DISCOVERY OF SIGNAL SUPPRESSION BY N-HYDROXY PIPERIDINE TO ENABLE ACTIVITY-BASED SENSING BY CHEMICAL EXCHANGE SATURATION TRANSFER MAGNETIC RESONANCE IMAGING

YEN JANETTE TRUONG

Thesis submitted to the University of Ottawa in partial fulfillment of the requirements for the Masters of Science in Chemistry degree

Department of Chemistry and Biomolecular Science
Faculty of Science
University of Ottawa

Abstract

Fluorescent probes are useful tools for studying chemical biology, available in a wide variety of colours and applicable to different biochemical processes. One of their hallmarks is the ability to tune their chemistry and allow them to selectively "turn on" in response to different biomolecular targets of interest. However, fluorescence is largely limited by shallow tissue depth of penetration. Magnetic resonance imaging (MRI) can overcome the depth of penetration limitations to better map these biochemical processes and mechanisms with contrast agents. Chemical exchange saturation transfer (CEST) MRI is an alternative method to generating contrast in MR imaging that, like fluorescence, can provide multiplexed imaging by varying the chemical shift of the exchangeable proton on the contrast agent. Previously, a paramagnetic CEST agent containing two tetramethylpiperidinyloxyl (TEMPO) moieties was shown to reduce the CEST signal of a lanthanide complex due to T_1 shortening effects on bulk water. Herein, we present a probe design strategy capable of suppressing the diamagnetic CEST (diaCEST) signal with the use of an *N*-hydroxy piperidine moiety. This discovery that *N*-hydroxy piperidine is capable of suppressing the diaCEST signal was applied to the study the activity of fibroblast activation protein-α (FAP). FAP is an enzyme involved in maintaining the tumour environment and its interactions can help understand tumour development, invasion and metastasis.

Acknowledgements

There are many people, without whom, this work would not have been possible. I would like to highlight a few selected individuals. First and foremost is Dr. Adam Shuhendler, my supervisor for the past few years. Thank you for providing me with the opportunity to join the Molecular Medicine Lab and making sure that I was never without work. Your guidance over the years has been invaluable and I was fortunate to continue my studies with such a mentor. Also, thank you for acquiring the CEST-MRI images.

Dr. Mojmir Suchy, our Research Associate and my tour guide for navigating the complex work of chemistry; thank you for your wealth of knowledge and guidance in all things chemistry. Many of the reactions below would not have been possible without your consultation and insight. Your mentorship has made me into the "chemist" that I am today.

Over the years, I have had the chance to work with many talented and hard-working individuals in the Molecular Medicine Lab and on Marion 2. It has been a pleasure to share the joys and pains of life and research. I am grateful for the opportunity to grow as a scientist

Table of Contents

List of Tables

List of Figures

List of Abbreviations

APT	amide proton transfer
BBOF	double resonance broadboad observed
Boc	tert-butyloxycarbonyl
BSA	bovine serum albumin
CAF	cancer associated fibroblasts
CEST	chemical exchange saturation transfer
CEST-MRI	chemical exchange saturation transfer magnetic resonance imaging
CT	compouted tomography
diaCEST	diamagnetic chemical exchange saturation transfer
DIPEA	N,N-diisopropylethylamine
DOTA	1, 4, 7, 10 tetraazacyclododecane
DTPA	diethylenetriaminepentaacetic acid
EDC-HCl	1-ethyl-3-(3-dimethylaminopropyl)carbodiimide
EI	electron impact
EPI	echo-planar imaging
EPR	electron paramagnetic resonance
equi	equivalent
ESI	electrospray ionization
FAP	fibroblast activation protein
FAPI	fibroblast activation protein inhibitor
FDG	fluorodeoxyglucose
FMOC	fluorenylmethoxycarboxyl
FOV	field of view
gluCEST	glutamate chemical exchange saturation transfer
glucoCEST	glucose chemical exchange saturation transfer
GP-AMC	glycine proline 7-amino-4-methylcoumarin
HATU	hexafluorophosphate azabenzotriazole tetramethyl uronium
HBTU	hexafluorophosphate benzotriazole tetramethyl uronium
HOBT	hydroxybenzotraizole
HPLC	high pressure liquid chromatography
HRMS	high resolution mass spectrometry
IRFSE	inversion recovery fast spin echo
MEMS	multi-echo multi-shot
MR	magnetic resonance
MRI	magnetic resonance imaging
MS	mass spectrum
MTR	magnetization transfer ratio
MTRasym	asymetric magnetization transfer ratio
NAD	nicotinamide adenine dinucleotide
NMR	nuclear magnetic resonance

NSF	nephrogenic systemic fibrosis
PARACEST	paramagnetic chemical exchange saturation transfer
PBS	phosphate-buffered saline
PDA	photo dioxde array
PET	positron emission tomography
ROI	region of interest
SMA	smooth muscle actin
TE	echo time
TEMPO	2,2,6,6-tetramethyl piperidinyloxyl
TEMPOL	4-hydroxy-2,2,6,6,-tetramethyl piperidinooxy
TEMPOMe	4-methoxy-2,2,6,6-tetramethyl piperidinooxy
TI	inversion time
TLC	thin layer chromatography
TR	repetition time
Tris	trisaminomethane
US	ultrasound
UV	ultraviolet
WASSR	water saturation shift referencing

Introduction

Magnetic Resonance Imaging and Chemical Exchange Saturation Transfer

Molecular imaging is an important technique that allows researchers to investigate and understand complex biochemical processes. It can be defined as the non-invasive, real-time visualization of biochemical events at the cellular and molecular level within cell and tissue samples, as well as live subjects (*in vivo*).[1–4] There are several different modalities that can be used for *in vivo* molecular imaging, including magnetic resonance imaging (MRI), positron emission tomography (PET), computed tomography (CT) and ultrasound (US).[5] One of the main advantages of MRI is that it can provide whole body images at the anatomical level without requiring ionizing radiation (Table 1).

Table 1. Summary of selected clinically relevant molecular imaging modalities and the related advantages.

Modality	Anatomical	Functional	Molecular	Ionizing Radiation	Spatial Resolution
MRI	✔	☐	☐	✗	1 mm
PET	☐	☐	☐	☐	5 – 7 mm
CT	☐	☐	☐	☐	0.5 – 1 mm
US	☐	☐	☐	☐	0.01 – 2 mm*

* depending on depth of penetration

MRI can allow for anatomical structures to be imaged non-invasively and with high spatial resolution. The basis of MRI relies on the use of a strong magnet, typically 1.5 T or 3 T in the clinical setting,[6] and radiofrequencies to visual the internal structures of the body. During the scan, a sample is placed inside the magnet and this can cause specific atomic nuclei in that sample to orient themselves along the field of the magnet, acting as a magnetic dipole. The most common nuclei imaged by MRI is ^{1}H due to its abundance in magnetically active isotopes and presence in water molecules in the body.[5] Once a radiofrequency pulse is applied, the magnetic dipole is tipped off its equilibrium point and will relax back to the initial equilibrium position. Relaxation can take place in two forms: longitudinal/spin-lattice (T_1) and transverse/spin-spin

(T_2).[7–9] Contrast in MRI, defined as image brightening or darkening of specific tissue and targets, is generated by different relaxation rates of water in different tissue types in the body. For example, magnetic dipoles of proton nuclei in fat tissue have shorter relaxation times and will return to equilibrium faster than those in an aqueous environment.[10] This difference in relaxation can be exploited by preferentially looking at the longitudinal or transverse relaxation for T_1- or T_2-weighted images (Figure 1).

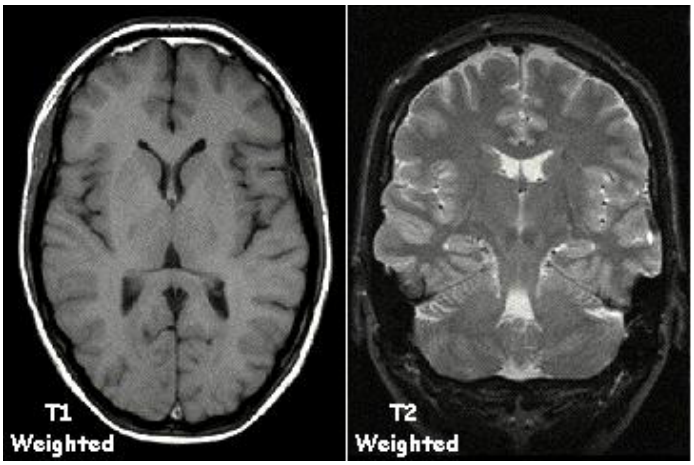

Figure 1. Example of T_1-weighted and T_2-weighted images of the brain. *In T_1-weighted images (left), the cerebrospinal fluid appears dark and the white matter of the brain and other fat appears light. In T_2-weight images (right), the cerebrospinal fluid is bright, while white matter is dark. Both fat and inflammation appear bright in the T_2-weighted images as well.*[11]

Contrast agents can also be employed to enhance the contrast of the image and report on the presence or activity of a given target. These contrast agents work by altering the T_1 and T_2 relaxation time or interactions with water to result in imaging brightening for T_1 and image darkening in T_2 scans.[12] Historically, MRI contrast agents have been based around gadolinium chelates.[13] However, gadolium-based contrast agents were associated with nephrogenic systemic fibrosis (NSF) in patients with pre-existing renal impairments[14,15] and can lead to poor kidney function. Additionally, it was discovered that some amount of the gadolinium (III) remained in the body for long periods of time. The build up of the remaining gadolinium (III) was detectable

by MRI.[16] Remaining gadolinium (III) can interfere with the signal intensity of future MRI scans and can lead to other toxic effects, including nephrotoxicity,[17,18] hematotoxicity,[19] hepatotoxicity[20] and neurotoxicity.[21,22] These findings contributed to growing efforts to develop other types of contrast agents, particularly those that are metal-free. There are several other ways to generate contrast in MR images, which can include physical properties (diffusion-weighted imaging),[23–25] functional properties (blood oxygen level dependent imaging)[26–28] and chemical composition (MR spectroscopy).[29,30]

Chemical exchange saturation transfer (CEST) is another method to generate contrast in MRI, using interactions of the agent with bulk water. In CEST, magnetic saturation is transferred from the contrast agent to bulk water through exchangeable protons.[31–33] Saturation in this case is when no net magnetization is observed. During the imaging session, a radiofrequency pulse is applied at the resonance frequency of the proton of interest on the contrast agent (Figure 2). It temporarily becomes invisible in the MRI because there is no net magnetization. Since this proton is exchangeable, it can exchange with the surrounding non-saturated water molecules to transfer the saturation from the contrast agent to bulk water. This will result in a decrease in the water signal, which can be detected by MR imaging sequences to determine the concentration of the agent of interest. The CEST exchange is dependent on a number of factors, including pH, temperature and concentration,[34] and the exchange rate must be on the slow to intermediate NMR timescale to lead to useful contrast.[35,36] The exchange rate varies according to the proton of interest and chemical shift ($k_{ex} < \Delta\omega$), but is generally in the range of ~30 – 7100 Hz.[37–43] Although water molecules vastly outnumber the contrast agent, continuous exchange between the contrast agent and bulk water over the course of the 5 s saturation pulse can amplify the

signal and have a summation effect so that the change in the water signal is observable. The CEST signal can be calculated as the percent decrease in bulk water intensity according to the following equation:

$$\frac{M_z}{M_0} = 100\left(1 + \frac{cqT_1}{55.5\tau_M}\right)^{-1} \quad (1)$$

where c is the concentration, q is the number of exchanging protons, T_1 is the longitudinal relaxation time of bulk water and τ_M is the exchange lifetime of the exchanging protons.

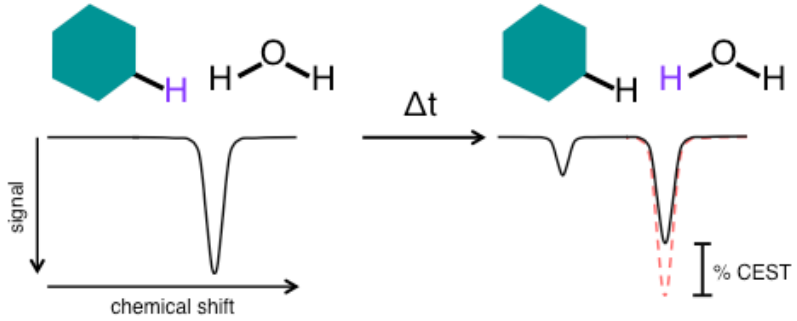

Figure 2. An illustration of the chemical exchange of the saturated proton on the contrast agent with bulk water. *Following a radiofrequency pulse at the resonance frequency of the exchangeable proton, the proton becomes saturated and invisible. The proton can exchange with bulk water, to transfer the saturation onto the water molecule. This results in a decrease of the measured water signal.*

The CEST effect can be analyzed by looking at the Z-spectrum (Figure 3), where the signal reduction (S/S_0) is plotted against the saturation frequency relative to water.[44] Water is used as the reference point, and is set to 0 ppm. In the absence of a CEST-active molecule, saturation around the resonance frequency of water is symmetrical. If a CEST-active molecule is present, then a CEST effect can be measured by comparing the signal intensity on each side of the water peak ($\Delta\omega$) and ($-\Delta\omega$) to give the magnetization transfer ratio (MTR).[45] In the Z-spectrum below, the %MTR is also plotted using the right y-axis. The net CEST effect can be observed by the location and magnitude of the MTR peak(s).

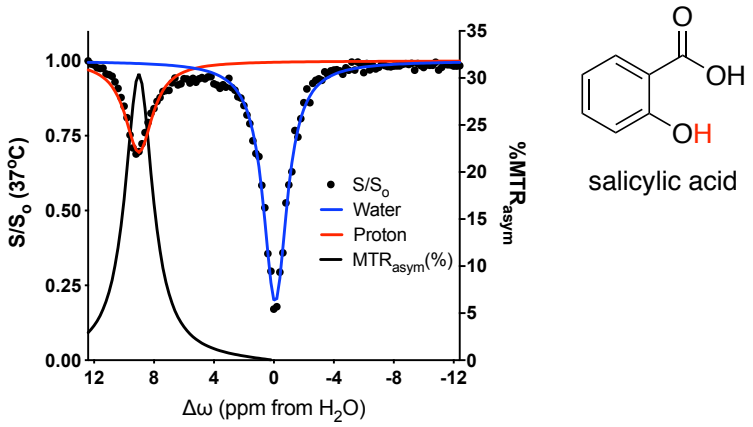

Figure 3. Z-spectrum of salicylic acid. *The exchangeable CEST proton of salicylic acid (red) is well separated from water, at 9.2 ppm. The peak is reflected on the x-axis and the CEST signal (%MTR$_{asym}$) can be read from the right y-axis.*

CEST contrast agents must contain an exchangeable proton, either –NH,[42,46,47] –SH[48] or –OH.[49–52] There have been many compounds studied for the exchange effects with water. Typically, the compounds can be grouped into 2 categories based on the presence or absence of a paramagnetic metal: paramagnetic CEST (PARACEST) and diamagnetic (diaCEST). PARACEST contrast agents involve a metallic ion and have large chemical shifts away from bulk water. In contrast, compounds that fall under the diaCEST category are generally small organic molecules, with chemical shifts close to water. The metal-free nature of diaCEST makes it an attractive alternative to gadolinium-based contrast agents. However, one of the difficulties in developing a diaCEST agent is that the chemical shift of the exchangeable proton must be sufficiently separated from water.[45]

Babalan *et al.* initially reported several organic small molecules with exchangeable protons at different sites as the first diaCEST agents in a landmark paper in 2000.[53] This list included sugars, amino acids, imino acids, nucleosides and barbiturates. However, the chemical shifts of these compounds were limited to 1 – 6 ppm. Regardless, some diaCEST agents have

been found to be useful for *in vivo* imaging. Glucose CEST, called glucoCEST, can be used to map glucose distribution to gain insight on tumour detection and staging[50]. Since the chemical shift difference between the hydroxyl protons of glucose and water is small, it is difficult to map the endogenous glucose distribution and instead exogenous glucose is administered as a contrast agent. GlucoCEST can also be applied to imaging glioma with comparable contrast enhancement to a gadolinium-based contrast agent.[54] Glutamate and creatine are two sources of endogenous diaCEST agents that have exchangeable amine protons for CEST. Glutamate is a neurotransmitter and mapping the distribution of glutamate by CEST, through gluCEST, is important in neurological and neurodegenerative diseases.[55,56] One of the most commonly used functional groups for CEST imaging is amide, often referred to as amide proton transfer (APT).[46] APT images the amide protons of proteins and peptides for the detection of cancer and ischemic stroke.[39,57] Typically, these protons have a chemical shift at around 3.5 ppm.[46] In 2013, Yang *et al* first reported the use of salicylic acid as a diaCEST agent.[58] The exchangeable proton of salicylic acid resonated at 9.3 ppm from water, which was further than any other organic diaCEST agent at the time. Since then, salicylic acid has been incorporated into many other diaCEST agents.[40,59] The McMahon group has continued working to find new diaCEST agents with sufficient separation from water, including anthranilic acid analogues.[42] An overview of common classes of diaCEST agents and their chemical shift is presented in Figure 4.

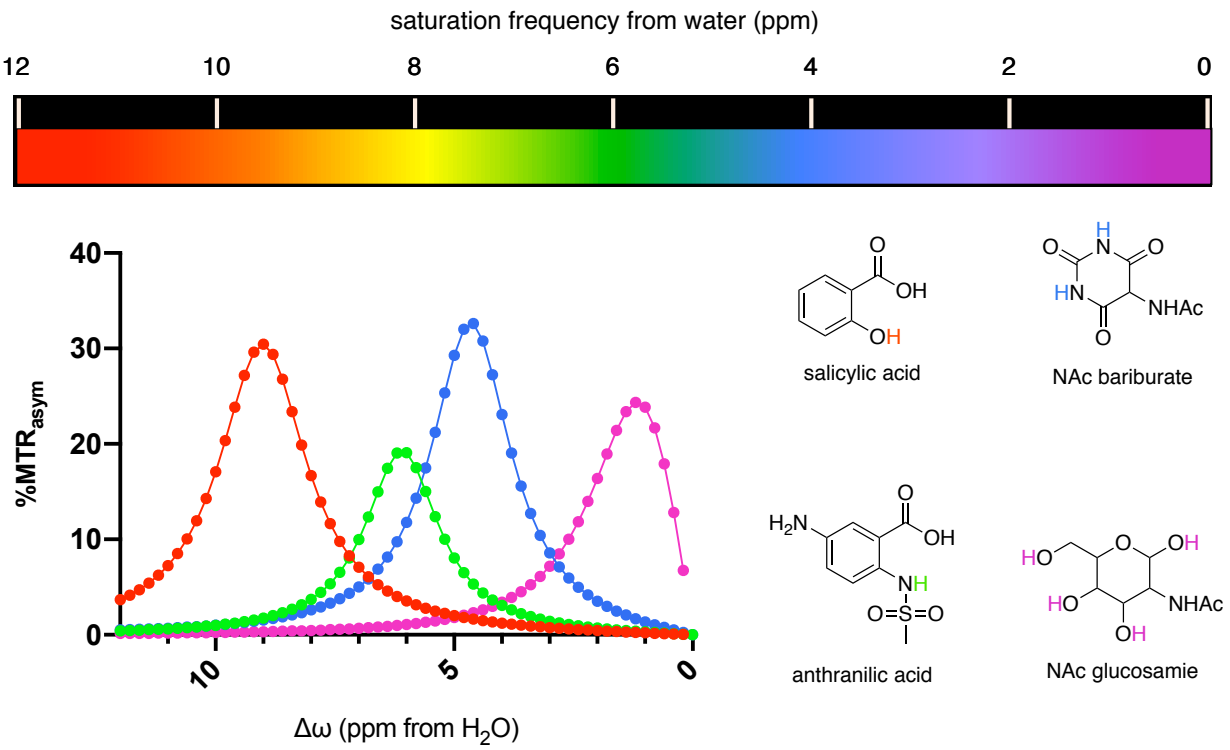

Figure 4. Applying the chemical shift of diaCEST exchangeable protons to a colour scale. *CEST signal measured from salicylic acid, barbituric acid, D-glucosamine, and anthranilic acid. The chemical shift of the exchangeable proton differs among the contrast agents, providing an opportunity for multicolour MRI.*

Activatable Probes for CEST MRI

The development of imaging probes that can respond to different environmental conditions or biomarkers are a growing area of interest. Often in disease conditions, the environment can have altered pH, enzymatic activity or chemical potential (reduction/oxidation), which are characteristic of the biological process and pathology.[60] Contrast agents providing activity-based sensing, or "smart" probes, can respond to the changing environment and give an altered signal upon interaction with their biomolecular target of interest. While traditional targeted agents can localize and accumulate in a specific site due to protein interactions or cell internalization, activatable probes undergo a chemical change and this affects the output signal. Through this process, activatable probes can be used to understand different pathways by studying the

functional activity of enzymes. There have been many examples of probes activated by pH changes, enzymatic activity and changing redox conditions used for CEST-MRI (Table 2).

Table 2. Activatable CEST-MRI agents. *Probes can be "turned on" by a variety of stimuli including pH changes, enzyme activity and redox conditions.*

Probe	Biological Relevance (target)	Reference
5, 6-dihydrouracil 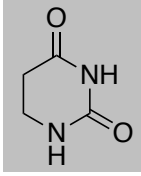	Determine pH changes	Ward *et al* [32]
Poly-L-lysine 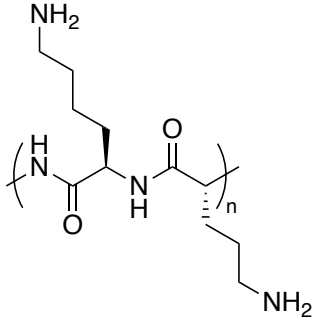	Determine pH changes	McMahon *et al* [61]
Imidazole-4, 5-dicarboxamide 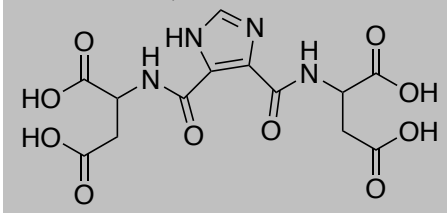	Ischemia (pH changes)	Yang *et al* [43]
Cytosine 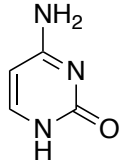	Deamination for prodrug activation in cancer therapy	Liu *et al* [51]
(Phe-Arg)-4-amino-2-hydroxy benzoic acid 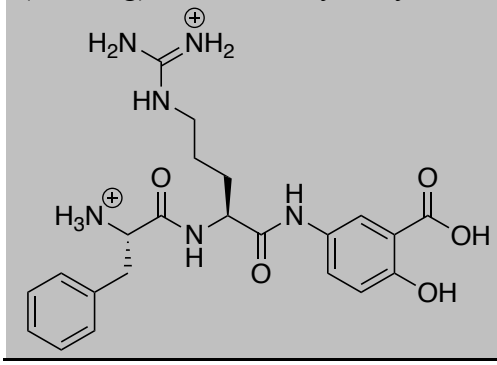	Monitor tumour initiation, proliferation, invasion and metastasis (cathepsin B)	Hingorani *et al* [62]

4-acedamino-2-(sulfoxy)benzoic acid 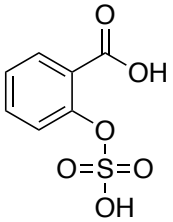	Developmental abnormailites, hormone-dependent cancer, bacterial pathogenesis (sulfates)	Sinharay *et al* [63]
Fosfosfal 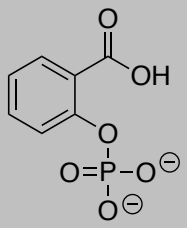	Osterogenic sarcoma, primary sclerosis cholangitis, metabolic syndrome (alkaline phosphatase)	Daryaei *et al* [64]
Yb-based complex 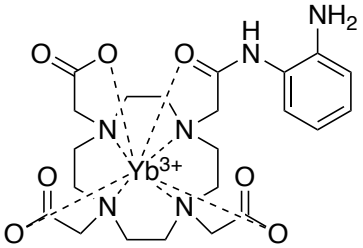	Monitor redox changes (nitric oxide)	Liu *et al* [65]
Eu-based complex 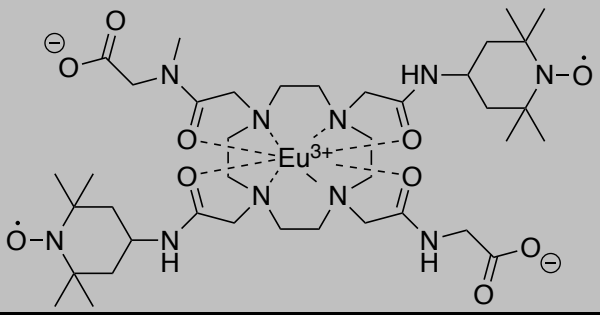	Monitor redox changes by the presence of L-ascorbic acid	Ratnakar *et al* [66]

The activity of enzymes underlies a large majority of molecular and cellular functions. In disease conditions, enzymes can be upregulated or have increased expression or activity on the cell surface and extracellular space. Detection of the activity of enzymes can be important in understanding the pathology of the disease. Liu *et al* first reported a "turn-off" diaCEST agent for cytosine deaminase, where cytosine is deaminated to uracil and results in the loss of the CEST signal.[51] In 2016, Hingorani *et al* used a probe containing a dipeptide followed by a salicylic acid analogue.[62] Cathepsin B cleaves the dipeptide linker to release 4-amino 2-

hydroxybenzoic acid and restores the CEST signal. Salicylic acid has been a core feature in other "turn-on" diaCEST agents that can be used to detect the activity of other enzymes including sulfates[63] and alkaline phosphatase.[64]

The reduction-oxidation potential of the cell environment is important for physiological processes. Generally, it is controlled by metabolites including NAD/NADH, peroxides and thiols/disulfides and oxidase enzymes.[67] In disease conditions, the redox environment can be disrupted and imaging the redox conditions can give us a better understanding of the pathophysiology of diseases. CEST probes that respond to changing redox conditions have largely used paramagnetic ions. Pagel and co-workers presented a ytterbium-based contrast agent capable of detecting nitric oxide in the presence of oxygen.[65] The probe undergoes an irreversible reaction to convert the CEST-active amide and amine into a triazine, thus losing the CEST ability of the molecule. Ratnakar *et al* used redox-sensitive nitroxyl radicals on their probe with an europium core.[66] As the T_1 decreases, as shown in Equation 1, the measured CEST signal also decreases. The radicals can shorten the T_1 relaxation time of bulk water to quench the PARACEST signal. Reduction of the radicals to the diamagnetic hydroxylamine can result in lengthened T_1 relaxation to restore the CEST signal.

Molecular Imaging of Tumour Stroma

The tumour environment can be characterized by hypoxia, vascular changes, low pH, increased interstitial fluid and increased aerobic glycolysis.[68] It is important for the tumour to adapt its metabolism to best suit the environment in order to ensure growth and survival. Alterations in the metabolic pathways used by the tumour can also affect cell signalling and cell differentiation.[69–72] While a lot of work has been done to understand tumour cells themselves, the

tumour environment also has an important role in its development and progression.[71,73–75] The tumour stroma consists of the extracellular matrix, stromal cells and immune cells. Cancer cells are responsible for recruiting and reprogramming the metabolism of stromal cells,[71,74,76] as well as remodelling the extracellular matrix, to promote tumour growth.[77–80]

The extracellular matrix is complex and composed of many elements, including collagen, proteoglycans and fibronectin. MRI can be used to image collagen in the tumour environment. Previously EP-3533 has been used as a peptide-based MR probe targeting collagen.[81,82] A cyclic chelate (Gd-DOTA) has also been developed by Farrar *et al* to study fibrosis by MR imaging.[83] Shiftan *et al* developed an activatable contrast agent to detect the activity of hyaluronidase by MRI.[84] Proteoglycans, like hyaluronan, contain high molecular weight glycosaminoglycans that can be degraded by hyaluronidase to alter the tumour microenvironment. Gd-DTPA covalently linked to hyaluronan showed attenuated relaxivity and the R1, R2 relaxation rates were altered upon cleavage by hyaluronidase. Park *et al* used a peptide that binds specifically to fibronectin conjugated to superparamagnetic iron oxide nanoparticles to detect fibronectin by MRI.[85] The contrast agent was administered intravenously and fibronectin was detectable after 24 hours. Thus far, MR imaging of the extracellular matrix has been done with Gd-based contrast agents and iron oxide nanoparticles, but the use of small molecule contrast agents has not been explored.

Cancer associated fibroblasts (CAF) are fibroblasts inside the tumour or tumour margins, and are responsible for promoting drug resistance, remodelling of the extracellular matrix, stimulating chronic inflammation and contributing to tumour invasiveness.[71,86,87] CAF are the

most prevalent cell type in the tumour stroma and can be found in several types of cancer, including breast,[88,89] non-small cell lung carcinoma,[90] colorectal,[91–93] liver[94] and prostate.[95] There are several markers that can be used to identify CAF, including α-smooth muscle actin (α-SMA), vimentin and fibroblast activation protein α (FAP).[96] FAP was first reported by Rettig *et al* in 1986 as a surface protein on reactive stromal fibroblast of epithelial cancers.[97] FAP is a dipeptidyl peptidase and has post-proline exopeptidase activity.[98] Typically, FAP is expressed during development and rarely seen in healthy adult tissue.[99] However, expression of FAP can be upregulated on fibroblasts with active tissue remodelling, including wound healing, fibrosis and cancer.[100]

FAP is described as an important marker for CAF, related to tumour growth and progression, and stimulation of the immune system.[101,102] The presence of FAP can also contribute to the invasiveness of the tumour. It is important for the stroma to be active for cancer cell invasion and metastasis.[100] The extracellular matrix is degraded by cancer cells and enzymes with protease activity, like FAP, are important in the matrix remodelling process for tumour invasion and metastasis.[103–105] In addition to remodelling the extracellular matrix, FAP has been linked with increased microvascular density, where the expression of FAP was associated with the secretion of pro-angiogenic factors.[106] FAP also promotes the growth of stromal fibroblasts and their transformation into CAF.[107,108] The expression of FAP on stromal cells also contributes to the stimulatory effects of CAF on the proliferation of tumour cells.[109–111] Overall, the presence and expression of FAP contributes to tumour invasion and aggressiveness.

Granot *et al* previously designed an MRI probe to track CAF *in vivo*.[112] CAF were pre-labelled with biotin-BSA-Gd-DTPA or iron oxide particles and could be monitored over several days to study the recruitment into the tumour stroma. Recently, Giesel *et al* published a quinolone-based PET tracer capable of acting as an FAP inhibitor (FAPI).[113] The probe, ^{68}Ga-FAPI, has the potential to be used in the diagnostic imaging of cancer patients. Currently, ^{18}F-FDG (fluorodeoxyglucose) is widely used for this purpose. Further characterization found tracer uptake in 28 different types of cancer, with the highest uptake in lung, breast and esophageal cancers.[114] However, the probe functions as an inhibitor and can only report on the expression of FAP, rather than activity. The use of a probe that targets FAP as a potential substrate can report its enzymatic activity and may more accurately reflect the function and interactions of the target. An activatable, near-IR fluorescent probe was also reported for FAP that can be used to image the activity.[115] Using the post-proline endopeptidase activity of FAP, the quencher group (QSY21) is cleaved from the fluorescent group (Cy5.5) to restore the fluorescent signal. Unfortunately, fluorescence probes have a limited depth of penetration (<1 cm),[5] which can make clinical translation difficult. Incorporation of a proline site recognized by FAP to make a substrate-based probe can be straightforward and allow for activity-based sensing of the marker. Combined with the limitless depth of penetration from MRI, this can present itself as an opportunity to further understand the role and interactions of FAP in the tumour environment.

Goals and Objectives

Conventional strategies for developing selective probes can often rely on molecular recognition and binding based on a lock and key model. This can be used to report on the expression or presence of a biomolecule. However, an approach using activity-based sensing can provide useful information based on the function and activity of the target of interest that can provide better insight on the interactions within a complex system. Activatable probes using fluorophore quencher pairs have become very important for chemical biology to study different pathways. Unfortunately, this activatable concept has not been broadly reinterpreted for molecular imaging and specifically CEST-MRI using metal-free probes. While there has been some work in creating activatable probes for CEST-MRI, the activation mechanism is largely dependent on the enzyme and difficult to adapt to different targets or generalize.

Ratnakar *et al* synthesized a PARACEST contrast agent where the signal was modulated by changes in the relaxation of bulk water.[66] The signal could be restored by reduction of the nitroxyl radical by ascorbate. However, the presence of europium at its core can lead to toxic effects and the *in vivo* stability of TEMPO is limited. Based off of this report, we were inspired to adapt this idea for a diaCEST model. The use of a small molecule can avoid lanthanide metal toxicity issues. Signal suppression could be achieved through similar changes in the relaxation of bulk water, however replacing TEMPO for a group with greater *in vivo* stability. Since this signal suppression mechanism is independent of the contrast agent used (lanthanide metal complex or small molecule) it has the potential to be generalized to a wide range of diaCEST agents.

The goal of this work is to develop a generalizable signal suppression group that can be applied to a wide range of targets. The mechanism of signal suppression will be studied and applied to other classes of diaCEST agents. Specifically, the activatable signal suppression effect can be used to image FAP using activity based-sensing to understand more about the tumour stroma and environment. This functionality of signal suppression can be used to generate a library of activatable CEST-MRI probes, similar to fluorophore-quencher pairs, to further study biochemical pathways and processes in understanding the progression and prognosis of disease.

To achieve these goals, our objectives are the following:

1. Characterize a new signal suppression moiety for diaCEST-MRI
2. Propose a mechanism for CEST signal suppression
3. Design and test an activatable probe for activity-based sensing of FAP, an enzyme biomarker of CAFs relevant to tumour imaging

If successful, then this work can be used as a new strategy for designing activity-based imaging probes for CEST-MRI. The signal suppression moiety can be paired with a diaCEST contrast agent and applied to a target of interest to generate a library of activatable contrast agents.

Materials and Methods

Experimental Procedures

Z-Spectra Acquisition by NMR

CEST spectra were acquired on a Bruker AVANCE II 300 MHz NMR spectrometer equipped with a 5 mm BBOF probe. A pseudo 2D pulse sequence was used with a variable frequency list consisting of 201 values ranging from 20 ppm to -20 ppm, with water at 4.7 ppm. At each frequency, 1.15 mW of presaturation power was applied during the 3 second recycle delay followed by a hard 90 degree pulse (centred at 2.5 ppm). The proton 90 degree pulse was 12.75 microseconds. Four scans were averaged for each spectrum. The free induction decays were Fourier transformed and the integral of the water resonance was plotted as a function of the saturation frequency to give a CEST plot. Samples were composed of 1:1 PBS:D_2O solutions of the complexes (adjusted to pH 6.95-7.05). During the scans, the sample was heated to 37°C using heated forced air through a Model 1025 Small Animal Monitoring and Gating System. Z-spectra were processed using MatLab and invoking the Interactive Peak Fitter code to fit Lorentzian curves to the acquired data. Spectra were plotted in GraphPad Prism.

EPR Sample Preparation and Absolute Spin Counting

To determine the appropriate settings for EPR spin counting, TEMPO was dissolved in chloroform to make solutions at 0.05 mM, 0.1 mM, 0.5 mM and 1 mM. The attenuation and power were adjusted to centre the signal and the q value at each concentration was recorded. The attenuation and q value were entered as EPR parameters after tuning to measure the absolute spin count of each sample.

The compound was dissolved in chloroform to make a 1 mM solution. Nitrogen gas was bubbled through the sample for 5 minutes before EPR acquisition. The sample was placed in a tube with an interior diameter of 2 mm and the height of the sample was approximately 4 mm. The EPR spectrum was acquired using a Bruker EPR spectrometer and the attenuation was adjusted to 36 dB after tuning (for a sample at 1 mM). A 1D field sweep acquired the spectrum over 3 scans. Absolute spin counting was done to confirm the concentration of the sample within 10% of the expected value (0.9 mM – 1.1 mM).

Serum Stability Assay by NMR

The compound was prepared in 1:1 mouse serum:D_2O and adjusted to pH 7.0. The NMR spectrum was acquired on a Bruker AVANCE II 300 MHz NMR spectrometer equipped with a 5 mm BBOF probe. A scan was acquired every 20 minutes for a total of 2 hours. During the scan, the sample was heated to 37°C using heated air forced through a Model 1025 Small Animal Monitoring and Gating System.

Serum Stability Assay by EPR

The compound was prepared as a 20mM sample in mouse serum. The EPR spectrum was acquired on a Bruker EPR spectrometer. The spectrometer was tuned using a sample of the compound prepared in PBS buffer. A scan was acquired every 20 minutes for a total of 2 hours. The sample was maintained at room temperature for the duration of the scans.

Acquisition of T_1- and T_2-weighted Images and Relaxivity by MRI

All images were acquired on an MRS 3000 3T MRI (MR Solutions, Inc., Guildford, UK) using a mouse body coil. Samples were prepared in NMR tubes and suspended in a phantom comprised of ultrasound imaging gel. Once position of phantom was optimized by standard localizer protocol, an imaging routine and a relaxation quantitation routine was implemented. For imaging, single slice T_1-weighted images were acquired by standard Fast Spin Echo pulse sequence (FOV 40 mm, Thickness 5.0 mm, Flip Angle 90°, TR 720 ms, TE 11 ms, Views 240, Echo Train 4, Echo Spacing 11, Average 4). Additionally, single slice T_2-wegithed imaging were acquired by standard Fast Spin Echo pulse sequence (FOV 40 mm, Thickness 5.0 mm, TR 4800 ms, TE 68 ms, Views 240, Echo Train 8, Echo Spacing 17, Average 4). All images were prepared using the Fiji implementation of ImageJ.[116]

Relaxation times were determined by Inversion Recovery Fast Spin Echo (IRFSE) or Multi-Echo Multi-Shot (MEMS) pulse sequences for transverse and longitudinal relaxation rates (R_1 and R_2, respectively), where $R_n=(T_n)^{-1}$. For IRFSE, a single slice image of the phantom was acquired with the following parameters: FOV 40 mm, Thickness 5.0 mm, TE 17 ms, TR 5000 ms, Views 240, Echo Train 8, Echo Spacing 17, Average 1. An image was acquired for each of the following inversion times (TI): 50, 100, 200, 300, 400, 600, 800, 1200, 2400, and 4000 ms. Regions of interest (ROIs) were drawn around samples and the transverse relaxation rates for 50, 100, 200, and 400 μM contrast agent were extracted using ‘mapping2.mat’, a MATLAB-based analysis routine from Dr. J. Rioux at Dalhousie University, which was modified from a routine generated by J. Barral, M. Etezadi-Amoli, E. Gusmundson, and N. Stikov at Stanford University (2009). The value of transverse relaxivity (r_1) was extracted as the slope of the line from a plot of

contrast agent concentration versus R_1. For MEMS, a single slice image of the phantom was acquired with the following parameters: FOV 40 mm, Thickness 5.0 mm, Views 128, TR 7500 ms, TE step 15 ms, Number of Echoes 10, Average 1. Regions of interest (ROIs) were drawn around samples and the longitudinal relaxation rates for 50, 100, 200, and 400 μM contrast agent were extracted by fitting a plot of TE versus signal intensity (M(t)) to equation 2 using Prism (v. 8.1.1, GraphPad Software Inc.).

$$M(t) = M_o e^{-\frac{TE}{T_2}} \qquad (2)$$

The value of longitudinal relaxivity (r_2) was extracted as the slope of the line from a plot of contrast agent concentration versus R_2.

Acquisition of CEST Scan by MRI

CEST-MRI was performed at 3T on an MR Solutions system using a mouse body coil. The phantom consisted of a 50 mL Falcon tube filled with ultrasonography gel and fitted with a sample holder cap. Standard NMR tubes were used to hold the samples. CEST acquisition used a single slice 2D EPI sequence for the WASSR and Z-spectrum images, both using a slice thickness of 5.0 and field of view of 40. For the WASSR sequence images, CEST acquisition started at 200 Hz with -25 Hz steps for 17 steps at a saturation amplitude of 1%. The following parameters were used: TE = 25 ms, samples = 8160, switches = 60, crusher = 1500 ms and the total acquisition time was 3 minutes and 3 seconds. For the Z-spectrum sequence, acquisition started at 2000 Hz with a -50 Hz step for 81 steps at a saturation amplitude of 4%. All other parameters were the same as the WASSR sequence, with a total acquisition time of 13 minutes and 56 seconds. Finally, a T_1-weighted Fast Spin Echo sequence was performed (averages = 4,

TE = 11 ms, TR = 720 ms). CEST maps were generated using the code defined by Liu *et al*[117] and run in MatLab. The code was modified to accept data acquired of the MR Solutions system by Ruslan Garipov and Gerd Melkus.

Fluorescence Intensity Assay for hFAP

50 μg GP-AMC or probe was incubated with 0.01 μg (1X), 0.05 μg (5X) or 0.1 μg (10X) hFAP at 25°C. The fluorescence intensity was measured using excitation at 380 nm and emission at 460 nm every 1 minute over 15 minutes. The Plate Reader Synergy Hybrid Reader H4 (Biotek) was used to monitor fluorescence increase. The assay buffer consisted of 50 mM Tris, 1.0 M NaCl, 0.1 % BSA (w/v), adjusted to pH 7.5, or 1X PBS at pH 7.4.

HPLC Assay for hFAP

50 μg GP-AMC or probe was incubated with 0.01 μg (1X), 0.05 μg (5X) or 0.1 μG (10X) hFAP in assay buffer (50 mM Tris, 1.0 M NaCl, 0.1 % BSA (w/v), adjusted to pH 7.5, or 1X PBS at pH 7.4. The samples were incubated in a bead bath at 37°C in the dark. After 3 hours, the reaction was quenched by the addition of cold acetonitrile. Water was also added to the sample to make the total volume 1 mL. The sample was centrifuged at 5000 g for 1 minute before being subjected to HPLC analysis. HPLC was done using a Luna C-18 100 Å column (particle size 5 μm; 21.2 x 250 mm), on analytical mode at a flow rate of 1 mL/minute, with the following gradient profile: 99% water + 0.1% TFA : 1% acetonitrile + 0.1% TFA to 100% acetonitrile + 0.1% TFA over 25 minutes. The absorbance was monitored using a PDA detector set to 310 nm.

Results

Synthesis of Probes and Controls

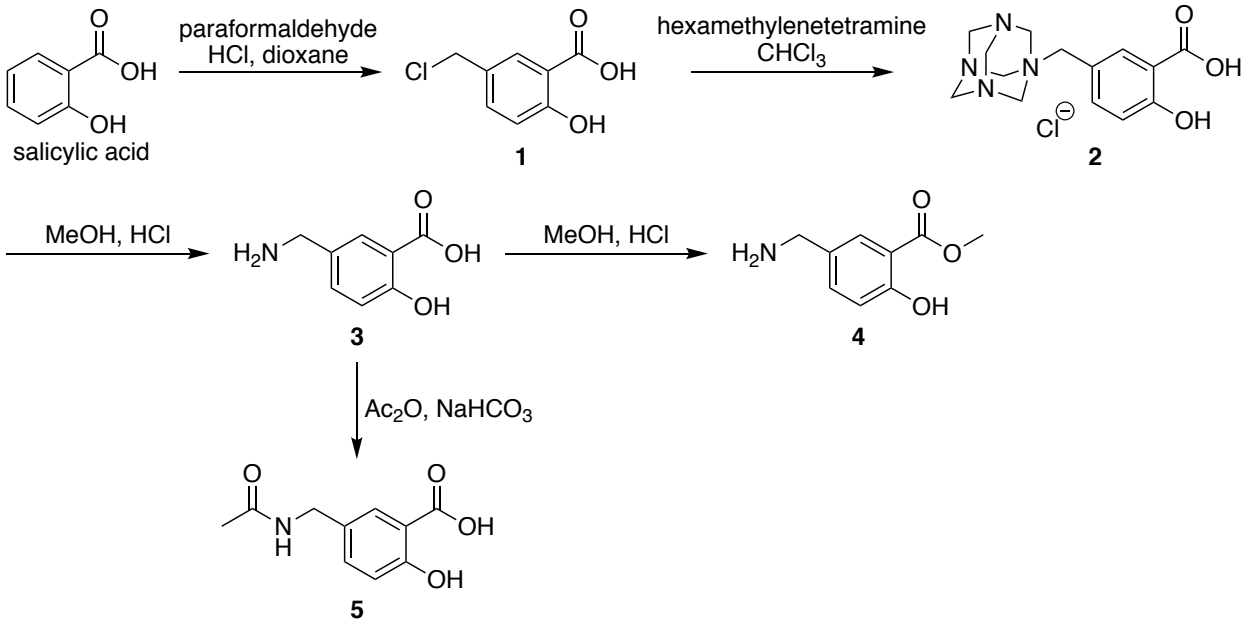

Scheme 1. Synthetic pathway to 5-aminomethyl salicylate methyl ester (4).

Salicylic acid was functionalized at the 5 position to introduce a chloromethyl group (**1**). This was converted into an adamantine intermediate (**2**) and was later hydrolyzed under acidic conditions to give 5-aminomethyl salicylate (**3**). Fischer esterification of compound **3** resulted in compound **4**, 5-aminomethyl salicylate methyl ester. Carboxylic acids were coupled to the amine to study its effect on the CEST signal. Acetylation of compound **3** gave compound **5**, which was used to study the effects of the amide bond.

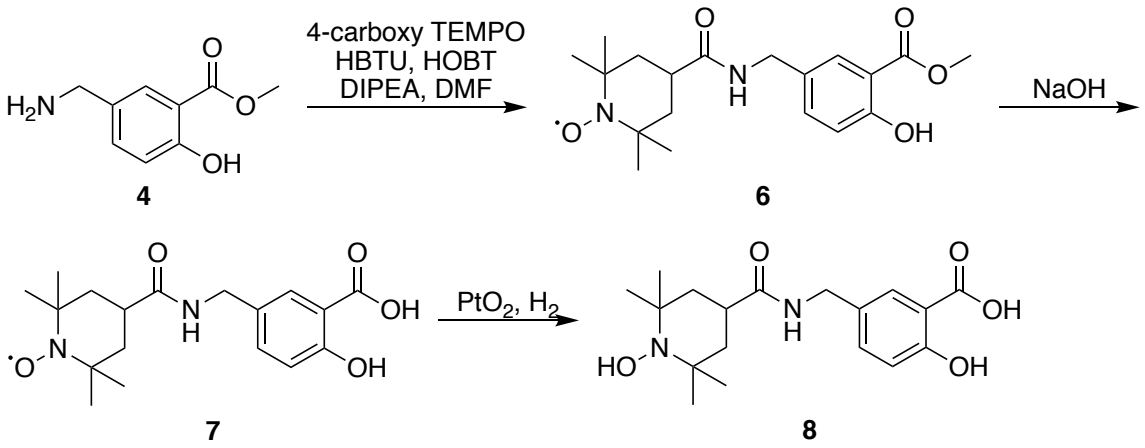

Scheme 2. Synthesis of compound 8.

From 5-aminomethyl salicylate methyl ester (**5**), we use HBTU/HOBT coupling conditions to attach 4-carboxy TEMPO to salicylate (**6**). Hydrolysis of the methyl ester afforded compound **7**. The nitroxyl radical was reduced using platinum (IV) oxide to give compound **8**.

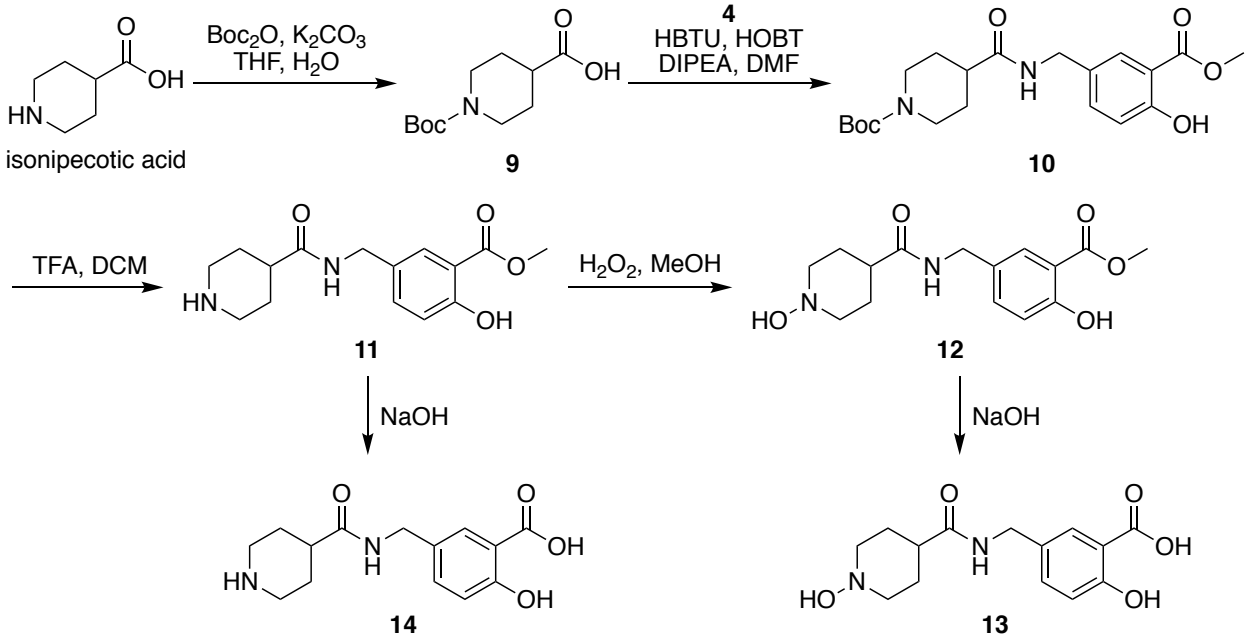

Scheme 3. Synthetic scheme to make compounds 13 and 14.

Commercially available isonipecotic acid was Boc-protected to mask a potentially competing nucleuophile, the secondary amine. Compound **9** was coupled to 5-aminomethyl salicylate

methyl ester (**4**) using HBTU/HOBT and resulted in compound **10**. Removal of the Boc group under acidic conditions (**11**), followed by oxidation using hydrogen peroxide (**12**), and finally hydrolysis with sodium hydroxide resulted in compound **13**.

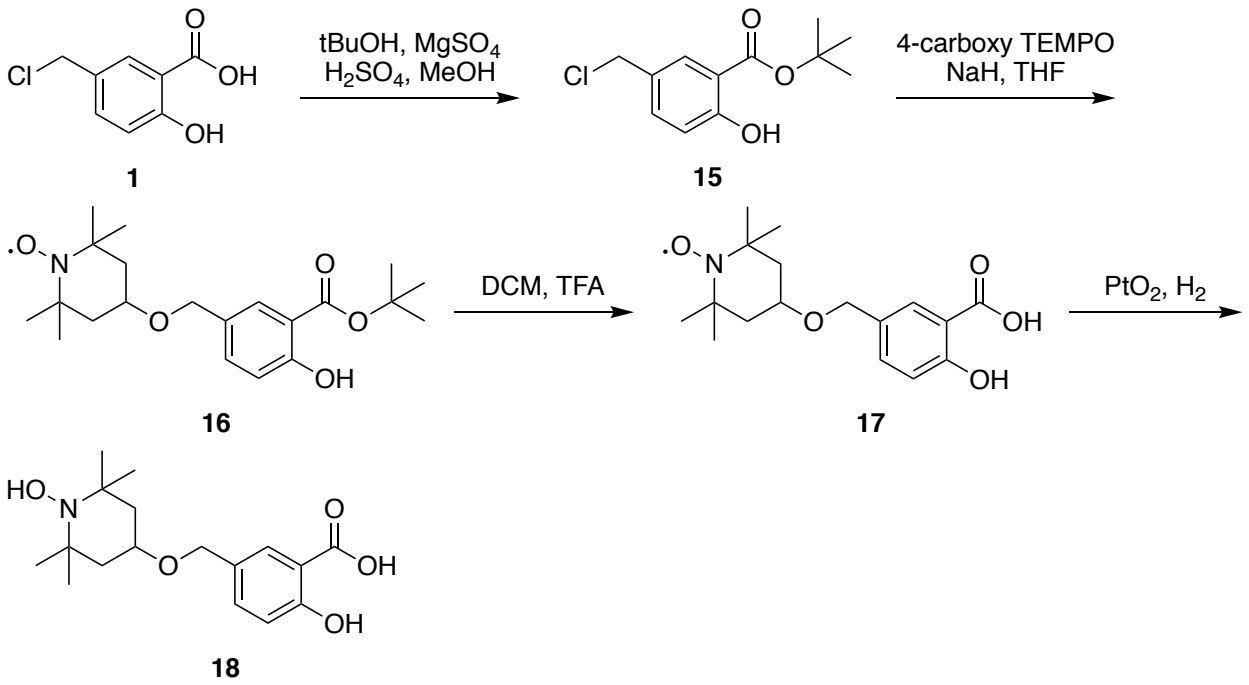

Scheme 4. Synthesis of compound 18.

5-chloromethyl salicylic acid (**1**) was converted into a t-butyl ester (**15**). The chloro compound underwent a nucleophilic substitution to result in compound **16**. The t-butyl group was removed under acidic conditions (**17**), and the nitroxyl radical was reduced using platinum (IV) oxide (**18**).

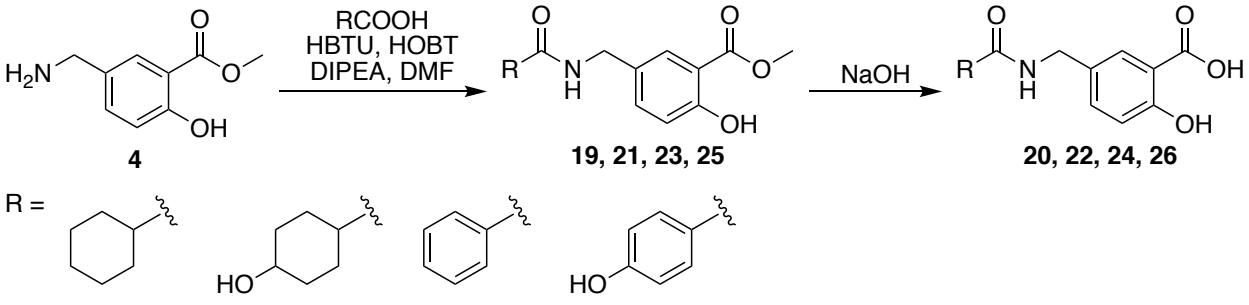

Scheme 5. Synthetic scheme for the synthesis of compounds 20, 22, 24, 26.

Various 6-membered aliphatic and aromatic carboxylic acids were coupled to 5-aminomethyl salicylate methyl ester **(4)** under HOBT/HBTU peptide coupling conditions. The methyl ester was removed using sodium hydroxide to reveal the coupled salicylic acids (**20**, **22**, **24**, **26**).

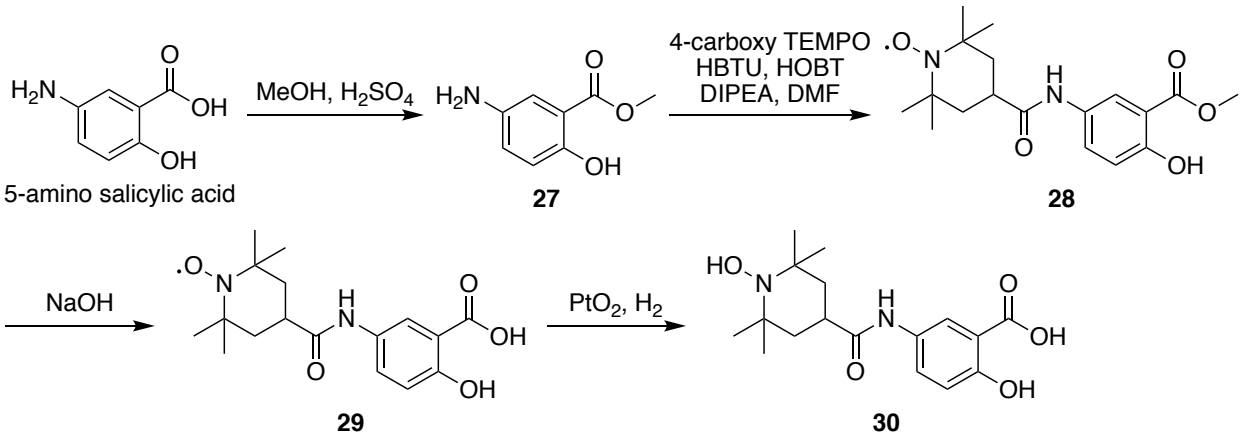

Scheme 6. Synthesis of compound 30.

Commercially available 5-amino salicylic acid underwent Fischer esterification to protect the carboxylic acid (**27**). 4-carboxy TEMPO was coupled to the amine (**28**) and the methyl ester was hydrolyzed to restore salicylic acid (**29**). The nitroxyl radical was reduced using platinum (IV) oxide with hydrogen (**30**).

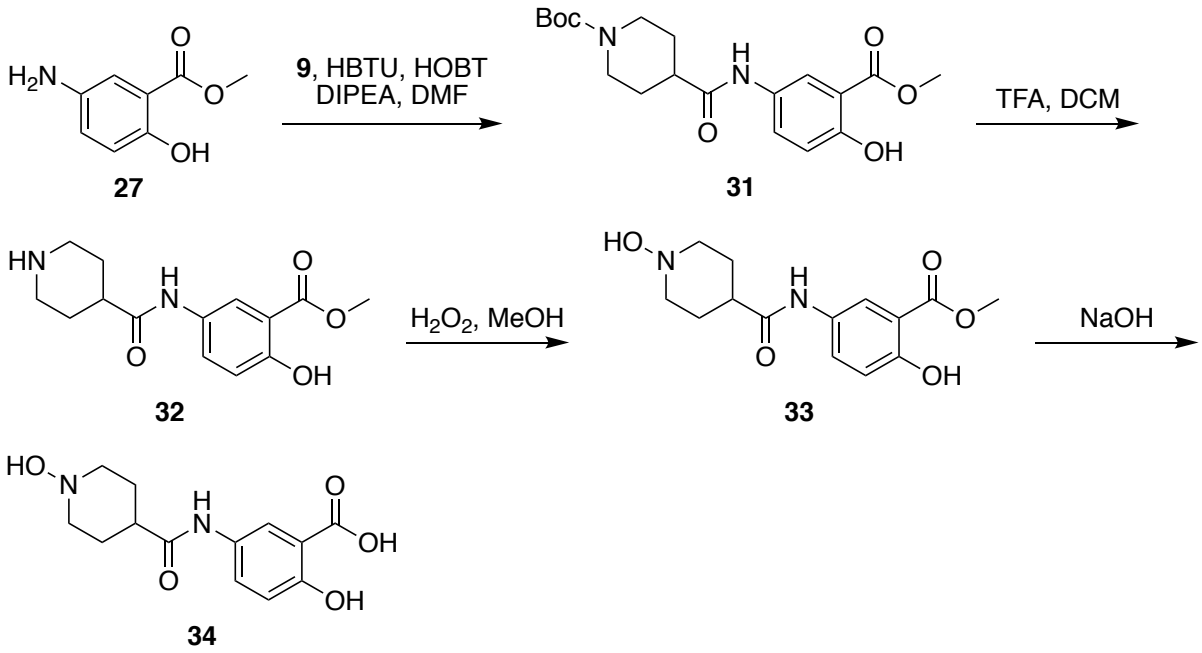

Scheme 7. Synthesis of compound 34.

Compound **27** was coupled to Boc-protected isonipecotic acid (**9**) to give compound **31**. The Boc group was removed (**32**), the piperidine was oxidized (**33**), and the methyl ester was hydrolyzed to afford compound **34**.

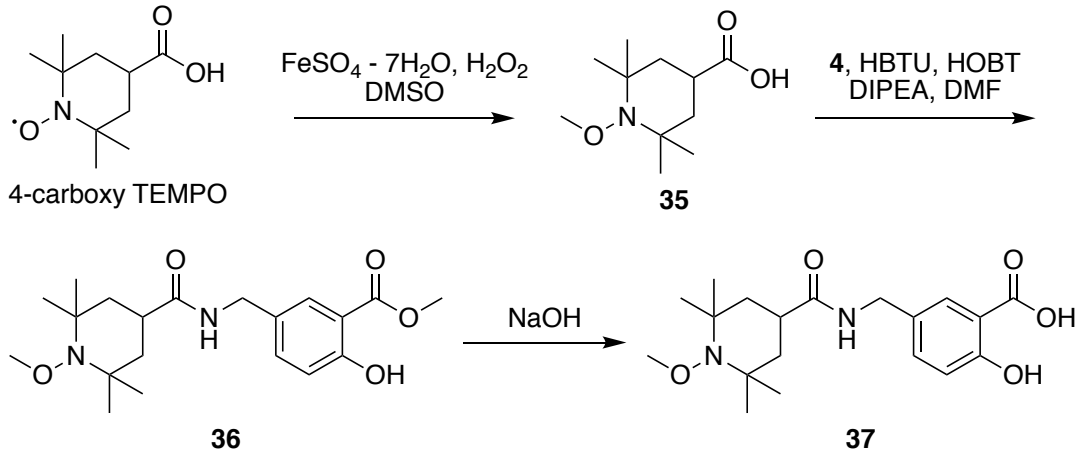

Scheme 8. Synthesis of compound 37.

4-carboxy TEMPO was methylated using DMSO as the methyl donor (**35**). It was then coupled to compound **4** (**36**) and the methyl ester was removed with sodium hydroxide (**37**).

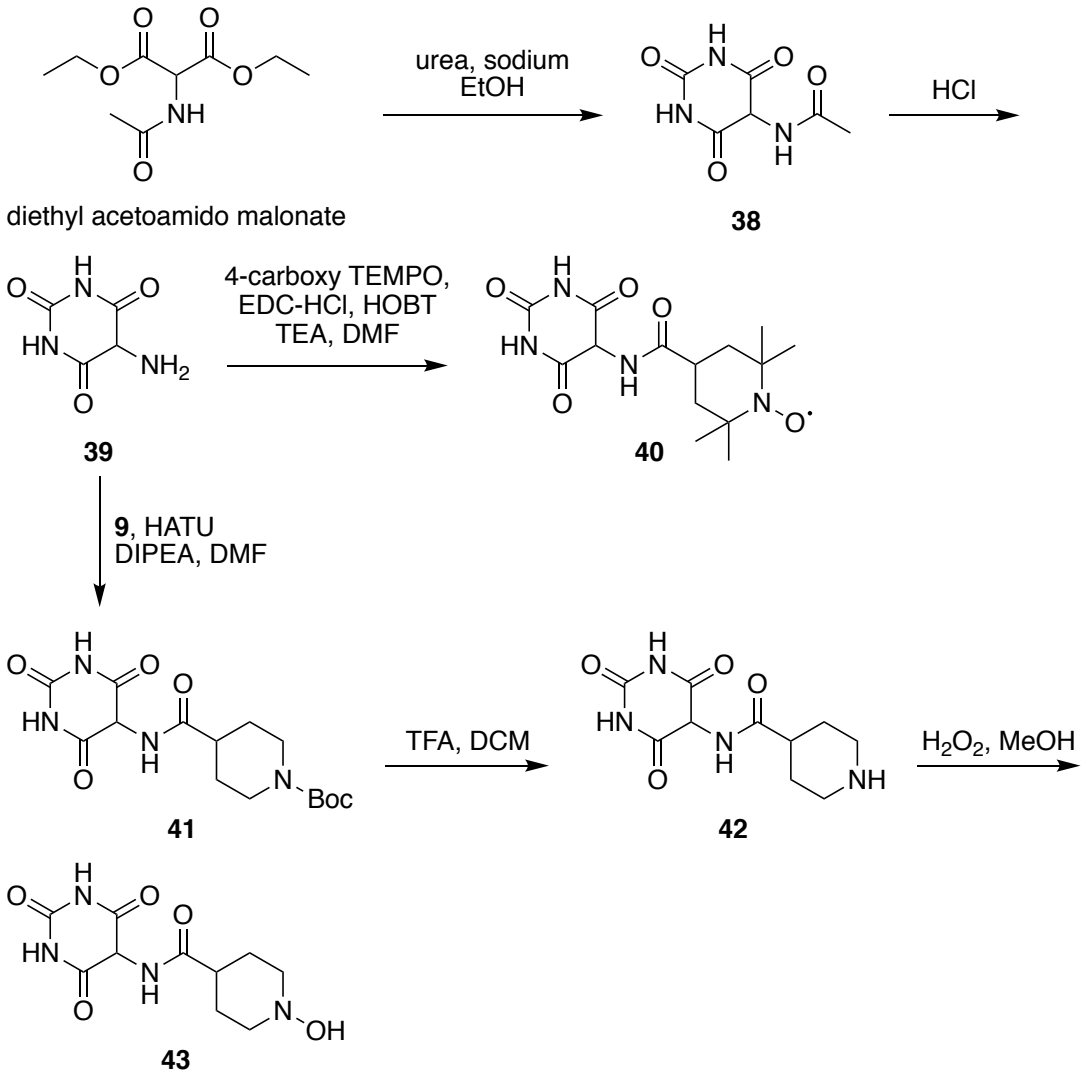

Scheme 9. Scheme to synthesize compounds 40 and 43.

N-acetyl 5-amino barbiturate acid (**38**) was synthesized from diethyl acetamido malonate and urea. The acetyl group was removed under acidic conditions to give compound **39**, which was coupled to 4-carboxy TEMPO to give compound **40**. Compound **39** was also coupled to

compound **9** and removal of the Boc group (**42**), followed by oxidation (**42**), resulted in compound **43**.

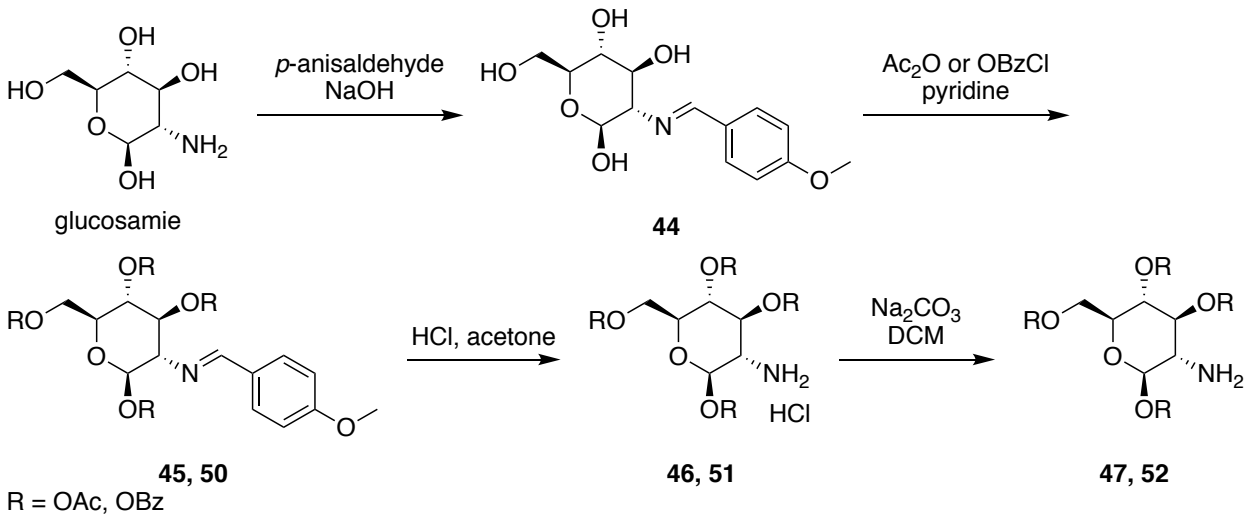

Scheme 10. Protection of glucosamine to make compounds 47 and 52.

Glucosamine was protected using acetyl (**47**) or benzoyl groups (**52**).

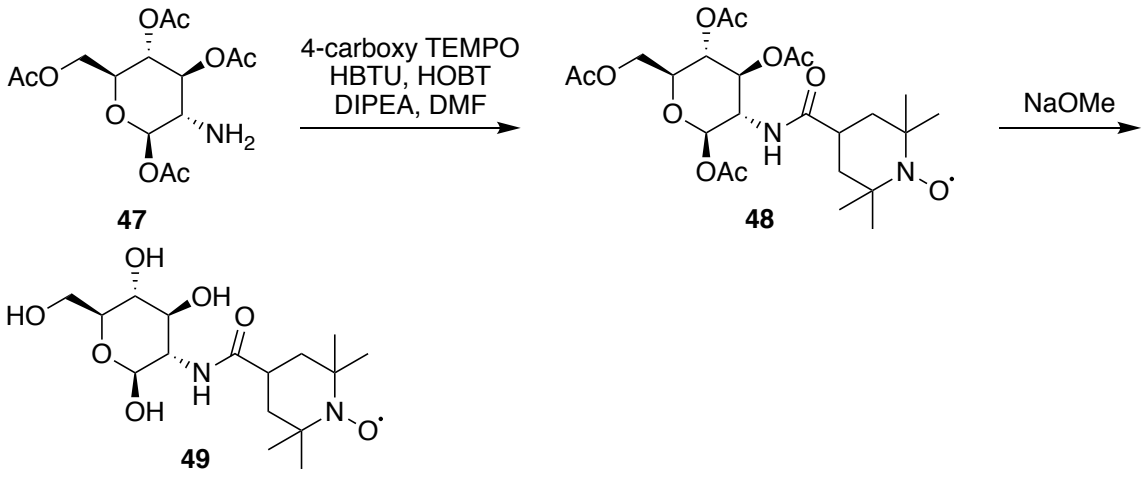

Scheme 11. Synthesis of compound 49.

Compound **47** was coupled to 4-carboxy TEMPO to result in compound **48**. The acetyl groups were removed to give compound **49**.

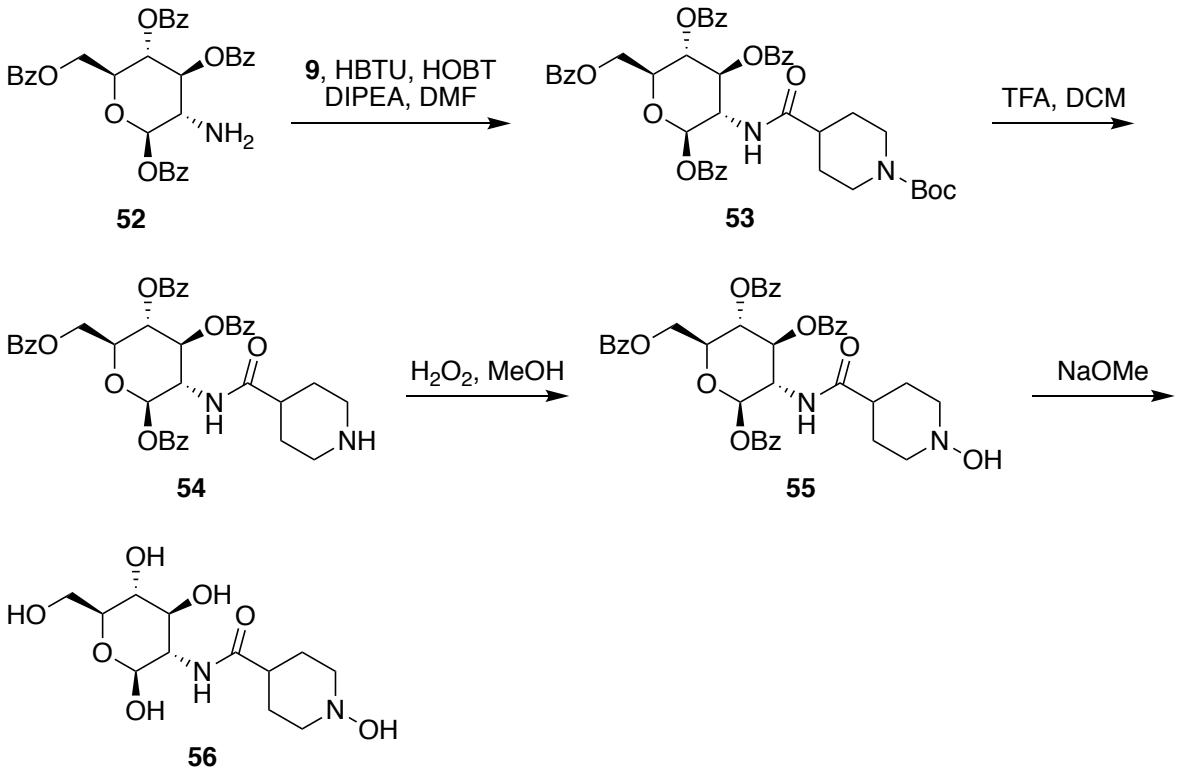

Scheme 12. Synthesis of compound 56.

Compound **52** was coupled to compound **9** to result in compound **53**. Boc deprotection (54) followed by oxidation with hydrogen peroxide gave compound **55**. The acetyl groups were removed to give compound **56**.

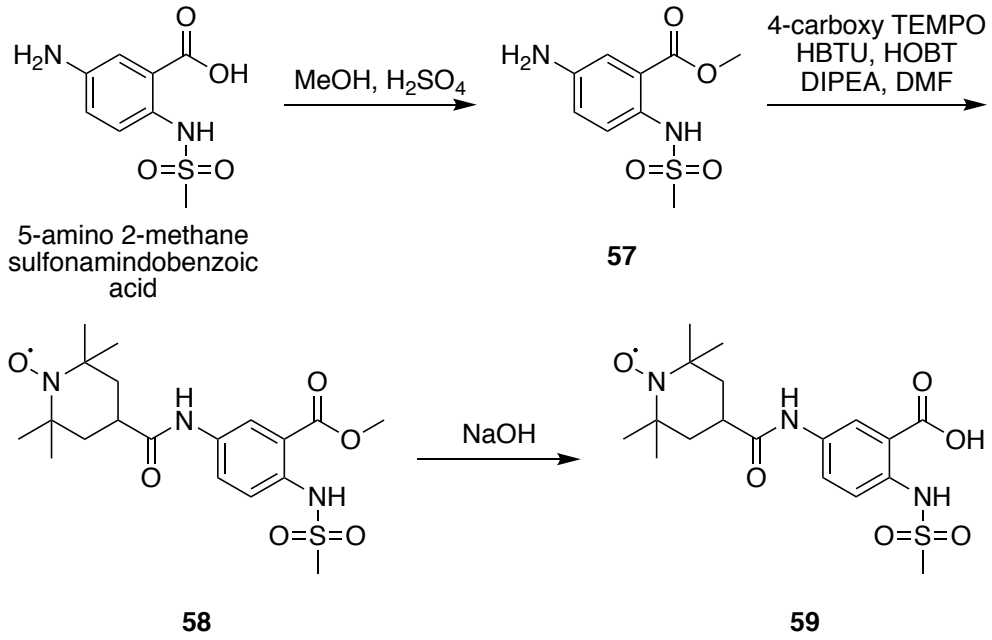

Scheme 13. Synthesis of anthranilate compound 59.

Commercially available 5-amino 2-methane sulfonamidobenzoic acid underwent Fischer esterification to give compound **57**. Compound **57** was coupled to 4-carboxy TEMPO (**58**). The methyl ester of compound **58** was hydrolyzed to give compound **59**.

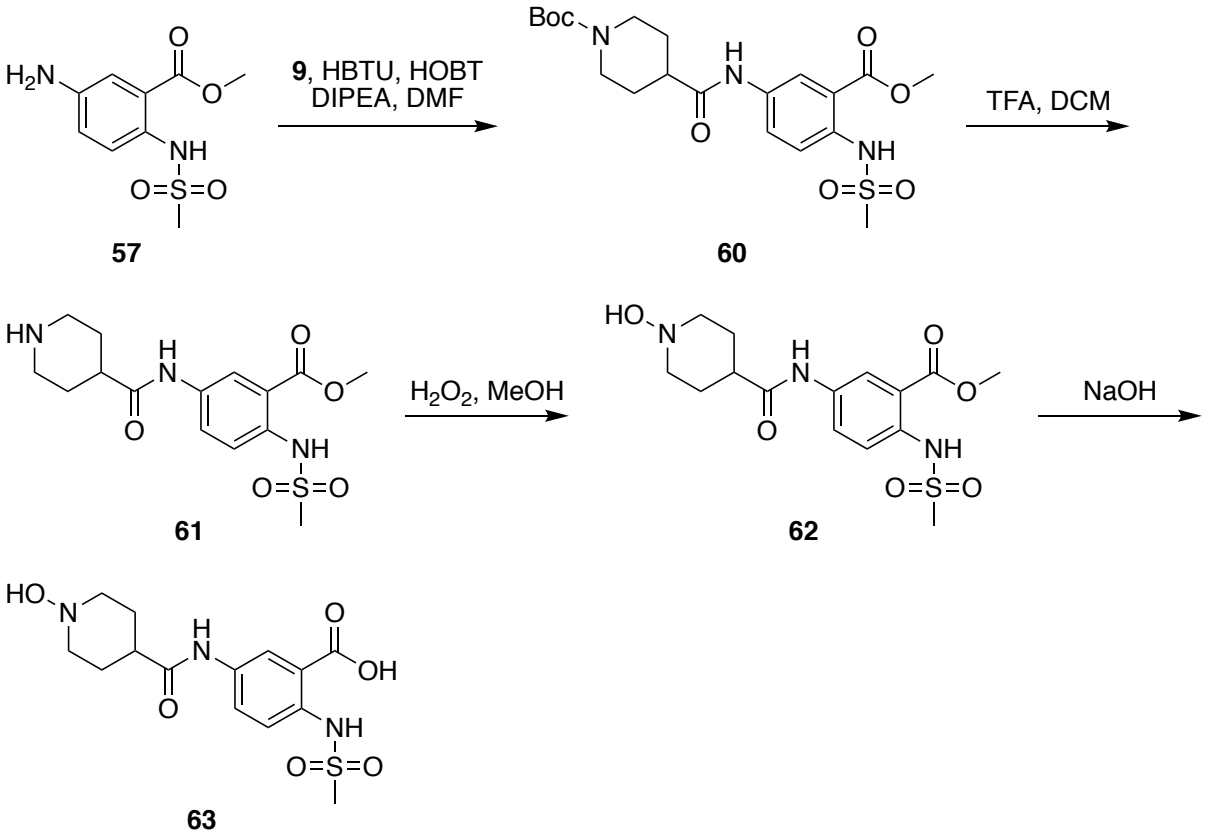

Scheme 14. Synthesis of anthranilate compound 63.

Compound **57** was coupled to compound **9** to give compound **60**. Boc deprotection (**61**), oxidation (**62**), followed by removal of the methyl ester with sodium hydroxide resulted in compound **63**.

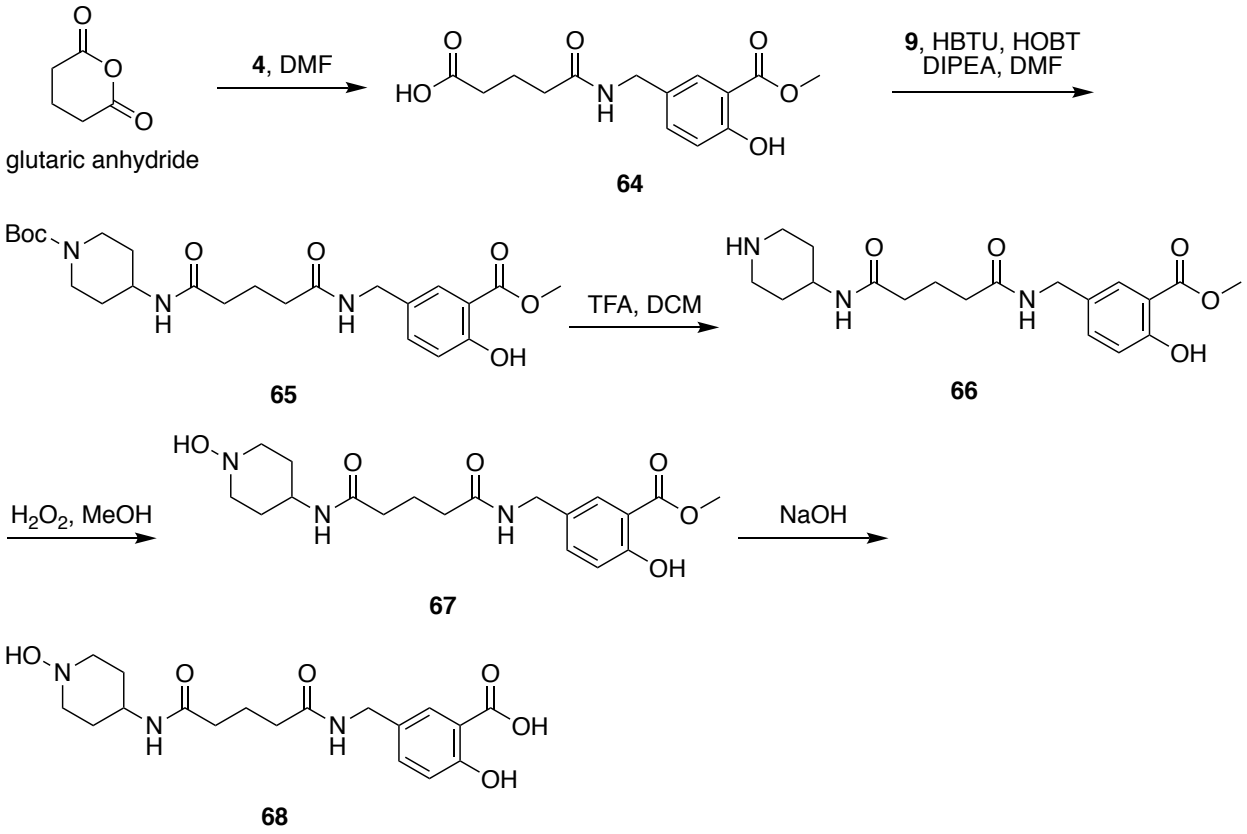

Scheme 15. Synthesis of compound 68.

Glutaric anhydride was mixed with 5-aminomethyl salicylate methyl ester (**4**), to result in compound **64**. Compound **9** was coupled to the newly revealed carboxylic acid. Boc deprotection of compound **65**, followed by oxidation with hydrogen peroxide (**67**) and hydrolysis of the methyl ester resulted in compound **68**.

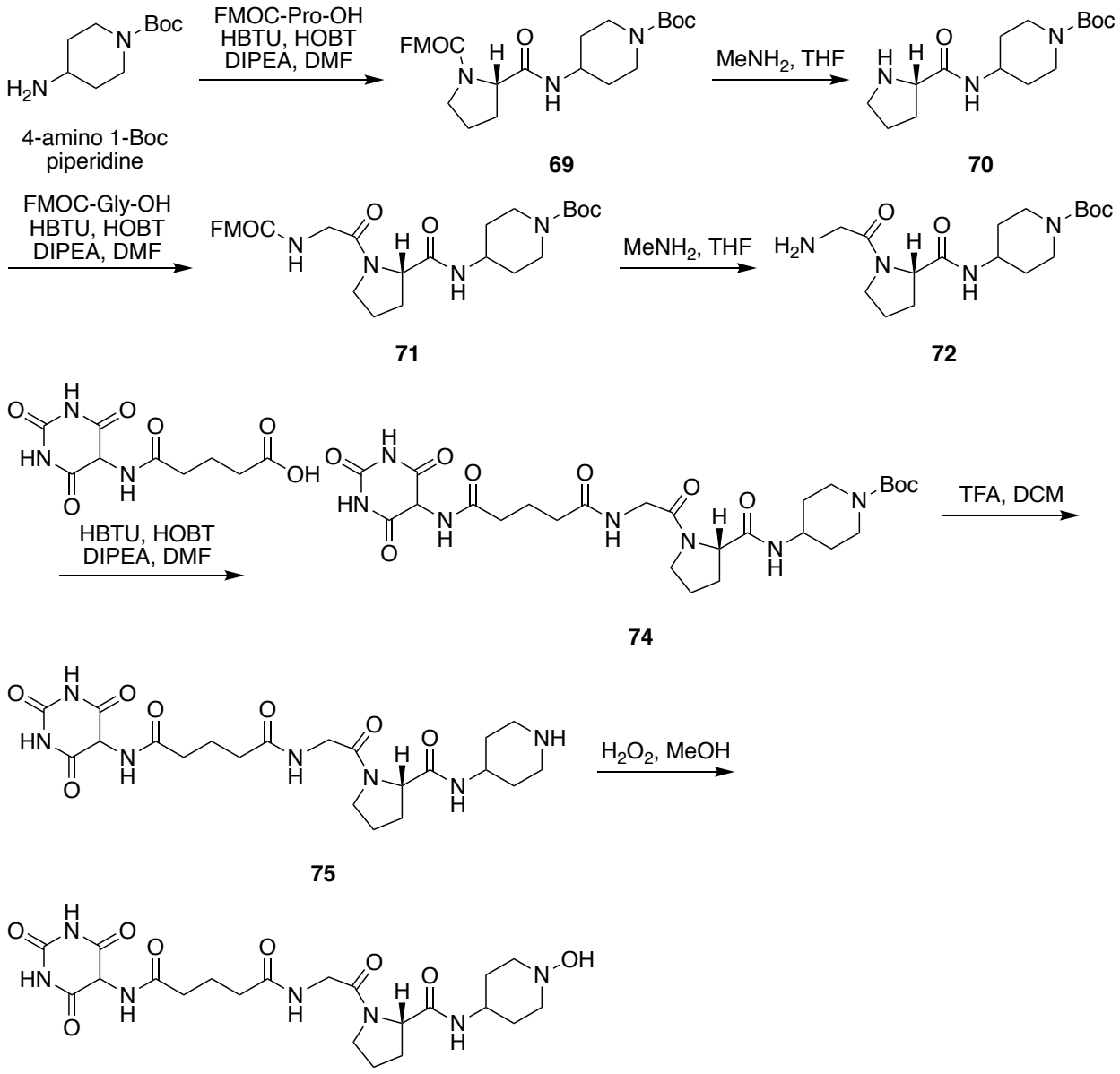

Scheme 16. Synthesis of FAP probe (76).

4-amino 1-Boc piperidine was coupled to FMOC-Pro-OH (**69**). The FMOC group was removed (**70**) to allow the FMOC-Gly-OH to be coupled to the new N-terminus (**71**). A second FMOC deprotection (**72**) allowed barbiturate to be incorporated into the molecule through a short glutarate linker (**74**). Boc deprotection (**75**) followed by oxidation (**76**), resulted in the FAP probe, compound **76**.

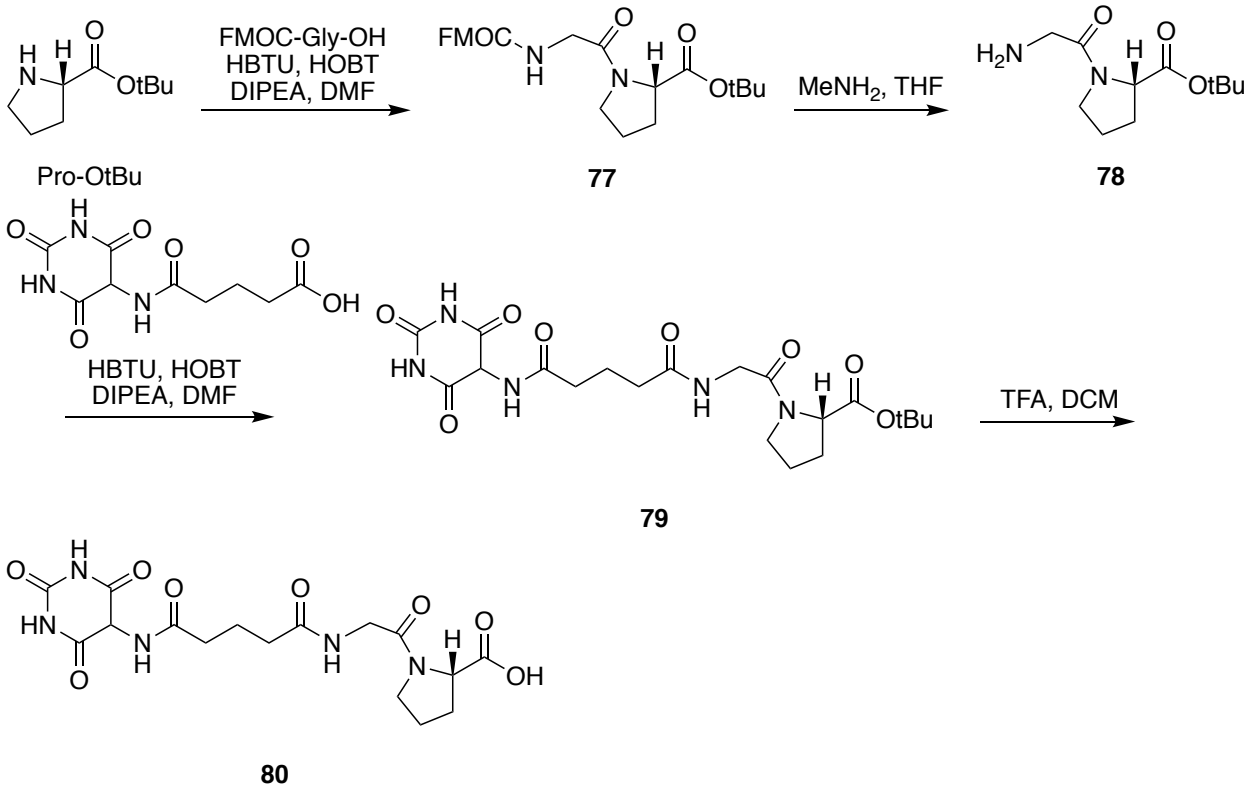

Scheme 17. Synthesis of FAP hydrolysis control (80).

Pro-OtBu was coupled to FMOC-Gly-OH to give a dipeptide (**77**). The FMOC group was removed using methylamine and barbiturate was attached to the molecule using a short glutarate linker. Removal of the t-butyl ester under acidic conditions resulted in compound **80**.

Understanding Structural Requirements for CEST Signal Suppression

Previously Ratnakar *et al* [66] altered the T_1 relaxation time of bulk water protons to modulate the CEST signal of an europium-based PARACEST complex. The probe contained two nitroxyl radical groups that effectively quenched the CEST signal. Inspired by this work, we wanted to investigate whether this same effect held true for metal-free diaCEST compounds. 4-carboxy TEMPO was coupled to 5-aminomethyl salicylic acid (SaliMeTEMPO, compound **7**) (Figure 5A), and a weak CEST signal was observed (less than 1%), supporting the suppression of CEST. This signal reduction is similar to what was observed by the Kovacs Lab from their

Eu-complex containing TEMPO.[66] As previously reported by Ratnakar *et al*, reduction of the nitroxyl radical by sodium ascorbate resulted in the re-appearance of the CEST signal. Interestingly, when the nitroxyl radical of compound **7** was reduced (SaliMeTEMPOH, compound **8**), the measured signal remained less than 1% MTR_{asym}, and no signal restoration was observed. However, methylation of the *N*-oxide (compound **37**) recovers a CEST signal that is similar to the uncoupled salicylic acid ($SaliMeNH_2$, compound **3**). In order to begin to identify the minimal structural unit required to suppress the diaCEST effect, a salicylic acid analog was synthesized comprising of the N-hydroxy piperdine moiety (SaliMeNOH, compound **13**), which also displayed a suppression of the CEST signal to less than 1% MTR_{asym}.

To investigate the CEST-suppressive role of ring structures similar to N-hydroxy piperidine, cyclohexanoic acids, mimicking the piperidine ring, and benzoic acids, a planar model, were coupled to 5-aminomethyl salicylic acid (compounds **20**, **22**, **24** and **26**). These compounds did not show the same signal suppression effect as the N-hydroxy piperidine structure. Acetylation of the amine (SaliMeNHAc, compound **5**) also did not suppress the measured CEST signal. It appears that the N-hydroxy piperidine moiety is the minimal required functional unit inducing the observed CEST signal suppression.

CEST signal suppression was also studied with different connections to the salicylic acid ring (Figure 5B). Similar to 5-aminomethyl salicylic acid, when 5-amino salicylic acid was coupled to 4-carboxy TEMPO (SaliTEMPO, compound **29**), the CEST signal was weak and reduction of the nitroxyl radical (SaliTEMPOH, compound **30**) did not restore the CEST signal. The simplified piperidine ring (compound **34**) maintained CEST signal suppression

functionality. Acetylation of the amine (N-acetyl 5-aminosalicylic acid) did not reduce the CEST signal substantially, where signal suppression was observed only in compounds containing a nitroxyl radical or the N-hydroxy piperidine variant.

In addition to the linkage of the CEST beacon (salicylic acid) to CEST suppressor through amide bonds, the use of an ether bond was also evaluated (Figure 5C). 5-Chloromethyl salicylic acid (SaliMeCl, compound **1**) was alkylated to 4-hydroxy TEMPO to yield compound **17**. As with the previous TEMPO compounds, the measured CEST signal was weak (1% MTR_{asym}). Reduction of the nitroxyl radical (compound **18**) still shows some signal suppression, although observed signal suppression was more limited with the ether linkage than the amide bonded TEMPOH (compounds **8** and **30**). Overall, the signal suppression effect is observed in all three types of bond linkages connecting the signal-generating moiety (salicylic acid) and the signal-suppressing moiety (TEMPO or N-hydroxy piperidine).

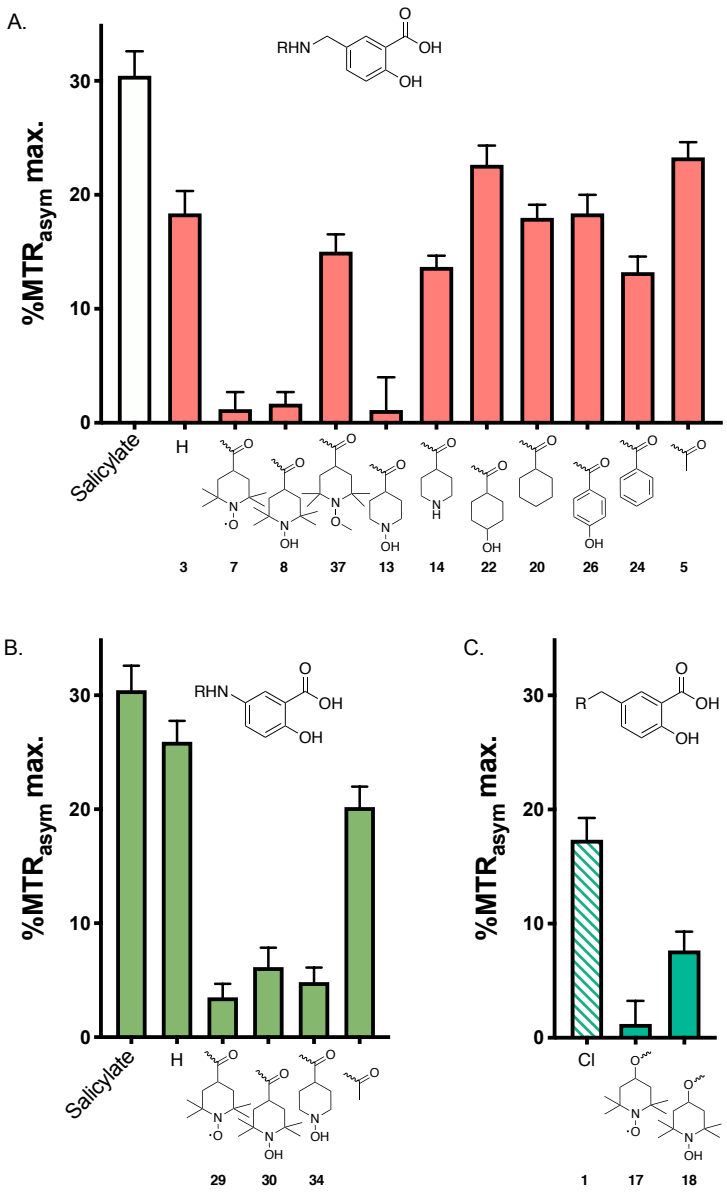

Figure 5. Structure-signal relationship for CEST signal suppression. *The coupling of (A) 5-aminomethyl salicylic acid and (B) 5-amino salicylic acid and alkylation of (C) 5-chloromethyl salicylic acid to TEMPO and N-hydroxy piperidine resulted in a suppresed CEST signal. Reduction of nitroxyl radical to TEMPOH maintains some CEST signal suppression. Methylation to TEMPOMe restores the signal strength to be equivalent to the uncoupled salicylic acid. Additional cyclohexyl and benzyl rings indicated in the plots were evaluated, but do not show the same signal suppression effect. The CEST signals were acquired on a 300 MHz NMR spectrometer at 37°C. The samples were prepared as 20 mM solutions in 1:1 PBS:D_2O and adjusted to pH 6.95-7.05. Error bars represent uncertainty of fitting the Laurenztian curves to the Z-spectrum.*

Linker Effects on the diaCEST Signal

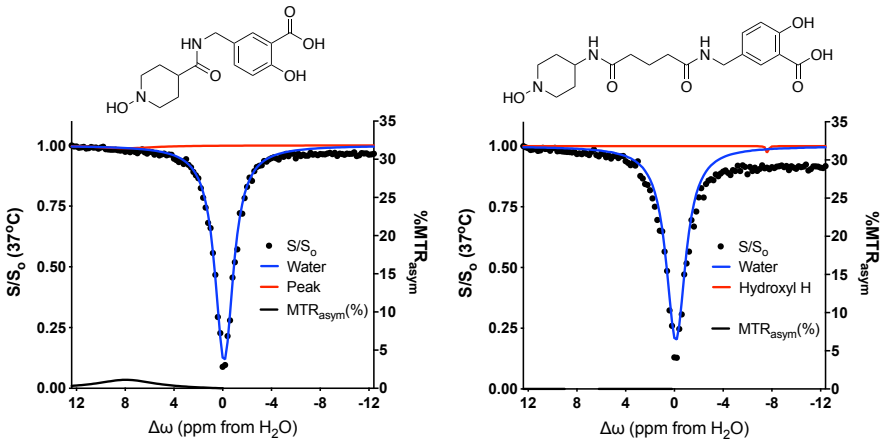

Figure 6. Increased spacing between salicylic acid and N-hydroxy piperidine maintains CEST signal suppression effect. *Compounds 13 and 68 were prepared as 20 mM samples in 1:1 PBS:D_2O and adjusted to pH 6.95-7.05. The CEST spectra were acquired on a 300 MHz NMR spectrometer at 37°C. The addition of a glutarate linker does not seem to change the CEST signal and in both cases, the CEST signal was measured to be less than 1%.*

Next, we wanted to study further structural requirements between the signal-generating moiety and signal-suppressing moiety. A short glutarate linker was incorporated between 5-aminomethyl salicylic acid and N-hydroxy piperidine. Increasing the spacing between salicylic acid and N-hydroxy piperidine did not appear to affect CEST signal suppression (Figure 6). When N-hydroxy piperidine was directly coupled to 5-aminomethyl salicylic acid (compound **13**), the CEST signal was less than 1% MTR_{asym}. Importantly, the introduction of a glutarate linker adds length and flexibility, and maintains the signal suppression effect. The addition of the linker allows for more variability in length and structure between the signal-generating moiety and signal-suppressing moiety, permissive of the development of activity-based sensing probes for diaCEST MRI using the signal suppression moiety we have described.

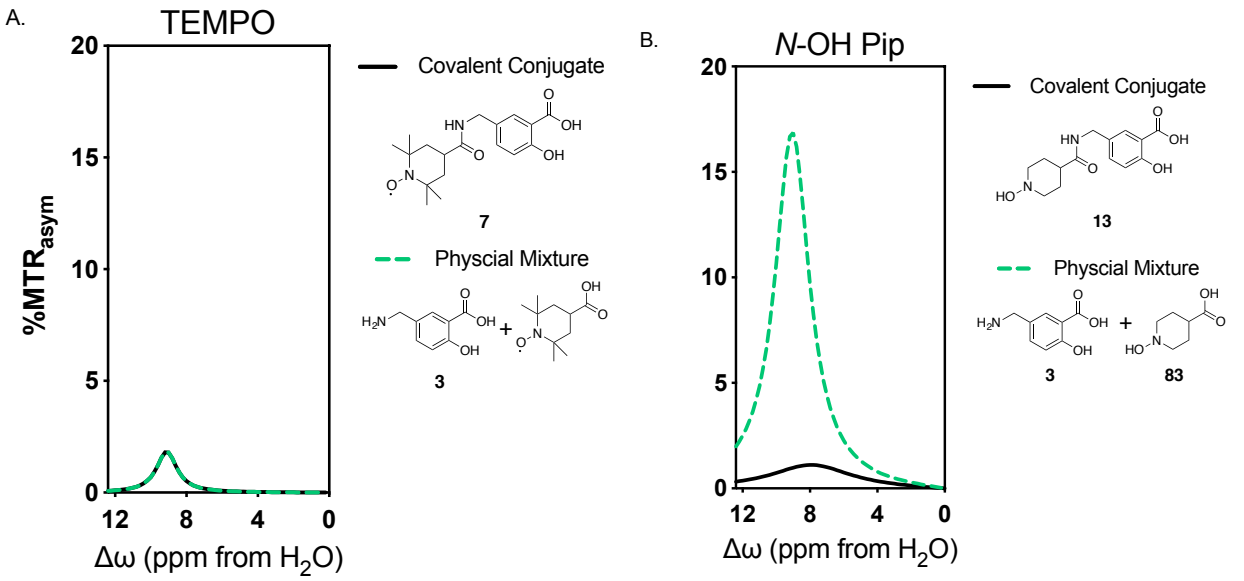

Figure 7. CEST signal suppression by N-hydroxy piperidine requires covalent conjugation. *The following samples were prepared in 1:1 PBS:D_2O at 20mM: compound **7**, compounds **3** + 4-carboxy TEMPO, compound **13**, and compounds **3** + **83**. The CEST spectra were acquired using a 300 MHz NMR spectrometer at 37°C. In the case of the TEMPO-containing samples (A), the CEST signal was the same for both when the compound was joined by a covalent bond, and when the salicylic acid and TEMPO were separated. With the N-hydroxy piperidine (B), the signal of the physical mixture is about 17% CEST MTR_{asym}, similar to the CEST signal of 5-aminomethyl salicylic acid. The covalent conjugate sample has a reduced signal, less than 1% CEST MTR_{asym}.*

In order to investigate the design parameters for CEST suppression, the requirement for direct linkage for the signal-suppression moiety was evaluated. An intramolecular mechanism would require the signal-generating moiety and signal-suppressing moiety to be in close proximity. To further understand the structural requirements, the measured CEST signal from the presence of the signal-suppression moiety was compared for a covalent mixture and physical mixture. In the covalent mixture, a signal-generating moiety and signal-suppression moiety (TEMPO or N-hydroxy piperdine) were joined together through an amide bond. In the physical mixture, the two compounds are separated and mixed together in the NMR sample tube. In the presence of the nitroxyl radical from TEMPO (Figure 7A), both the covalent conjugate and physical mixture have a decreased CEST signal. When looking at the N-hydroxy piperidine, only

the covalent conjugate has a suppressed CEST signal. The physical mixture of 5-aminomethyl salicylic acid (compound **3**) and N-hydroxy piperidine (compound **83**) resulted in a measured CEST signal of 17% MTR_{asym}, which was similar to that of compound **3** on its own (Figure 7B). From this experiment, it appears that a covalent bond is required for CEST signal suppression only when the quencher moiety is the N-hydroxy piperidine. This functional group has the potential to be applied to the development of a broad set of activity-based sensing probes for CEST-MRI, where cleavage of the covalent bond and removal of the signal-suppressing moiety is necessary to restore the CEST signal.

While both TEMPO and N-hydroxy piperidine show comparable signal suppression effects, only the N-hydroxy piperidine-mediated signal suppression can be reversed by cleavage of the covalent bond. Previous studies using EPR have shown the progressive loss of the nitroxyl radical from TEMPO upon its incubation with cells.[118] In order to study the stability of the two signal suppression moieties in standard biochemical environments, we incubated each of the signal-suppressor compounds in serum, and in PBS supplemented with 4 mM of sodium ascorbate, a standard screening test for studying nitroxyl stability.[118,119] Typically, the rate of reduction correlates to the *in vivo* half-life of the nitroxyl. Previous studies have shown almost complete reduction of the nitroxyl within one hour at room temperature when looking at the relative EPR peak height.[119] With these standard methods, the stability of TEMPO was studied by following the EPR signal amplitude of the nitroxyl radical over time. The paramagnetic nature of the TEMPO radical prevents the compound from being characterized by traditional NMR spectroscopy, however the stability of N-hydroxy piperidine was able to be monitored by ^{1}H-NMR.

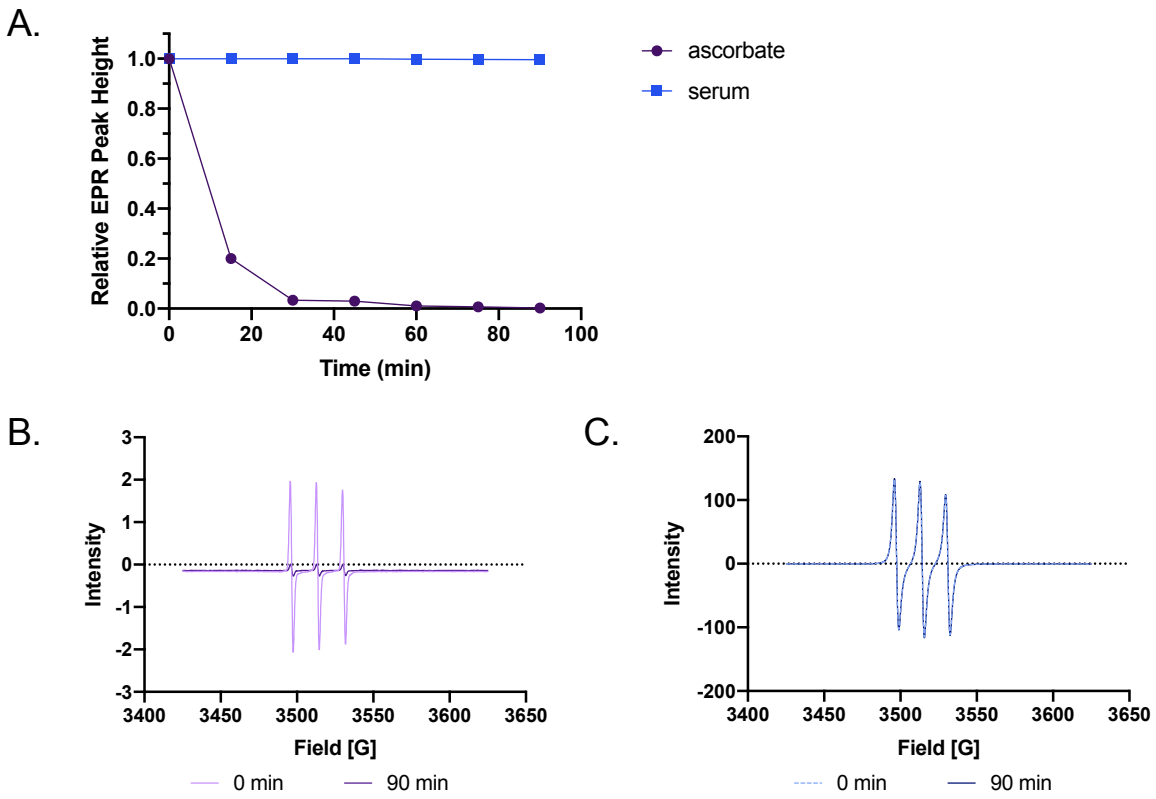

Figure 8. Relative EPR peak signal from nitroxyl radical of TEMPO in mouse serum and ascorbate over time. *TEMPO was prepared as a 5 mM solution in a buffer of 4 mM sodium ascorbate in PBS at pH 7.4, or mouse serum for 2 hours at room temperature (A). After 2 hours, signal intensity in mouse serum is equal to the initial signal intensity. In the ascorbate buffer, the signal intensity rapidly decreases after 15 minutes and the low signal is maintained over 90 minutes. When comparing the EPR spectra at 0 minutes versus, 90 minutes, the signal intensity decreases in ascorbate buffer (B), but the intensity and pattern is consistent in mouse serum (C).*

Incubation of 4-carboxy TEMPO in mouse serum (Figure 8A and C) did not show a change in the signal pattern or amplitude over 2 hours at room temperature. When 4-carboxy TEMPO was incubated in a buffer containing PBS and ascorbate (Figure 8A and B), as described by Paletta et al[119], the signal amplitude of the characteristic triplet pattern was greatly reduced after 15 min and remained reduced for the duration of the 90 minute assay. While TEMPO appears stable in mouse serum, the nitroxyl is not stable in the ascorbate buffer, confirming literature results that TEMPO may have a short *in vivo* half-life.[119]

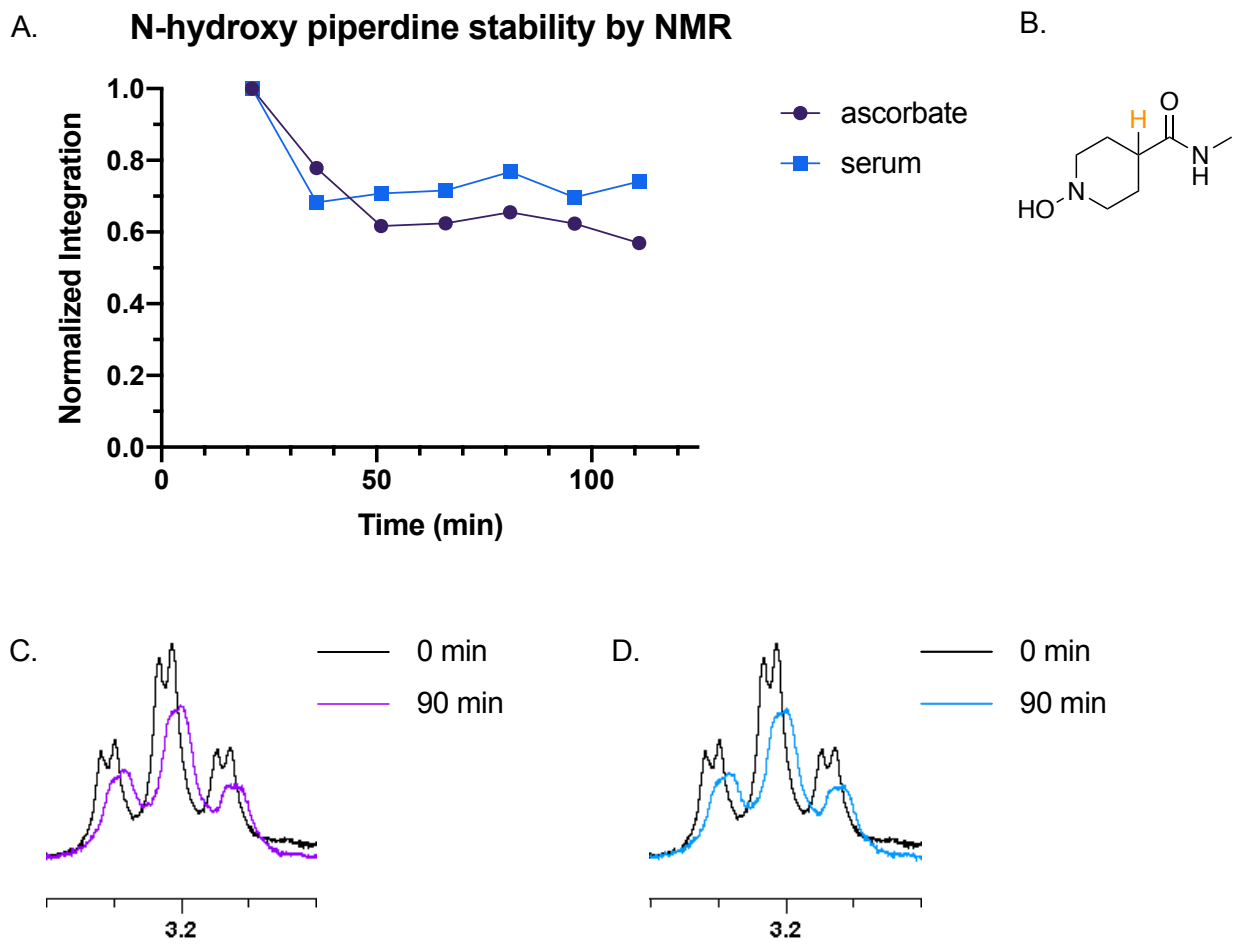

Figure 9. N-hydroxy piperidine (83) appears stable by NMR in mouse serum and ascorbate buffer. *N-hydroxy piperidine was incubated in mouse serum or PBS containing 4 mM sodium ascorbate at pH 7.4 for 2 hours at room temperature. NMR scans were acquired on a 300 MHz NMR spectrometer at 20 minute intervals. The normalized NMR signal from N-hydroxy piperidine in mouse serum and ascorbate buffer shows stability of the compound over time (A). The ^{1}H at the C4 position of the piperidine ring was used to monitor the stability (B). NMR spectra from 0 minutes and 90 minutes in ascorbate (C) and mouse serum (D) show similar coupling pattern and height after 90 minutes.*

N-hydroxy piperidine (**83**) was similarly prepared in mouse serum and ascorbate buffer. ^{1}H-NMR scans were acquired using a 300 MHz NMR spectrometer every 20 minutes while the sample was incubated at room temperature over 2 hours. The integration value of the proton at the C4 position was normalized to the initial time point and plotted over the incubation time (Figure 9). In both the serum and buffer, the integration signal for N-hydroxy piperidine is more stable than that observed for TEMPO, remaining above 60% after 2 h incubation. This suggests

that the N-hydroxy piperidine may be the preferred signal suppression moiety, due to its greater stability in *in vivo*-like conditions. However, in both the serum and buffer samples, there is a both a peak shift and broadening effect. This may be due to changes in the relaxation of the compound, which is further investigated later with T_1- and T_2-weighted scans. Previously, Rabenstein *et al* have reported that hydroxylamine can be responsible for decreasing the relaxation[120] and this can be responsible for the observed broadening in the stability scans. This, along with its activatable and reversible signal suppression effect, makes it an ideal signal suppression moiety for *in vivo* imaging.

Applying CEST Signal Suppression Across diaCEST Agents

In addition to salicylic acid, there are several classes of well-known and frequently used diaCEST agents (Figure 10). Barbiturates were among the first known diaCEST-active compounds.[53] Anthranilates are another class of often studied diaCEST agents,[42,121] with a structure similar to salicylates and signalling mechanism based on intramolecular hydrogen bonding of the exchangeable proton. Carbohydrates, glucose in particular, are often used in *in vivo* applications due to the abundance of glucose found in the body, specifically in the brain.[122–124] Similar amide coupling strategies as used for aminomethyl salicylate were applied to couple 4-carboxy TEMPO and N-hydroxy piperidine to anthranilates, barbiturates and glucosamine (compounds **7, 13, 40, 43, 49, 56, 59,** and **63**). Across all classes, both TEMPO and N-hydroxy piperidine effectively suppressed the CEST signal of the diaCEST agents. The signal suppression observed for salicylate has been demonstrated to be generally applicable to other classes of diaCEST agents in dependent of their proton chemical shift. Since each class of diaCEST agent has a different exchangeable CEST proton, the chemical shift of the CEST signal is also different. Using a combination of multiple diaCEST agents, we can take advantage of the

different chemical shifts for multi-target imaging, each with a different CEST-encoded "colour". Interestingly, when coupled to N-hydroxy piperidine, a common broad peak around 8 ppm away from water appears in all 4 diaCEST classes.

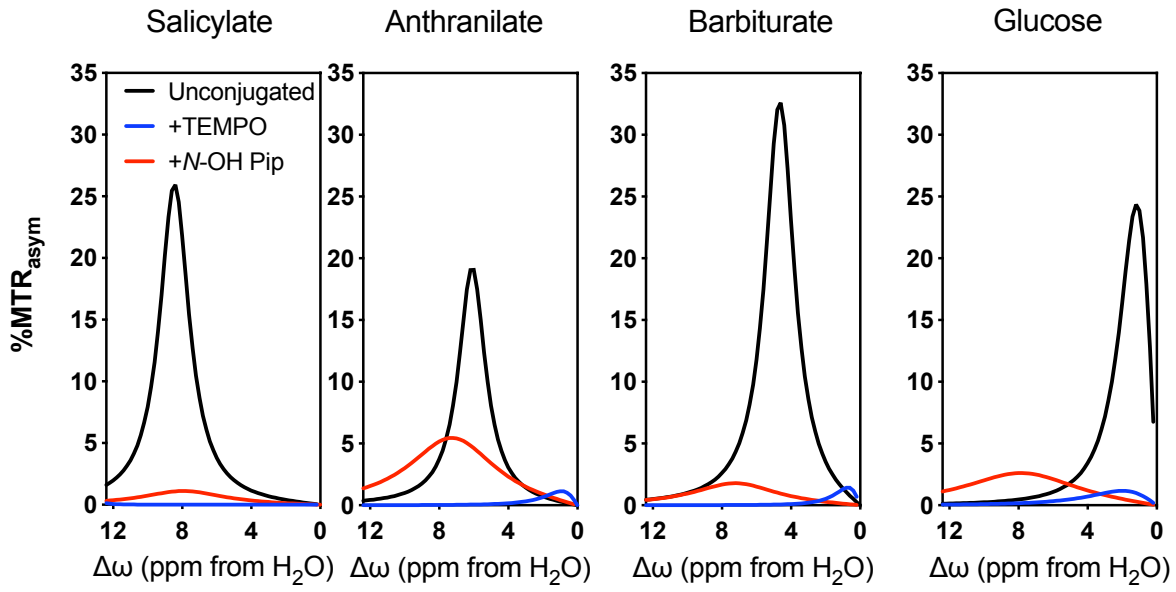

Figure 10. CEST signal suppression by N-hydroxy piperidine and TEMPO observed across several classes of diaCEST agents. *5-aminomethyl salicylate, 5-amino-2-methanesulfoamido benzoic acid, 5-amino barbiturate and glucosamine were coupled to 4-carboxy TEMPO or 4-carboxy N-hydroxy piperidine. The compounds were prepared in solutions of 1:1 PBS:D_2O at 20 mM and the CEST spectra were acquired using a 300 MHz NMR spectrometer at 37°C. The Z-spectra from 12-0 ppm of each diaCEST class is overlayed in the panels above. In all cases, coupling to TEMPO or N-hydroxy piperidine reduces the CEST signal to less than 5% MTR_{asym}.*

Elucidating the Mechanism of CEST Signal Suppression

To further understand the mechanism and investigate the potential of intramolecular interactions, CEST signal production from 5-amino salicylic acid and compound **34** were studied at different concentrations (Figure 11). Our hypothesis was that if signal suppression was through an intramolecular mechanism, then the concentration should be independent of the signal suppression effect. As a control, 5-amino salicylic acid was prepared as a 20 mM, 10 mM and 5 mM solution in PBS/D_2O at pH 7.0. The measured CEST signal decreases as the concentration of the compound decreases, as expected. In the case of the compound coupled to

the signal-suppression moiety (compound **34**), the CEST signal is suppressed at all concentrations, 20 mM, 10 mM and 5 mM. The observed CEST signal suppression is independent of concentration and suggests an intramolecular mechanism.

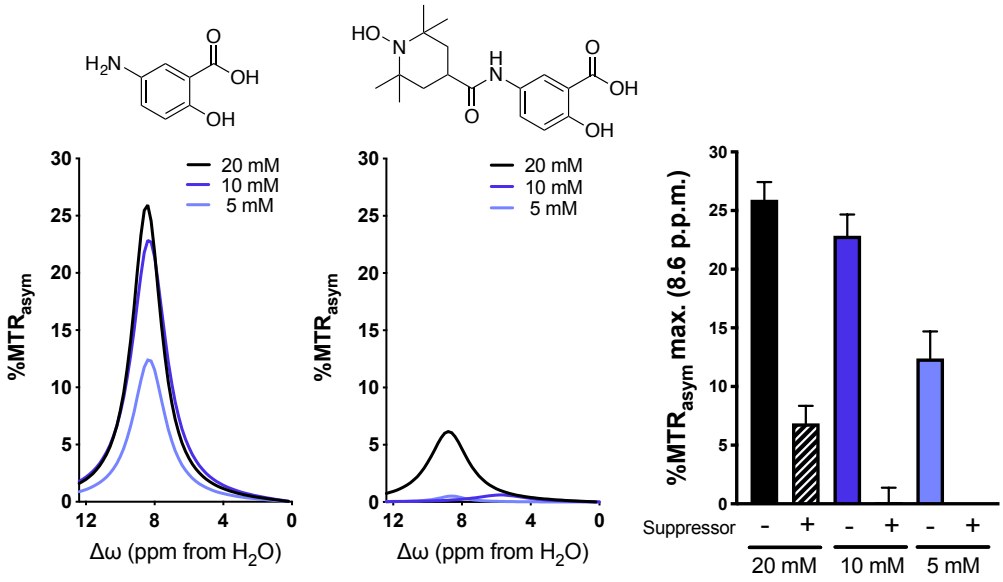

Figure 11. CEST signal suppression by N-hydroxy piperidine is independent of concentration. *Samples of 5-amino salicylic acid and 4-carboxy TEMPOH coupled to 5-aminomethyl salicylic acid were prepared in a 1:1 PBS:D_2O solution, adjusted to pH 6.95-7.05 at 20 mM, 10 mM and 5 mM. The CEST spectra were measured using a 300 MHz NMR spectrometer at 37°C. The CEST signal of 5-amino salicylic acid decreases as the concentration decreases. For the TEMPOH-coupled compound, the signal is less than 1% at 10 mM and 5 mM. The CEST signal is also compared at 20 mM, 10 mM and 5 mM in the presence and absence of the N-OH from TEMPOH. Error bars represent uncertainty of fitting the Laurenztian curves to the Z-spectrum*

Ratnakar *et al* synthesized a europium-based complex that suppresses the PARACEST signal by shortening the T_1 of bulk water mediated by the nitroxyl radical on TEMPO.[66] We have observed similar CEST signal suppression with the non-radical N-hydroxy piperidine in addition to the radical-mediated mechanism. To verify the absence of a radical, EPR spectra of the signal-suppression moieties were acquired (Figure 12). A strong EPR signal was observed from 4-carboxy TEMPO (Figure 12A) as expected. Upon reduction of the radical to the hydroxylamine (compound **81**, Figure 12B), a weak EPR signal was observed with the triplet pattern. The

methylated TEMPO (compound **35**, Figure 12C) and N-hydroxy piperidine (compound **83**, Figure 12D) also do not have an EPR signal, suggesting that these are diamagnetic species. Therefore, the signal suppression effect observed by N-hydroxy piperidine may follow a non-paramagnetic mechanism, different to that of TEMPO. The hydroxylamine of N-hydroxy piperidine has been reported to decrease the relaxation of exchanging protons[120] and this could be the underlying mechanism to CEST signal suppression.

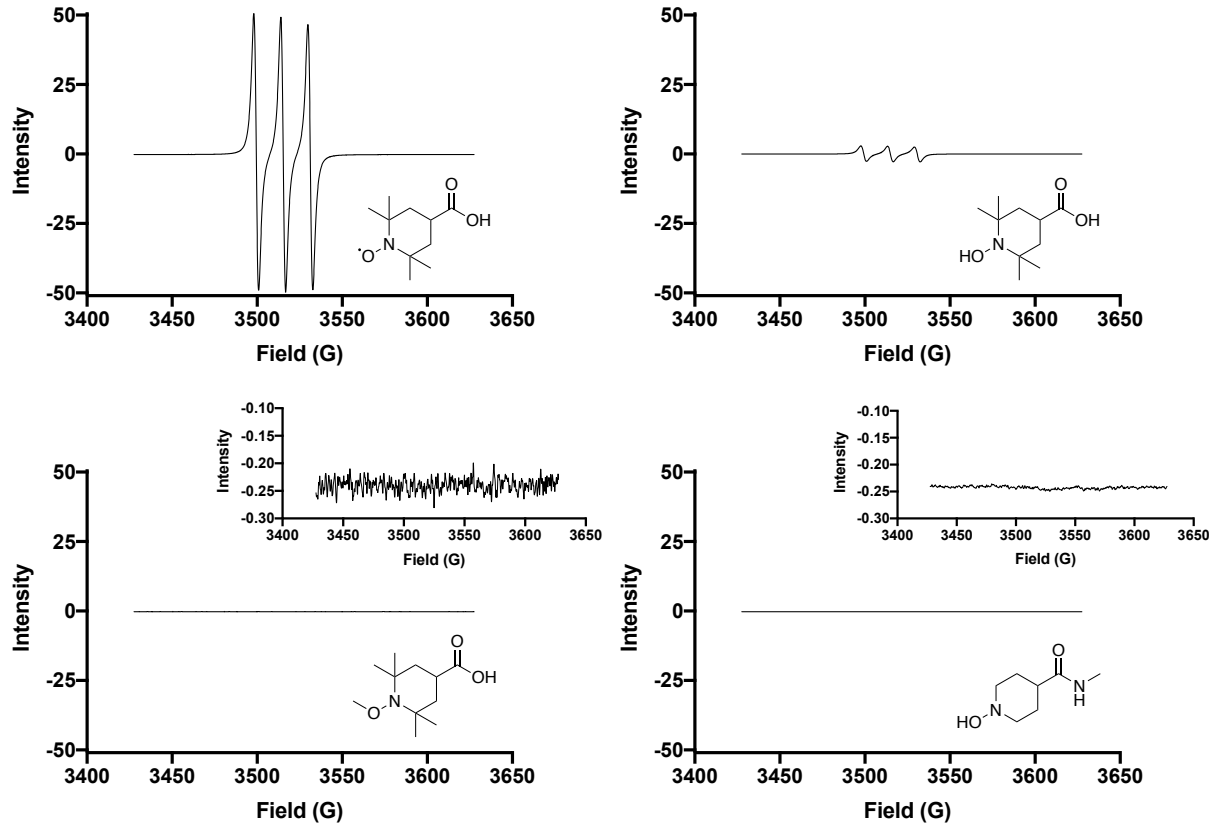

Figure 12. EPR spectra of TEMPO and piperidine-related compounds. *The compounds above were prepared in a solution of PBS and adjusted to pH 6.95-7.05. The EPR spectra were acquired using an EPR spectrometer, tuned according to the sample in PBS buffer. A total of 5 scans were acquired and the sample was maintained at room temperature for the duration of the scans. Only the 4-carboxy TEMPO compound displayed an EPR signal.*

Signal broadening was observed from the NMR stability assay in mouse serum and ascorbate buffer that may have suggested a relaxation effect. From the EPR data, it appears that this relaxation is not paramagnetic in nature for N-hydroxy piperidine. The diamagnetic *versus*

paramagnetic character of the putative signal suppressor moieties was further assessed by MRI in order to provide a full assessment of their T_1 contributions. T_1- and T_2-weighted images of 4-carboxy TEMPO and compounds **35**, **81** and **83** were acquired at 3T, (Figure 13) and the transverse relaxivity (r_1) was measured (Figure 14). The TEMPO compound containing a stable-radical showed a strong T_1-shortening effect (r_1 = 2.27 $mM^{-1}s^{-1}$) as reported[125], almost comparable to Gadovist, a gadolinium chelate use clinically. In contrast, but surprisingly, the N-hydroxy (**83**) (r_1 = 1.42 $mM^{-1}s^{-1}$) and TEMPOH (**81**) (r_1 = 1.53 $mM^{-1}s^{-1}$) compounds displayed mild T_1-shortening effect even though no paramagnetism was detected by EPR. This may elude to a signal suppression mechanism through non-radical, weak T_1-shortening interactions. Importantly, TEMPOMe (**35**) showed no T_1 shortening effect, which may rationalize the inability of this moiety to suppress CEST signal generation. None of the compounds showed detectable T_2 effects.

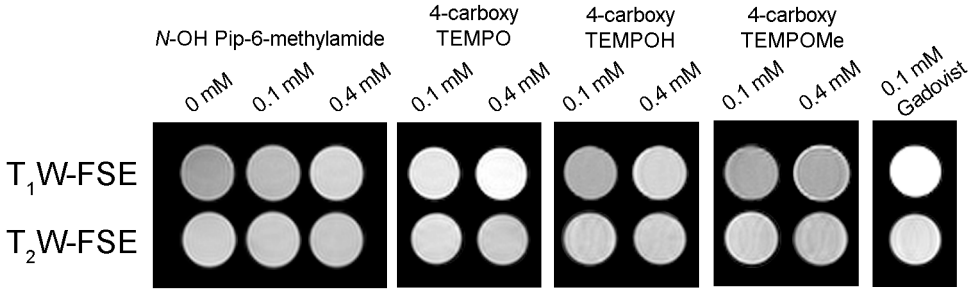

Figure 13. T_1-weighted and T_2-weighted images of compounds 35, 81, 83 and 4-carboxy TEMPO with mild T_1 shortening effect from N-hydroxy piperidine. *4-carboxy TEMPO and compounds 35, 81 and 83 were prepared as 0.4 mM and 0.1 mM solutions in PBS buffer, adjusted to pH 6.95-7.05. Images were acquired at 3T using a fast spin echo (T1) or gradient echo (T2) pulse sequence. Strong T_1 effect is observed from 4-carboxy TEMPO and a weaker effect from N-hydroxy piperidine and 4-carboxy TEMPOH. The 4-carboxy TEMPOMe compound does not show much T_1 brightening, as expected. No T_2 effect was observed from any of the compounds.*

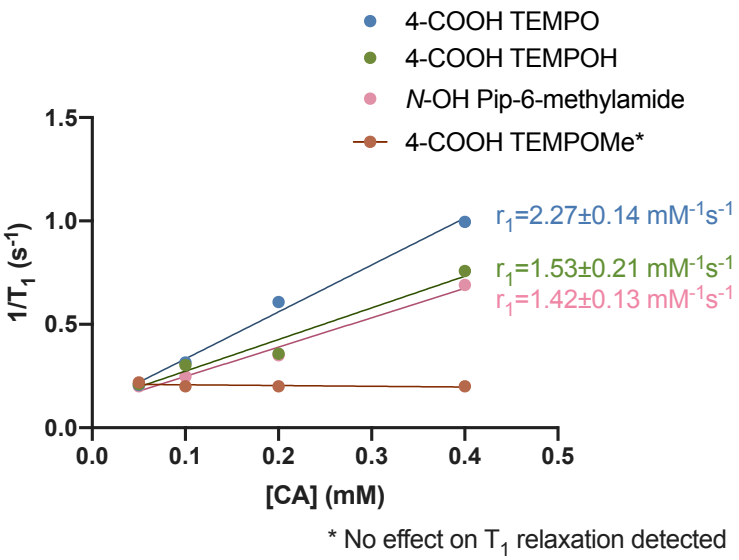

Figure 14. Quantitation of transverse relaxivity (r_1) for CEST suppression moieties. *4-carboxy TEMPO and compounds 35, 81 and 83 were prepared as solutions in PBS buffer, adjusted to pH 6.95-7.05. Strong T_1 relaxation was observed from 4-carboxy TEMPO. Weaker T_1 relaxation was measured for 4-carboxy TEMPOH and N-hydroxy piperidine, where there is also a more moderate suppression of the CEST signal. No T_1 relaxation was observed for 4-carboxy TEMPOMe.*

Enzyme Assay for Studying FAP Activity

In order to apply the signal suppression effect to a real probe, we incorporated the signal generating moiety and signal suppression moiety into a substrate recognized by enzymes with hydrolytic activity. Fibroblast activator protein α (FAP) is a serine protease that can be excreted into the plasma. The expression of FAP is associated with epithelial cancer-associated fibroblasts.[97,126] In studying the activity of FAP, we can understand more about the growth of a tumour, its metastasis and extracellular matrix remodelling.

Since FAP is a proline-specific enzyme and can cleave following a proline residue,[127] we have designed a probe containing the signal generating moiety and signal suppressing moiety separated by a short glycine-proline linker used for commercially available fluorescent probes for FAP. FAP can recognize the Gly-Pro site and through endopeptidase activity, the signal

suppressing moiety is cleaved from the signal generating moiety. Upon separation of these two groups, we expected to see an increase in the CEST-MRI signal (Figure 15).

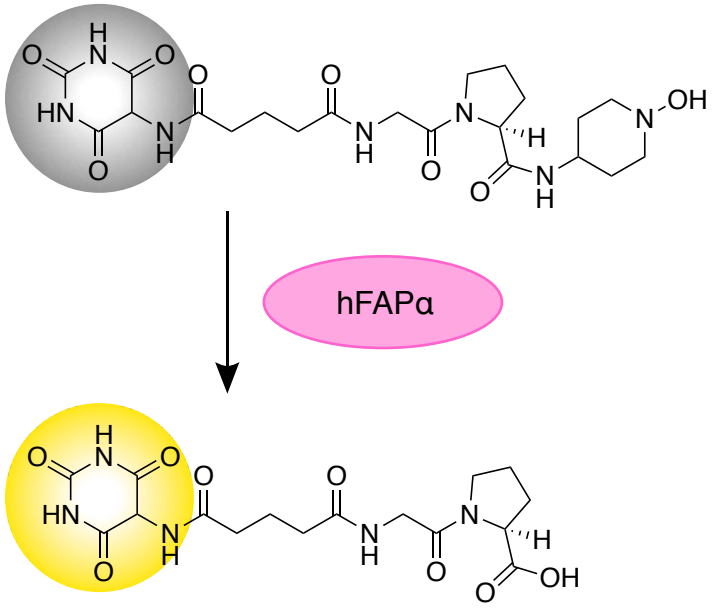

Figure 15. Schematic of CEST signal turn on by hFAP. *The CEST signal of the intact probe is suppressed. hFAP cleaves following the proline, to release 4-amino N-hydroxy piperdine and the remainder of the probe containing barbiturate. The released probe has its CEST signal restored and can be measured.*

Initially, FAP assay conditions were verified using the known fluorogenic peptide substrate, Gly-Pro-AMC.[128,129] The assay buffer and procedure was adapted from the manufacturer, BioLegend. Briefly, human FAP (hFAP) and the substrate, Gly-Pro-AMC, were loaded onto a 96-well plate and the fluorescence increase was measured using a plate reader with exaction at 380 nm and emission at 460 nm (Figure 16). An increase in fluorescence indicates substrate cleavage and release of AMC. At higher enzyme concentrations, there is a greater rate of fluorescence increase. However, we were concerned with the interference of BSA in the CEST acquisition and also used a simplified buffer, PBS, in place of the assay buffer (Figure 16B). Although no fluorescence increase was observed at 0.5 µg/mL (1X) and 2.5 µg/mL (5X) hFAP, fluorescence increase was observed with 5 µg/mL (10X) hFAP, which indicates that PBS can be a suitable buffer in place of the original assay buffer. When comparing the rate of

fluorescence increase for all buffer and enzyme concentration combinations, it was found that 5 µg/mL hFAP in PBS had the greatest increase. This was chosen as the enzyme assay buffer and enzyme concentration for further studies.

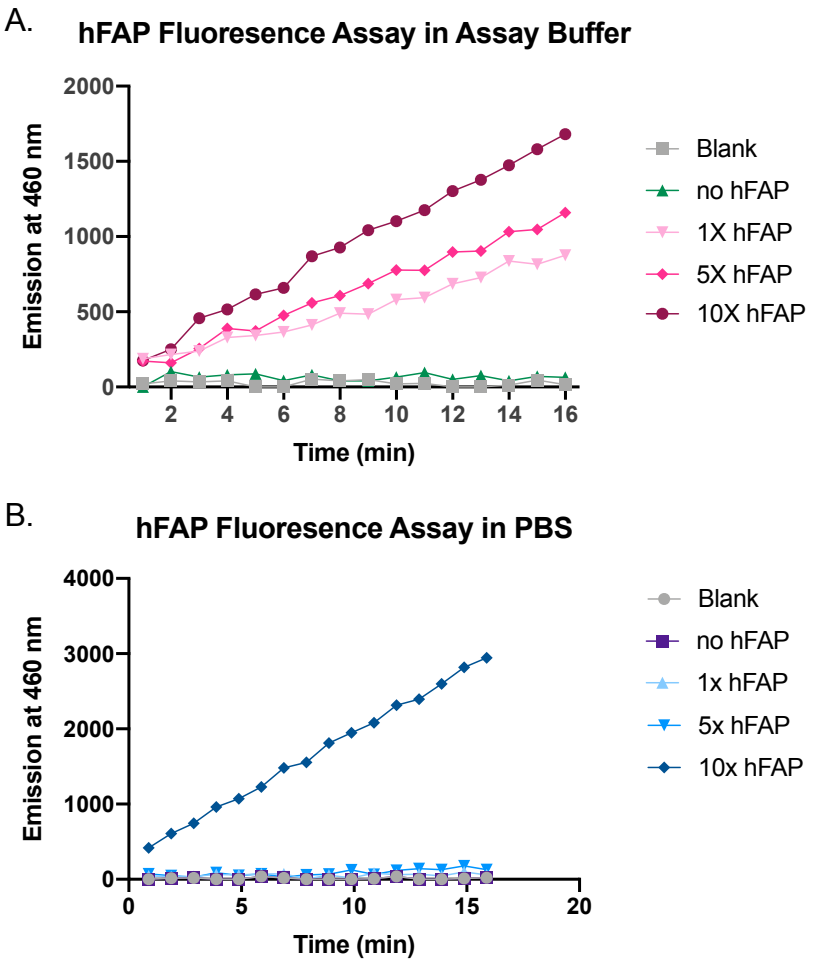

Figure 16. Fluorescence intensity increase of GP-AMC incubated with hFAP in various buffers. *50 µM GP-AMC was incubated with 0.01 µg (1X), 0.05 µg (5X) or 0.1µg (10X) hFAP at 25°C in buffers. The assay buffer consisted of 50 mM Tris, 1.0 M NaCl, 0.1% BSA (w/v), adjusted to pH 7.5 (A). Increasing the amount of hFAP in each well also increased the rate of fluorescence increase. 1X PBS at pH 7.4 was also used as an assay buffer (B). Activity in PBS was only observed using 10X the amount of hFAP. The fluorescence intensity using a plate reader with excitation at 380 nm and emission at 460 nm was measured every 1 minute over 15 minutes. When comparing the enzyme amount and two assay buffers, 10X hFAP in PBS showed the greatest fluorescence increase.*

Since no changes in the fluorescence or absorbance were expected upon cleavage of our CEST probe (**76**) by hFAP to release the signal suppression moiety, HPLC was used to monitor

the progress of the reaction (Figure 17). A change in the chromatogram pattern of the assay aliquot indicates that the substrate is hydrolyzed by the enzyme. A hydrolysis product was also synthesized and used to compare to the aliquots of the reaction.

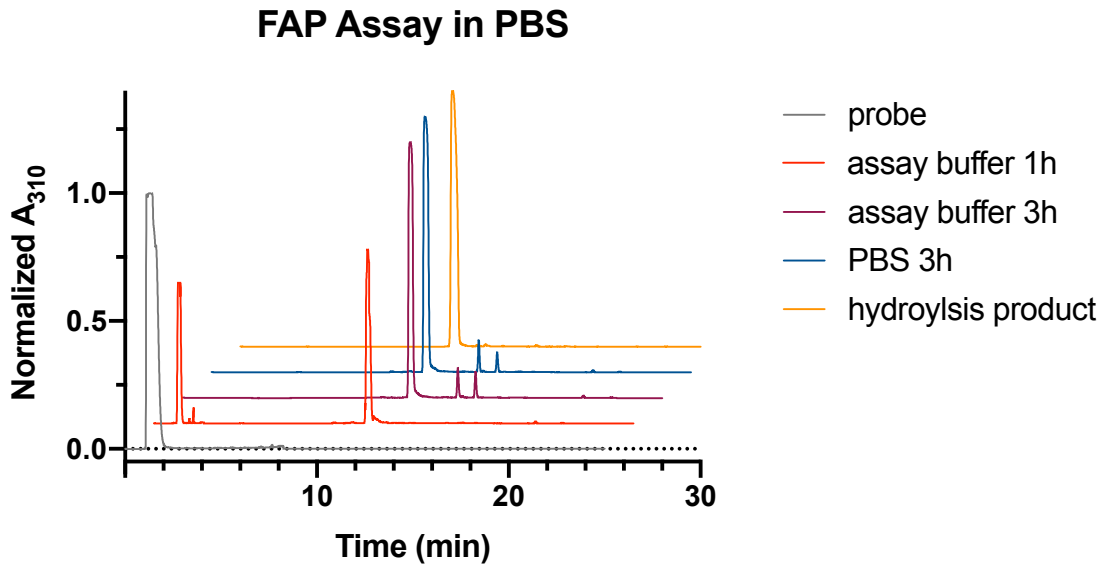

Figure 17. HPLC chromatogram of hFAP assay using compound 76 in various buffers. *0.1 µg hFAP was incubated with 5 mM (76) in assay buffer (50 mM Tris, 1.0 M NaCl, 0.1% BSA (w/v) at pH 7.4), or 1X PBS at pH 7.4 for 1 hour (assay buffer only) or 3 hours at 37°C. The reaction was then quenched with 100 µL cold acetonitrile and the volume was topped to 1 mL using water. The sample was centrifuged at 5000 g for 1 minute before subjected to HPLC analysis. The chromatograms in assay buffer and PBS after 3 hours incubation both show a major peak with an elution time of 11.1 minutes, the same as the hydrolysis product. No major peak for compound 76 was* ***observed.*** *HPLC conditions: Using a C-18 column and gradient method: 1% acetonitrile + 0.1% TFA to 100% acetonitrile + 0.1% TFA in water + 0.1% TFA over 25 minutes. The absorbance was monitored by a PDA detector at 310 nm.*

Initially the synthesized probe prepared in a sample of the assay buffer has an elution time of 2 minutes. Incubation of compound **76** with hFAP at 37°C for 3 hours shows no early peak corresponding to the probe and a large peak shifted to 11 minutes. This peak appeared to have the same elution time as the hydrolysis product that was synthesized (compound **80**). When the same assay was repeated in PBS under the same conditions, the reaction aliquot shows a similar chromatogram, with a large peak at 11 minutes corresponding to the hydrolysis product.

It appears that compound **76** is a substrate recognized by hFAP and the product of the enzyme reaction corresponds to the hypothesized hydrolysis product where the signal suppression moiety is hydrolyzed.

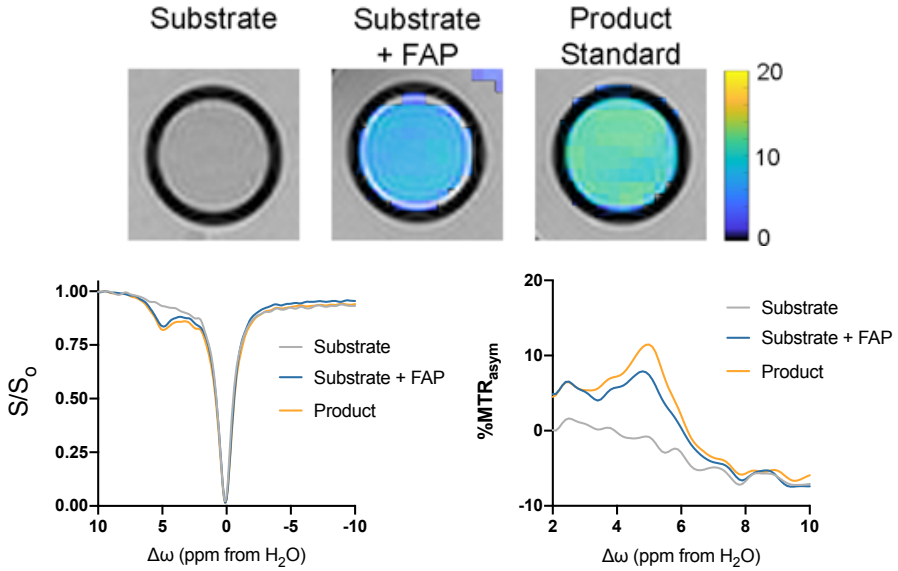

Figure 18. CEST-MRI signal increase upon incubation of compound 76 with hFAP. *Compound 76 was incubated in PBS with hFAP at 37°C for 3 hours. A phantom image (A) and the Z-spectra (B) were acquired at 3T. The incubated sample (substrate + FAP) was also compared to the synthesized product standard (80). No signal was measured from the intact substrate, suggesting that there is signal suppression. The signal of the incubated substrate is comparable to the product standard prepared at the same concentration. The chemical shift of the CEST signal appears at the same range around 5ppm.*

The next step was to study the changes in the CEST-MRI signal upon incubation of compound **76** with hFAP. The probe was incubated with 10X hFAP in PBS at 37°C for 3 hours, as previously done for HPLC to track the progress of the reaction. A CEST-MRI image of the sample was acquired, along with compound **76** and hydrolysis product (Figure 18). No CEST-MRI signal was observed from compound **76**,as expected. When compound **76** was incubated with hFAP for 3 hours, there is an increase in the signal, matching the chemical shift of the hydrolysis product standard. However, the signal intensity of the incubated sample is slightly lower than the hydrolysis product and may indicate that some of the probe has not been cleaved

to remove the signal suppression moiety by hFAP. Compound **76** was found to be a substrate for hFAP and the CEST signal is restored upon cleavage by the enzyme. This allows compound **76** to be used in further activity-based sensing studies to further understand the role of FAP in tumour stroma.

Discussion

Understanding Structural Requirements for CEST Signal Suppression

Salicylic acid has often been described as the gold standard for diaCEST agents.[130] The signal strength is strong and the CEST signal appears at a frequency far away from bulk water to be applicable to *in vivo* situations. Unlike PARACEST agents relying on a paramagnetic inorganic core, salicylic acid owes its favourable CEST qualities to the 1,2 position of the carboxylic acid and hydroxyl group on the aromatic ring.[131,132] Initial studies in this work introducing chloromethyl (**1**) and aminomethyl (**3**) groups at the 5 position found that these modifications did not greatly reduce the measured CEST signal, but allowed the potential for functionalization and modulation of the CEST signal depending on what group was incorporated into the molecule.

Ratnakar *et al* have previously synthesized a PARACEST complex containing two nitroxyl radicals, capable of effectively suppression the CEST signal.[66] Herein, we synthesized diaCEST agents containing the nitroxyl radical of TEMPO and observed a similar reduction in the CEST signal (Figure 5A). In the Ratnakar work, when the nitroxyl radical of the PARACEST complex was reduced by sodium ascorbate to the hydroxylamine, the PARACEST signal was restored and appeared to be the same as the original PARACEST complex without the nitroxyl radicals.[66] In the case of our synthesized diaCEST agents, reduction of the nitroxyl radical by platinum(IV) oxide and hydrogen gas to the hydroxylamine did not restore the CEST signal. SaliMeTEMPOH (**8**) displayed a similar signal suppression effect to the nitroxyl radical of SaliMeTEMPO (**7**). Therefore, unlike the PARACEST complex, reduction of the diaCEST contrast agent did not remove CEST signal suppression. However, we did find that alkylation of

TEMPO to quench the nitroxyl radical was effective in restoring the CEST signal. SaliMeTEMPOMe (**37**) gives a CEST signal similar to the unconjugated salicylate, $SaliMeNH_2$ (**3**). It was apparent to us that both the nitroxyl radical of TEMPO and hydroxylamine of TEMPOH have some signal suppression effect, an effect we sought to understand and exploit to enable unprecedented probes for activity-based sensing by CEST-MRI.

Based off of the SaliMeTEMPOH (**8**) results, which showed signal suppression without the nitroxyl radical, we prepared a simplified piperidinyl ring, removing the gem-dimethyl at position 2 and 6. SaliMeNOH (**13**) displayed a similar signal suppression effect to compound **8**. It appears that although the gem-dimethyl groups contribute to some physical distortion of the ring, they are not important in the suppression of the CEST signal. N-hydroxy piperidine alone can also suppress the CEST signal of salicylic acid to below 1% MTR_{asym}.

To further understand the structural requirements of the signal suppression moiety N-hydroxy piperidine, we coupled 5-aminometyl salicylate (**4**) to various cyclohexanoic acids and benzoic acids (Figure 5A). The cyclohexanoic acid structure is comparable to the piperidine, whereas the benzoic acids have a flatter, planar structure that more closely resembles the puckered ring of TEMPO,[133] compared to the chair conformation adopted by cyclohexanoic acid and piperidine. Additionally, the cyclohexanoic acid and benzoic acid were substituted with a hydroxyl group at the 4 position to mimic the hydroxylamine of TEMPOH and N-hydroxypiperidine. The rings substituted with the hydroxyl group (**22** and **26**) both showed greater CEST signal than their unsubstitued counterparts (**20** and **24**, respectively). The planar aromatic ring also lowered the CEST signal compared to the unsaturated cyclohexane rings.

Previously, Yang *et al* have seen that the introduction of a hydroxyl substitution can increase the CEST signal by increasing the exchange rate of the proton.[58] However, all of these compounds had measured CEST signals in the range of 15-20% MTR_{asym}, similar to 5-aminomethyl salicylic acid (**3**), and were not capable of suppressing the CEST signal. While a planar structure and hydroxyl substitution can have some effects on the CEST signal, it does not appear important in the mechanism of CEST suppression of interest. From these results, we can see the importance of the N-hydroxy group. While no signal suppression was observed for the cyclic and aromatic structures with a hydroxyl group (**22** and **26**), there was a signal reduction in the hydroxylamine of piperidine.

Initially, 5-aminomethyl salicylic acid (**3**) was used as the base structure to create the library of salicylates. The presence of the methyl spacer between the aromatic ring and amide prevents any resonance structures that might disrupt the interactions between the 1,2 carboxylic acid and hydroxyl groups responsible for the CEST signal. However, we wanted to investigate whether this methyl spacer was necessary and if its presence or absence had any effect on the observed CEST signal. 5-amino salicylic acid was coupled to 4-carboxy TEMPO to form SaliTEMPO (**29**) (Figure 5B). Similar to SaliMeTEMPO (**8**), the CEST signal was low, due to the presence of the nitroxyl radical. When SaliTEMPO (**29**) was reduced to the hydroxylamine, SaliTEMPOH (**30**), the CEST signal was still weak. Coupling 5-amino salicyclic acid to N-hydroxy piperidine (**34**) also displayed a similar signal suppression effect. It appears that the methyl spacer is not necessary for the signal suppression effect because a reduced signal is observed in both the case of SaliMeNOH (**13**) and SaliNOH (**34**). In this set of molecules, the signal suppressing moiety and signal generating moiety are closer in proximity, but the

suppression is still observed. This suggests that there can be some flexibility and variability in the positioning of the signal generating and signal suppressing moieties.

Studying more variability on how the signal generating and signal suppressing can be joined, we also synthesized compounds containing an ether linkage (Figure 5C). 4-hydroxy TEMPO was alkylated to 5-chloromethyl salicylate t-butyl ester to form compound **15**. SaliOTEMPO (**15**) showed very little CEST signal, similar to the other TEMPO-coupled salicylic acids (**8**, **29**). However, reduction of the nitroxyl radical to the hydroxylamine (SaliOTEMPOH, **16**) did not have a signal suppression effect to the same extent. SaliOTEMPOH had a measured CEST signal of 7.7%. MTR_{asym}. This indicates that the signal suppression effect is less effective with an ether bond. It is possible that the ether interferes with the signal suppression. This may be due to the stronger activation effects from an ether compared to the amide. Yang et al saw that the CEST signal can increase when there is a strong activating group at the 5 position of salicylic acid, compared to a deactivating group.[134] It is possible the effect of suppression is weakened because the CEST signal is increased by the alkyoxy group. In the PARACEST probe synthesized by Ratnakar *et al*, two nitroxyl radicals were incorporated into the arms of DOTA chelate.[66] This allows them to have sufficient signal suppression of the Eu-complex. Since the exchange rate of the PARACEST complex is higher, greater suppression through shortening the T_1 relaxation is required. As a result, two TEMPO groups were added to the design of the probe. In diaCEST agents, the exchange rate is limited by the difference in chemical shift from bulk water ($k_{ex} < \Delta\omega$), and less T_1 shortening is required for signal suppression.[135] Thus, in our diaCEST probe, we have signal suppression with only one nitroxyl radical.

The nitroxyl radical of TEMPO is capable of suppressing the diaCEST signal of salicylic acid conjugates, similar to the PARACEST complex of Ratnakar *et al*.[66] However, reduction of the radical to the hydroxylamine (TEMPOH) still maintains some signal suppression effect. Looking at its simplified structure, the N-hydroxy piperidine core feature is required to observe CEST signal suppression. This effect can be observed with different linkages to salicylic acid, both directly and with a methyl spacer.

While the methyl spacer seemed to have little effect in the CEST signal of 5-aminomethyl salicylic acid (**3**) compared to 5-amino salicylic acid, we wanted to further investigate structural requirements relating to the distance between the signal generating and signal suppressing moieities (Figure 6). A glutarate linker was incorporated between salicylic acid and N-hydroxy piperidine (**68**). This linker was used to separate the two ends of the molecule further and can introduce more flexibility. From a synthetic perspective, glutarate is a useful molecule because it contains two carboxylic acids that can be used for coupling to easily functionalize the molecule. Reacting glutaric anhydride, a masked carboxylic acid, with an amine forms an amide and opens the ring to reveal a second carboxylic acid that can be used in another coupling reaction.[136] Using this strategy, both carboxylic acids of glutarate can be used for coupling without additional protecting groups. The measured CEST signal of compound **68** appeared to be suppressed compared to 5-aminomethyl salicylic acid (**3**). The additional linker, space and flexibility did not affect the signal suppression effect of N-hydroxy piperidine. This result suggests that there can be some variation in the design of the molecule while maintaining the signal suppression effect. The addition of the glutarate linker separates the signal generating moiety from the signal suppressing moiety by 8 bonds, compared to the 3 bond spaces between SaliMeNOH (**13**). These additional bond spaces have the potential to introduce other targeting

groups into the design of the molecule. Since the signal suppression effect is still observed with a short linker, we expect that the pair of salicylic acid and N-hydroxy piperidine can be applied to a wide variety of substrates for enzymes and still maintain CEST signal suppression.

One of the defining characteristics that differentiate the signal suppression effect of TEMPO from N-hydroxy piperidine is the requirement of physical conjugation through a covalent bond (Figure 7). We observed that a physical mixture of 4-carboxy TEMPO and 5-aminomethyl salicylic acid (**3**) has the same measured CEST signal as the covalently bound compound (SaliMeTEMPO, **8**). However, when we replace the signal suppressing moiety with N-hydroxy piperidine, only the covalent conjugate, SaliMeNOH (**13**) displays signal suppression. A physical mixture of N-hydroxy piperidine with compound **3** shows a CEST signal of 17% MTR_{asym}, similar to that of 5-aminomethyl salicylic acid alone (Figure 7B). It appears that the by separating the signal generating moiety and the signal suppressing moiety, we are able to introduce enough distance so that there is no interaction and no resulting signal suppression. Since the results of the physical mixture study are different between TEMPO and N-hydroxy piperidine, this suggests that the effect of CEST signal suppression varies depending if TEMPO or N-hydroxy piperidine is used. Signal suppression is stronger with TEMPO, likely because it is paramagnetic.

The requirement of the covalent linkage is a key design feature for activity-based sensors, where turn on is required upon modification by the target molecule. There are several examples of model probes that are turned on by degradation or cleavage.[137–142] Fluorophore-quencher pairs have become an important tool in chemical biology that allow different targets to be studied.[143–

[150] Once separated from the quencher, the fluorophore can be activated or turned on to give greater signal sensitivity. Activatable probes are preferred because the signal is specific and can have a higher signal-to-noise ratio. Unlike traditional "always on" probes that develop the signal based on accumulation of the probe at the target of interest,[151] activatable probes are initially turned off and become activated upon interaction with the target. This allows the activatable probe to have greater signal-to-noise ratio by minimizing the background.[152–154] Conventional probes may also have selectivity from molecular recognition, similar to a lock and key approach. The binding of the probe can give information on the expression of an enzyme or presence of the target of interest. However, activity-based sensing uses the molecular reactivity to achieve specificity and can report on the activity of the target.[155]

Similar to the fluorophore quencher model, this signal generating/signal suppression pair for diaCEST has the potential to be adapted to be used as an activity-based sensor. Signal suppression by covalent conjugation to N-hydroxy piperidine is analogous to fluorescence quenching in activity-based sensing probes. A labile linker can be included in the design of the probe so that in the presence of the biomolecule or target of interest, the N-hydroxy piperidine is removed and the signal is restored. This allows the biomolecule or activity of the target of interest to be visualized, even at a low signal.

Moving forward in the design of an activatable CEST probe, we needed to decide which signal suppressing moiety to incorporate. Previous studies have suggested that the nitroxyl radical of TEMPO is unstable and can become quickly reduced under physiological conditions.[119] The reduction of nitroxyl radicals in cells is primarily intracellular, with ascorbate

having a significant role in reduction of certain cell types (erythrocytes, hepatocytes, kidney cells).[156–158] In mouse serum, the EPR signal typical of TEMPO was consistent and stable over 2 hours at room temperature. This may be due to the lack of ascorbate, glutathione and other antioxidants in the serum. However in PBS containing 4 mM sodium ascorbate, the EPR signal of the nitroxyl radical rapidly diminished after 15 minutes at room temperature (Figure 8). Generally, it is accepted that the rate of reduction of the nitroxyl radicals in physiological ascorbate solutions correlates to the *in vivo* half-life of the molecule.[159,160] Since TEMPO was quickly reduced in the presence of sodium ascorbate, it suggests that the nitroxyl radical will have a short *in vivo* half-life. Bobko *et al* have also reported reversible reoxidation of a hydroxylamine similar to TEMPO back to the nitroxyl radical form.[161] The redox reactions between nitroxyl radicals and hydroxylamine in ascorbate-containing environments were significantly affected by the presence of glutathione. This suggests that an equilibrium exists between the paramagnetic radical and hydroxylamine. However, the equilibrium and reoxidation was not observed in the stability studies, perhaps due to the limited time points (acquisition every 15 minutes). Regardless TEMPO as the signal suppression moiety can lead to inconsistent signal suppression if there is an equilibrium between the nitroxyl radical and hydroxylamine. N-hydroxy piperidine had similar stability in both mouse serum and PBS containing sodium ascorbate. Since the N-hydroxy piperidine shows better stability under the physiological conditions tested, in addition to the turn on effect when separated from the signal generating moiety, it is the preferred signal suppression moiety.

Applying CEST Signal Suppression Across diaCEST Agents

Aside from salicylic acid, there is a wide variety of useful diaCEST agents. While the chemical shift of the exchangeable proton must be sufficiently separated from bulk water, if the

exchange rate of the proton is suitable for the NMR timescale, then a CEST signal can be measured. There are several functional groups with protons meeting these specific criteria, including amide[162,163] (barbiturate)[53], hydroxyl[164] (glucose)[50,122,165] and amine[166–169] (anthranilate). Each of these functional groups can result in a diaCEST agent where the CEST signal appears at a different chemical shift, based on its chemical environment. Specifically, barbiturate has a chemical shift at 4.8 ppm, glucose at 1.0 ppm and anthranilate at 6.2 ppm, compared to salicylate where the CEST signal appears at 9.2 ppm (Figure 4). Using the different chemical shifts of each exchangeable CEST proton can be analogous to the different colours of fluorophore that allow for multiplexed imaging. Similar to how fluorophores with different emission spectra can be used for multicolour staining, multiple diaCEST agents, each with a distinct chemical shift, can be used in combination to make a multi-coloured CEST image. Imaging several diaCEST agents together can give insight on the interaction of the targeted agents. For example, fibroblast activation protein, collagen and fibronection are all important components of the tumour stroma,[71] and there has been literature supporting the interaction of these components to contribute to tumour growth and invasiveness.[170] Imaging the components together in real-time can give more insight on the interactions and a more holistic understanding of the tumour environment.

In order to study the breadth of the signal suppression effect across different diaCEST agents, 4-carboxy TEMPO and N-hydroxy piperidine were coupled to anthranilates, barbiturates and glucosamine (Figure 10). 4-carboxy TEMPO reduced the measured CEST signal across all classes of diaCEST agents studied to less than 1% MTR_{asym}. This was expected because 4-carboxy TEMPO has paramagnetic character due to its unpaired electron, which can broaden the

observed signal such that no CEST peak is measured from the z-spectra. When looking at the compounds coupled to N-hydroxy piperidine, the CEST signal is also suppressed across all diaCEST agent. However, there appears to be a broad peak around 8 ppm for all diaCEST classes studied as well. This may be the exchanging N-hydroxy proton. Future kinetic experiments can be done to determine the rate of proton exchange (k_{sw}) to see if it is within a viable diaCEST range.[171] In this case, signal suppression is mediated by an alternative non-radical mechanism, different from TEMPO. The signal suppression moiety can reduce the CEST signal for the diaCEST agents studied, indicating that the chemical shift of the diaCEST proton is not involved in the mechanism.

Elucidating Mechanism of CEST Signal Suppression

An initial hypothesis for the signal suppression mechanism was based off an intramolecular H-bond between the N-hydroxy piperidine and salicylic acid. If this were true, then the signal suppression effect should still be observed at all concentrations. The signal strength of the sample is related to its concentration (Figure 11). As the concentration decreases, the CEST signal also decreases. This is observed when a sample of 5-aminosalicylic acid was prepared as a 20 mM, 10 mM and 5 mM solution. When the corresponding TEMPOH coupled compound (**34**) was measured under the same conditions, there is no correlation to the concentration and the signal suppression effect is still observed at all concentrations. It appears that the signal suppression is mediated through an intramolecular mechanism, perhaps through interactions with bulk water.

In the PARACEST complex synthesized by Ratnakar *et al*[66], the CEST signal was hypothesized to be suppressed due to T_1-shortening effects on bulk water mediated by the

nitroxyl radical on TEMPO. The CEST signal can be represented as the percent decrease in bulk water intensity according to the following equation:

$$\frac{M_z}{M_0} = 100\left(1 + \frac{cqT_1}{55.5\tau_M}\right)^{-1} \quad (1)$$

where c is the concentration of the CEST agent, q is the number of exchanging protons, T_1 is the longitudinal relaxation time of bulk water and τ_M is the exchange lifetime of the exchanging protons. We can see that as T_1 decreases, the measured CEST signal also decreases. As a result of the T_1 shortening by the nitroxyl radical of TEMPO, the authors observed a decrease in the PARACEST signal.

Of the synthesized signal-suppression moiety, we measured the EPR signal to assess the presence of any paramagnetic character (Figure 12). The presence of a radical can be responsible for the paramagnetic EPR signal observed. 4-carboxy TEMPO is a stable radical and a strong EPR signal was measured. The reduction (**81**) and methylation (**35**) products lacked an EPR signal because the radical was reduced to the hydroxylamine or methylated, respectively. The lack of the radical is observed in the lack of EPR signal. N-hydroxy piperidine (**83**) also had no EPR signal, suggesting that it is not paramagnetic. Unlike 4-carboxy TEMPO, N-hydroxy piperidine is not paramagnetic and cannot have a signal suppression mechanism based off paramagnetic interactions. As a result, we suggest that N-hydroxy piperidine is mediating CEST signal suppression by a non-radical mechanism.

T_1-weighted and T_2-weighted images were acquired of the signal-suppression moieties to assess a potential T_1-mediated mechanism to CEST signal suppression (Figure 13). 4-carboxy TEMPO showed a strong T_1 shortening effect and N-hydroxy piperidine (**83**) had weaker T_1

shortening effect while not being paramagnetic according to EPR. This suggests that N-hydroxy piperdine can be suppressing the CEST signal through a T_1 shortening mechanism, similar to what was proposed by Ratnakar *et al*, although through a non-radical mechanism.

When comparing the effect of nitroxyl reduction between the Ratnakar PARACEST probe[66] and the diaCEST probe described, it is interesting that reduction is capable of restoring the CEST signal in the PARACEST case, but not for diaCEST. This could be due to the difference in water residence time (τ_M) between the two classes of agents. The water residence time for PARACEST agents is generally around 70 μs[172], whereas it is in the range of 500 μs for diaCEST.[173] Upon reduction, Ratnakar observed a 10-fold change in the T_1 relaxation. In our diaCEST case, a change of 1.4-fold was observed upon introduction of the N-hydroxy piperidine to the salicylate compound. For our studied diaCEST compounds, we observed a smaller change in the T_1 with the introduction of N-hydroxy piperidine compared to the change in T_1 that results from the TEMPO nitroxyl radical. This small T_1 effect, in combination with the longer water residence time for diaCEST agents, seems to be capable of reducing the diaCEST signal to result in signal suppression. Looking at equation 1, we can see that τ_M is inversely proportional to the strength of the signal and T_1 is proportional to the signal observed. Although the change in T_1 from N-hydroxy piperidine is small, it can be overcome by the large τ_M inherent to diaCEST compounds. Therefore, given the extended water residence time of diaCEST agents, we hypothesized that the weak T_1 contribution from N-hydroxy piperidine was sufficient to cause the CEST signal suppression that we observed.

Enzyme Assay for Studying the Activity of FAP

The tumour environment is dynamic and made up of many different components including the extracellular matrix, stromal cells and immune cells. Stromal cells are the most abundant component of the tumour stroma.[174] Stromal fibroblasts of epithelial tumours can often be characterized by overexpression of FAP, making it a good target for the diagnosis and treatment of cancer.[97,126] FAP recognizes a glycine-proline dipeptide sequence and cleaves following the proline residue.[127] This design feature was incorporated into (**76**) to create a probe targeting FAP, which will allow us to study the activity of FAP in live subjects. Upon cleavage by FAP, the signal suppression moiety is released and the CEST signal is expected to be restored. The expected hydrolysis product was also synthesized and used as the positive control sample in the enzyme assays.

There were initial concerns of the assay buffer due to a potential interference of BSA and the high sodium chloride concentration.[175] A simplified buffer of PBS at pH 7.4 was also used to validate the assay conditions (Figure 16). Although no fluorescence increase was observed at low hFAP concentrations (1X, 5X), comparable fluorescence increase was observed at 10X hFAP. It appears that hFAP can still function and hydrolyze the substrate in the simplified assay buffer. Moving forward in the study, PBS was used as the assay buffer in place of the cocktail recommended by Biolegend. When the assay buffer and PBS were directly compared, the rate of fluorescence increase is higher in PBS than it was with the assay buffer. The use of PBS avoids interference of BSA in the CEST images.

Following the validated assay protocol, (**76**) was incubated with hFAP at 37°C for 3 hours and monitored by HPLC to determine if it was a suitable substrate (Figure 17). When

comparing the chromatograms, (**76**) has an elution time of 2 minutes and (**80**) elutes through the column after 11 minutes. Aliquots of the enzyme reaction in the manufacture assay buffer and PBS after 3 hours of incubation resulted in similar chromatograms, both with a major peak at 11 minutes. This peak is consistent with (**80**) and suggests that the product following enzymatic cleavage is the hypothesized (**80**). The aliquots of the enzyme reaction after 3 hours also do not have a peak at 2 minutes, indicating that the substrate is no longer present and has been hydrolyzed by hFAP or degraded in the buffer over the incubation period. Regardless, these results are promising and can be used to verify that (**76**) is a substrate for hFAP, with the product matching (**80**).

We hypothesized that cleavage of the covalent linker connecting the signal generating moiety and signal suppressing moiety would be sufficient in restoring the CEST signal. Through the HPLC chromatograms, we can see that hFAP is capable of hydrolyzing the linker between the signal generating moiety (barbiturate) and the signal suppression moiety (N-hydroxy piperidine). To confirm the restoration of the signal, the CEST-MRI images were acquired of the incubated sample with hFAP (Figure 18). The substrate, (**76**), on its own does not generate a CEST signal. In this molecule, the signal generating moiety and signal suppressing moiety are joined through a short dipeptide linker consisting of glycine and proline. Following incubation with hFAP for 3 hours at 37°C, there is a CEST signal appearing at 4.6 ppm of 8% MTR_{asym}. Incubation with hFAP allows the enzyme to hydrolyze the probe and release the signal suppressing moiety and relieves the signal suppression effect. When the CEST signal is compared to the (**80**), we can see that the chemical shift is about the same. However, the

measured signal of (**80**) is slightly stronger, 11% MTR_{asym}. It is possible that the reaction has not gone to completion and some intact probe remains where the signal is still suppressed.

Increase of the CEST signal following incubation with hFAP supports our hypothesis of the signal suppression mechanism. Upon cleavage of the short covalent linker, the signal generating moiety and signal suppressing moiety are separated and the CEST signal is restored. Structural investigations suggest that there can be variability in how the signal generating moiety and signal suppressing moiety are connected. Similar to how fluorophore and quencher pairs can be applied to a wide range of cleavable linkers, there is the same potential for a signal generating moiety and signal suppressing moiety to be used as an activatable probe.

In the design of the probe targeting FAP, barbiturate was selected as the signal generating moiety. However, this diaCEST molecule can also be easily replaced with another class of diaCEST agents and the same signal suppression and activation upon cleavage can be observed. This is due to the breadth of signal suppression from the N-hydroxy piperidine. Since the weak T_1 interaction underlying CEST signal suppression was observed across several diaCEST agents, we would expect signal reduction from any pair that includes N-hydroxy piperidine. The simplicity of this design means that several probes can be synthesized, each with a signal generating moiety targeting a different target. The combination of these probes can give insight on the interactions between the targets in their environment, as long as there is sufficient resolution between the exchanging CEST protons of each signal generating moiety.

The discovery of N-hydroxy piperidine to suppress the signals of diaCEST agents has allowed us to study a new activatable probe and mechanism by CEST-MRI. By joining N-hydroxy piperidine with a diaCEST agent, we synthesized a probe that can be used for activity-based sensing of hFAP. The activity of hFAP, along with its interactions with other components in the tumour stroma, is important in the progression and invasion of tumours. This activatable CEST-MRI mechanism can be applied to other relevant targets in the tumour environment to help understand its interactions in tumour development with multicolour CEST imaging.

Conclusion and Future Directions

Both TEMPO and N-hydroxy piperidine were found to have a signal suppression effect on the diaCEST signal. Signal suppression was observed in several different classes of diaCEST agents include salicylates, barbiturates and carbohydrates, thus suggesting that it follows a general mechanism applicable to the range of diaCEST agents. Signal suppression is predicted to be due to a weak T_1 effect that alters the relaxation time of bulk water. A covalent linkage was necessary for signal suppression from N-hydroxy piperidine; cleavage of the linker relieves the suppression effect and the diaCEST signal is restored.

Signal suppression by N-hydroxy piperidine was applied to the design of a probe used to detect the activity of FAP. FAP is an enzyme relevant in the tumour environment and important to tumour growth, invasion and metastasis. Barbiturate and N-hydroxy piperidine were joined together by a linker containing proline, recognized by FAP. Incubation of the synthesized probe with FAP resulted in signal increase after 3 hours, indicating that the probe was hydrolyzed and N-hydroxy piperidine was separated from the diaCEST-generating baribiturate. While this is one of the few examples of an activatable probe sensing enzyme activity, it is the first one that uses a generalizable signal suppression mechanism.

Further work can be done to study the activity of FAP using this activatable probe *in vitro* and *in vivo* settings. Additionally, since the signal suppression mechanism is generalizable and applicable to different classes of diaCEST agents, a second probe can be designed targeting another element of the tumour environment using a different CEST beacon, such as salicylic acid. Since the diaCEST agents have exchangeable protons at unique chemical shifts, it can allow for multi-colour diaCEST imaging to help understand the interactions of these targets in the tumour environment.

Overall, this work has found a new group, N-hydroxy piperidine, that is capable of suppressing the diaCEST signal of a wide range of small molecules. This has been adapted to study the activity of FAP and showed a signal increase upon incubation with the enzyme. Having a generalizable signal suppression mechanism can contribute to the growth of a modular toolbox of activatable diaCEST probes to study interactions and reactivity on a molecular level.

Experimental

General Synthetic Procedures

Reagents were commercially available, or prepared as stated below. All solvents were HPLC grade, except water (18.2 Ω cm Millipore water) and CH_2Cl_2 (dried in a solvent purification system). Flash column chromatography (FCC) was carried out using silica gel (SiO_2), mesh size 230 – 400 Å. Thin-layer chromatography (TLC) was carried out on Al-backed silica gel plates with compounds visualized by anisaldehyde stain, 5% ninhydrin stain, orcinol stain, bromocersol green stain and UV light. NMR spectra were recorded on a 300 MHz 400 MHz spectrometer. For ^1H NMR spectra δ values were recorded as follows: DMSO-D_6 (2.50 ppm), D_2O (4.79 ppm) and ^{13}C NMR spectra δ values were recorded as follows: DMSO-D_6 (39.52 ppm). Mass spectra (MS) were obtained using electron impact (EI) or electrospray ionization (ESI).

Model Compounds: Salicylates

Synthesis of 5-chloromethyl salicylic acid (1).

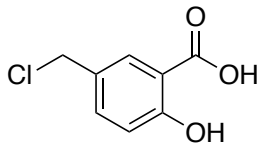

Compound 1 was prepared following modified procedures from Shindo et al[176], Friedman et al[177] and Quelet et al.[178] Salicylic acid (1.38 g, 10 mmol, 1 equi.) was dissolved in 10mL of dioxane in a round bottom flask. Paraformaldehyde (2.00 g, 6 mmol, 0.6 equi.) was added to the flask with 20 mL concentration HCl. The mixture was stirred at room temperature for 18 hours as a white precipitate was formed. Afterwards, the flask was placed in the fridge for 6 hours. Suction

filtration of the reaction mixture gave a white solid that was washed with cold water and dried at room temperature overnight. The white solid was recrystallized using chloroform to give white crystals. The crystals were obtained by suction filtration and washed with cold chloroform, before being dried at room temperature overnight. A white crystalline solid was obtained in 64% yield. ^{1}H NMR (400 MHz, DMSO-D_6): δ 11.33 (broad s, 1H), 7.87 (d, J = 2.2 Hz, 1H), 7.58 (dd, J = 8.5, 2.3 Hz, 1H), 6.97 (d, J = 8.5 Hz, 1H), 4.75 (s, 3H). ^{13}C NMR (400 MHz, DMSO-D_6): δ 171.51, 161.03, 136.37, 130.85, 128.62, 117.62, 112.89, 45.74. HRMS (EI): calculated for $C_8H_7ClO_3$ 186.0084; found 186.0065.

Synthesis of compound 2.

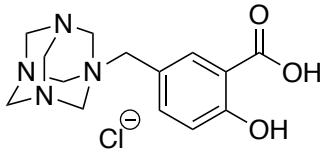

Compound 2 was prepared following the procedure outlined from Shindo et al[176]. 5-chloromethyl salicylic acid (**1**) (186 mg, 1 mmol, 1 equi.) was stirred in 5 mL of chloroform in a round bottom flask. Hexamethylenetetramine (218.4 mg, 1.56 mmol, 1.56 equi.) was added to the flask and the mixture was stirred at room temperature for 4 hours. A white solid was obtained by suction filtration that was washed with cold chloroform and dried at room temperature over night. A crude white powdered solid was isolated and used without further purification.^{1}H NMR (400 MHz, DMSO-D_6): δ 7.81 (d, J = 2.4 Hz, 1H), 7.38 (dd, J = 8.6, 2.6 Hz, 1H), 6.87 (d, J = 8.4 Hz,1 H), 5.02 (s, 6H), 4.49 (dd, J = 12.6, 5.9 Hz, 6H), 3.99 (s, 2H). ^{13}C NMR (400 MHz, DMSO-D_6): δ 171.02, 163.90, 137.00, 134.24, 117.42, 113.76, 77.39, 71.10, 69.90, 59.21. Unable to acquire HRMS due to high boiling point of molecule and instability under ESI conditions.

Synthesis of 5-aminomethyl salicylic acid (3).

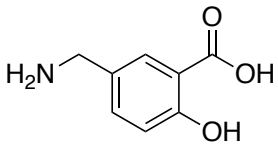

Compound **2** (326 mg, 1 mmol 1 equi.) was stirred in 2 mL of MeOH in a round bottom flask. 0.5 mL of concentrated HCl was added and the mixture was refluxed (at 90°C) for 1.5 hours. After 1.5 hours, the flask was cooled to room temperature and a white solid precipitates. The white solid was removed by gravity filtration and mother liquor was concentrated *in vacuo* to give a white solid. The white solid was dissolved in 1 mL of a 20% aqueous NaOH solution and stirred at 70°C for 2 hours with an air condenser. After 2 hours, the flask was cooled to room temperature and diluted with brine. The pH was adjusted using dilute HCl until the pH was 1. The crude product was extracted using ethyl acetate and dried over sodium sulphate, before being concentrated *in vacuo* to give a light yellow solid in 53% yield. ^{1}H NMR (400 MHz, DMSO-D_6): δ 7.82 (d, J = 2.6 Hz, 1H), 7.50 (broad s, 3H), 7.25 (dd, J = 8.3, 2.4, 1H), 6.65 (d, J = 8.2, 1H), 3.87 (s, 2H). ^{13}C NMR (400 HMz, DMSO-D_6): δ 171.18, 163.28, 132.72, 131.17, 121.12, 119.91, 116.03, 42.23. HRMS (EI) calculated for $C_8H_9NO_3$ 167.16; found 167.1597.

Synthesis of 5-aminomethyl salicylate methyl ester (4).

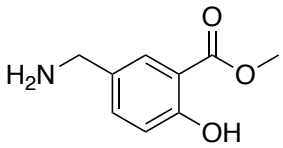

Compound **2** (326 mg, 1 mmol, 1 equi.) was stirred in 2 mL of MeOH in a round bottom flask. 0.5 mL of concentrated HCl was added and the mixture was refluxed (at 90°C) for 1.5 hours.

After 1.5 hours, the flask was cooled to room temperature and a white solid precipitates. The white solid was removed by gravity filtration and mother liquor was concentrated *in vacuo* to give a white solid. The crude product was redissolved in 5 mL of MeOH and H_2SO_4 (2.5 uL, 0.05 mmol, 0.05 equi.) was added to the reaction mixture. The mixture was heated to 65°C for 2 days with an air condenser. After 2 days, the solvent was concentrated *in vacuo* to give a yellow residue. The residue was redissolved in saturated sodium bicarbonate and adjusted to neutral pH. The crude product was extracted using ethyl acetate and dried over sodium sulphate, before being concentrated *in vacuo* to give a light yellow solid in 36% yield. ^{1}H NMR (400 MHz, DMSO-D_6): δ 7.71 (d, J = 2.2 Hz, 1H), 7.45 (dd, J = 8.5, 2.3 Hz, 1H), 6.89 (d, J = 8.5 Hz, 1H), 3.89 (s, 3H), 3.65 (s, 2H). ^{13}C NMR (400 MHz, DMSO-D_6): δ 169.46, 158.65, 134.92, 128.13, 117.07, 112.32, 52.42, 44.62. HRMS (EI) calculated for $C_9H_{11}NO_3$ 181.0739; found 181.0727.

N-acetyl 5-aminomethyl salicylic acid (5).

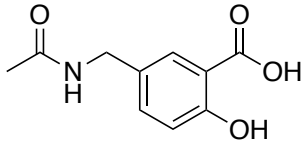

This procedure was adapted from Di Antonio et al[179]. 5-aminomethyl salicylic acid (**3**) (120 mg, 0.5 mmol, 1 equi.) was added to a round bottom flask and stirred in a solution 3 mL of saturated sodium bicarbonate at room temperature. Acetic anhydride (52 uL, 0.55 mmol, 1.1 equi.) was added to the flask and the mixture was stirred for an additional 1.5 hours. The reaction mixture was diluted with brine and the pH was adjusted to 1 using dilute HCl. The crude compound was extracted using ethyl acetate. The combined organic phases were dried over sodium sulphate and concentrated *in vacuo* to give the compound without further purification. A light yellow solid was obtained in 54% yield. ^{1}H NMR (400 MHz, DMSO-D_6): δ 11.30 (broad s, 1H), 8.32 (t, J =

5.36 Hz, 1H), 7.67 (d, J = 2.3 Hz, 1H), 7.39 (dd, J = 8.2, 2.3 Hz, 1H), 6.91 (d, J = 8.6 Hz, 1H), 4.16 (d, J = 6.1 Hz, 2H), 1.85 (s, 3H). ^{13}C NMR (400 MHz, DMSO-D_6): δ 171.84, 169.13, 160.06, 135.14, 130.41, 128.98, 117.07, 112.47, 41.36, 22.54. HRMS (EI) calculated for $C_{10}H_{11}NO_4$ 209.0688; found 209.0676.

Synthesis of compound 6.

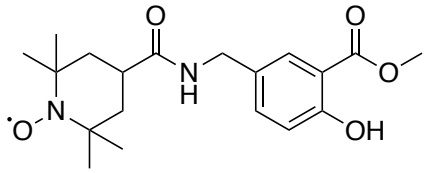

4-carboxy TEMPO (100 mg, 0.5 mmol, 1 equi.) was stirred in a round bottom flask containing DIPEA (175 uL, 2 mmol, 4 equi.) in 1 mL of DMF. HBTU (189.6 mg, 0.5 mmol, 1 equi.) and HOBT (20.2 mg, 0.625 mmol, 0.3 equi.) were added to the flask and cooled to 0°C. The mixture was stirred on ice for 5 minutes before 5-aminomethyl salicylate methyl ester (**4**) (90.6 mg, 0.5 mmol 1 equi.) was added and the mixture was continued to be stirred at room temperature for 18 hours/overnight. The next morning the reaction mixture was diluted with brine and extracted using ethyl acetate. The organic phases were combined and washed with brine before being dried over sodium sulphate and concentrated *in vacuo*. The crude compound was purified by silica column chromatography using 2:1 hexanes:acetone as the solvent system. An orange residue was obtained in 83% yield. HRMS (ESI) calculated for $C_{19}H_{27}N_2O_5Na^+$ 386.1829; found 386.1818.

Synthesis of compound 7.

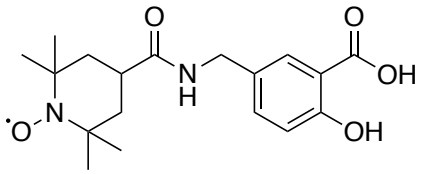

The methyl ester (**7**) (90.9, 0.25 mmol, 1 equi.) was stirred in a round bottom flask with 0.5 mL of dioxane and 1.5 mL of a 20% NaOH solution. The mixture was stirred at 70°C for 2 hours with an air condenser. After 2 hours, the flask was cooled to room temperature and diluted with brine. The mixture was acidified with dilute HCl to adjust to the pH to 1. The crude compound was extracted using ethyl acetate. The combined organic layers were dried over sodium sulphate and concentrated *in vacuo*. The product was obtained in 43% yield as an orange solid without further purification. HRMS (ESI) calculated for $C_{18}H_{25}N_2O_5Na^+$ 372.1687; found 372.1661.

Synthesis of compound 8.

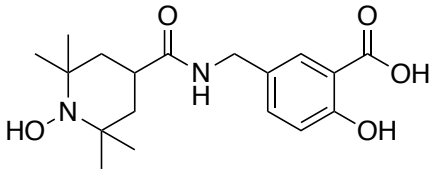

The reduction of the nitroxyl radical was adapted from Mitchell et al[180]. The nitroxyl radical (**8**) (87.3 mg, 0.25 mmol, 1 equi.) was stirred in a round bottom flask with 2 mL of MeOH and platinum(IV) oxide (5.6 mg, 0.025 mmol, 10% mol equi.) and evacuated under vacuum at room temperature for 45 minutes. An H_2 balloon was then added and the reaction mixture was stirred at room temperature for an additional 2 hours as the orange colour disappeared to give a colourless solution with a black dark grey solid. The mixture was filtered through a Pasteur pipette with cotton and then concentrated *in vacuo* to give reduced compound without further purification. An orange residue was obtained in 68% yield.

^{1}H NMR (400 MHz, DMSO-D_6): δ 8.41 (t, J = 5.5 Hz, 1H), 7.68 (d, J = 2.2 Hz, 1H), 7.37 (dd, J = 8.5, 2.4 Hz, 1H), 6.91 (d, J = 8.5 Hz, 1H), 4.19 (d, J = 5.8 Hz, 2H), 2.85-2.73 (m, 1H), 1.89-1.75 (m, 4H), 1.51-1.42 (m, 2H), 1.30 (s, 6H), 1.24 (s, 6H). ^{13}C NMR (400 MHz, DMSO-D_6): δ 171.28, 169.36, 158.95, 134.23, 130.73, 128.43, 117.56, 112.71, 78.76, 42.22, 28.04, 27.34, 25.92, 25.13. HRMS (ESI) calculated for $C_{18}H_{26}N_2O_5Na^+$ 373.1734; found 373.1739.

Synthesis of N-Boc isonipecotic acid (9).

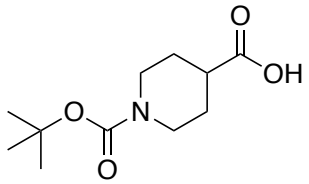

Compound 9 was synthesized following the procedure outline in Klein et al[181]. Briefly, Di-tert-butyl dicarbonate (414.7 mg, 1.9 mmol, 1.9 equi.) was added to 1 mL of THF in a small vial. Isonipecotic acid (129.1 mg, 1 mmol, 1 equi.) was added to a round bottom flask with potassium carbonate (262.6 mg, 1.9 mmol, 1.9 equi.) and 2mL of water. The flask was cooled to 0°C on ice. The di-tert-butyl dicarbonate solution in THF was added dropwise to the round bottom flask and the mixture was stirred at room temperature for 4 hours. After 4 hours, the solvent was concentrated *in vacuo* to give a white solid. The solid was dissolved with brine and washed twice with ether. The pH of the aqueous phase was adjusted to pH 1 using dilute HCl and the crude compound was extracted using ethyl acetate. The combined organic phases were dried over sodium sulphate before being concentrated *in vacuo*. The compound was used without further purification. (Yield = 83.7%) ^{1}H NMR (DMSO-D_6): δ 12.18 (broad s, 1H), 3.83 (d, J = 14.7 Hz, 2H), 2.81 (broad s, 2H), 2.44-2.34 (m, 1H), 1.77 (dd, J = 13.1, 3.2 Hz, 2H), 1.46-1.33 (m, 11 H).

^{13}C NMR (400 MHz, DMSO-D_6): δ 175.74, 153.92, 78.62, 28.09, 27.74. HRMS (EI) calculated for $C_7H_{11}NO_4$ 173.0688; found 173.0707 (loss of t-butyl group).

Synthesis of compound 10.

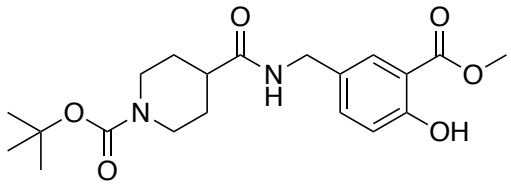

Compound 10 was obtained by coupling compound **4** and **9**, following the procedure outlined for compound **6**. The crude compound was purified using silica column chromatography with 2:1 hexanes:acetone as the solvent system. A light yellow oil was obtained in 88% yield.
^{1}H NMR (400 MHz, DMSO-D_6): δ 10.39 (s, 1H) 8.33 (t, J = 6.0 Hz, 1H), 7.63 (d, J = 2.5 Hz, 1H), 7.38 (dd, J = 9.1, 3.3 Hz, 1H), 6.94 (d, J = 8.7 Hz, 1H), 4.18 (d, J = 6.0 Hz, 2H), 3.88 (s, 3H), 2.69 (s, 1H), 2.37-2.27 (m, 1H), 1.70-1.62 (m, 2H), 1.48-1.34 (m, 11H). ^{13}C NMR (400 MHz, DMSO-D_6): δ 173.93, 169.11, 158.92, 153.87, 134.79, 130.65, 128.47, 117.43, 112.57, 78.56, 52.43, 41.64, 41.04, 38.23, 28.28, 28.07. HRMS (ESI) calculated for $C_{20}H_{28}N_2O_6Na^+$ 415.1861; found 415.1845.

Synthesis of compound 11.

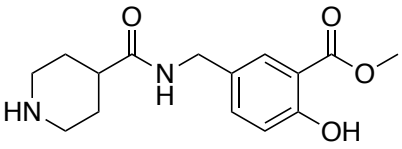

The Boc protected compound (**10**) (117 mg, 0.3 mmol, 1 equi.) was added to a round bottom flask and stirred in a solution of 2 mL DCM and 0.5 mL TFA at room temperature. After TLC showed conversion of the starting material to product (2.5 hours), the reaction mixture was

concentrated *in vacuo* with excess DCM. The product was obtained as a light yellow oil in quantitative yield without further purification. ^{1}H NMR (300 MHz, DMSO-D_6): δ 10.40 (broad s, 1H), 8.45 (t, J = 7.1 Hz, 1H), 7.65 (d, J = 2.6 Hz, 1H), 7.39 (dd, J = 8.8 Hz, 2.7 Hz, 1H), 6.95 (d, J = 8.8, 1H), 4.19 (d, 7.7 Hz, 2H), 3.89 (s, 3H), 3.35-3.18 (m, 2H), 3.00-2.80 (m, 2H), 2.02-1.59 (m, 6H). ^{13}C NMR (400 MHz, DMSO-D_6): δ 172.97, 169.05, 158.88, 134.83, 130.49, 128.58, 117.46, 112.69, 52.46, 42.52, 41.14, 25.19. HRMS (ESI) calculated for $C_{15}H_{20}N_2O_4Na^+$ 315.1344; found 315.1321.

Synthesis of compound 12.

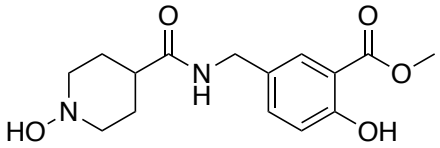

Compound **11** was stirred in a solution of dioxane/methanol at 0°C. 30% H_2O_2 was added dropwise. The mixture was stirred on ice for 1 hour, and then continued at room temperature for 5 hours. The solvent was evaporated *in vacuo* and the remaining residue was dissolved in brine. The compound was extracted using ethyl acetate, dried over sodium sulphate and evaporated *in vcauo* to give a light yellow residue. ^{1}H NMR (300 MHz, DMSO-D_6): δ 10.33 (broad s, 1H), 8.47 (t, J = 7.1 Hz, 2H), 7.65 (d, J = 2.6 Hz, 1H), 7.39 (dd, J = 8.8, 2.7 Hz, 1H), 6.95 (d, J = 8.8 Hz, 1H), 4.19 (d, 7.7 Hz, 2H), 3.88 (s, 3H), 3.35-3.18 (m, 2H), 3.00-2.80 (m, 2H), 2.02-1.59 (m, 6H). ^{13}C NMR (400 MHz, DMSO-D_6): δ 169.04, 158.87, 134.83, 130.55, 128.59, 117.42, 112.68, 51.85, 43.05, 41.25, 25.30. HRMS (ESI) calculated for $C_{15}H_{20}N_2O_5Na^+$ 331.33; found 331.32.

Synthesis of compound 13.

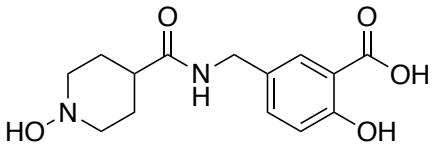

Compound 13 was obtained following the procedure outlined for compound **7**. ^{1}H NMR (400 MHz, DMSO-D_6): δ 11.19 (broad s, 1H), 8.52 (broad s, 1H), 8.43(t, J = 6.8 Hz, 1H), 8.21 (broad s, 1H), 7.64 (d, J = 2.4 Hz, 1H), 7.40 (dd, J = 8.9, 2.4 Hz, 1H), 6.89 (d, J = 8.8 Hz, 1H), 4.21 (d, J = 5.8 Hz, 2H), 3.32-3.18 (m, 4H), 2.97-2.80 (m, 3H), 2.69 (s, 4H), 1.99-1.62 (m, 6H). ^{13}C NMR (400 MHz, DMSO-D_6): δ 169.12, 158.92, 153.92, 134.77, 130.65, 128.47, 117.40, 112.57, 78.57, 52.34, 41.66, 41.04, 38.27. HRMSI (ESI) calculated for $C_{14}H_{18}N_2O_5Na^+$ 317.1113; found 317.1115.

Synthesis of compound 14.

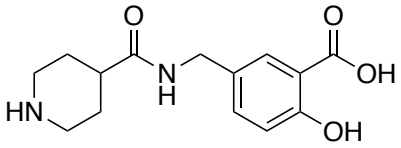

Compound 14 was prepared following the procedure outlined for compound **7** from compound **11**. ^{1}H NMR (400 MHz, DMSO-D_6): δ 11.18 (broad s, 1H), 8.50 (broad s, 1H), 8.44 (t, J = 6.9 Hz, 1H), 8.22 (broad s, 1H), 7.66 (d, J = 2.4 Hz, 1H), 7.38 (dd, J = 9.1, 2.4 Hz, 1H), 6.91 (d, J = 8.8 Hz, 1H), 4.19 (d, J = 5.8 Hz, 2H), 3.32-3.20 (m, 4H), 2.96-2.81 (m, 3H), 2.69 (s, 4H), 2.01-1.61 (m, 6H). ^{13}C NMR (400 MHz, DMSO-D_6): δ 170.09, 159.13, 153.72, 134.57, 130.42, 128.40, 117.54, 111.34, 78.67, 52.37, 41.60, 40.97, 37.78. HRMS (ESI) calculated for $C_{19}H_{26}N_2O_6Na^+$ 401.1704; found 401.1689.

5-chloromethyl salicylate t-butyl ester (15).

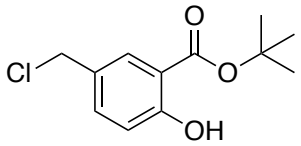

Formation of the t-butyl ester was prepared following the procedure outlined by Wright et al[182]. Magnesium sulphate (480 mg, 4 mmol, 4 equi.) was stirred with 10 mL of DCM in a round bottom flask. H_2SO_4 (53 mg, 1 mmol, 1 equi.) was added to the flask and the mixture was vigorously stirred at room temperature for 15 minutes. 5-chloromethyl salicyclic acid (**1**) (186 mg, 1mmol, 1 equi.) was added to the flask along with tert-butanol (474 uL, 5 mmol, 5 equi.). The mixture was stirred at room temperature for 18 hours/overnight. The next morning, the mixture was diluted with saturated sodium bicarbonate and addition DCM was added. The crude product was drawn off from the organic phase and the combined organic layers were washed with bring and dried over sodium sulphate before being concentrated *in vacuo* to give a light coloured residue. The crude compound was purified using silica column chromatography (3:1 hexanes:acetone). The product was obtained as a light yellow residue in 73% yield.
^{1}H NMR (400 MHz, DMSO-D_6): δ 10.81 (s, 1H), 7.79 (d, J = 2.5 Hz, 1H), 7.56 (dd, J = 8.6, 2.8 Hz, 1H), 6.97 (d, J = 8.9 Hz, 1H), 4.76 (s, 2H), 1.58 (s, 9H). ^{13}C NMR (400 MHz, DMSO-D_6): δ 168.39, 160.35, 136.19, 130.58, 128.65, 117.82, 113.77, 83.09, 45.73, 27.76. HMRS (EI) calculated for $C_{12}H_{15}ClO_3$ 242.07; found 242.0710.

Synthesis of compound 16.

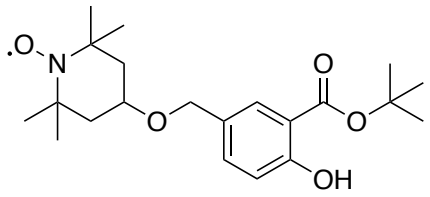

The procedure was adapted from Dessolin et al[183]. TEMPOL (86.6 mg, 0.5 mmol, 1 equi.) was stirred in a round bottom flask in 5 mL of THF. The flask was flushed with N_2 for 10 minutes while cooled on ice to 0°C. NaH (23 mg, 0.575 mmol, 1.15 equi.) was added to the reaction flask and the mixture was stirred at room temperature for an additional hour under N_2. After 1 hour, 5-chloromethyl salicylate t-butyl ester (**15**) (152.9 mg, 0.63 mmol, 1.25 equi.) dissolved in 2 mL of THF was added to the round bottom flask and the mixture was stirred at room temperature for 18 hours/overnight. The solvent was evaporated *in vacuo* to give a residue. The residue was re-dissolved in brine and the crude compound was extracted using ethyl acetate. The combined organic layers were dried over sodium sulphate before evaporation *in vacuo*. The crude compound was purified by column chromatography using 5:1 hexanes:acetone as the solvent system. The product was obtained as an orange residue in 58% yield. HRMS (ESI) calculated for $C_{21}H_{32}NO_5Na^+$ 401.2180; found 401.2178.

Synthesis of compound 17.

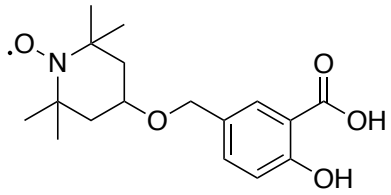

The t-butyl ester (**16**) (189.2 mg, 0.5 mmol, 1 equi.) was stirred in a round bottom flask and stirred 2 mL of DCM and 0.5 mL of TFA. The reaction was left at room temperature for 18 hours/overnight until TLC showed disappearance of the starting material. The reaction mixture was concentrated *in vacuo* with excess DCM. The product was obtained as an orange solid without further purification (89% yield). HRMS (ESI) calculated for $C_{17}H_{24}NO_5Na^+$ 345.1553; found 345.1630.

Synthesis of compound 18.

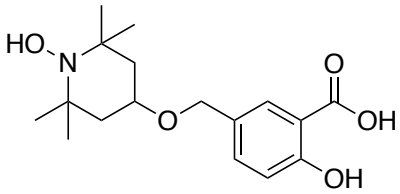

Compound 18 was obtained following the procedure outline for compound **12**. An orange residue was obtained in 65% yield. ^{1}H NMR (400 MHz, DMSO-D_6): δ 11.52 (broad s, 1H), 9.87 (s, 1H), 8.33 (d, J = 2.3 Hz, 1H), 7.99 (dd, J = 8.4, 2.4 Hz, 1H), 7.10 (d, J = 8.5 Hz, 1H), 4.33 (d, J = 5.6 Hz, 2H), 3.25 (s, 2H), 3.16 (s, 1H), 1.91-1.78 (m, 4H), 1.34 (s, 12H). ^{13}C NMR (400 MHz, DMSO-D_6): δ 169.34, 159.14, 134.45, 130.35, 128.27, 117.84, 112.84, 82.94, 42.56, 27.96, 27.35, 25.86, 24.98. HRMS (ESI) calculated for $C_{12}H_{25}NO_5Na^+$ 346.1623; found 346.1630.

Synthesis of compound 19.

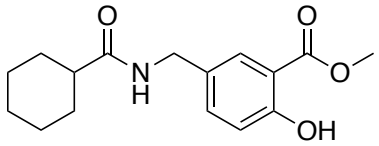

Compound 19 was obtained following the procedure outlined for compound **6**. The compound was purified by column chromatography using 1:1 hexanes:acetone as the solvent system. The product was obtained as an orange residue in 72% yield. ^{1}H NMR (400 MHz, DMSO-D_6): δ 11.18 (broad s, 1H), 8.20 (t, J = 5.9 Hz, 1H), 7.64 (d, J = 2.5 Hz, 1H), 7.36 (dd, J = 8.5, 2.4 Hz, 1H), 6.94 (d, J = 8.4 Hz, 1H), 4.16 (d, J = 6.1 Hz, 2H), 3.88 (s, 3H), 2.13 (tt, J = 11.5, 3.2 Hz, 1H), 1.70-1.59 (m, 4H), 1.38-1.12 (m, 6H). ^{13}C NMR (400 MHz, DMSO-D_6): δ 175.18, 171.90,

159.98, 134.67, 130.62, 128.61, 117.05, 112.50, 43.99, 40.94, 29.25, 25.47, 25.27. HRMS (EI) calculated for $C_{16}H_{21}NO_4$ 291.35; found 291.1

Synthesis of compound 20.

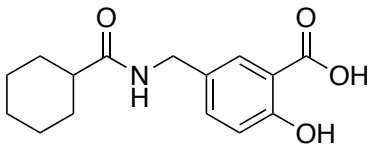

The methyl ester (**19**) (69.3 mg, 0.25 mmol, 1 equi.) was stirred in a round bottom flask with 0.5 mL of dioxane and 1.5 mL of a 20% NaOH solution. The mixture was stirred at 70°C for 2 hours with an air condenser. After 2 hours, the flask was cooled to room temperature and diluted with brine. The mixture was acidified with dilute HCl to adjust to the pH to 1. A white precipitate formed and was filtered to give the product without further purification (71% yield).
^{1}H NMR (400 MHz, DMSO-D_6): δ 10.38 (broad, s, 1H), 8.19 (t, J = 5.6 Hz, 1H), 7.64 (d, J = 2.5 Hz, 1H), 7.38 (dd, J = 8.4, 2.3 Hz, 1H), 6.94 (d, J = 8.5 Hz, 1H), 4.17 (d, J = 6.1 Hz, 2H), 3.88 (s, 3H), 2.18-2.08 (m, 1H), 1.74-1.56 (m, 4H), 1.41-1.06 (m, 4H). ^{13}C NMR (400 MHz, DMSO-D_6): δ 175.17, 171.85, 159.98, 134.68, 130.62, 128.60, 117.06, 112.51, 43.98, 40.93, 29.27, 25.48, 25.28. HMRS (EI) calculated for $C_{15}H_{19}NO_4$ 277.3; found 288.1315.

Synthesis of compound 21.

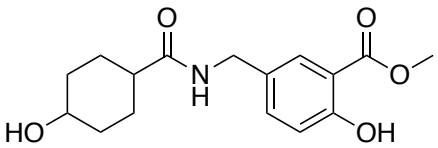

Compound **21** was obtained follow the procedure outlined for compound **6**. The compound was purified by column chromatography using 95:5 DCM:MeOH. A yellow solid was obtained in

68% yield. ^{1}H NMR (400 MHz, DMSO-D_6): δ 10.38 (s, 1H), 8.18 (t, J = 5.9 Hz, 1H), 7.64 (d, J = 2.3 Hz, 1H), 7.37 (dd, J = 8.5, 2.4 Hz, 1H), 6.93 (d, J = 8.4 Hz, 1H), 4.30 (d, J = 3.2 Hz, 1H), 3.88 (s, 3H), 2.14 (m, 1H), 1.87-1.57 (m, 4H), 1.48-1.35 (m, 4H). ^{13}C NMR (400 MHz, DMSO-D_6): δ 175.18, 171.90, 159.98, 134.67, 130.62, 128.61, 117.05, 112.50, 53.67, 43.99, 40.94, 29.25, 25.47, 25.27. HRMS (EI) calculated for $C_{16}H_{21}NO_5$ 307.14; found 307.1420.

Synthesis of compound 22.

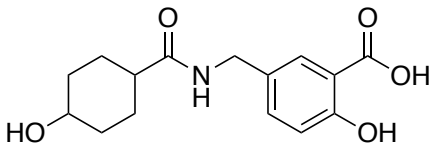

This compound was obtained following the procedure outlined for the compound **7**. A white glassy residue was obtained in 36% yield. ^{1}H NMR (400 MHz, DMSO-D_6): δ (400 MHz, DMSO-D_6): δ 10.38 (s, 1H), 8.18 (t, J = 5.9 Hz, 1H), 7.64 (d, J = 2.3 Hz, 1H), 7.37 (dd, J = 8.5, 2.4 Hz, 1H), 6.93 (d, J = 8.4 Hz, 1H), 4.30 (d, J = 3.2 Hz, 1H), 4.17 (d, J = 6.0 Hz, 2H), 2.14 (m, 1H), 1.87-1.57 (m, 4H), 1.48-1.35 (m, 4H), 1.18-1.06 (m, 1H). ^{13}C NMR (400 MHz, DMSO-D_6): δ 175.18, 171.90, 159.98, 134.67, 130.62, 128.61, 117.05, 112.50, 43.99, 40.94, 29.25, 25.47, 25.27. HRMS (EI) calculated for $C_{15}H_{19}NO_5$ 292.32; found 293.1252

Synthesis of compound 23.

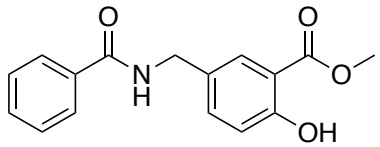

Compound **23** was obtained following the procedure outlined for the compound **6**. The crude compound was purified by column chromatography with 2:1 hexanes:acetone as the solvent

system. A light yellow residue was obtained in 74% yield. ^{1}H NMR (400 MHz DMSO-D_6): δ 10.42 (s, 1H), 9.04 (t, J = 5.9 Hz, 1H), 7.92-7.83 (m, 4H), 7.75 (d, J = 2.2 Hz, 1H), 7.69-7.58 (m, 1H), 7.56-7.44 (m, 6H), 6.96 (d, J = 9.3 Hz, 1H), 4.40 (d, J = 7.5 Hz, 2H), 3.88 (s, 3H). ^{13}C NMR (400 MHz, DMSO-D_6): δ 171.84, 167.37, 166.14, 160.06, 135.12, 134.24, 132.92, 131.31, 130.77, 130.49, 129.28, 129.02, 128.59, 128.35, 128.21, 127.21, 117.10, 112.49, 53.56, 41.91. HRMS (EI) calculated for $C_{16}H_{15}NO_4$ 285.10; found 285.0986.

Synthesis of compound 24.

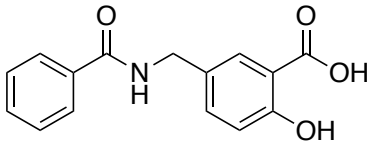

Compound **24** was obtained following the procedure outlined for compound **7**. A light yellow solid was obtained in 42% yield. ^{1}H NMR (400 MHz, DMSO-D_6): 11.04 (broad s, 1H), 9.03 (t, J = 5.8 Hz, 1H), 7.98-7.85 (m, 8H), 7.66-7.60 (m, 3H), 7.56-7.43 (m, 10H), 6.93 (d, J = 9.1 Hz, 1H), 4.40 (d, J = 6.0 Hz, 2H). ^{13}C NMR (400 MHz, DMSO-D_6): δ 171.84, 167.37, 166.12, 160.07, 135.11, 132.90, 130.76, 129.28, 128.59, 128.37, 127.21, 117.09, 112.49, 41.88. HRMS (EI) calculated for $C_{15}H_{13}NO_4$ 271.27; found 271.0861.

Synthesis of compound 25.

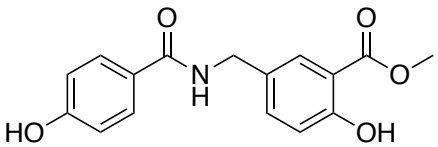

This procedure was adapted from Gopin et al[184]. 4-hydroxy benzoic acid (41.4 mg, 0.3 mmol, 1 equi.) was added to a round bottom flask with EDC-HCl (69.0 mg, 0.36 mmol, 1.2 equi.) and

HOBT (20.3 mg, 0.15 mmol, 0.5 equi.) in 2 mL of DMF. The mixture was stirred on ice at 0°C for 10 minutes. 5-aminomethyl salicylate methyl ester (**4**) (58.4 mg, 0.3 mmol, 1 equi.) was added to the round bottom flask and the mixture was stirred at room temperature for an additional 18 hours/overnight. Afterwards, the mixture was diluted with brine and the crude compound was extracted using ethyl acetate. The organic phases were combined and washed with brine before being dried over sodium sulphate. The solvent was evaporated *in vacuo* to give a yellow residue, which was then purified by silica column chromatography using a solvent system of 1:1 hexanes: acetone. A yellow oil was obtained as the purified product in 72% yield. ^{1}H NMR (400 MHz, DMSO-D_6): δ 10.41 (s, 1H), 9.98 (s, 1H), 8.77 (t, J = 5.8 Hz, 1H), 7.76-7.71 (m, 3H), 7.47 (dd, J = 8.5, 2.4, 1H), 6.95 (d, J = 8.6 Hz, 1H), 6.81-6.76 (m, 2H), 4.36 (d, J = 6.0 Hz, 2H), 3.88 (s, 3H). ^{13}C NMR (400 MHz, DMSO-D_6): δ 169.17, 165.81, 160.18, 158.92, 135.13, 131.07, 129.15, 128.741 124.92, 117.35, 114.82, 112.56, 52.45, 41.73, 30.71, 29.61. HRMS (EI) calculated for $C_{15}H_{13}NO_5$ 301.10; found 301.0968.

Synthesis of compound 26.

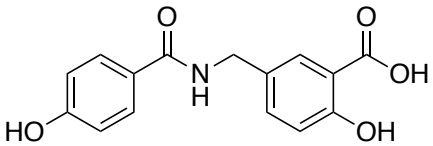

Compound **25** was hydrolyzed following the procedure outlined for compound **7**. A white solid was obtained in 78% yield. ^{1}H NMR (400 MHz, DMSO-D_6): δ 11.16 (broad s, 1H), 9.97 (s, 1H), 8.77 (t, J = 6.0 Hz, 1H), 7.80-7.70 (m, 3H), 7.46 (dd, J = 8.7, 2.5 Hz, 1H), 6.91 (d, J = 7.5 Hz, 1H), 6.83-6.76 (m, 2H), 4.36 (d, J = 6.1, 2H). ^{13}C NMR (400 MHz, DMSO-D_6): δ 169.20, 165.80, 160.20, 158.93, 135.16, 131.09, 129.16, 128.74, 124.95, 117.33, 114.86, 112.54, 41.74. HRMS (EI) calculated for $C_{15}H_{13}NO_5$ 287.27; found 287.0793.

Synthesis of 5-aminomethyl salicylate methyl ester (27).

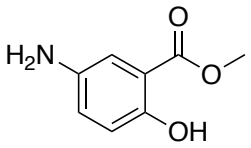

5-aminomethyl salicylic acid (153.13 mg, 1 mmol, 1 equi.) was added to a round bottom flask with 5 mL of methanol and H_2SO_4 (2.5 uL, 0.05 mmol, 0.05 equi.). The mixture was stirred at 65°C for 2 days using an air condenser. After 2 days, the solvent was concentrated *in vacuo* to give a dark brown residue. The residue was dissolved in a saturated solution of sodium bicarbonate and the crude product was extracted using ethyl acetate. The combined organic layers were dried over sodium sulphate and the solvents were concentrated *in vacuo*. The product was obtained as a light brown solid in 78% yield. ^{1}H NMR (400 MHz, DMSO-D_6): δ 10.29 (s, 1H), 8.89-8.27 (broad s, 2H), 7.50 (d, J = 8.0 Hz, 1H), 7.25 (d, J = 2.8 Hz, 1H), 6.98 (dd, J = 9.3, 3.0 Hz, 1H), 3.82 (s, 3H). ^{13}C NMR (400 MHz, DMSO-D_6): δ 167.63, 146.21, 126.54, 124.91, 122.00, 119.10, 114.74, 52.32. HRMS (EI) calculated for $C_8H_9NO_3$ 167.17; found 167.0894.

Synthesis of compound 28.

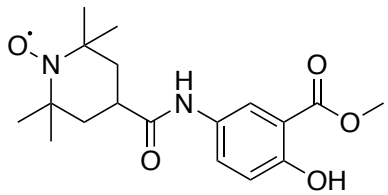

The compound was obtained following the procedure outlined for compound **7**. The crude product was purified by silica column chromatography using 95:5 DCM:MeOH as the solvent system. The product was obtained as a yellow oil in 82% yield. HRMS (ESI) calculated for $C_{18}H_{25}N_2O_5Na^+$ 372.1663; found 372.1661.

Synthesis of compound 29.

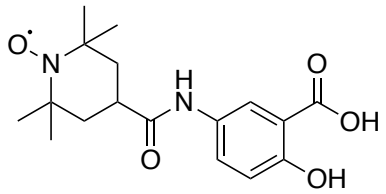

The compound was obtained following the procedure outlined **7**. The product was a light orange solid, obtained in 54% yield. HRMS (ESI) calculated for $C_{17}H_{23}N_2O_5Na^+$ 358.1503; found 358.1505.

Synthesis of compound 30.

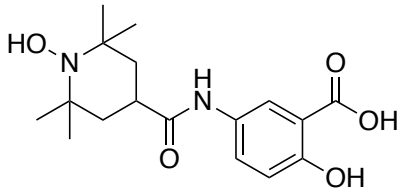

The compound was obtained following the procedure outlined for **8**. The product was obtained as a light orange solid in 49% yield. ^{1}H NMR (400 MHz, DMSO-D_6): δ 9.91 (broad s, 1H), 8.04 (d, J = 2.6 Hz, 1H), 7.64 (dd, J = 9.2, 2.9 Hz, 1H), 6.85 (d, J = 8.8 Hz, 1H), 1.88-1.70 (m, 2H), 1.65-1.52 (m, 4H), 0.91-0.85 (m, 12H). ^{13}C NMR (400 MHz, DMSO-D_6): 171.25, 169.03, 146.32, 126.54, 125.06, 122.46, 119.38, 114.75, 76.85, 27.96, 27.21, 29.86, 25.24. HRMS (ESI) calculated for $C_{17}H_{24}N_2O_5Na^+$ 359.16; found 359.1583.

Synthesis of compound 31.

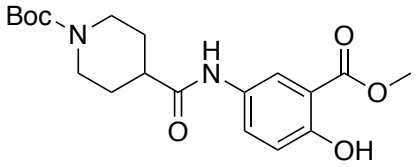

Compounds **9** and **27** were coupled following the procedure outlined for compound **6**. The crude compound was purified by column chromatography using 1:1 hexanes:acetone as the mobile phase. A light yellow residue was obtained in 74% yield. ^{1}H NMR (400 MHz, DMSO-D_6): δ 10.25 (s, 1H), 9.90 (s, 1H) 8.16 (d, J = 2.7 Hz, 1H), 7.63 (dd, J = 8.9, 5.3 Hz, 1H), 6.93 (d, J = 8.8 Hz, 1H), 3.97 (d, J = 12.1 Hz, 2H), 3.89 (s, 3H), 2.76 (broad s, 2H), 2.48-2.41 (m, 1H), 1.79-1.72 (m, 2H), 1.53-1.43 (m, 2H) 1.40 (s, 9H). ^{13}C NMR (400 MHz, DMSO-D_6): δ 172.75, 169.05, 155.85, 153.86, 131.22, 127.33, 120.06, 117.51, 112.34, 78.64, 52.46, 42.48, 28.13, 28.07. HRMS (ESI) calculated for $C_{19}H_{26}N_2O_6Na^+$ 401.1704; found 401.1689.

Synthesis of compound 32

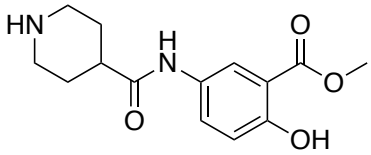

Compound **32** was obtained following the Boc deprotection procedure outlined for compound **11**. The product was obtained as a light yellow oil without further purification. ^{1}H NMR (400 MHz, DMSO-D_6): δ 10.34-10.17 (broad s, 1H), 10.02 (s, 1H), 8.66-8.54 (m, 1H), 8.42-8.27 (m, 1H), 8.15 (d, J = 2.8 Hz, 1H), 7.63 (dd, J = 9.7, 3.4 Hz, 1H), 6.94 (d, J = 8.9 Hz, 1H), 3.89 (s, 3H), 2.93 (q, J = 11.9 Hz, 2H), 2.63-2.54 (m, 1H), 1.96-1.90 (m, 2H), 1.86-1.73 (m, 2H). ^{13}C NMR (400 MHz, DMSO-D_6): δ 172.77, 169.06, 155.87, 153.89, 131.24, 127.42, 120.08, 117.51,

112.44, 78.66, 52.48, 42.48. HRMS (ESI) calculated for $C_{14}H_{18}N_2O_4Na^+$ 301.30; found 301.2995.

Synthesis of compound 33

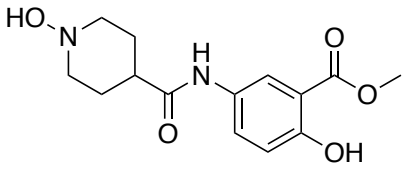

Compound **33** was obtained following the oxidation procedure outlined for compound **12**. The product was obtained as a light yellow residue without further purification. ^{1}H NMR (400 MHz, DMSO-D_6): δ 10.35-10.13 (broad s, 1H), 10.03 (s, 1H), 8.67-8.53 (m, 1H), 8.41-8.26 (m, 1H), 8.15 (d, J = 2.7 Hz, 1H), 7.63 (dd, J = 8.9, 3.2 Hz, 1H), 6.94 (d, J = 8.9 Hz, 1H), 3.89 (s, 3H), 3.33 (d, J = 12.5 Hz, 2H), 2.93 (q, J = 11.9 Hz, 2H), 2.65-2.58 (m, 1H), 1.97-1.88 (m, 2H), 1.87-1.71(m, 2H). ^{13}C NMR (400 MHz, DMSO-D_6): δ 172.77, 169.06, 155.87, 153.89, 131.24, 127.42, 120.08, 117.51, 112.44, 78.66, 52.48, 42.48. HMRS (ESI) calculated for $C_{14}H_{18}N_2O_5Na^+$ 317.1113; found 317.1114.

Synthesis of compound 34

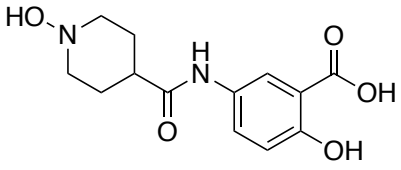

The methyl ester of compound **33** was removed following the hydrolysis procedure outlined for compound **7**. The product was obtained in 45% yield without further purification. ^{1}H NMR (400 MHz, DMSO-D_6): δ 10.35-10.13 (broad s, 1H), 10.03 (s, 1H), 8.67-8.53 (m, 1H), 8.41-8.26 (m, 1H), 8.15 (d, J = 2.7 Hz, 1H), 7.63 (dd, J = 8.9, 3.2 Hz, 1H), 6.94 (d, J = 8.9 Hz, 1H), 3.33 (d, J =

12.5 Hz, 2H), 2.93 (q, J = 11.9 Hz, 2H), 2.65-2.58 (m, 1H), 1.97-1.88 (m, 2H), 1.87-1.71(m, 2H).[13]C NMR (400 MHz, DMSO-D_6): δ 172.76, 169.04, 155.83, 153.93, 131.26, 127.42, 120.04, 117.53, 112.46, 78.66, 52.36. HMRS (ESI) calculated for $C_{13}H_{16}N_2O_5Na^+$ 303.10; found 303.0957.

Synthesis of 4-carboxy-1-carboxy-2,2,6,6-tetramethylpiperidine (35).

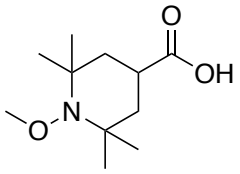

This compound was obtained following a procedure as described by Verderosa et al.[185] Briefly, 4-carboxy TEMPO (50 mg, 0.25 mmol, 1 equi.) was stirred in 1.5 mL of DMSO. $FeSO_4 – 7\ H_2O$ (160.5 mg, 0.675 mmol, 2.7 equi.) was added and 100 µL H_2O_2 (1.075 mmol, 4.3 equi.), dropwise. The mixture was stirred on ice for 10 minutes, and then an additional 1.5 hours at room temperature. The reaction mixture was diluted with brine and the pH was adjusted to pH 1 using dilute HCl. The crude compound was extracted with diethyl ether. The combined organic phases were washed with dilute HCl and dried over sodium sulphate. The solvent was evaporated *in vacuo* to give a white solid in 35% yield. [1]H NMR (300 MHz, DMSO-D_6): δ 3.55 (s, 3H), 2.54 (s, 3H), 1.72-1.62 (m, 2H), 1.50-1.34 (m, 2H), 1.15 (s, 6H), 1.05 (s, 6H). [13]C NMR 400 MHz, DMSO-D_6): δ 175.43, 78.67, 51.68, 28.98, 27.63 25.45, 25.32. HRMS (EI) calculated for $C_{11}H_{21}NO_3$ 215.15; found 215.1521.

Synthesis of compound 36.

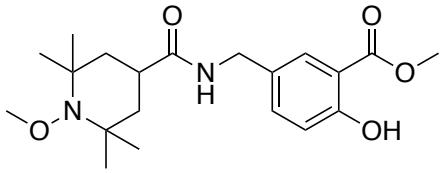

This compound was obtained coupling compound **4** and **35**, following the procedure outlined for compound **6**. The crude compound was purified by column chromatography using 2:1 hexanes: acetone as the mobile phase. A colourless oil was isolated in 49% yield. ^{1}H NMR (400 MHz, DMSO-D_6): δ 10.05 (s, 1H), 8.18 (t, J = 3.4 Hz, 1H), 7.65 (d, J = 2.4 Hz, 1H), 7.38 (dd, J = 8.5, 2.4 Hz, 1H), 6.92 (d, J = 8.4 Hz, 1H), 3.88 (s, 3H), 2.54 (s, 3H), 1.87-1.57 (m, 3H), 1.48-1.35 (m, 3H), 1.16 (s, 6H), 1.04 (s, 6H). ^{13}C NMR (400 MHz, DMSO-D_6): δ 175.18, 171.90, 159.98, 134.67, 130.62, 128.61, 117.05, 112.50, 53.67, 43.99, 40.94, 29.25, 25.47, 25.27. HRMS (ESI) calculated for $C_{20}H_{30}N_2O_5Na^+$ 401.2023; found 401.2053.

Synthesis of compound 37.

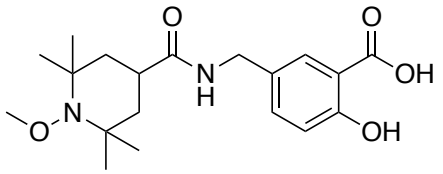

This compound was obtained following the procedure outlined for compound **7**. A yellow solid was isolated in 67% yield. ^{1}H NMR (400 MHz, DMSO-D_6): δ 10.05 (s, 1H), 8.18 (t, J = 3.4 Hz, 1H), 7.65 (d, J = 2.4 Hz, 1H), 7.38 (dd, J = 8.5, 2.4 Hz, 1H), 6.92 (d, J = 8.4 Hz, 1H), 3.88 (s, 3H), 2.54 (s, 3H), 1.87-1.57 (m, 3H), 1.48-1.35 (m, 3H), 1.16 (s, 6H), 1.04 (s, 6H). ^{13}C NMR (400 MHz, DMSO-D_6): δ 175.18, 171.90, 159.98, 134.67, 130.62, 128.61, 117.05, 112.50, 53.67, 43.99, 40.94, 29.25, 25.47, 25.27. HRMS (ESI) calculated for $C_{19}H_{28}N_2O_5Na^+$ 387.1897; found 387.1896.

Model Compounds: Barbiturates

Synthesis of N-acetyl 5-amino barbituric acid (38).

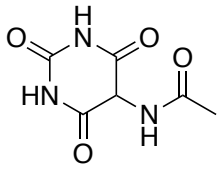

Compound 38 was prepared following a procedure adapted from Hurst et al[186] and Cavalieri et al[187]. Diethyl acetoamindo malonate (2.17 g, 10 mmol, 1 equi.) and urea (600 mg, 10 mmol, 1 equi.) were added to a round bottom flask woth 15 mL of ethanol. Sodium metal (380 mg, 16.5 mmol, 1.65 equi.) was added to the flask and the mixture was stirred until everything was dissolved. The flask was then heated to 95°C and refluxed for 3 hours. After 3 hours, the flask was cooled to room temperature and a yellow precipitate formed. Warm water was added to dilute the reaction mixture and concentrated HCl was added dropwise until the solution was acidic. The flask was placed in the refrigerator for 1 hour to form more precipitate. A light yellow solid was obtained by suction filtration in 56% yield. ^{1}H NMR (400 MHz, DMSO-D_6): δ 11.29 (s, 2H), 8.91 (d, J = 6.0 Hz, 1H), 4.90 (d, J = 6.3 Hz, 1H), 1.86 (s, 3H). ^{13}C NMR (400 MHz, DMSO-D_6): δ 169.79, 167.47, 150.45, 54.31, 21.48. HRMS (EI) calculated for $C_6H_7N_3O_4$ 185.14; found 185.0456.

Synthesis of 5-amino barbituric acid (39).

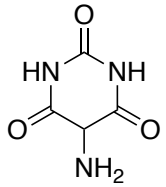

The procedure for removal of the acetyl group was adapted from Cavalieri et al[187]. N-acetyl 5-amino barbituric acid (**38**) (143 mg, 1 mmol, 1 equi.) was added to a round bottom flask. 0.5 mL of concentrated HCl was added to the flask and the mixture was stirred at 95°C for 15 minutes. The reaction flask was cooled to room temperature and water was added dropwise until a light yellow precipitate forms. The flask was left in the refrigerator for 18 hours/overnight. A pink solid was obtained by suction filtration in 15% yield. ^{1}H NMR (400 MHz, D_2O): δ 3.35 (s, 1H). ^{13}C NMR (400 MHz, D_2O): δ 164.86, 12.70, 92.06. HRMS (EI) calculated for $C_4H_5N_3O_3$ 143.10; found 143.0359.

Synthesis of compound 40.

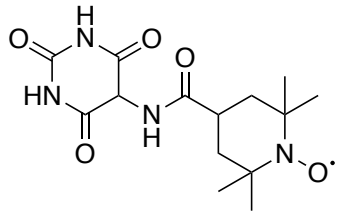

4-carboxy TEMPO (48 mg, 0.24 mmol, 1 equi.) was stirred in DMF with triethylamine (13.9 μL, 0.1 mmol, 0.41 equi.). EDC-HCl (46 mg, 0.24 mmol, 1 equi.) and HOBT (32.4 mg, 0.24 mmol, 1 equi.) were both added to the round bottom flask. The mixture was stirred at 0°C for 5 minutes. Amino barbiturate (**39**) (28.6 mg, 0.2 mmol, 0.83 equi.) was added to the flask and the mixture was stirred for an additional 18 hours at room temperature. The next day, the reaction mixture was diluted with brine and the crude compound was extracted using ethyl acetate. The combined organic phases were washed with brine and dried over sodium sulphate. The solvent was evaporated *in vacuo* to give an orange residue that was purified by column chromatography using 3:1 hexanes:acetone as the mobile phase. The product was isolated as an orange solid in 24% yield. HMRS (EI) calculated for $C_{14}H_{21}N_4O_5$ 325.15; found 325.1512.

Synthesis of compound 41.

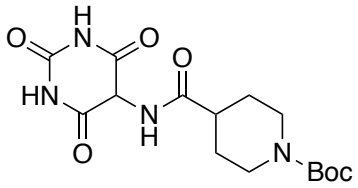

Boc-protected piperidine (**9**) (45 mg, 0.20 mmol, 1 equi.) was stirred in a round bottom flask with DMF, DIPEA (176 µL, 1 mmol, 5 equi.) and HATU (100 mg, 0.26 mmol, 1.3 equi.) at room temperature. After 15 minutes, amino barbiturate (**39**) (35 mg, 0.24 mmol, 1.2 equi.) was added to the flask and the mixture was stirred at room temperature for 18 hours. The next day, the reaction mixture was diluted with brine and the crude compound was extracted using ethyl acetate. The combined organic phases were washed with additional brine and dried over sodium sulphate. The solvent was evaporated *in vacuo* to give a brown residue. The crude compound was purified by column chromatography using 2:1 hexanes:acetone as the solvent system. The product was isolated in 56% yield. ^{1}H NMR (400 MHz, DMSO-D_6): δ 11.35 (s, 2H), 8.89 (d, J = 5.9 Hz, 1H), 4.86 (d, J = 6.4 Hz, 1H), 3.85 (d, J = 15.2 Hz, 2H), 2.87 (broad s, 2H), 2.46-2.32 (m, 1H), 1.75 (dd, J = 13.4, 3.1 Hz, 2H), 1.47-1.32 (m, 11H). ^{13}C NMR (400 MHz, DMSO-D_6): δ 175.23, 169.84, 167.43, 150.46, 78.63, 28.04, 27.34, 21.45. HMRS (ESI) calculated for $C_{15}H_{22}N_4O_6Na^+$ 377.14; found 377.1437.

Synthesis of compound 42.

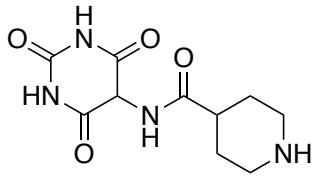

This compound was obtained following the procedure outlined for compound **11**. The product was isolated in quantitative yield and used without further purification. ^{1}H NMR (400 MHz, DMSO-D_6): δ 11.34 (s, 2H), 8.92 (d, J = 5.8 Hz, 1H), 4.92 (d, J = 6.5 Hz, 1H), 3.89 (d, J = 15.1 Hz, 2H), 2.86 (broad s, 2H), 2.43-2.31 (m, 1H), 1.78 (dd, J = 14.4, 3.7 Hz, 2H), 1.45-1.39 (m, 2H). ^{13}C NMR (400 MHz, DMSO-D_6): δ 169.82, 167.48, 150.62, 78.84, 27.97, 27.35. HMRS (ESI) calculated for $C_{10}H_{14}N_4O_4Na^+$ 277.09; found 277.0912.

Synthesis of compound 43.

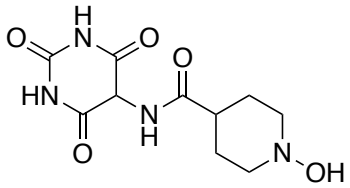

This compound was obtained following the procedure outlined for compound **22**. ^{1}H NMR (400 MHz, DMSO-D_6): δ 11.52 (s, 2H), 8.92 (d, J = 5.2 Hz, 1H), 4.96 (d, J = 6.7 Hz, 1H), 3.92 (d, J = 14.8 Hz, 2H), 2.91 (broad s, 2H), 2.39-2.28 (m, 1H), 1.74 (dd, J = 14.7, 4.1 Hz, 2H), 1.52-1.43 (m, 2H). ^{13}C NMR (400 MHz, DMSO-D_6): δ 169.48, 167.82, 150.27, 78.19, 27.52, 27.14. HMRS (ESI) calculated for $C_{10}H_{14}N_4O_5Na^+$ 293.09; found 293.0862.

Model Compounds: Carbohydrates

Synthesis of 2-deoxy-2-[p-methoxybenzylidene(amino)]-D-glucopyranose (44).

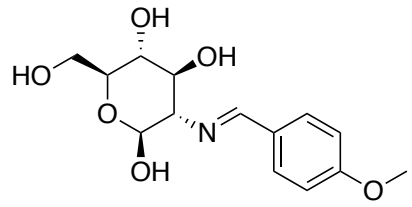

Protection of the glucosamine was followed by the procedure outlined by Biswas et al[188]. Glucosamine HCl (431 mg, 2 mmol, 1 equi.) was added to a round bottom flask. 2 mL of 1 M NaOH solution was added along with p-anisaldehyde (291 uL, 2.08 mmol, 2.08 equi.) dropwise. The mixture was stirred on ice at 0°C for 2 hours. A white solid formed and was obtained by suction filtration. The solid was washed with cold water and diethyl ether. A white solid was obtained in 85% yield and used without further purification. ^{1}H NMR (400 MHz, DMSO-D_6): δ 8.11 (s, 1H), 7.68 (d, J = 8.8 Hz, 2H), 6.98 (d, J = 8.6 Hz, 2H), 6.52 (d, J = 6.5 Hz, 1H), 4.93 (d, J = 4.9 Hz, 1H), 4.81 (d, J = 5.5 Hz, 1H), 4.68 (t, J = 6.8 Hz, 1H), 4.54 (t, J = 5.5 Hz, 1H), 3.80 (s, 3H), 3.75-3.68 (m, 1H), 3.52-3.38 (m, 2H), 3.26-3.09 (m, 2H), 2.82-2.75 (m, 1H). ^{13}C NMR (400 MHz, DMSO-D_6): δ 161.22, 160.05, 129.64, 129.12, 113.91, 95.64, 78.21, 76.89, 74.61, 70.38, 61.29, 55.29. HRMS (EI) calculated for $C_{14}H_{19}NO_6$ 297.31; found 297.1237.

Synthesis of 1, 3, 4, 6-tetra-O-acetyl-2-deoxy-2-[p-methoxybenzylidene(amino)]-β-D-glucopyranose (45).

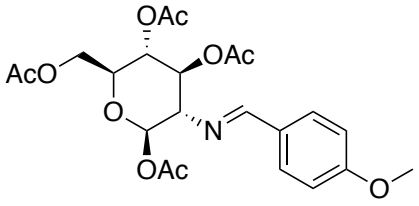

Protection of the glucosamine was followed by the procedure outlined by Biswas et al[188]. Compound **40** (387.4 mg, 1.3 mmol, 1 equi.) was added to a round bottom flask with 2 mL of pyridine. The flask was stirred under N_2 on ice at 0°C for 5 minutes. Acetic anhydride (552 uL, 5.3 mmol, 4.07 equi.) was added dropwise. The reaction mixture was stirred on ice for an additional 2 hours, then at room temperature for 18 hours/overnight. Ice cold water was added to the flask and a white solid precipitated. The white solid was obtained by suction filtration in 72%

yield and used without further purification. ^{1}H NMR (400 MHz, DMSO-D_6): δ 8.28 (s, 1H), 7.65 (d, J = 8.7 Hz, 2H), 6.99 (d, J = 8.2 Hz, 2H), 6.06 (d, J = 8.4 Hz, 2H), 5.44 (t, J = 10.3 Hz, 1H), 4.96 (t, J = 9.6 Hz, 1H), 4.30-4.18 (m, 2H), 4.03-3.97 (m, 1H), 3.79 (s, 3H), 3.44 (dd, J = 9.6, 8.5 Hz, 1H), 2.01 (s, 3H), 1.98 (s, 3H), 1.98 (s, 3H), 1.81 (s, 3H). ^{13}C NMR (400 MHz, DMSO-D_6): δ 170.064 169.45, 168.99, 168.61, 164.45, 161.82, 129.92, 128.26, 114.21, 92.52, 72.33, 72.22, 71.52, 67.80, 61.65, 55.37, 20.55, 20.46, 20.45, 20.22. HRMS (ESI) calculated for $C_{22}H_{27}NO_{10}$ 465.46Na^{+} 488.1535; found 488.1533.

Synthesis of 1, 3, 4, 6-tetra-O-acetyl-β-D-glucosamine hydrochloride (46).

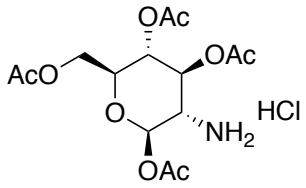

Protection of the glucosamine was followed by the procedure outlined by Biswas et al[188]. The acetyled glucosime (**41**) (178 mg, 0.37 mmol, 1 equi.) was added to a round bottom flask with 1.25 mL of acetone and 0.8 mL of 5 M HCl. The mixture was stirred at room temperature for 30 minutes. Afterwards 10 mL of diethyl ether was added and the flask was stirred for an additional hour at room temperature. A white solid precipitated and was obtained by suction filtration. The product was obtained as a white solid in 64% without further purification. ^{1}H NMR (400 MHz, DMSO-D_6): δ 8.61 (s, 3H), 5.89 (d, J = 10.2 Hz, 1H), 5.34 (t, J = 8.7 Hz, 1H), 4.93 (t, J = 8.8 Hz, 1H), 4.19 (dd, J = 12.6, 4.4 Hz, 1H), 4.10-3.96 (m, 2H), 3.57 (t, J = 10.2 Hz, 1H), 2.17 (s, 3H), 2.03 (s, 3H), 2.00 (s, 3H), 2.00-1.98 (m, 6H). ^{13}C NMR (400 MHz, DMSO-D_6): δ 169.94,

169.79, 169.29, 168.63, 90.19, 71.59, 71.59, 70.40, 67.77, 61.24, 52.13, 20.89, 20.81, 20.47. HRMS (ESI) calculated for $C_{14}H_{21}NO_9Na^+$ 370.1129; found 370.1114.

Synthesis of 1, 3, 4, 6-tetra-O-acetyl-β-D-glucosamine (47).

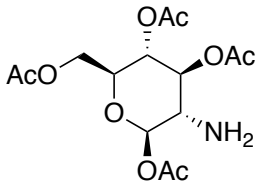

Protection of the glucosamine was followed by the procedure outlined by Biswas et al[188]. Peracetylated glucosamine hydrochloride (**42**) (90 mg, 0.23 mmol, 1 equi.) was added to a round bottom flask with 1.5 mL of DCM and 1.5 mL of a 1 M solution of sodium carbonate. The mixture was stirred at room temperature for 30 minutes. Afterwards, the mixture was diluted with brine and product was extracted using DCM. The combined organic phases were washed with brine and dried over sodium sulphate. The solvent was evaporated *in vacuo* to give a white solid in 92% yield. The product was used without further purification. ^{1}H NMR (400 MHz, DMSO-D_6): δ 5.54 (d, J = 8.1 Hz, 1H), 5.04 (t, J = 10.1 Hz, 1H), 4.80 (t, J = 9.8 Hz, 1H), 4.15 (dd, J = 12.8, 5.0 Hz, 1H), 3.98-3.91 (m, 2H), 2.74 (dd, J = 18.7, 10.2 Hz, 1H), 2.10 (s, 3H), 1.99-1.96 (m, 9H), 1.65 (broad s, 2H). ^{13}C NMR 170.00, 169.91, 169.35, 169.14, 94.71, 74.57, 71.32, 68.32, 61.69, 55.09, 20.71, 20.64, 20.49, 20.41. HRMS (ESI) calculated for $C_{14}H_{21}NO_9Na^+$ 370.1129; found 370.1114.

Synthesis of compound 48.

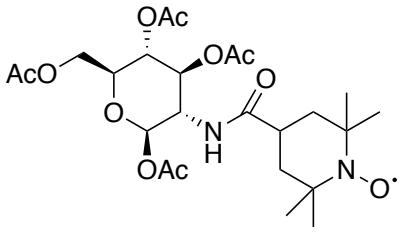

This compound was obtained by coupling compound **43** to 4-carboxy TEMPO, following the procedure outlined for compound **6**. The crude compound was purified by column chromatography using 2:1 hexanes:acetone as the mobile phase. The product was isolated as a light yellow residue that crystalizes in 80% yield. HRMS (ESI) calculated for $C_{24}H_{37}N_2O_{11}Na^+$ 552.2291; found 552.2295.

Synthesis of compound 49.

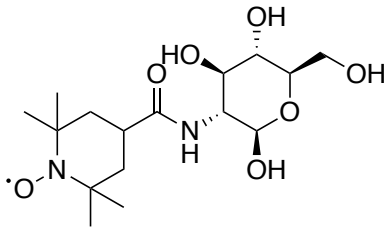

The peracetylated glucosamine (**44**) (106 mg, 0.2 mmol, 1 equi.) was stirred in dry methanol at 0°C under N_2. 25% NaOMe (2 mL) was added to the reaction flask and the mixture was stirred at room temperature for 24 hours. To work up the reaction, Amberlyst resin was added to neutralize the reaction and the filtered through a Pasteur pipette with cotton at the bottom. The solvent was evaporated *in vacuo* to give a brown residue. HRMS (ESI) calculated for $C_{16}H_{29}N_2O_7Na^+$ 384.19; found 384.1872.

Synthesis of 1, 3, 4, 6-tetra-O-benzoyl-2-deoxy-2-[p-methoxybenzylidene(amino)]-β-D-glucopyranose (50).

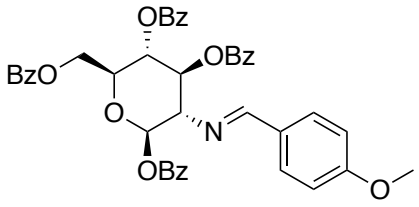

Compound **44** (350 mg, 1.17 mmol, 1 equi.) was stirred in DCM. Triethylamine (1.79 mL, 12.87 mmol, 11 equi.) and benzoyl chloride (1.22 mL, 10.53 mmol, 9 equi.) were added to the round bottom flask. The mixture was stirred at room temperature. After 18 hours, the mixture was diluted with saturated sodium bicarbonate solution. The crude compound was extracted using DCM and the combined organic phases were washed with saturated sodium bicarbonate solution. The organic phases were dried over sodium sulphate and the solvent was evaporated *in vacuo* to give a golden residue. The product obtained without further purification in 84% yield. ^{1}H NMR (400 MHz, DMSO-D_6): δ 8.05 (s, 1H), 8.17-8.12 (m, 10H), 7.97-7.92 (m, 5H), 7.89-7.75 (m, 10H), 7.69-7.59 (m, 14H), 7.57-7.35 (m, 13H), 6.85 (d, J = 9.6 Hz, 2H), 6.52 (d, J = 8.1 Hz, 1H), 6.09 (t, J = 8.8 Hz, 1H), 5.65 (t, J = 10.3 Hz, 1H), 4.82 (td, J = 10.0, 3.1 Hz, 1H), 4.59-4.48 (m, 2H), 4.06 (dd, J = 9.6, 8.2 Hz, 1H), 3.86 (s, 1H), 3.69 (s, 3H). ^{13}C NMR (400 MHz, DMSO-D_6): δ 191.32, 167.39, 162.40, 135.17, 132.87, 131.82, 130.75, 129.36, 129.28, 128.57, 128.03, 114.53, 114.18, 93.36, 73.30, 71.97, 69.10, 62.45, 55.70, 55.28. HRMS (ESI) calculated for $C_{45}H_{46}N_2O_{12}Na^+$ 829.2964; found 829.2948.

Synthesis of 1, 3, 4, 6-tetra-benzoyl-β-D-glucosamine hydrochloride (51).

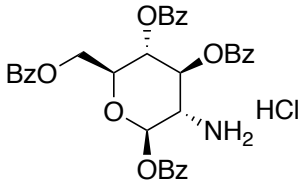

The compound was obtained following the procedure outlined for compound **46**. The product was obtained as a fine white solid in 67% yield. ^{1}H NMR (400 MHz, DMSO-D_6): δ 8.98-8.79 (broad s, 3H), 8.20-8.12 (m, 10H), 7.97-7.87 (m, 5H), 7.85-7.78 (m, 6H), 7.68-7.59 (m, 13H), 7.53-7.42 (m, 7H), 6.43 (d, J = 8.5 Hz, 1H), 5.99 (t, J = 9.8 Hz, 1H), 5.61 (t, J = 9.6 Hz, 1H), 4.60 (dt, J = 10, 3.5 Hz, 1H), 4.48 (d, J = 3.7 Hz, 2H), 4.18 (t, J = 9.5 Hz, 1H). ^{13}C NMR (400 MHz, DMSO-D_6): δ 171.21, 170.45, 167.32, 165.33, 165.22, 164.75, 163.81, 162.27, 135.19, 130.42, 130.19, 129.55, 129.38, 129.27, 128.73, 128.58.

Synthesis of 1, 3, 4, 6-tetra-benzozyl-β-D-glucosamine (52).

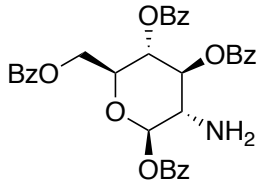

The compound was obtained following the procedure outlined for **47**. The product was obtained as a white solid in 78% yield. ^{1}H NMR (400 MHz, DMSO-D_6): δ 8.80 (d, J = 9.4 Hz, 1H), 8.00-7.33 (m, 36H), 6.28 (d, J = 9.8, 1H), 5.92 (t, J = 10.0 Hz, 1H), 5.69 (t, J = 9.7 Hz, 1H), 4.82 (q, J = 9.5 Hz, 1H), 4.60-4.51 (m, 3H). ^{13}C NMR (400 MHz, DMSO-D_6): δ 167.36, 167.07, 165.37, 165.35, 164.73, 164.24, 134.29, 134.04, 133.82, 133.70, 133.52, 132.82,131.53, 130.89, 129.49, 129.29, 129.27, 129.13, 129.03, 128.79, 128.70, 128.64, 128.56, 128.43, 128.22, 126.88, 93.11, 73.20, 71.99, 69.19, 62.41, 52.81. HRMS (ESI) calculated for $C_{34}H_{29}NO_9Na^+$ 618.1740; found 618.1719.

Synthesis of compound 53.

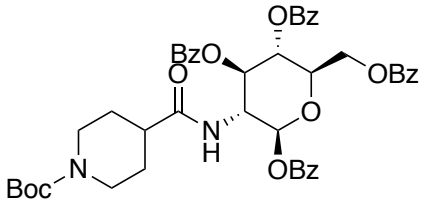

The compound was obtained by coupling compound **52** and **9** following the procedure outlined for compound **6**. The crude compound was purified by silica column chromatography using 2:1 hexanes:acetone. The product was obtained in 67% yield. ^{1}H NMR (400 MHz, DMSO-D_6): δ 12.29 (broad s, 1H), 8.80 (d, J = 9.7 Hz, 2H) 7.99-7.92 (m, 9H), 7.88-7.84 (m, 4H), 7.80-7.76 (m, 5H), 7.70-7.38 (m, 38H), 6.28 (d, J = 8.6 Hz, 2H), 5.91 (t, J = 10.1 Hz), 5.68 (t, J = 9.0 Hz, 3H), 4.18 (q, J = 9.3 Hz, 2H), 4.60-4.48 (m, 6H), 3.88-3.77 (m, 2H), 2.91-2.72 (m, 2H), 2.44-2.35 (m, 1H), 1.78 (dd, J = 13.0, 3.0 Hz, 2H), 1.44-1.28 (m, 12H). ^{13}C NMR (DMSO-D_6): δ 175.68, 167.05, 165.36, 164.71, 164.23, 153.87, 134.03, 133.82, 133.70, 133.51, 131.54, 129.49, 129.29, 129.25, 129.04, 128.79, 128.44, 12822, 126.88, 93.09, 78.62, 73.22, 71.99, 69.20, 52.20, 28.07. HRMS (ESI) calculated for $C_{45}H_{46}N_2O_{12}Na^+$ 829.2964; found 829.2948.

Synthesis of compound 54.

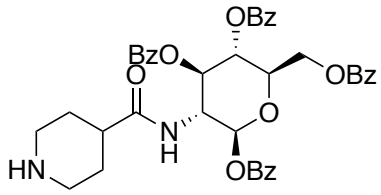

The compound was obtained following the procedure outlined for compound **11**. The product was isolated as dark yellow crystals in quantitative yield and used without further purification.

^{1}H NMR (400 MHz, DMSO-D_6): δ 8.71 (broad s, 1H), 8.37 (d, J = 8.6 Hz, 1H), 8.17-7.40 (m, 25 H), 6.36 (d, J = 9.2 Hz, 1H0, 6.18 (d, J = 8.2 Hz, 1H), 5.94 (q, J = 9.2 Hz, 1H), 5.78 (t, J = 10.3 Hz, 1H), 5.66-5.60 (m, 1H), 4.55-4.47 (m, 2H), 3.28 (m, 2H), 2.61-2.52 (m, 1H), 2.00-1.91 (m, 2H), 1.74-1.60 (m, 2H). ^{13}C NMR (400 MHz, DMSO-D_6): δ 174.80, 167.36, 132.95, 129.58, 129.42, 129.29, 129.24, 129.06, 129.02, 128.90, 128.80, 128.71, 128.59, 128.46, 128.29, 128.18, 128.14, 127.47, 126.89, 42.48, 37.65, 24.66. HRMS (ESI) calculated for $C_{40}H_{28}N_2O_{10}Na^+$ 729.24; found 729.2424.

Synthesis of compound 55.

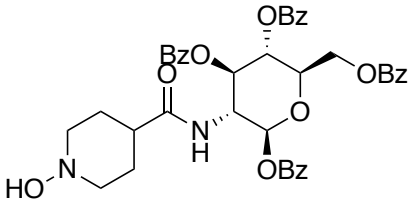

This compound was obtained following the procedure outlined for compound **12**.

^{1}H NMR (400 MHz, DMSO-D_6): δ 8.71 (broad s, 1H), 8.37 (d, J = 8.6 Hz, 1H), 8.17-7.40 (m, 25 H), 6.36 (d, J = 9.2 Hz, 1H0, 6.18 (d, J = 8.2 Hz, 1H), 5.94 (q, J = 9.2 Hz, 1H), 5.78 (t, J = 10.3 Hz, 1H), 5.66-5.60 (m, 1H), 4.55-4.47 (m, 2H), 3.28 (m, 2H), 2.61-2.52 (m, 1H), 2.00-1.91 (m, 2H), 1.74-1.60 (m, 2H). ^{13}C NMR (400 MHz, DMSO-D_6): δ 174.84, 167.33, 165.49, 165.33, 158.32, 134.49, 134.35, 134.27, 134.09, 133.85, 133.60, 130.80, 129.57, 129.43, 129.30, 129.08, 129.02, 128.93, 128.80, 128.75, 128,60, 128.16, 127.45, 126.87, 91.22, 73. 17, 70.49, 69.64, 63.65, 42.46, 37.67, 24.67. HRMS (ESI) calculated for $C_{40}H_{38}N_2O_{11}Na^+$ 745.24; found 745.2373.

Synthesis of compound 56.

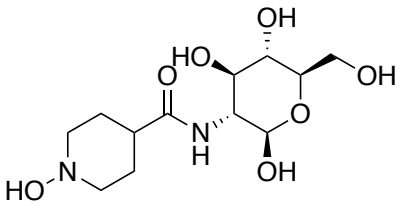

This compound was obtained following the procedure outlined for compound **49**. The product was obtained was a brown residue in 49% yield. ^{1}H NMR (400 MHz, DMSO-D_6): δ 8.13 (s, 1H), 6.32 (d, J = 6.1 Hz, 1H), 4.83 (d, J = 5.2 Hz, 1H), 4.92 (d, J = 5.9 Hz, 1H), 4.73 (t, J = 6.8 Hz, 1H), 4.47 (t, J = 5.2 Hz, 1H), 3.89 (d, J = 15.1 Hz, 2H), 3.81-3.72 (m, 2H), 2.81 (broad s, 2H), 2.41-2.29 (m, 1H), 1.69 (dd, J = 14.8, 2.9 Hz, 2H).^{13}C NMR (400 MHz, DMSO-D_6): δ 153.80, 129.56, 129.21, 114.19, 85.62, 78.61, 74.23, 70.39, 28.42, 27.96. HMRS (ESI) calculated for $C_{12}H_{22}N_2O_7Na^+$ 329.13; found 329.1324.

Model Compounds: Anthranilates

Synthesis of compound 57.

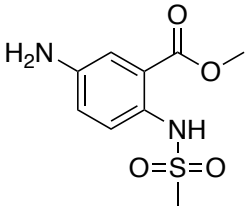

5-amino-2-methanesulfonamido benzoic acid (230 mg, 1 mmol, 1 equi.) was added to a round bottom flask with 5 mL of MeOH and H_2SO_4 (2.5 uL, 0.05 mmol, 0.05 equi.). The mixture was stirred at 65°C for 2 days using an air condenser. After 2 days, the solvent was concentrated *in vacuo* to give a dark red residue. The residue was dissolved in a saturated solution of sodium bicarbonate and the crude product was extracted using ethyl acetate. The combined organic layers were dried over sodium sulphate and the solvents were concentrated *in vacuo*. The product

was obtained as a light brown solid in 83% yield. ^{1}H NMR (400 MHz, DMSO-D_6): δ 9.16 (s, 1H), 7.19 (d, J = 8.6 Hz, 1H), 7.12 (d, J = 2.5 Hz, 1H), 6.80 (dd, J = 8.6, 2.7 Hz, 1H), 5.35 (s, 2H), 3.82 (s, 3H), 2.91 (s, 3H). ^{13}C NMR (400 MHz, DMSO-D_6): δ 167.60, 146.24, 126.55, 124.93, 122.01, 119.12, 114.76, 52.32. HRMS (EI) calculated for $C_9H_{12}N_2O_4S$ 244.27; found 224.0419.

Synthesis of compound 58.

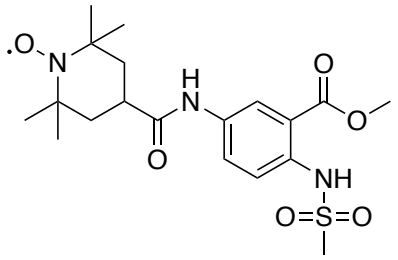

This compound was obtained by coupling compounds **57** and 4-carboxy TEMPO, following the procedure outlined for compound **6**. The compound was purified by column chromatography using 1:1 hexanes:acetone. An orange residue was isolated in 71% yield. HRMS (ESI) calculated for $C_{19}H_{28}N_3O_6SNa^+$ 449.1596; found 449.1596.

Synthesis of compound 59.

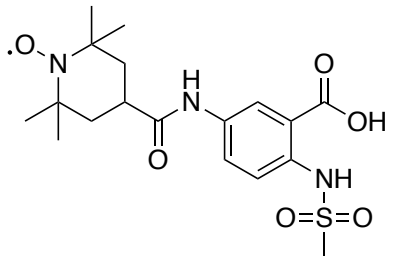

This compound was obtained following the procedure outlined for compound **7**. The product was obtained as a dark orange solid in 65% yield. HRMS (ESI) calculated for $C_{18}H_{26}N_3O_6SNa^+$ 435.1440; found 435.1522.

Synthesis of compound 60.

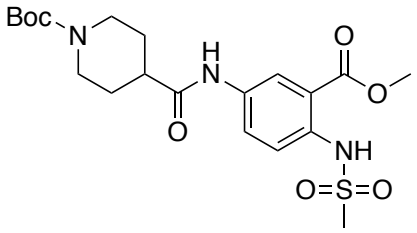

Compound **60** was obtained following the procedure outlined for compound **6**. The crude compound was purified by column chromatography using 2:1 hexanes:acetone as the mobile phase. A dark brown residue was isolated in 74% yield. ^{1}H NMR (DMSO-D_6): δ 10.13 (s, 1H), 8.32 (d, J = 2.6 Hz, 1H), 7.77 (dd, J = 8.5, 2.4 Hz, 1H), 7.50 (d, J = 9.0 Hz, 1H), 4.04 -3.93 (m, 2H), 3.88 (s, 3H), 3.86-3.79 (m, 1H), 3.09 (s, 3H), 2.69 (s, 4H), 2.08 (s, 3H), 1.81-1.72 (m, 3H), 1.54-1.44 (m, 2H), 1.41 (s, 9H). ^{13}C NMR (400 MHz, DMSO-D_6): 175.76, 167.18, 145.98, 126.73, 124.93, 122.04, 119.21, 114.65, 78.32, 50.27, 28.05, 27.48. HRMSI (ESI) calculated for $C_{20}H_{29}N_3O_7SNa^+$ 478.1630; found 478.1624.

Synthesis of compound 61.

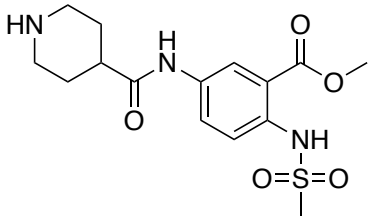

Compound **61** was obtained following the procedure outlined for compound **11**. The product was isolated as dark brown residue in quantitative yield and used without further purification.

Synthesis of compound 62.

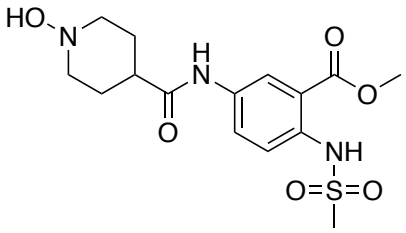

Compound **62** was obtained following the procedure outlined for compound **12**. The product was isolated as a brown residue in 45% yield. ^{1}H NMR (400 MHz, DMSO-D_6): δ 10.18 (s, 1H), 9.36 (broad s, 1H), 8.35 (d, J = 2.7 Hz, 1H), 7.79 (dd, J = 8.4, 2.7 Hz, 1H), 7.48 (d, J = 8.2 Hz, 1H), 4.03-3.95 (m, 2H), 3.89 (s, 3H), 3.84-3.78 (m, 1H), 3.04 (s, 3H), 2.69-2.56 (m, 2H). ^{13}C NMR (400 MHz, DMSO-D_6): δ 167.27, 161.34, 145.93, 126.82, 125.04, 122.65, 119.93, 114.72, 78.35, 76.24, 50.22, 29.06, 28.14. HMRS (ESI) calculated for $C_{15}H_{21}N_3O_6SNa^+$ 394.10; found 394.1049.

Synthesis of compound 63.

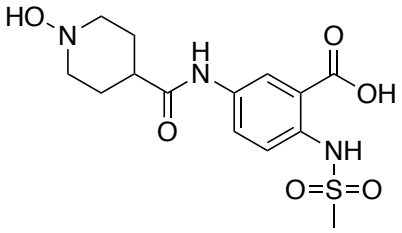

Compound **63** was obtained following the procedure outlined for compound **7**. The product was isolated as a dark brown solid in 64% yield. ^{1}H NMR (400 MHz, DMSO-D_6): δ 10.26 (s, 1H), 9.31 (broad s, 1H), 8.34 (d, J = 2.5 Hz, 1H), 7.79 (dd, J = 8.7, 2.6 Hz, 1H), 7.48 (d, J = 8.5 Hz,

1H), 4.02-3.92 (m, 2H), 3.80-3.69 (m, 1H), 3.03 (s, 3H), 2.68-2.59 (m, 2H). ^{13}C NMR (400 MHz, DMSO-D_6): δ 167.27, 161.34, 145.93, 126.82, 125.04, 122.65, 119.93, 114.72, 78.35, 76.29, 29.06, 28.14. HMRS (ESI) calculated for $C_{14}H_{19}N_3O_6SNa^+$ 380.09; found 380.0893.

Synthesis of Compound for Linker Studies

Synthesis of compound 64.

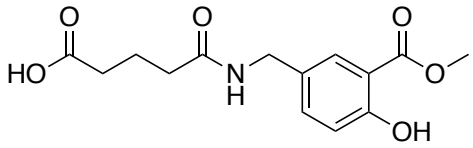

5-aminomethyl salicylate methyl ester (**4**) (181 mg, 1 mm, 1 equi.) was stirred in a solution of 1 mL of DMF with glutaric anhydride (114 mg, 1 mmol, 1 equi.) for 18 hours at room temperature. The reaction mixture was diluted with brine and dilute HCl added to make the solution acidic. The compound was extracted using ethyl acetate. The combined organic phases were washed with brine and dilute HCl and dried over sodium sulphate. The solvent was evaporated *in vacuo*. The product was isolated as a light coloured residue without further purification in 60% yield. ^{1}H NMR (400 MHz, DMSO-D_6): δ 12.04 (broad s, 2H), 10.42 (s, 1H), 8.33 (t, J = 6.4 Hz, 1H), 7.95 (s, 1H), 7.65 (d, J = 2.2 Hz, 1H), 7.40 (dd, J = 8.5, 2.4 Hz, 1H), 6.94 (d, J = 8.4 Hz, 1H), 4.18 (d, J = 6.0 Hz, 2H), 3.89 (s, 3H), 2.76-2.67 (m, 2H), 2.29-2.13 (m, 2H), 1.77-1.69 (m, 2H). ^{13}C NMR (400 MHz, DMSO-D_6): δ 173.25, 169.82, 168.43, 156.68, 135.41, 132.58, 121.54, 116.21, 112.84, 52.84, 44.16, 33.05, 32.85, 20.94. HMRS (ESI) calculated for $C_{14}H_{17}NO_6Na^+$ 318.0954; found 318.0935.

Synthesis of compound 65.

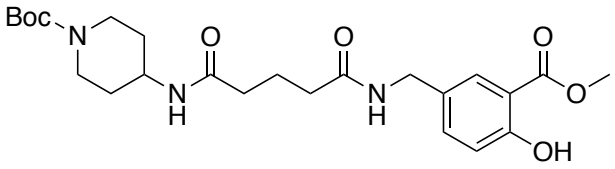

Compound **65** was synthesized following the procedure for compound **6**. The product was isolated as an yellow-orange residue by column chromatography using 95:5 DCM:MeOH in 67% yield. ^{1}H NMR (400 MHz, DMSO-D_6): δ 10.40 (s, 1H), 8.30 (t, J = 6.3 Hz, 1H), 7.73 (d, J = 8.0 Hz, 1H), 7.65 (d, J = 2.2 Hz, 1H), 7.39 (dd, J = 8.4, 2.2 Hz, 1H), 6.93 (d, J = 8.4 Hz, 1H), 4.19 (d, J = 5.9 Hz, 2H), 3.89 (s, 3H), 2.89-2.76 (broad s, 2H), 2.69 (s, 2H), 2.16-2.03 (m, 2H), 1.83-1.63 (m, 2H), 1.40 (s, 9H), 1.26-1.16 (m, 2H). ^{13}C NMR (400 MHz, DMSO-D_6): δ 175.96, 174.12, 169.82, 169.72, 156.93, 136.48, 131.59, 122.85, 116.73, 112.93, 79.28, 53.44, 42.83, 35.26, 34.12, 27.94, 25.24, 21.17. HMRS (ESI) calculated for $C_{24}H_{35}N_3O_7Na^+$ 500.2366; found 500.2373.

Synthesis of compound 66.

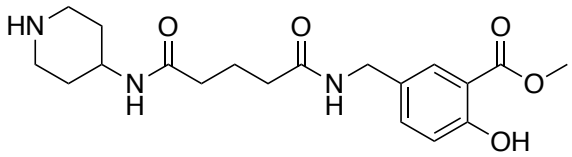

The Boc-deprotection of compound **65** was done following the procedure outlined for compound **11**. The product was isolated in quantitative yield without further purification. HMRS (ESI) calculated for $C_{19}H_{27}N_3O_5Na^+$ 400.1828; found 400.1848.

Synthesis of compound 67.

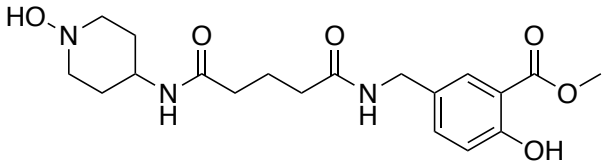

The product was prepared following the procedure outlined for compound **12**. ^{1}H NMR (400 MHz, DMSO-D_6): δ 7.72 (d, J = 2.5 Hz, 1H), 7.43 (dd, J = 8.4, 2.6 Hz, 1H), 6.91 (d, J = 8.2 Hz, 1H), 4.15 (d, J = 5.9 Hz, 1H), 3.91 (s, 3H), 2.79-2.65 (m, 4H), 2.42-2.38 (m, 1H), 2.19-2.08 (m, 2H), 1.93 (m, 2H), 1.49 (m, 2H). ^{13}C NMR (400 MHz, DMSO-D_6): δ 173.74, 170.49, 169.93, 162.53, 146.84, 129.30, 126.94, 121.03, 118.49, 79.64, 52.39, 44.92, 34.95, 32.10, 28.31, 27.59, 21.47. HMRS (ESI) calculated for $C_{19}H_{27}N_3O_6Na^+$ 416.18; found 416.1794.

Synthesis of compound 68.

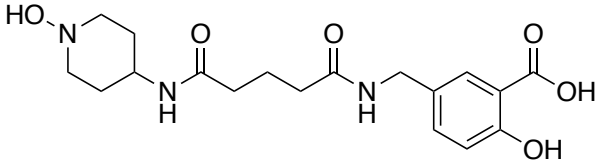

The product was prepared following the procedure outlined for compound **7**. ^{1}H NMR (400 MHz, DMSO-D_6): δ 7.72 (d, J = 2.5 Hz, 1H), 7.43 (dd, J = 8.4, 2.6 Hz, 1H), 6.91 (d, J = 8.2 Hz, 1H), 4.15 (d, J = 5.9 Hz, 1H), 2.79-2.65 (m, 4H), 2.42-2.38 (m, 1H), 2.19-2.08 (m, 2H), 1.93 (m, 2H), 1.49 (m, 2H).^{13}C NMR (400 MHz, DMSO-D_6): δ 173.74, 170.49, 169.93, 162.53, 146.84, 129.30, 126.94, 121.03, 118.49, 79.64, 44.92, 34.95, 32.10, 28.31, 27.59, 21.47.HMRS (ESI) calculated for $C_{16}H_{25}N_2O_6Na^+$ 402.16; found 402.1646.

Synthesis of Probe Targeted for FAP

Synthesis of compound 69.

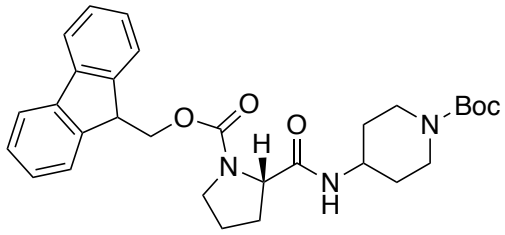

FMOC-Pro-OH (337 mg, 1 mmol, 1 equi.) was stirred a round bottom flask containing DIPEA (175 µL, 2 mmol, 2 equi.) and 1.5 mL DMF. HBTU (379 mg, 1 mmol, 1 equi.) and HOBT (40.4 mg, 0.3 mmol, 0.3 equi.) were added and the flask was stirred at 0°C on ice for 5 minutes. 4-amino-1-Boc-piperidine (200 mg, 1 mmol, 1 equi.) was then added to the flask and the reaction was stirred at room temperature overnight. After 18 hours, the mixture was diluted with brine, and the crude compound was extracted using ethyl acetate. The combined organic layers were dried over sodium sulphate and filtered. The remaining liquid was evaporated *in vacuo* to get a light yellow residue that was purified by column chromatography using 2:1 hexanes: acetone. A sticky, light yellow product was isolated in 89% yield. ^{1}H NMR (400 MHz, DMSO-D_6): δ 8.00-7.26 (m, 8H), 4.30-4.20 (m, 2H), 4.17-4.03 (m, 1H), 3.87-8.71 (m, 2H), 3.51-3.40 (m, 2H), 2.90-2.72 (broad s, 2H), 1.92-1.71 (m, 2H), 1.69-1.58 (m, 2H), 1.37 (s, 9H). ^{13}C NMR (400 MHz, DMSO-D_6): δ 171.39, 171.16, 164.70, 154.11, 154.05, 153.95, 143.95, 143.73, 140.87, 140.69, 127.76, 127.42, 127.22, 125.32, 120.25, 109.68, 78.72, 67.01, 66.53, 59.92, 59.63, 477.29, 46.79, 46.74, 46.56, 45.86, 45.73, 38.31, 31.62, 30.79, 30.28, 28.13, 28.11, 24.00, 23.03. HMRS (ESI) calculated for $C_{30}H_{37}N_3O_5Na^+$ 542.2601; found 542.2596.

Synthesis of compound 70.

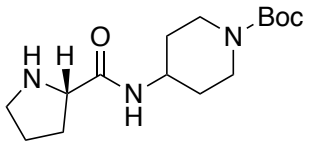

Compound **69** (407 mg, 0.75 mmol, 1 equi.) was stirred in a 2.0 M solution of methylamine in THF for 1 hour at room temperature. The solvent was evaporated *in vacuo* after TLC indicated that the start material was no longer present in the reaction mixture. The crude product was purified by column chromatography in 90:9:1 DCM: MeOH: NH_4OH. A yellow oil was isolated in 90% yield. ^{1}H NMR (400 MHz, DMSO-D_6): δ 7.82 (d, J = 8.3 Hz, 1H), 3.83 (d, J = 12.1 Hz, 2H), 3.74-3.63 (m, 1H), 3.47-3.42 (m, 2H), 2.83-2.74 (m, 4H), 1.96-1.85 (m, 1H), 1.69-1.61 (m, 2H), 1.61-1.51 (m, 2H), 1.39 (s, 9H), 1.34-1.21 (m, 2H). ^{13}C NMR (400 MHz, DMSO-D_6): δ 173.65, 153.91, 78.67, 60.24, 46.75, 45.43, 30.59, 28.11, 25.80. HMRS (ESI) calculated for $C_{15}H_{27}N_3O_3Na^+$ 320.1950; found 320.1965.

Synthesis of compound 71.

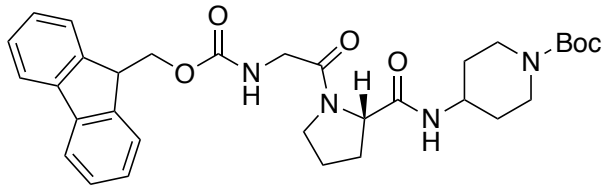

Compound **71** was prepared following the procedure outlined for compound **69**, by coupling FMOC-protected glycine to compound **70**. The crude compound was purified by column chromatography using 95:5 DCM:MeOH to run the column. Compound **71** was isolated as a yellow oil in 74% yield. ^{1}H NMR (400 MHz, DMSO-D_6): δ 7.89 (d, J = 7.5 Hz, 2H), 7.75-7.67 (m, 2H), 7.44-7.29 (m, 4H), 4.33-4.19 (m, 3H), 3.89-3.68 (m, 2H), 3.57-3.41 (m, 2H), 2.05-1.57 (m, 4H), 1.38 (s, 9H), 1.31-1.61 (m, 2H). ^{13}C NMR (400 MHz, DMSO-D_6): δ 170.84, 167.31,

162.36, 156.54, 153.91, 143.88, 140.76, 127.66, 127.13, 125.30, 120.15, 78.68, 78.63, 65.74, 59.77, 58.91, 46.66, 45.62, 38.27, 35.82, 30.82, 29.38, 28.09, 24.32, 22.14. HRMS (ESI) calculated for $C_{32}N_{40}N_4O_6Na^+$ 599.2846; found 599.2845.

Synthesis of compound 72.

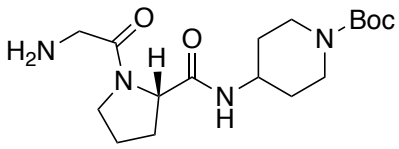

Compound **72** was prepared following the procedure for compound **70**. The crude compound was purified by column chromatography using the same solvent system as well (90:9:1 DCM: MeOH: NH_4OH). The product was isolated as a yellow solid in 70% yield. ^{1}H NMR (400 MHz, DMSO-D_6): δ 8.03-7.71 (m, 2H), 4.33-4.17 (m, 1H), 3.87-3.77 (m, 3H), 2.88 (s, 2H), 2.72 (s, 2H), 2.04-1.94 (m, 1H), 1.93-1.81 (m, 2H), 1.80-1.72 (m, 1H), 1.71-1.57 (m, 2H), 1.39 (s, 9H), 1.32-1.19 (m, 2H). ^{13}C NMR (400 MHz, DMSO-D_6): δ 170.83, 167.30, 78.60, 65.75, 54.97, 46.73, 45.63, 42.74, 35.76, 30.76, 29.41, 28.11, 24.30, 22.09. HMRS (ESI) calculated for $C_{17}H_{30}N_4O_4Na^+$ 388.2165; found 377.2169.

Synthesis of compound 73.

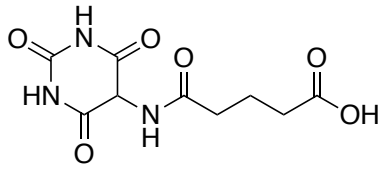

Compound **73** was prepared following the procedure outlined for compound **64**. ^{1}H NMR (400 MHz, DMSO-D_6): δ 11.31 (s, 2H), 8.82 (broad s, 1H), 2.42-2.32 (m, 4H), 1.89-1.78 (m, 2H). ^{13}C

NMR (400 MHz, DMSO-D_6): δ 174.14, 168.34, 32.75, 29.32, 19.97, 15.64. HRMS (EI) calculated for $C_9H_{11}N_3O6$ 257.0$_6$; found 257.0648.

Synthesis of compound 74.

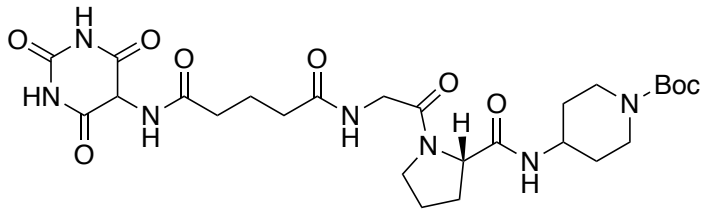

Compound **74** was prepared by coupling compounds **72** and **73**, using the procedure outlined for compound **6**. The crude compound was purified by column chromatography using 9:1 EtOAc: MeOH and the product was isolated as a light yellow solid in 46% yield. ^{1}H NMR (400 MHz, DMSO-D_6): δ 10.93 (s, 2H), 8.93 (broad s, 1H), 3.94-3.84 (m, 3H), 2.80 (s, 2H), 2.74 (s, 2H), 2.39-2.31 (m, 6H), 2.01-1.87 (m, 1H), 1.87-1.72 (m, 2H), 1.53 (s, 9H). ^{13}C NMR (400 MHz, DMSO-D_6): δ 173.89, 170.42, 169.50, 167.39, 166.74, 162.95, 78.92, 75.97, 54.75, 53.46, 46.76, 45.87, 42.04, 35.24, 30.72, 29.43, 28.22, 24.56, 22.55. HRMS (EI) calculated for $C_{26}H_{39}N_7O_9Na^+$ 616.2707; found 616.2698.

Synthesis of compound 75.

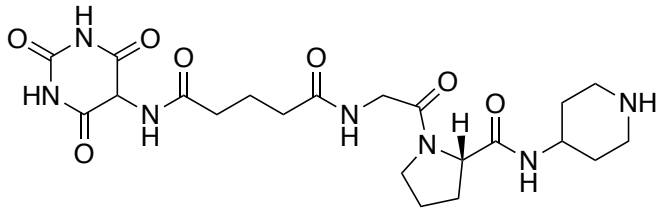

Compound **75** was prepared following the deprotection procedure outlined for compound **11**. The product was isolated without further purification or characterization.

Synthesis of compound 76.

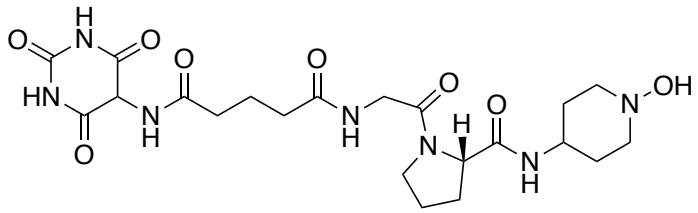

Compound **76** was prepared following the oxidation procedure outlined for compound **12**. The product was isolated in 42% yield as a light pink solid. ^{1}H NMR (400 MHz, DMSO-D_6): δ 11.29 (s, 2H), 9.10 (broad s, 1H), 4.01-3.96 (m, 3H), 3.89-3.82 (m, 2H), 2.84 (s, 2H), 2.76 (s, 2H), 2.41-2.37 (m, 7H), 2.12-1.99 (m, 1H), 1.89-1.81 (m, 2H) 1.49-1.42 (m, 2H). ^{13}C NMR (400 MHz, DMSO-D_6): δ 173.45, 171.92, 170.84, 169.73, 169.41, 168.30, 79.42, 78.49, 72.63, 71.48, 56.24, 53.76, 46.88, 36.51, 35.93, 28.05, 27.96, 25.98. HRMS (EI) calculated for $C_{21}H_{31}N_7O_8Na^+$ 532.3132; found 532.3128.

Synthesis of compound 77.

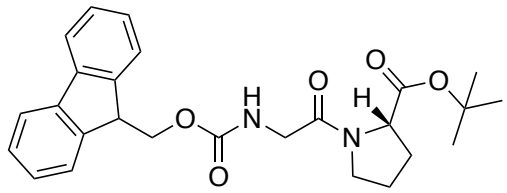

Compound **77** was prepared by coupling FMOC-protecting glycine to t-buyl protected proline using the procedure outlined for compound **69**. The crude compound was purified by column chromatography using a solvent system of 2:1 hexanes: acetone. Compound **77** was isolated in 58% yield as a light yellow residue. ^{1}H NMR (400 MHz, DMSO-D_6): δ 7.86 (d, J = 7.5 Hz, 2H), 7.69 (d, J = 6.8 Hz, 2H), 7.40 (t, J = 7.2 Hz, 2H), 7.31 (t, J = 7.5 Hz, 2H), 4.30-4.11 (m, 4H), 3.50-3.34 (m, 5), 2.07 (s, 2H), 1.35 (s, 9H), 1.12 (s , 1H). ^{13}C NMR (400 MHz, DMSO-D_6): δ 170.79, 169.75, 163.92, 156.87, 145.27, 140.31, 127.10, 125.62, 120.86, 78.39, 68.71, 59.30,

54.08, 46.41, 45.23, 43.12, 35.92, 30.04, 29.52, 28.33 HMRS (ESI) calculated for $C_{26}H_{30}N_2O_5Na^+$ 472.2052; found 473.2069.

Synthesis of compound 78.

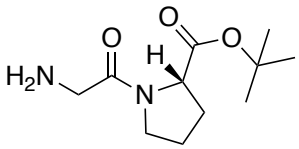

Compound **78** was prepared following the FMOC deprotection procedure outlined for compound **70**. The crude compound was purified by column chromatography with 90:9:1 DCM: MeOH: NH_4OH as the mobile phase. The product was isolated in 69% yield as a yellow residue. ^1H NMR (400 MHz, DMSO-D_6): δ 4.19 (dd, J = 8.6, 1.9 Hz, 1H), 3.45-3.37 (m, 3H), 3.27 (d, J = 7.8 Hz, 2H), 2.23-2.03 (m, 2H), 1.93-1.74 (m, 4H), 1.38 (s, 9H). ^{13}C NMR (400 MHz, DMSO-D_6): δ 169.28, 163.85, 58.00, 45.91, 44.64, 27.90, 27.61, 22.06. HMRS (EI) calculated for $C_{11}H_{20}N_2O_3$ 228.15; found 228.1476.

Synthesis of compound 79.

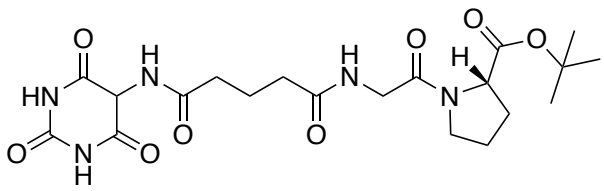

Compound **79** was prepared following the procedure outlined for compound **6**, by coupling compounds **73** and **78**. The crude compound was purified by column chromatography using 9:1 DCM:MeOH as the mobile phase. Compound **79** was isolated in 49% yield as a light yellow residue. ^1H NMR (400 MHz, DMSO-D_6): δ 10.86 (s, 2H), 8.93 (broad s, 1H), 4.59 (m, 2H), 4.23-4.19 (m, 2H), 3.49-3.41 (m, 2H), 3.27 (m, 2H), 2.43-2.31 (m, 6H), 2.24-2.19 (m, 2H), 1.92-

1.78 (m, 2H), 1.42 (s, 9H). ^{13}C NMR (400 MHz, DMSO-D_6): δ 170.41, 169.93, 169.25, 168.29, 162.30, 160.57, 58.23, 53.42, 45.29, 43.95. 35.61, 33.51, 27.08, 23.45, 23.14. HRMS (ESI) calculated for $C_{20}H_{29}N_5O_8Na^+$ 490.1914; found 490.1910.

Synthesis of compound 80.

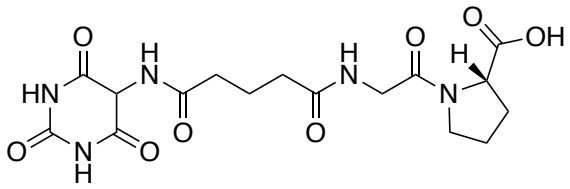

Compound **80** was prepared following the procedure outlined for compound **17**. The product was obtained without further purification. ^{1}H NMR (400 MHz, DMSO-D_6): δ 10.52 (s, 2H), 8.93 (broad s, 1H), 4.72 (m, 2H), 4.35-4.27 (m, 2H), 3.83-3.68 (m, 2H), 3.21 (m, 2H), 2.42-2.30 (m, 6H), 2.19-2.12 (m, 2H), 1.89-1.76 (m, 2H).^{13}C NMR (400 MHz, DMSO-D_6): δ 170.48, 169.11, 168.37, 162.29, 160.58, 58.23, 52.59, 45.62, 43.06, 35.44, 33.09, 23.47. HRMS (ESI) calculated for $C_{16}H_{21}N_5O_8Na^+$ 434.1288; found 434.1291.

Piperidine Analogues for Control Compounds

Synthesis of 4-carboxy TEMPOH (81).

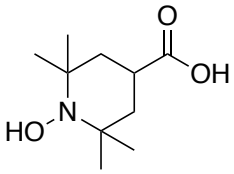

4-carboxy TEMPO was reduced to 4-carboxy TEMPOH (**81**) following the procedure outlined for compound **8**. The product was isolated as a white solid in 58% yield. ^{1}H NMR (400 MHz, DMSO-D_6): δ 2.42-2.36 (m, 1H) 1.80-1.73 (m, 2H), 1.54-1.42 (m, 2H), 1.14 (s, 6H), 1.07 (s,

6H).[13]C NMR (400 MHz, DMSO-D_6): δ 175.67, 78.42, 28.39, 27.65, 25.36, 25.29. HRMS (EI) calculated for $C_{10}H_{19}NO_3$ 201.1365; found 201.1368.

Synthesis of compound 82.

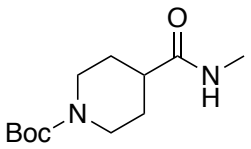

Compound **9** (183 mg, 0.8 mmol, 1 equi.) was stirred in a solution of DIPEA (707 µL, 1.06 mmol, 5.125 equi.) and 1 mL DMF. HATU (401.8 mg, 1.06 mmol, 1.325 equi.) was added to the round bottom flask and the reaction was left on ice. After 5 minutes, methylamine HCl (71.6 mg, 1.06 mmol, 1.325 equi.) was added to the reaction mixture and stirring continued overnight at room temperature. The mixture was diluted with 1 M NaOH and extracted using ethyl acetate. The combined organic phases were washed with brine and dilute HCl, before being dried over sodium sulphate. The solvent was evaporated *in vacuo* and the crude product was purified by column chromatography using 2:1 hexanes: acetone as the mobile phase. Compound **82** was isolated in 48% yield as a light yellow residue. [1]H NMR (400 MHz, DMSO-D_6): δ 3.91 (d, J = 15.2 Hz, 2H), 3.76 (s, 3H) 2.79 (broad s, 2H), 2.44-2.36 (m, 1H), 1.78 (dd, J = 13.4, 2.8 Hz, 2H), 1.49-1.37 (m, 11H). [13]C NMR (400 MHz, DMSO-D_6): δ 175.26, 169.42, 83.59, 51.80, 29.14, 27.49, 25.63, 25.21. HRMS (EI) calculated for $C_{12}H_{22}N_2O_3$ 242.16; found 242.1634.

Synthesis of compound 83.

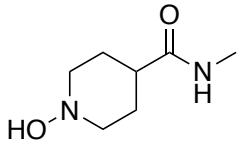

Compound **82** under went Boc deprotection following the procedure outlined for compound **11**, following by oxidation using the procedure outlined for compound **12**. Compound **83** was isolated as a light residue in 39% yield over 2 steps. ^{1}H NMR (400 MHz, DMSO-D_6): δ 3.59 (d, J = 14.8 Hz, 3H), 3.39 (s, 2H), 2.88 (broad s, 2H), 2.39-2.28 (m, 2H), 1.79 (m, 2H), 1.47-1.38 (m, 2H). ^{13}C NMR (400 MHz, DMSO-D_6): δ 175.26, 84.29, 53.48, 29.42, 27.83. HRMS (EI) calculated for $C_7H_{14}N_2O_2$ 158.11; found 158.1055.

References

(1) Massoud, T. F.; Gambhir, S. S. *Genes Dev.* **2003**, *17* (5), 545.
(2) Osborn, E. A.; Jaffer, F. A. *Current Opinion in Cardiology*. November 2008, pp 620–628.
(3) Weissleder, R.; Mahmood, U. *Radiology* **2001**, *219* (2), 316.
(4) Weissleder, R.; Pittet, M. J. *Nature* **2008**, *452* (7187), 580.
(5) James, M. L.; Gambhir, S. S. *Physiol. Rev.* **2012**, *92* (2), 897.
(6) van Osch, M. J. P.; Webb, A. G. *Current Radiology Reports*. Springer New York LLC August 14, 2014, pp 1–8.
(7) Buxton, R. B. *Introduction to Functional Magnetic Resonance Imaging*; Cambridge University Press: Cambridge, 2009.
(8) De Graaf, R. A. *In vivo NMR spectroscopy : principles and techniques*; John Wiley & Sons, 2007.
(9) Levitt, M. H. *Spin dynamics : basics of nuclear magnetic resonance*.
(10) Massoud, T. F.; Gambhir, S. S. *Genes Dev.* **2003**, *17* (5), 545.
(11) File:T1t2PD.jpg - Wikimedia Commons https://commons.wikimedia.org/wiki/File:T1t2PD.jpg (accessed Jun 25, 2020).
(12) Xiao, Y. D.; Paudel, R.; Liu, J.; Ma, C.; Zhang, Z. S.; Zhou, S. K. *International Journal of Molecular Medicine*. Spandidos Publications November 1, 2016, pp 1319–1326.
(13) Runge, V. M. *Invest. Radiol.* **2017**, *52* (6), 317.
(14) Grobner, T. *Nephrol. Dial. Transplant.* **2006**, *21* (4), 1104.
(15) Marckmann, P.; Skov, L.; Rossen, K.; Dupont, A.; Damholt, M. B.; Heaf, J. G.; Thomsen, H. S. *J. Am. Soc. Nephrol.* **2006**, *17* (9), 2359.
(16) Kanda, T.; Fukusato, T.; Matsuda, M.; Toyoda, K.; Oba, H.; Kotoku, J.; Haruyama, T.; Kitajima, K.; Furui, S. *Radiology* **2015**, *276* (1), 228.
(17) Akgun, H.; Gonlusen, G.; Cartwright, J.; Suki, W. N.; Truong, L. D. *Arch. Pathol. Lab. Med.* **2006**, *130* (9), 1354.
(18) Elmståhl, B.; Nyman, U.; Leander, P.; Chai, C. M.; Golman, K.; Björk, J.; Almén, T. *Eur. Radiol.* **2006**, *16* (12), 2712.
(19) Chen, R.; Ling, D.; Zhao, L.; Wang, S.; Liu, Y.; Bai, R.; Baik, S.; Zhao, Y.; Chen, C.; Hyeon, T. *ACS Nano* **2015**, *9* (12), 12425.
(20) Blasco-Perrin, H.; Glaser, B.; Pienkowski, M.; Peron, J. M.; Payen, J. L. *Pancreatology* **2013**, *13* (1), 88.
(21) Ray, D. E.; Cavanagh, J. B.; Nolan, C. C.; Williams, S. C. R. *Am. J. Neuroradiol.* **1996**, *17* (2), 365.
(22) Hui, F. K.; Mullins, M. *American Journal of Neuroradiology*. American Journal of Neuroradiology January 1, 2009, pp e1–e1.
(23) Moseley, M. E.; Cohen, Y.; Mintorovitch, J.; Chileuitt, L.; Shimizu, H.; Kucharczyk, J.; Wendland, M. F.; Weinstein, P. R. *Magn. Reson. Med.* **1990**, *14* (2), 330.
(24) Bains, L. J.; Zweifel, M.; Thoeny, H. C. *Cancer Imaging* **2012**, *12* (2), 395.
(25) Mori, S.; Barker, P. B. *Anat. Rec.* **1999**, *257* (3), 102.
(26) Logothetis, N. K.; Pfeuffer, J. *Magn. Reson. Imaging* **2004**, *22* (10), 1517.
(27) Logothetis, N. K. *Nature* **2008**, *453* (7197), 869.
(28) Forster, B. B.; MacKay, A. L.; Whittall, K. P.; Kiehl, K. A.; Smith, A. M.; Hare, R. D.; Liddle, P. F. *Can. Assoc. Radiol. J.* **1998**, *49* (5), 320.
(29) Soares, D. P.; Law, M. *Clin. Radiol.* **2009**, *64* (1), 12.

(30) Gujar, S. K.; Maheshwari, S.; Bj??rkman-Burtscher, I.; Sundgren, P. C. *J. Neuro-Ophthalmology* **2005**, *25* (3), 217.
(31) Aime, S.; Delli Castelli, D.; Terreno, E. *Angew. Chemie Int. Ed.* **2002**, *41* (22), 4334.
(32) Ward, K. M.; Balaban, R. S. *Magn. Reson. Med.* **2000**, *44* (5), 799.
(33) De Leon-Rodriguez, L. M.; Lubag, A. J. M.; Malloy, C. R.; Martinez, G. V.; Gillies, R. J.; Sherry, A. D. *Acc. Chem. Res.* **2009**, *42* (7), 948.
(34) Wu, B.; Warnock, G.; Zaiss, M.; Lin, C.; Chen, M.; Zhou, Z.; Mu, L.; Nanz, D.; Tuura, R.; Delso, G. *EJNMMI Phys.* **2016**, *3* (1), 19.
(35) Soesbe, T. C.; Wu, Y.; Dean Sherry, A. *NMR Biomed.* **2013**, *26* (7), 829.
(36) Sherry, A. D.; Wu, Y. *Curr. Opin. Chem. Biol.* **2013**, *17* (2), 167.
(37) Hills, B. P.; Cano, C.; Belton, P. S. *Macromolecules* **1991**, *24* (10), 2944.
(38) Zhou, J.; Zijl, P. C. M. va. *Progress in Nuclear Magnetic Resonance Spectroscopy*. Elsevier May 30, 2006, pp 109–136.
(39) Zhou, J.; Payen, J.-F.; Wilson, D. A.; Traystman, R. J.; van Zijl, P. C. M. *Nat. Med.* **2003**, *9* (8), 1085.
(40) Banerjee, S. R.; Song, X.; Yang, X.; Minn, I.; Lisok, A.; Chen, Y.; Bui, A.; Chatterjee, S.; Chen, J.; van Zijl, P. C. M.; McMahon, M. T.; Pomper, M. G. *Chem. - A Eur. J.* **2018**, *24* (28), 7235.
(41) Yang, X.; Yadav, N. N.; Song, X.; Ray Banerjee, S.; Edelman, H.; Minn, I.; van Zijl, P. C. M.; Pomper, M. G.; McMahon, M. T. *Chemistry* **2014**, *20* (48), 15824.
(42) Song, X.; Yang, X.; Ray Banerjee, S.; Pomper, M. G.; McMahon, M. T. *Contrast Media Mol. Imaging* **2015**, *10* (1), 74.
(43) Yang, X.; Song, X.; Ray Banerjee, S.; Li, Y.; Byun, Y.; Liu, G.; Bhujwalla, Z. M.; Pomper, M. G.; McMahon, M. T. *Contrast Media Mol. Imaging* **2016**, *11* (4), 304.
(44) Bryant, R. G. *Annual Review of Biophysics and Biomolecular Structure*. Annual Reviews Inc. 1996, pp 29–53.
(45) Guivel-Scharen, V.; Sinnwell, T.; Wolff, S. D.; Balaban, R. S. *J. Magn. Reson.* **1998**, *133* (1), 36.
(46) Yan, K.; Fu, Z.; Yang, C.; Zhang, K.; Jiang, S.; Lee, D.-H.; Heo, H.-Y.; Zhang, Y.; Cole, R. N.; Van Eyk, J. E.; Zhou, J. *Mol. Imaging Biol.* **2015**, *17* (4), 479.
(47) Harris, R. J.; Cloughesy, T. F.; Liau, L. M.; Prins, R. M.; Antonios, J. P.; Li, D.; Yong, W. H.; Pope, W. B.; Lai, A.; Nghiemphu, P. L.; Ellingson, B. M. *Neuro. Oncol.* **2015**, *17* (11), 1514.
(48) Chen, J.; Yadav, N. N.; Stait-Gardner, T.; Gupta, A.; Price, W. S.; Zheng, G. *NMR Biomed.* **2020**, *33* (1).
(49) Van Zijl, P. C. M.; Yadav, N. N. .
(50) Chan, K. W. Y.; McMahon, M. T.; Kato, Y.; Liu, G.; Bulte, J. W. M.; Bhujwalla, Z. M.; Artemov, D.; van Zijl, P. C. M. *Magn. Reson. Med.* **2012**, *68* (6), 1764.
(51) Liu, G.; Liang, Y.; Bar-Shir, A.; Chan, K. W. Y.; Galpoththawela, C. S.; Bernard, S. M.; Tse, T.; Yadav, N. N.; Walczak, P.; McMahon, M. T.; Bulte, J. W. M.; van Zijl, P. C. M.; Gilad, A. A. *J. Am. Chem. Soc.* **2011**, *133* (41), 16326.
(52) Van Zijl, P. C. M.; Jones, C. K.; Ren, J.; Malloy, C. R.; Sherry, A. D. *Proc. Natl. Acad. Sci. U. S. A.* **2007**, *104* (11), 4359.
(53) Ward, K. .; Aletras, A. .; Balaban, R. . *J. Magn. Reson.* **2000**, *143* (1), 79.
(54) Wang, J.; Weygand, J.; Hwang, K.-P.; Mohamed, A. S. R.; Ding, Y.; Fuller, C. D.; Lai, S. Y.; Frank, S. J.; Zhou, J. *Sci. Rep.* **2016**, *6* (1), 30618.

(55) Haris, M.; Nath, K.; Cai, K.; Singh, A.; Crescenzi, R.; Kogan, F.; Verma, G.; Reddy, S.; Hariharan, H.; Melhem, E. R.; Reddy, R. *NMR Biomed.* **2013**, *26* (4), 386.
(56) Ametamey, S. M.; Treyer, V.; Streffer, J.; Wyss, M. T.; Schmidt, M.; Blagoev, M.; Hintermann, S.; Auberson, Y.; Gasparini, F.; Fischer, U. C.; Buck, A. *J. Nucl. Med.* **2007**, *48* (2), 247.
(57) Zhou, J.; Tryggestad, E.; Wen, Z.; Lal, B.; Zhou, T.; Grossman, R.; Wang, S.; Yan, K.; Fu, D.-X.; Ford, E.; Tyler, B.; Blakeley, J.; Laterra, J.; van Zijl, P. C. M. *Nat. Med.* **2011**, *17* (1), 130.
(58) Yang, X.; Song, X.; Li, Y.; Liu, G.; Banerjee, S. R.; Pomper, M. G.; McMahon, M. T. *Angew. Chem. Int. Ed. Engl.* **2013**, *52* (31), 8116.
(59) Lesniak, W. G.; Oskolkov, N.; Song, X.; Lal, B.; Yang, X.; Pomper, M.; Laterra, J.; Nimmagadda, S.; McMahon, M. T. *Nano Lett.* **2016**, *16* (4), 2248.
(60) Wahsner, J.; Gale, E. M.; Rodríguez-Rodríguez, A.; Caravan, P. *Chem. Rev.* **2019**, *119* (2), 957.
(61) McMahon, M. T.; Gilad, A. A.; Zhou, J.; Sun, P. Z.; Bulte, J. W. M.; van Zijl, P. C. M. *Magn. Reson. Med.* **2006**, *55* (4), 836.
(62) Hingorani, D. V.; Montano, L. A.; Randtke, E. A.; Lee, Y. S.; Cárdenas-Rodríguez, J.; Pagel, M. D. *Contrast Media Mol. Imaging* **2016**, *11* (2), 130.
(63) Sinharay, S.; Fernández-Cuervo, G.; Acfalle, J. P.; Pagel, M. D. *Chem. - A Eur. J.* **2016**, *22* (19), 6491.
(64) Daryaei, I.; Mohammadebrahim Ghaffari, M.; Jones, K. M.; Pagel, M. D. *ACS Sensors* **2016**, *1* (7), 857.
(65) Liu, G.; Li, Y.; Pagel, M. D. *Magn. Reson. Med.* **2007**, *58* (6), 1249.
(66) Ratnakar, S. J.; Soesbe, T. C.; Lumata, L. L.; Do, Q. N.; Viswanathan, S.; Lin, C.-Y.; Sherry, A. D.; Kovacs, Z. *J. Am. Chem. Soc.* **2013**, *135* (40), 14904.
(67) Go, Y. M.; Jones, D. P. *Biochimica et Biophysica Acta - General Subjects*. NIH Public Access November 2008, pp 1273–1290.
(68) Ramamonjisoa, N.; Ackerstaff, E. *Frontiers in Oncology*. Frontiers Media S.A. January 31, 2017,.
(69) De Vitto, H.; Pérez-Valencia, J.; Radosevich, J. A. *Tumor Biology*. Springer Netherlands February 1, 2016, pp 1541–1558.
(70) Marchiq, I.; Pouysségur, J. *Journal of Molecular Medicine*. Springer Verlag February 1, 2016, pp 155–171.
(71) Hanahan, D.; Weinberg, R. A. *Cell*. March 4, 2011, pp 646–674.
(72) Romero-Garcia, S.; Moreno-Altamirano, M. M. B.; Prado-Garcia, H.; Sánchez-García, F. J. *Frontiers in Immunology*. Frontiers Media S.A. 2016, p 52.
(73) Liotta, L. A.; Kohn, E. C. *Nature*. May 17, 2001, pp 375–379.
(74) Xing, Y.; Zhao, S.; Zhou, B. P.; Mi, J. *FEBS Journal*. Blackwell Publishing Ltd October 1, 2015, pp 3892–3898.
(75) Polet, F.; Feron, O. *Journal of Internal Medicine*. February 2013, pp 156–165.
(76) Hanahan, D.; Coussens, L. M. *Cancer Cell*. March 20, 2012, pp 309–322.
(77) Pickup, M. W.; Mouw, J. K.; Weaver, V. M. *EMBO Rep.* **2014**, *15* (12), 1243.
(78) Hagedorn, H. G.; Bachmeier, B. E.; Nerlich, A. G. *International journal of oncology*. April 2001, pp 669–681.
(79) Turley, S. J.; Cremasco, V.; Astarita, J. L. *Nature Reviews Immunology*. Nature Publishing Group November 1, 2015, pp 669–682.

(80) Friedl, P.; Bröcker, E. B. *Cellular and Molecular Life Sciences*. 2000, pp 41–64.
(81) Caravan, P.; Das, B.; Dumas, S.; Epstein, F. H.; Helm, P. A.; Jacques, V.; Koerner, S.; Kolodziej, A.; Shen, L.; Sun, W. C.; Zhang, Z. *Angew. Chemie - Int. Ed.* **2007**, *46* (43), 8171.
(82) Polasek, M.; Fuchs, B. C.; Uppal, R.; Schühle, D. T.; Alford, J. K.; Loving, G. S.; Yamada, S.; Wei, L.; Lauwers, G. Y.; Guimaraes, A. R.; Tanabe, K. K.; Caravan, P. *J. Hepatol.* **2012**, *57* (3), 549.
(83) Farrar, C. T.; Gale, E. M.; Kennan, R.; Ramsay, I.; Masia, R.; Arora, G.; Looby, K.; Wei, L.; Kalpathy-Cramer, J.; Bunzel, M. M.; Zhang, C.; Zhu, Y.; Akiyama, T. E.; Klimas, M.; Pinto, S.; Diyabalanage, H.; Tanabe, K. K.; Humblet, V.; Fuchs, B. C.; Caravan, P. *Radiology* **2018**, *287* (2), 581.
(84) Shiftan, L.; Israely, T.; Cohen, M.; Frydman, V.; Dafni, H.; Stern, R.; Neeman, M. *Cancer Res.* **2005**, *65* (22), 10316.
(85) Park, J.; Kim, S.; Saw, P. E.; Lee, I. H.; Yu, M. K.; Kim, M.; Lee, K.; Kim, Y. C.; Jeong, Y. Y.; Jon, S. *J. Control. Release* **2012**, *163* (2), 111.
(86) Cirri, P.; Chiarugi, P. *Cancer and Metastasis Reviews*. June 2012, pp 195–208.
(87) Zhang, J.; Liu, J. *Pharmacology and Therapeutics*. NIH Public Access February 2013, pp 200–215.
(88) Eck, S. M.; Côté, A. L.; Winkelman, W. D.; Brinckerhoff, C. E. *Mol. Cancer Res.* **2009**, *7* (7), 1033.
(89) Gao, M. Q.; Kim, B. G.; Kang, S.; Choi, Y. P.; Park, H.; Kang, K. S.; Cho, N. H. *J. Cell Sci.* **2010**, *123* (20), 3507.
(90) Hellevik, T.; Pettersen, I.; Berg, V.; Winberg, J. O.; Moe, B. T.; Bartnes, K.; Paulssen, R. H.; Busund, L. T.; Bremnes, R.; Chalmers, A.; Martinez-Zubiaurre, I. *Radiat. Oncol.* **2012**, *7* (1), 59.
(91) M., B.-A.; M.E., B.; A., L.-D.; A., V. V.; R., S.; M., M.-I.; C., S.; X., S.; A., V. V.; D.G., M.; Berdiel-Acer, M.; Bohem, M. E.; Lopez-Doriga, A.; Vidal, A.; Salazar, R.; Martinez-Iniesta, M.; Santos, C.; Sanjuan, X.; Villanueva, A.; Mollevi, D. G. *Neoplasia* **2011**, *13* (10), 931.
(92) Mueller, L.; Goumas, F. A.; Himpel, S.; Brilloff, S.; Rogiers, X.; Broering, D. C. *Cancer Lett.* **2007**, *250* (2), 329.
(93) Henriksson, M. L.; Edin, S.; Dahlin, A. M.; Oldenborg, P. A.; Öberg, Å.; Van Guelpen, B.; Rutegård, J.; Stenling, R.; Palmqvist, R. *Am. J. Pathol.* **2011**, *178* (3), 1387.
(94) Lin, Z. Y.; Chuang, Y. H.; Chuang, W. L. *Biomed. Pharmacother.* **2012**, *66* (7), 525.
(95) True, L. D.; Zhang, H.; Ye, M.; Huang, C. Y.; Nelson, P. S.; Von Haller, P. D.; Tjoelker, L. W.; Kim, J. S.; Qian, W. J.; Smith, R. D.; Ellis, W. J.; Liebeskind, E. S.; Liu, A. Y. *Mod. Pathol.* **2010**, *23* (10), 1346.
(96) Orimo, A.; Weinberg, R. A. *Cancer Biology and Therapy*. Landes Bioscience 2007, pp 618–619.
(97) Rettig, W. J.; Chesa, P. G.; Beresford, H. R.; Feickert, H. J.; Jennings, M. T.; Cohen, J.; Oettgen, H. F.; Old, L. J. *Cancer Res.* **1986**, *46* (12 Pt 1), 6406.
(98) Scanlan, M. J.; Raj, B. K. M.; Calvo, B.; Garin-Chesa, P.; Sanz-Moncasi, M. P.; Healey, J. H.; Old, L. J.; Rettig, W. J. *Proc. Natl. Acad. Sci. U. S. A.* **1994**, *91* (12), 5657.
(99) Niedermeyer, J.; Garin-Chesa, P.; Kriz, M.; Hilberg, F.; Mueller, E.; Bamberger, U.; Rettig, W. J.; Schnapp, A. *Int. J. Dev. Biol.* **2001**, *45* (2), 445.
(100) Jacob, M.; Chang, L.; Pure, E. *Curr. Mol. Med.* **2012**, *12* (10), 1220.

(101) Fassnacht, M.; Lee, J.; Milazzo, C.; Boczkowski, D.; Su, Z.; Nair, S.; Gilboa, E. *Clin. Cancer Res.* **2005**, *11* (15), 5566.
(102) Cheng, J. D.; Valianou, M.; Canutescu, A. A.; Jaffe, E. K.; Lee, H. O.; Wang, H.; Lai, J. H.; Bachovchin, W. W.; Weiner, L. M. *Mol. Cancer Ther.* **2005**, *4* (3), 351.
(103) Ghersi, G.; Dong, H.; Goldstein, L. A.; Yeh, Y.; Hakkinen, L.; Larjava, H. S.; Chen, W. T. *J. Biol. Chem.* **2002**, *277* (32), 29231.
(104) Chen, W.-T.; Kelly, T. *Cancer Metastasis Rev. 22* (2–3), 259.
(105) O'Brien, P.; O'Connor, B. F. *Biochimica et Biophysica Acta - Proteins and Proteomics*. Elsevier September 2008, pp 1130–1145.
(106) Koczorowska, M. M.; Tholen, S.; Bucher, F.; Lutz, L.; Kizhakkedathu, J. N.; De Wever, O.; Wellner, U. F.; Biniossek, M. L.; Stahl, A.; Lassmann, S.; Schilling, O. *Mol. Oncol.* **2016**, *10* (1), 40.
(107) Meng, M.; Wang, W.; Yan, J.; Tan, J.; Liao, L.; Shi, J.; Wei, C.; Xie, Y.; Jin, X.; Yang, L.; Jin, Q.; Zhu, H.; Tan, W.; Yang, F.; Hou, Z. *Tumor Biol.* **2016**, *37* (8), 10317.
(108) Yang, X.; Lin, Y.; Shi, Y.; Li, B.; Liu, W.; Yin, W.; Dang, Y.; Chu, Y.; Fan, J.; He, R. *Cancer Res.* **2016**, *76* (14), 4124.
(109) Ge, Y.; Zhan, F.; Barlogie, B.; Epstein, J.; Shaughnessy, J.; Yaccoby, S. *Br. J. Haematol.* **2006**, *133* (1), 83.
(110) Wen, X.; He, X.; Jiao, F.; Wang, C.; Yang, S.; Ren, X.; Li, Q. *Oncol. Res.* **2017**, *25* (4), 629.
(111) Santos, A. M.; Jung, J.; Aziz, N.; Kissil, J. L.; Puré, E. *J. Clin. Invest.* **2009**, *119* (12), 3613.
(112) Granot, D.; Addadi, Y.; Kalchenko, V.; Harmelin, A.; Kunz-Schughart, L. A.; Neeman, M. *Cancer Res.* **2007**, *67* (19), 9180.
(113) Giesel, F. L.; Kratochwil, C.; Lindner, T.; Marschalek, M. M.; Loktev, A.; Lehnert, W.; Debus, J.; Jäger, D.; Flechsig, P.; Altmann, A.; Mier, W.; Haberkorn, U. *J. Nucl. Med.* **2019**, *60* (3), 386.
(114) Kratochwil, C.; Flechsig, P.; Lindner, T.; Abderrahim, L.; Altmann, A.; Mier, W.; Adeberg, S.; Rathke, H.; Röhrich, M.; Winter, H.; Plinkert, P. K.; Marme, F.; Lang, M.; Kauczor, H. U.; Jäger, D.; Debus, J.; Haberkorn, U.; Giesel, F. L. *J. Nucl. Med.* **2019**, *60* (6), 801.
(115) Li, J.; Chen, K.; Liu, H.; Cheng, K.; Yang, M.; Zhang, J.; Cheng, J. D.; Zhang, Y.; Cheng, Z. *Bioconjug. Chem.* **2012**, *23* (8), 1704.
(116) ImageJ https://imagej.nih.gov/ij/download/ (accessed Mar 16, 2020).
(117) Liu, G.; Gilad, A. A.; Bulte, J. W. M.; van Zijl, P. C. M.; McMahon, M. T. *Contrast Media Mol. Imaging* **2010**, *5* (3), 162.
(118) Bačić, G.; Pavićević, A.; Peyrot, F. *Redox Biol.* **2016**, *8*, 226.
(119) Paletta, J. T.; Pink, M.; Foley, B.; Rajca, S.; Rajca, A. *Org. Lett.* **2012**, *14* (20), 5322.
(120) Rabenstein, D. L.; Fan, S. *Anal. Chem.* **1986**, *58* (14), 3178.
(121) Dang, T.; Suchy, M.; Truong, Y. J.; Oakden, W.; Lam, W. W.; Lazurko, C.; Facey, G.; Stanisz, G. J.; Shuhendler, A. J. *Chem. - A Eur. J.* **2018**, *24* (36), 9148.
(122) Walker-Samuel, S.; Ramasawmy, R.; Torrealdea, F.; Rega, M.; Rajkumar, V.; Johnson, S. P.; Richardson, S.; Gonçalves, M.; Parkes, H. G.; Årstad, E.; Thomas, D. L.; Pedley, R. B.; Lythgoe, M. F.; Golay, X. *Nat. Med.* **2013**, *19* (8), 1067.
(123) Tu, T.-W.; Ibrahim, W. G.; Jikaria, N.; Munasinghe, J. P.; Witko, J. A.; Hammoud, D. A.; Frank, J. A. *Sci. Rep.* **2018**, *8* (1), 669.

(124) Nasrallah, F. A.; Pagès, G.; Kuchel, P. W.; Golay, X.; Chuang, K.-H. *J. Cereb. Blood Flow Metab.* **2013**, *33* (8), 1270.
(125) Dharmarwardana, M.; Martins, A. F.; Chen, Z.; Palacios, P. M.; Nowak, C. M.; Welch, R. P.; Li, S.; Luzuriaga, M. A.; Bleris, L.; Pierce, B. S.; Sherry, A. D.; Gassensmith, J. J. *Mol. Pharm.* **2018**, *15* (8), 2973.
(126) Garin-Chesa, P.; Old, L. J.; Rettig, W. J. *Proc. Natl. Acad. Sci.* **1990**, *87* (18), 7235.
(127) Edosada, C. Y.; Quan, C.; Wiesmann, C.; Tran, T.; Sutherlin, D.; Reynolds, M.; Elliott, J. M.; Raab, H.; Fairbrother, W.; Wolf, B. B. *J. Biol. Chem.* **2006**, *281* (11), 7437.
(128) Lee, K. N.; Jackson, K. W.; Christiansen, V. J.; Lee, C. S.; Chun, J. G.; McKee, P. A. *Blood* **2006**, *107* (4), 1397.
(129) Aertgeerts, K.; Levin, I.; Shi, L.; Snell, G. P.; Jennings, A.; Prasad, G. S.; Zhang, Y.; Kraus, M. L.; Salakian, S.; Sridhar, V.; Wijnands, R.; Tennant, M. G. *J. Biol. Chem.* **2005**, *280* (20), 19441.
(130) Yang, X.; Song, X.; Li, Y.; Liu, G.; Banerjee, S. R.; Pomper, M. G.; McMahon, M. T. *Angew. Chem. Int. Ed. Engl.* **2013**, *52* (31), 8116.
(131) Maciel, G. E.; Savitsky, G. B. *J. Phys. Chem.* **1964**, *68* (2), 437.
(132) Mock, W. L.; Morsch, L. A. *Tetrahedron* **2001**, *57* (15), 2957.
(133) Marsh, D. *Spin-label electron paramagnetic resonance spectroscopy*; 2019.
(134) Yang, X.; Song, X.; Li, Y.; Liu, G.; Banerjee, S. R.; Pomper, M. G.; McMahon, M. T. *Angew. Chem. Int. Ed. Engl.* **2013**, *52* (31), 8116.
(135) Basharat, M.; deSouza, N. M.; Parkes, H. G.; Payne, G. S. *Magn. Reson. Med.* **2016**, *76* (3), 742.
(136) Huang, X.; Luo, X.; Roupioz, Y.; Keillor, J. W. *J. Org. Chem.* **1997**, *62* (25), 8821.
(137) Ogawa, M.; Kosaka, N.; Longmire, M. R.; Urano, Y.; Choyke, P. L.; Kobayashi, H. *Mol. Pharm.* **2009**, *6* (2), 386.
(138) Kamiya, M.; Kobayashi, H.; Hama, Y.; Koyama, Y.; Bernardo, M.; Nagano, T.; Choyke, P. L.; Urano, Y. *J. Am. Chem. Soc.* **2007**, *129* (13), 3918.
(139) Hama, Y.; Urano, Y.; Koyama, Y.; Kamiya, M.; Bernardo, M.; Paik, R. S.; In, S. S.; Paik, C. H.; Choyke, P. L.; Kobayashi, H. *Cancer Res.* **2007**, *67* (6), 2791.
(140) Guilbault, G. G.; Kramer, D. N. *Anal. Chem.* **1965**, *37* (1), 120.
(141) Rotman, B.; Zderic, J. A.; Edelstein, M. *Proc. Natl. Acad. Sci. U. S. A.* **1963**, *50*, 1.
(142) Rotman, B. *Proc. Natl. Acad. Sci. United States* **1961**, *47* (12), 1981.
(143) Kramer, D. N.; Guilbault, G. G. *Anal. Chem.* **1963**, *35* (4), 588.
(144) Kojima, H.; Nakatsubo, N.; Kikuchi, K.; Kawahara, S.; Kirino, Y.; Nagoshi, H.; Hirata, Y.; Nagano, T. *Anal. Chem.* **1998**, *70* (13), 2446.
(145) Xu, S.; Wang, Q.; Zhang, Q.; Zhang, L.; Zuo, L.; Jiang, J.-D.; Hu, H.-Y. *Chem. Commun.* **2017**, *53* (81), 11177.
(146) Biswas, S.; McCullough, B. S.; Ma, E. S.; LaJoie, D.; Russell, C. W.; Garrett Brown, D.; Round, J. L.; Ullman, K. S.; Mulvey, M. A.; Barrios, A. M. *Chem. Commun.* **2017**, *53* (14), 2233.
(147) Levine, M. N.; Hoang, T. T.; Raines, R. T. *Chem. Biol.* **2013**, *20* (4), 614.
(148) Lazebnik, Y. A.; Kaufmann, S. H.; Desnoyers, S.; Poirier, G. G.; Earnshaw, W. C. *Nature* **1994**, *371* (6495), 346.
(149) and, M. D. S.; Imperiali*, B. **2003**.
(150) Shults, M. D.; Carrico-Moniz, D.; Imperiali, B. *Anal. Biochem.* **2006**, *352* (2), 198.
(151) Lyu, Y.; Zhen, X.; Miao, Y.; Pu, K. *ACS Nano* **2017**, *11* (1), 358.

(152) Reichel, D.; Tripathi, M.; Butte, P.; Saouaf, R.; Perez, J. M. *Nanotheranostics* **2019**, *3* (2), 196.
(153) Lee, S.; Xie, J.; Chen, X. *Curr. Top. Med. Chem.* **2010**, *10* (11), 1135.
(154) Kobayashi, H.; Choyke, P. L. *Acc. Chem. Res.* **2011**, *44* (2), 83.
(155) Chang, C. J.; Editor, G.; James, T. D.; New, E. J.; Zhong Tang, B. *Acc. Chem. Res* **2020**, *2020*, 6.
(156) Rhodes, C. J. *Toxicology of the human environment : the critical role of free radicals*; Taylor & Francis Limited, 2000.
(157) Saphier, O.; Silberstein, T.; Shames, A. I.; Likhtenshtein, G. I.; Maimon, E.; Mankuta, D.; Mazor, M.; Katz, M.; Meyerstein, D.; Meyerstein, N. *Free Radical Research*. March 1, 2003, pp 301–308.
(158) Keana, J. F. W.; Pou, S.; Rosen, G. M. *Magn. Reson. Med.* **1987**, *5* (6), 525.
(159) Emoto, M.; Mito, F.; Yamasaki, T.; Yamada, K.-I.; Sato-Akaba, H.; Hirata, H.; Fujii, H. *Free Radic. Res.* **2011**, *45* (11–12), 1325.
(160) Rajca, A.; Wang, Y.; Boska, M.; Paletta, J. T.; Olankitwanit, A.; Swanson, M. A.; Mitchell, D. G.; Eaton, S. S.; Eaton, G. R.; Rajca, S. *J. Am. Chem. Soc.* **2012**, *134* (38), 15724.
(161) Bobko, A. A.; Kirilyuk, I. A.; Grigor'ev, I. A.; Zweier, J. L.; Khramtsov, V. V. *Free Radic. Biol. Med.* **2007**, *42* (3), 404.
(162) Sun, P. Z.; Cheung, J. S.; Wang, E.; Lo, E. H. *J. Cereb. Blood Flow Metab.* **2011**, *31* (8), 1743.
(163) Tietze, A.; Blicher, J.; Mikkelsen, I. K.; Østergaard, L.; Strother, M. K.; Smith, S. A.; Donahue, M. J. *NMR Biomed.* **2014**, *27* (2), 163.
(164) Haris, M.; Singh, A.; Cai, K.; Nath, K.; Crescenzi, R.; Kogan, F.; Hariharan, H.; Reddy, R. *J. Neurosci. Methods* **2013**, *212* (1), 87.
(165) Jin, T.; Autio, J.; Obata, T.; Kim, S.-G. *Magn. Reson. Med.* **2011**, *65* (5), 1448.
(166) Kogan, F.; Singh, A.; Debrosse, C.; Haris, M.; Cai, K.; Nanga, R. P.; Elliott, M.; Hariharan, H.; Reddy, R. *Neuroimage* **2013**, *77*, 262.
(167) Cai, K.; Haris, M.; Singh, A.; Kogan, F.; Greenberg, J. H.; Hariharan, H.; Detre, J. A.; Reddy, R. *Nat. Med.* **2012**, *18* (2), 302.
(168) Davis, K. A.; Nanga, R. P. R.; Das, S.; Chen, S. H.; Hadar, P. N.; Pollard, J. R.; Lucas, T. H.; Shinohara, R. T.; Litt, B.; Hariharan, H.; Elliott, M. A.; Detre, J. A.; Reddy, R. *Sci. Transl. Med.* **2015**, *7* (309), 309ra161.
(169) Kogan, F.; Haris, M.; Singh, A.; Cai, K.; Debrosse, C.; Nanga, R. P. R.; Hariharan, H.; Reddy, R. *Magn. Reson. Med.* **2014**, *71* (1), 164.
(170) Pietras, K.; Östman, A. *Experimental Cell Research*. Academic Press Inc. May 1, 2010, pp 1324–1331.
(171) Randtke, E. A.; Chen, L. Q.; Corrales, L. R.; Pagel, M. D. *Magn. Reson. Med.* **2014**, *71* (4), 1603.
(172) Zhang, S.; Merritt, M.; Woessner, D. E.; Lenkinski, R. E.; Sherry, A. D. *Acc. Chem. Res.* **2003**, *36* (10), 783.
(173) Parrott, D.; Fernando, W. S.; Martins, A. F. *Inorganics*. MDPI Multidisciplinary Digital Publishing Institute February 1, 2019, p 18.
(174) Denton, A. E.; Roberts, E. W.; Fearon, D. T. In *Advances in Experimental Medicine and Biology*; Springer New York LLC, 2018; Vol. 1060, pp 99–114.
(175) Aime, S.; Delli Castelli, D.; Lawson, D.; Terreno, E. *J. Am. Chem. Soc.* **2007**, *129* (9),

2430.
(176) Shindo, M.; Takaku, S.; Takamura, K. *Yakugaku Zasshi* **1971**, *91* (5), 590.
(177) Friedman, M. R.; Toyne, K. J.; Goodby, J. W.; Hird, M. *J. Mater. Chem.* **2001**, *11* (11), 2759.
(178) Quelet, R.; Dran, R.; Lallouz, E. *Bullentin la Soc. Chim. du Fr.* **1969**, *5* (303), 1698.
(179) Di Antonio, M.; Doria, F.; Richter, S. N.; Bertipaglia, C.; Mella, M.; Sissi, C.; Palumbo, M.; Freccero, M. *J. Am. Chem. Soc.* **2009**, *131* (36), 13132.
(180) Mitchell, J. B.; DeGraff, W.; Kaufman, D.; Krishna, M. C.; Samuni, A.; Finkelstein, E.; Ahn, M. S.; Hahn, S. M.; Gamson, J.; Russo, A. *Arch. Biochem. Biophys.* **1991**, *289* (1), 62.
(181) Klein, S. I.; Molino, B. F.; Czekaj, M.; Gardner, C. J.; Chu, V.; Brown, K.; Sabatino, R. D.; Bostwick, J. S.; Kasiewski, C.; Bentley, R.; Windisch, V.; Perrone, M.; Dunwiddie, C. T.; Leadley, R. J. *J. Med. Chem.* **1998**, *41* (14), 2492.
(182) Wright, S. W.; Hageman, D. L.; Wright, A. S.; McClure, L. D. *Tetrahedron Lett.* **1997**, *38* (42), 7345.
(183) Dessolin, J.; Schuler, M.; Quinart, A.; De Giorgi, F.; Ghosez, L.; Ichas, F. *Eur. J. Pharmacol.* **2002**, *447* (2–3), 155.
(184) Gopin, A.; Ebner, S.; Attali, B.; Shabat, D. *Bioconjug. Chem.* **2006**, *16* (6), 1432.
(185) Verderosa, A. D.; de la Fuente-Núñez, C.; Mansour, S. C.; Cao, J.; Lu, T. K.; Hancock, R. E. W.; Fairfull-Smith, K. E. *Eur. J. Med. Chem.* **2017**, *138*, 590.
(186) Hurst, D.; Atcha, S.; Marshall, K. *Aust. J. Chem.* **1991**, *44* (1), 129.
(187) Cavalieri, L. F.; Blair, V. E.; Brown, G. B. *J. Am. Chem. Soc.* **1948**, *70* (3), 1240.
(188) Biswas, N. N.; Yu, T. T.; Kimyon, Ö.; Nizalapur, S.; Gardner, C. R.; Manefield, M.; Griffith, R.; Black, D. S.; Kumar, N. *Bioorg. Med. Chem.* **2017**, *25* (3), 1183.
(189) Greenberg, C. S.; Birckbichler, P. J.; Rice, R. H. *FASEB J.* **1991**, *5* (15), 3071.
(190) Tucholski, J.; Lesort, M.; Johnson, G. V. W. *Neuroscience* **2001**, *102* (2), 481.
(191) Balajthy, Z.; Csomós, K.; Vámosi, G.; Szántó, A.; Lanotte, M.; Fésüs, L. *Blood* **2006**, *108* (6), 2045.
(192) Melino, G.; Annicchiarico-Petruzzelli, M.; Piredda, L.; Candi, E.; Gentile, V.; Davies, P. J.; Piacentini, M. *Mol. Cell. Biol.* **1994**, *14* (10), 6584.
(193) Lorand, L.; Graham, R. M. *Nature Reviews Molecular Cell Biology*. Nat Rev Mol Cell Biol February 1, 2003, pp 140–156.
(194) Wityak, J.; Prime, M. E.; Brookfield, F. A.; Courtney, S. M.; Erfan, S.; Johnsen, S.; Johnson, P. D.; Li, M.; Marston, R. W.; Reed, L.; Vaidya, D.; Schaertl, S.; Pedret-Dunn, A.; Beconi, M.; MacDonald, D.; Muñoz-Sanjuan, I.; Dominguez, C. *ACS Med. Chem. Lett.* **2012**, *3* (12), 1024.
(195) Akbar, A.; McNeil, N. M. R.; Albert, M. R.; Ta, V.; Adhikary, G.; Bourgeois, K.; Eckert, R. L.; Keillor, J. W. *J. Med. Chem.* **2017**, *60* (18), 7910.
(196) Lide, D. *CRC Handbook of Chemistry and Physics, 91th Edition*; 2006.
(197) Zhuang, Z. W.; Huang, Y.; Ju, R.; Maxfield, M. W.; Ren, Y.; Wang, X.; Wang, X.; Stacy, M. R.; Hwa, J. *Theranostics* **2019**, *9* (5), 1474.
(198) Souri, M.; Osaki, T.; Ichinose, A. *J. Biol. Chem.* **2015**, *290* (19), 12027.
(199) Ichinose, A. *Int. J. Hematol.* **2012**, *95* (4), 362.
(200) Tei, L.; Mazooz, G.; Shellef, Y.; Avni, R.; Vandoorne, K.; Barge, A.; Kalchenko, V.; Dewhirst, M. W.; Chaabane, L.; Miragoli, L.; Longo, D.; Neeman, M.; Aime, S. *Contrast Media Mol. Imaging* **2010**, *5* (4), 213.

(201) Kwon, M. H.; Jung, S. H.; Kim, Y. M.; Ha, K. S. *Anal. Chem.* **2011**, *83* (22), 8718.

Appendix A: Activatable Probes for Studying the Activity of Transglutaminase 2 (TG2) and Factor XIII (FXIII)

Methods

HPLC Assay for TG2

125 μM of the probe was incubated in 100 mM MOPS buffer, 3 mM $CaCl_2$ and 0.05 μM EDTA at pH 7.0. The reaction was initiated by the addition of 40 mU/mL TG2 enzyme. The substrate was incubated at 37°C for 1 hour before an aliquot was quenched with 100 μL cold acetonitrile and analyzed by HPLC. HPLC was done using a Luna C-18 Å column (particle size 5 μm; 21.2 x 250 mm), on analytical mode at a flow rate of 1 mL/minute, with the following gradient profile: 99% water + 0.1% TFA: 1% acetonitrile + 0.1 % TFA to 100% acetonitrile + 0.1% TFA over 25 minutes. The absorbance was monitored using a PDA detector set to 310 nm.

Fluorescence assay for TG2 at varying pH

AL5 (Keillor) was incubated in a buffer of 100 mM MOPS buffer, 3 mM $CaCl_2$ and 0.05 μM EDTA with TG2 at 37°C. The absorbance at 405 nm was measured every minute over 60 seconds. The pH of the buffer was 4.5, 5.0, 5.5 or 7. Measured absorbances were blank corrected.

Fluorescence assay for transamidation activity of FXIII(a)

Assay buffer (100 mM Tris, 15 mM $CaCl_2$ and 300 mM NaCl) containing dansylcadaverine and N,N-dimethyl casein was incubated with FXIII(a) and thrombin. Additional 3.7 mM Gly-OMe HCl in 1.4 mM TCEP-HCl was added to the buffer. The solutions were adjusted to pH 7.5. The assay was maintained at 37°C over 30 minutes as the fluorescence intensity was measured at 500 nm (excitation at 330 nm) every 1 minute.

Fluorescence assay for hydrolysis activity of FXIII(a) in PBS

A101 was prepared as a solution in DMSO with a final concentration of 100 μM. PBS was used as the buffer, supplemented with 15 mM $CaCl_2$. Additional 3.7 mM Gly-OMe HCl in 1.4 mM TCEP-HCl was added as the transamidation acceptor. The solutions were adjusted to pH 7.5 and the assay was held at 37°C. 3 μU FXIII(a) was added to the sample and the fluorescence was measured every 1 minute over 2 hours with excitation at 313 nm and emission at 418 nm.

Results and Discussion

A diaCEST probe was initially designed to be activated by the transamidation activity of transglutaminase 2 (TG2). TG2 is an enzyme best known for its cross-linking activity.[189] It has a role in may different physiological processes including cellular differentiation[190,191] and extracellular matrix assembly[192]. Increased TG2 activity has been linked to fibrosis and cancer.[193]

The design of the first generation was loosely based off compound **68**, which was used to study the effects of linker length. The benzyl chloroformate (Cbz) was included to confer specificity to TG2[194,195] and the glutarate is a useful design feature that can allow us to easily couple two different groups to each end of the molecule.[136] By starting with glutaric anhydride, we can selectively couple to one acid of glutarate without the need for additional protecting groups and protection/deprotection steps. The first generation TG2 activated probe (**A6**) was synthesized over 5 steps.

In order to test if the probe was activated by TG2, we incubated the probe in an assay buffer consisting of MOPS buffer, $CaCl_2$ and EDTA at 37°C and then took an aliquot for HPLC analysis (Figure A1). A new peak appearing with a different retention time could indicate that the probe is being processed by the enzyme to hydrolyze the N-hydroxy piperidine to relieve signal suppression and restore the CEST signal. A new peak was observed with a different retention time, but it does not appear to match the expected retention time of the hydrolysis product.

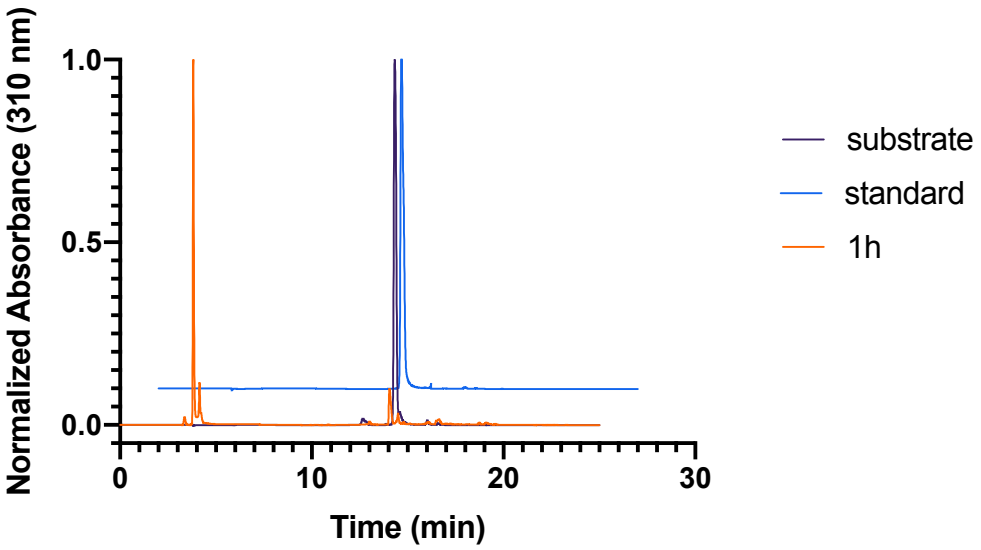

Figure A1. HPLC chromatograms of TG2 assay using first generation probe (A6). 125 μM of the probe was incubated in a buffer of 100 mM MOS buffer, 3 mM $CaCl_2$ and 0.05 μM EDTA at pH 7.0. The reaction was initiated by the addition of 40 mU/mL TG2 enzyme. The substrate was incubated at 37°C for 1 hour before an aliquot was quenched with cold acetonitrile and analyzed by HPLC.

A second generation TG2-activated probe (**A16**) was re-designed. This probe was based off a known TG2 inhibitor developed by the Keillor group.[195] Salicylic acid was used in place of the Cbz group, but the similar aromatic ring was expected to have similar specificity effects. The N-hydroxy piperidine was placed on the side chain of glutamate, where it can be removed by the transamidation or hydrolysis activity of TG2.

Similar HPLC assays were done as described above to see if the second generation was a viable probe. After 1 hour incubation at 37°C, the sample was analyzed by HPLC and a new peak appeared (Figure A2). Again, this peak did not match the elution time of the hydrolysis product and could be processed by the enzyme differently, or could be degrading under the assay conditions.

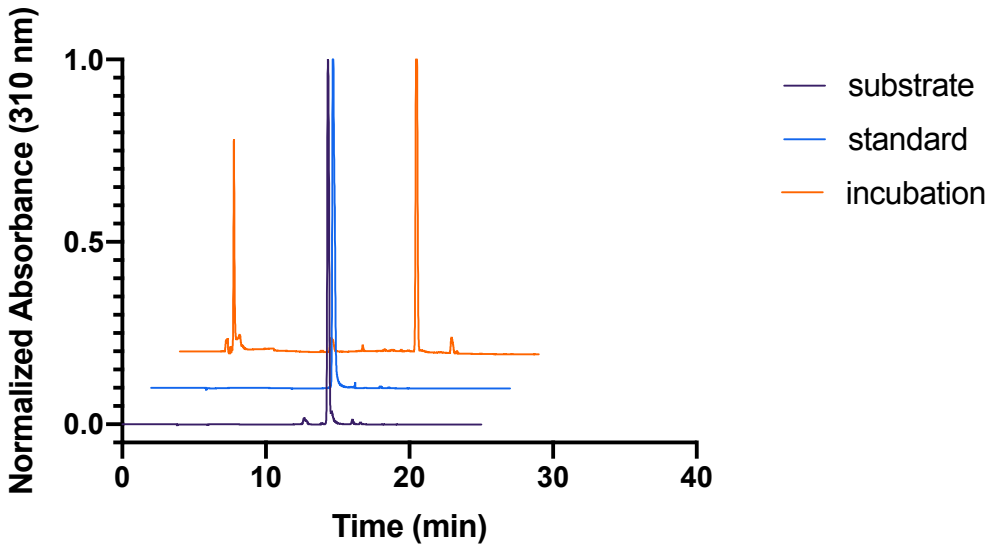

Figure A2. HPLC chromatograms of TG2 assay using first generation probe (A16). 125 μM of the probe was incubated in a buffer of 100 mM MOS buffer, 3 mM $CaCl_2$ and 0.05 μM EDTA at pH 7.0. The reaction was initiated by the addition of 40 mU/mL TG2 enzyme. The substrate was incubated at 37°C for 1 hour before an aliquot was quenched with cold acetonitrile and analyzed by HPLC.

Literature suggests that the binding pocket for the aromatic ring is highly hydrophobic.[194,195] It could be possible that the carboxylic acid of salicylic acid is interfering with the intermolecular interactions making it not suitable to fit in the active site. The pK_a of this carboxylic acid is 3.0[196] and under the assay conditions (pH 7), the carboxylic acid will be deprotonated to be carboxylate and carry a negative charge. We hypothesized that lowering the pH of the assay could protonate a greater proportion of the molecule to lose the negative charge so that it can fit in the binding pocket.

In order to test if the assay the assay at different pH, we incubated AL5 (a known TG2 substrate from the Keillor group) with a transamidation acceptor *para*-nitrophenolate and measured the absorbance over time (Figure A3). The assay was done at pH 4.5, 5.0, 5.5 and 7.0. Only at pH 7.0 did we observe an increase in absorbance at 405 nm over time to indicate

successful transamidation. While lower pH can protonate the carboxylate, the enzyme assay is not effective. The synthesized probe is not suitable for TG2.

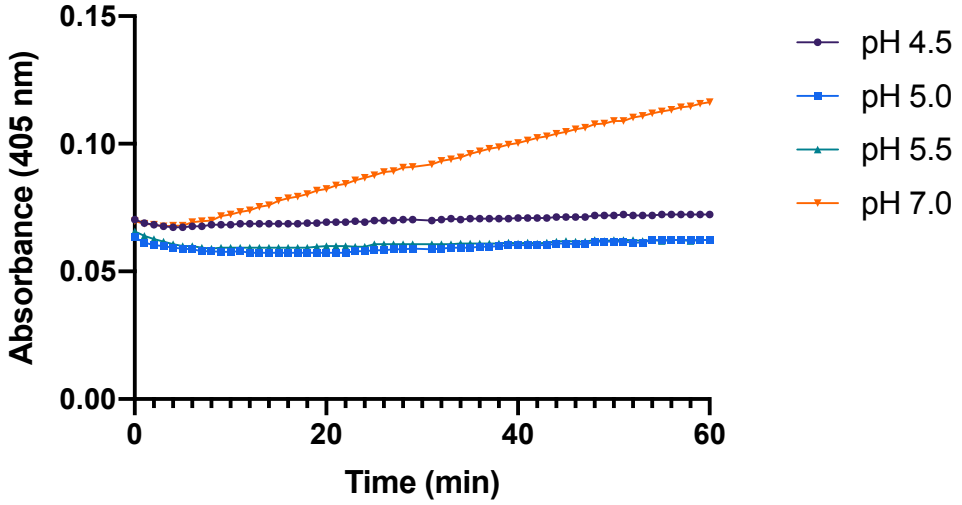

Figure A3. Absorbance of *para*-nitrophenolate (405 nm) at pH 4.5, 5.0, 5.5 and 7.0. AL5 was incubated in a buffer of 100 mM MOPS buffer, 3.0 mM $CaCl_2$, 0.05 µM EDTA with TG2 at 37°C and the absorbance at 405 nm was measured every 1 minute over 60 minutes. The pH of the buffer was 4.5, 5.0, 5.5 or 7.0. Absorbances were corrected for blank.

The second generation probe (**A16**) was repurposed for factor XIII (FXIII). FXIII is involved in several different physiological processes including blood clotting and cross-linking of small molecules.[197,198] FXIII gets activated by thrombin to become FXIIIa.[199] The binding pocket of FXIII more readily accepts a negative charge on the aromatic ring,[200,201] as present on salicylic acid. However, an assay looking at the transamidation and hydrolysis activity of FXIII was not established and this was necessary to test the probe.

In order to study the activity of FXIII, the known fluorogenic susbstrate, A101, was used as a control. A101 in DMSO was incubated in a buffer of Tris, $CaCl_2$ and NaCl, with additional Gly-OMe HCl in TCEP-HCl. The samples were kept at 37°C as the fluorescence intensity was measured over 2 hours (Figure A4). FXIIIa shows slow fluorescence increase both in the presence and absence of thrombin. However, FXIII supplemented with thrombin shows the

greatest increase in fluorescence. No increase in fluorescence was observed with FXIII when thrombin was omitted.

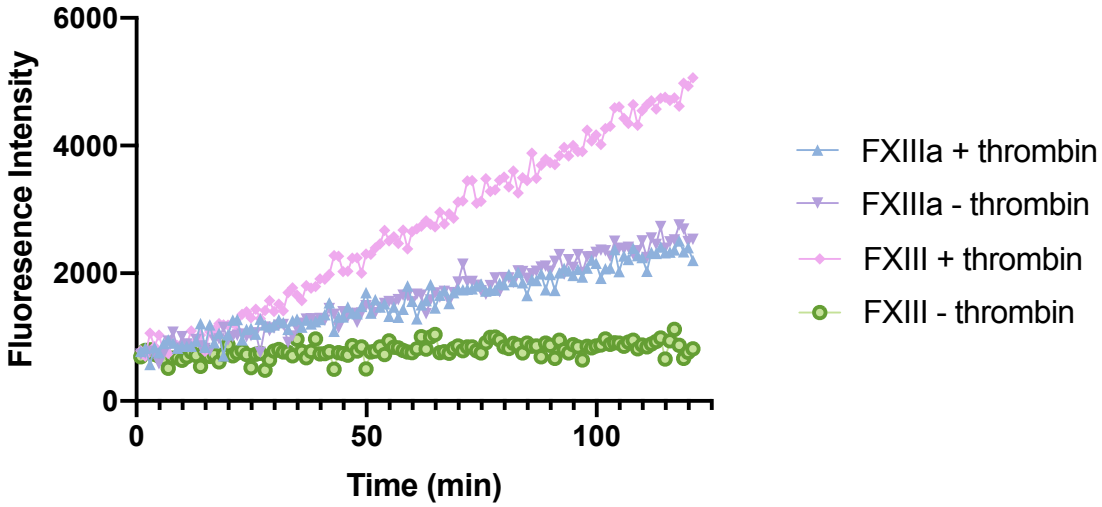

Figure A4. Fluorescence intensity monitoring the cleavage of A101 using FXIII(a) with thrombin. A101 was prepared as a solution in DMSO with a final concentration of 100 µM. The buffer consisted of 100 mM Tris, 15 mM $CaCl_2$ and 300 mM NaCl. Additional 3.7 mM Gly-OMe HCl in 1.4 mM TCEP-HCl was added as the transamidation acceptor. The solutions were adjusted to pH 7.5 and the assay was kept at 37°C. 3 µU of the appropriate FXIII(a) was added to the sample and the fluorescence was measured every 1 minute over 2 hours. Additional 3 µU thrombin was also added to the appropriate samples.

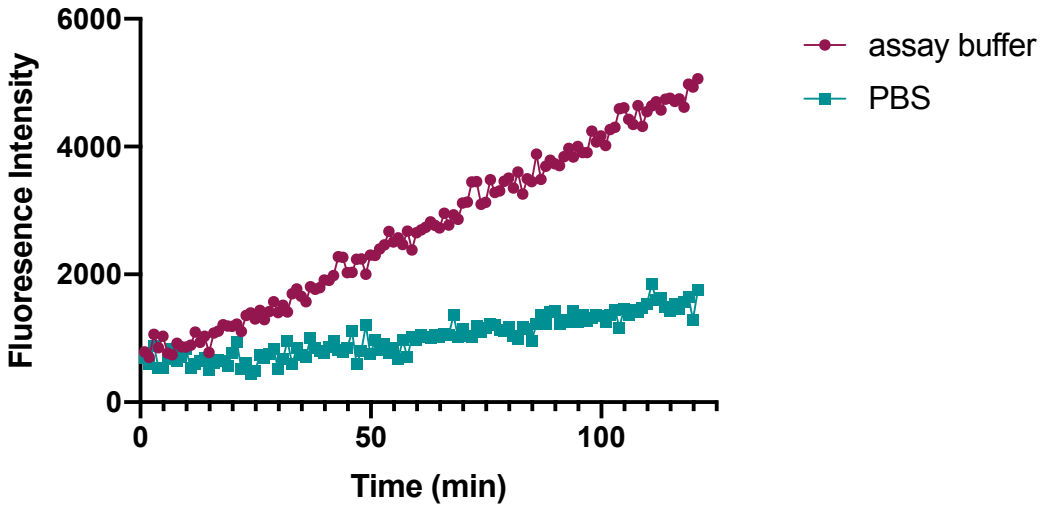

Figure A5. Fluorescence intensity increase of A101 with FXIII and thrombin in different buffers. Fluorescence intensity was measured with excitation at 313 nm and emission at 418 nm. 3.7 mM Gly-OMe HCl in 1.4 mM TCEP-HCl at pH 7.5 was added to each well as the transamidation acceptor. (Assay buffer: 100 mM Tris, 15 mM $CaCl_2$, 300 mM NaCl at pH 7.5; PBS: 1X PBS at pH 7.4 with 15 mM $CaCl_2$).

The next step in validating the FXIII assay was to compare the different possible buffers. An assay buffer consisting of Tris, $CaCl_2$ and NaCl was compared to PBS supplemented with $CaCl_2$. The fluorescence intensity was measured using the hydrolysis activity conditions described above, with excitation at 313 nm and emission at 418 nm (Figure A5). While both samples had in increase in fluorescence over 2 hours, there was a greater fluorescence increase in the assay buffer sample. This indicated that the preferred buffer for future FXIII hydrolysis activity assays was Tris, $CaCl_2$ and NaCl.

An HPLC assay was done using the second generation probe (**A16**) under the conditions for hydrolysis activity with FXIII. After 2 hours of incubation at 37°C, there was no change in the starting material chromatogram. This show that the probe is not a substrate for hydrolysis by FXIII.

A third generation probe was initially designed off the structure of A101, a known fluorogeneic substrate for FXIII. A101 is made up of a short peptide sequence with a quencher off the glutamate residue. Hydrolysis activity of FXIII can remove the quencher to result in an increase in fluorescence. Our design places the signal suppressor, N-hydroxy piperidine, in the same position and replaces the fluorogenic portion of the molecule with salicylic acid (Figure A6). Initial synthesis has begun to prepare the two unnatural amino acid monomers required in creating the probe: lysine containing salicylic acid off the side chain and glutamate containing N-hydroxy piperidine of its side chain. A peptide synthesizer can assemble the short peptide to form the third generation probe activated by transamidation/hydrolysis activity.

A.

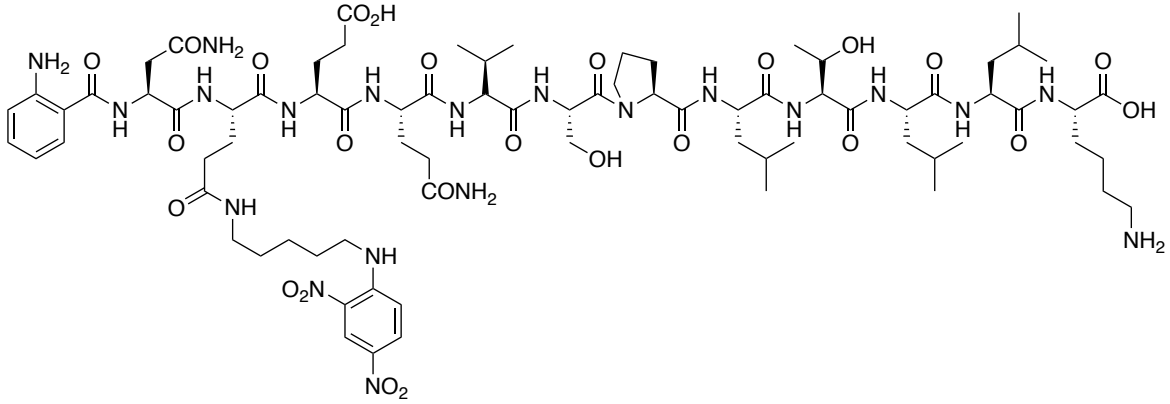

B.

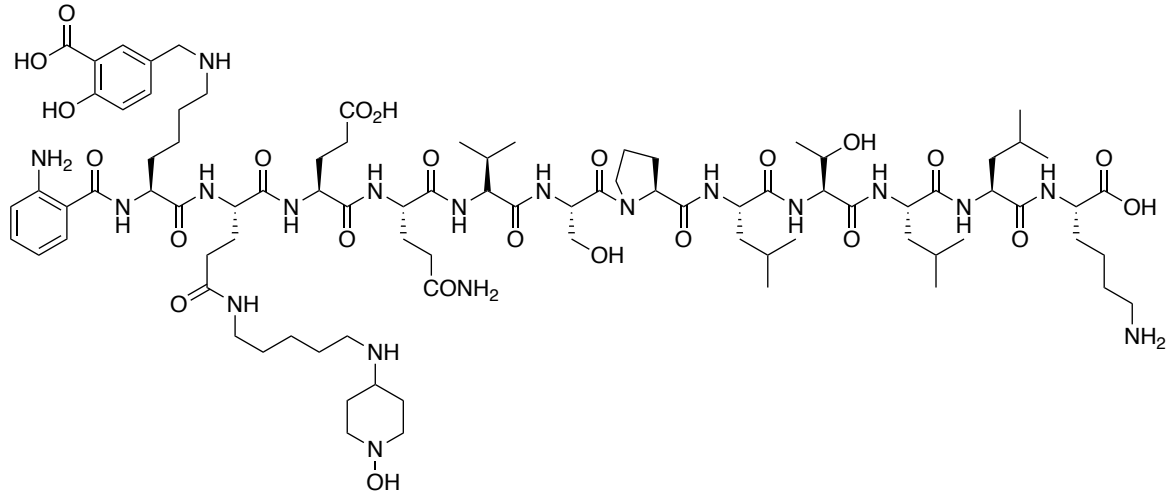

Figure A6. Structures of A101 (A) and third generation activatable probe (B).

A.

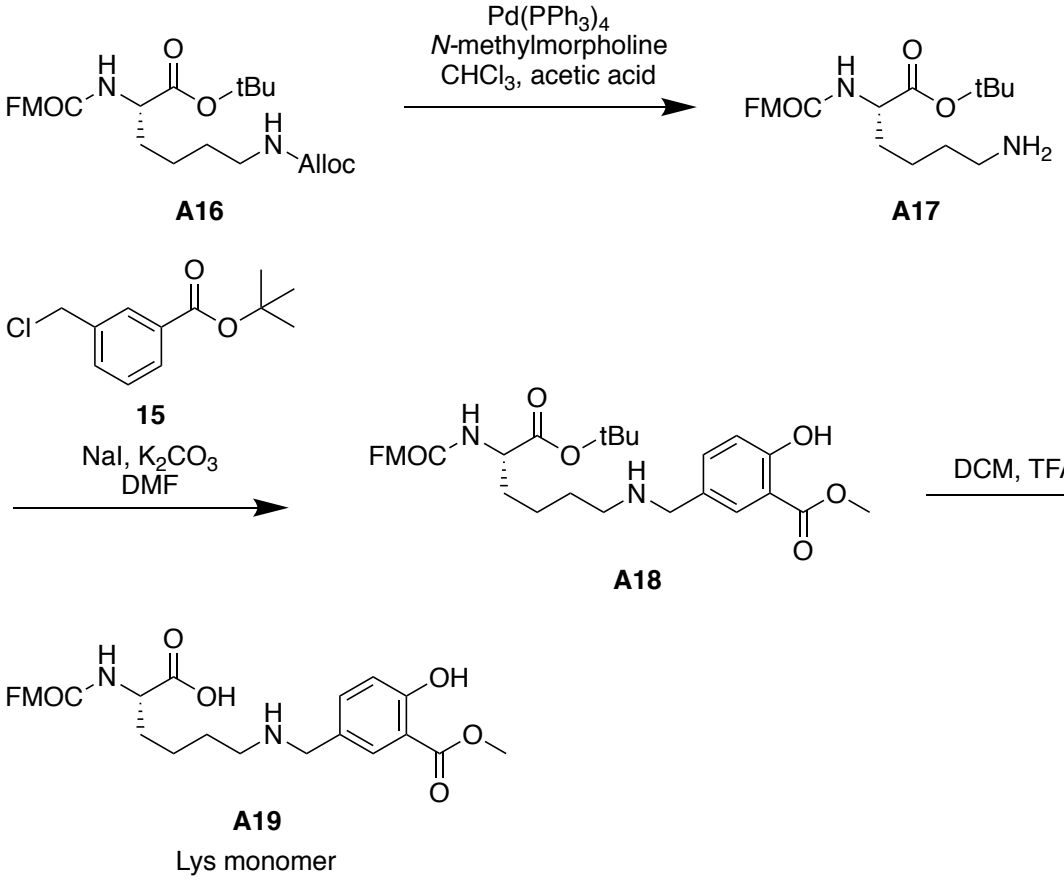

Lys monomer

B.

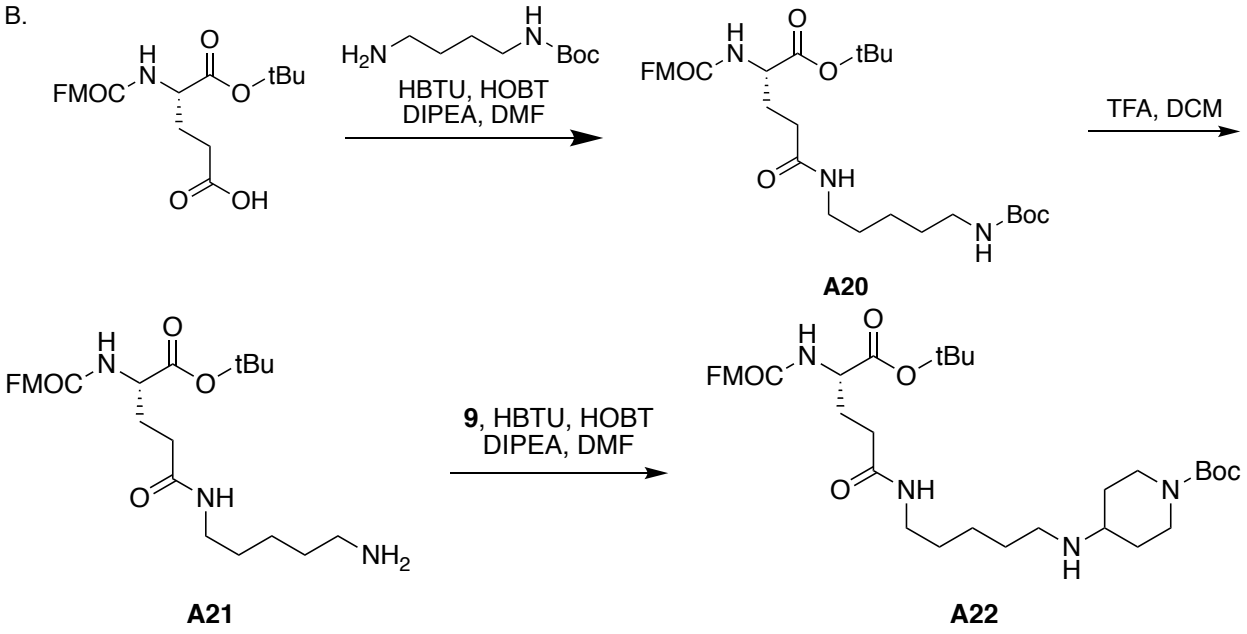

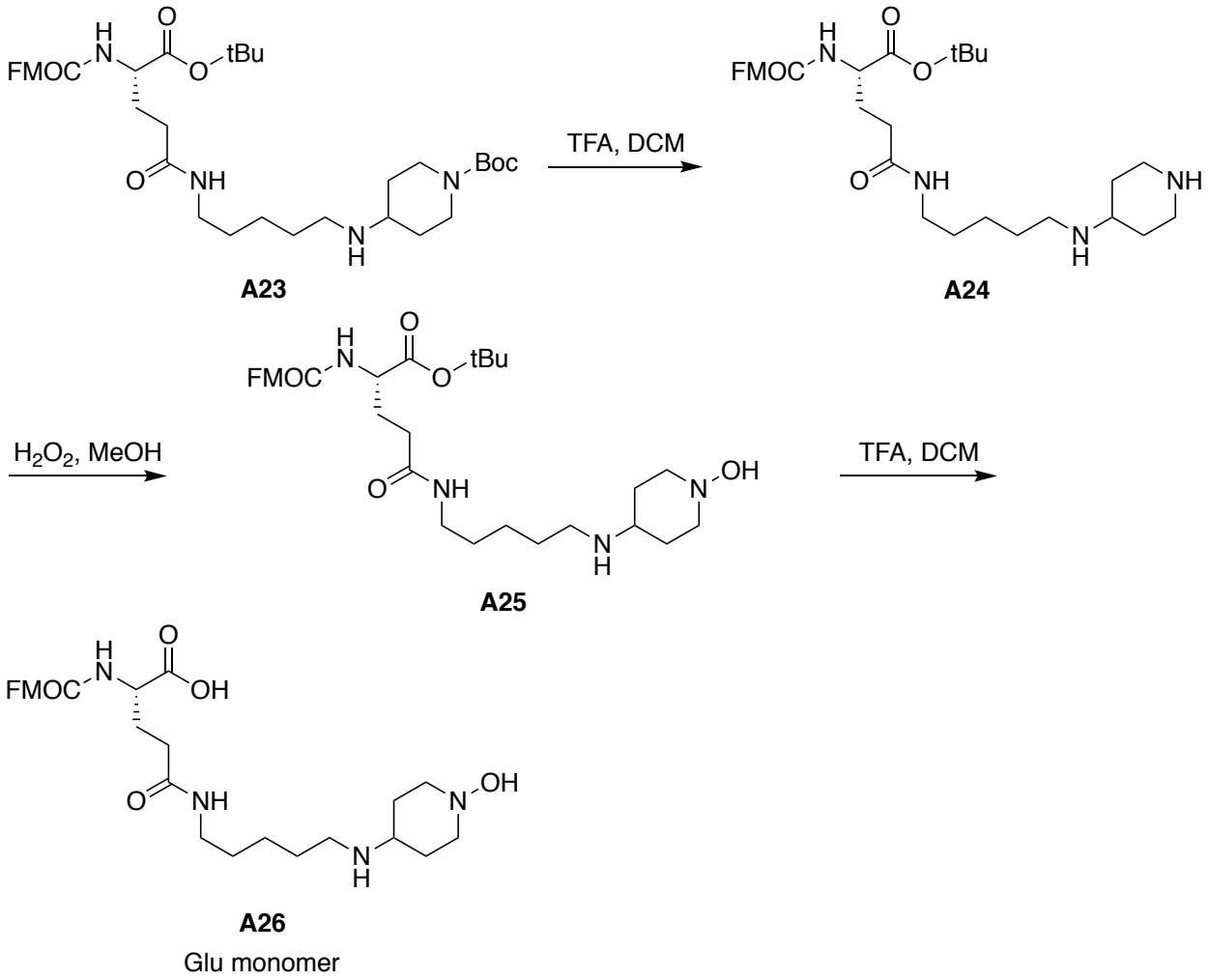

Figure A7. Synthesis of Lys (A) and Glu (B) monomers for third generation activatable probe.

Experimental

General Synthetic Procedures

Synthesis of TG2/FXIII-Targeted Probes

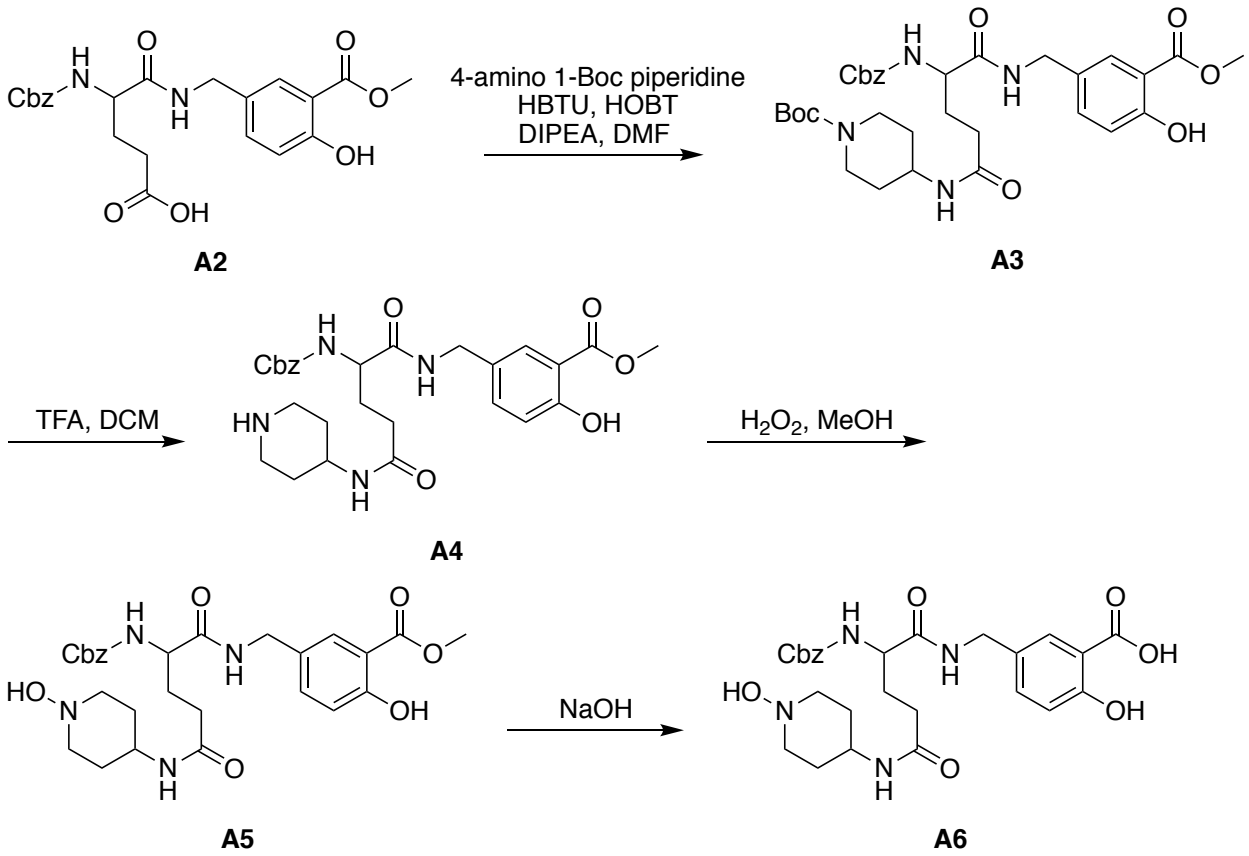

Scheme A1. Synthesis of first generation of TG2 activatable probe.

Synthesis of compound A1.

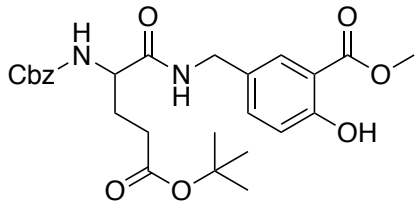

Cbz-protected glutaminc acid (Z-Glu(OtBu)-OH, 84.3 mg, 0.25 mmol, 1 equi.) was stirred in a solution of DIPEA (87.5 μL, 1 mmol, 4 equi.) and 0.5 mL DMF. HOBT (10.1 mg, 0.075 mmol, 0.3 equi.) and HBTU (94.8 mg, 0.25 mmol, 1 equi.) were added to the round bottom flask and

the reaction was put at 0°C for 10 minutes. Compound **4** (69.4 mg, 0.25 mmol, 1 equi.) was added to the reaction mixture and the flask was stirred at room temperature for an additional 18 hours. Afterwards, the mixture was diluted with brine and extracted using ethyl acetate. The combined organic phases were washed with brine and dried over sodium sulphate. The solvent was evaporated *in vacuo* to give the crude product as a yellow residue. The compound was purified by column chromatography using a mixture of 2:1 hexanes:acetone as the mobile phase. The product was isolated as a yellow solid in 52% yield. ^{1}H NMR (400 MHz, DMSO-D_6): δ 10.41 (s, 1H), 8.43 (t, J = 5.9 Hz, 1H), 7.68 (s, 1H), 7.50-7.26 (m, 7H), 6.93 (d, J = 10.9, 1H), 5.07-4.98 (m, 2H), 4.20 (t, J = 5.1 Hz, 2H), 4.05-3.95 (m, 1H), 3.33 (s, 3H), 2.20 (t, J = 8.2 Hz, 2H) ,1.94-1.67 (m 2H), 1.37 (s, 9H). ^{13}C NMR (400 MHz, DMSO-D_6): δ 171.84, 169.39, 165.13, 160.06, 135.14, 130.41, 128.98, 127.33, 127.03, 126.49, 126.35, 126.27, 125.94, 122.39, 121.84, 121.43, 117.07, 112.47, 90.23, 41.36, 28.39, 27.54, 25.61, 22.54. HRMS (ESI): calculated for $C_{26}H_{32}N_2O_6Na^+$ 523.2056; found 523.2068.

Synthesis of compound A2.

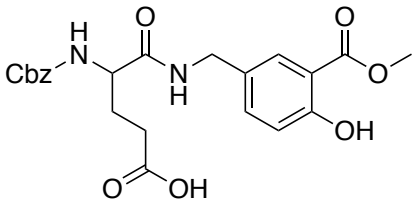

Compound **A1** was stirred in a solution of 2 mL DCM with 0.5 mL TFA for 2 hours at room temperature. The solvent was evaporated *in vacuo* with excess DCM to give the crude product as a light yellow solid. The solid was used without further purification. ^{1}H NMR (400 MHz, DMSO-D_6): δ 10.41 (s, 1H), 8.43 (t, J = 6.0 Hz, 1H), 7.67 (d, J = 2.0 Hz, 1H), 7.46 (d, J = 8.2

Hz, 1H), 7.42-7.28 (m, 6H), 6.93 (d, J = 8.8 Hz, 1H), 4.08-3.98 (m, 2H), 4.26-4.13 (m, 2H), 4.05-3.98 (m, 1H), 3.88 (s, 3H), 2.24 (t, J = 7.6 Hz, 2H), 1.96-1.67 (m, 2H).

HRMS (ESI): calculated for $C_{22}H_{24}N_2O_8Na^+$ 467.1430; found 467.1438.

Synthesis of compound A3.

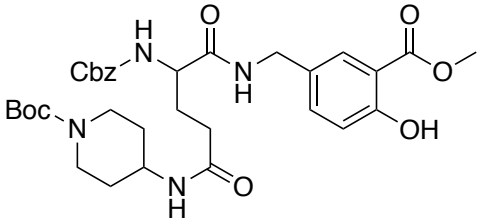

Compound **A3** was prepared following the same procedure as outlined for compound **A1**. Briefly, compound **A2** was stirred in a solution of 1 mL DMF with 43.8 μL DIPEA (0.5 mmol, 4 equi.). HOBT (5.05 mg, 0.0375 mmol, 0.3 equi.) and HBTU (47.4 mg, 0.12 mmol, 1 equi.) were added on ice. After 5 minutes, Boc-protected 4-amino piperidine (25 mg, 0.125 mmol, 1 equi.) was added to the flask and the mixture was stirred at room temperature for 18 hours. The crude compound was purified by column chromatography using a solvent system of 95:5 DCM:MeOH. The product was isolated as a white solid.

^{1}H NMR (400 MHz, DMSO-D_6): δ 10.40 (s, 1H), 8.40 (t, J = 5.8 Hz, 1H), 7.75 (d, J = 7.4 Hz, 1H), 7.67 (d, J = 2.0 Hz, 1H), 7.42-7.26 (m, 7H), 6.93 (d, J = 8.3 Hz, 1H), 5.07-4.98 (m, 2H), 4.00-3.93 (m, 1H), 3.88 (s, 3H), 3.85-3.75 (m, 2H), 3.75-3.66 (m, 1H), 2.88-2.76 (s, 1H), 2.18-2.05 (m, 2H), 1.96-1.84 (m, 1H), 1.81-1.61 (m, 3H), 1.39 (s, 9H), 1.28-1.14 (m, 3H). ^{13}C NMR (400 MHz, DMSO-D_6): 171.47, 168.82, 166.45, 161.67, 134.93, 130.57, 129.07, 127.68, 127.15, 126.82, 126.64, 126.38, 126.04, 122.49, 120.47, 120.29, 116.73, 112.69, 110.37, 105.69, 90.23, 70.23, 69.30, 41.36, 28.98, 27.29, 26.81, 22.24. HRMS (ESI): calculated for $C_{32}H_{42}N_4O_9Na^+$ 649.2849; found 649.2863.

Synthesis of compound A4.

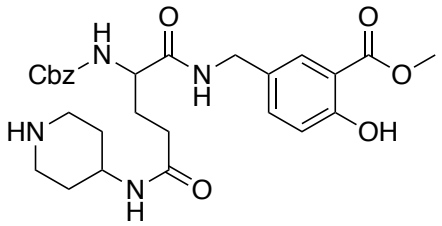

Compound **A4** was prepared from the same procedure as outlined for compound **A2**, starting with compound **A3**. The product was isolated as a colourless residue without further purification.

Synthesis of compound A5.

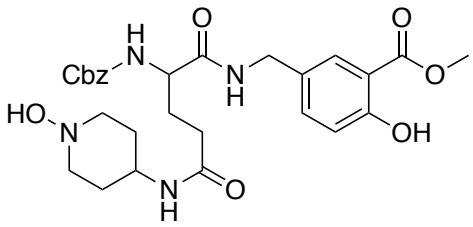

Compound **A5** was stirred in a solution of 30% H_2O_2 with 5 mL methanol at room temperature for 2 hours. The solvent was evaporated *in vacuo* and the residue was extracted using DCM. The combined organic phases were washed over brine and dried with sodium sulphate. The solvent was evaporated *in vacuo*. The compound was isolated as a white without further purification. ^{1}H NMR (400 MHz, DMSO-D_6): δ 10.38 (s, 1H), 8.41 (t, J = 5.9 Hz, 1H), 7.78 (d, J = 7.2 Hz, 1H), 7.67 (d, J = 2.1Hz, 1H), 7.42-7.26 (m, 7H), 6.93 (d, J = 8.4 Hz, 1H), 5.08-4.97 (m, 2H), 4.00-3.94 (m, 1H), 3.88 (s, 3H), 3.84-3.75 (m, 2H), 3.73-3.62 (m, 1H), 2.88-2.76 (s, 1H), 2.18-2.05 (m, 2H), 1.96-1.86 (m, 1H), 1.81-1.59 (m, 3H).^{13}C NMR (400 MHz, DMSO-D_6): 169.28, 168.58, 166.39, 161.72, 134.82, 130.76, 129.03, 127.83, 127.4, 126.27, 126.49, 126.37, 125.63,

122.89, 121.26, 120.93, 116.74, 112.35, 110.59, 105.02, 89.35, 70.19, 69.68, 41.49, 29.81, 26.93. HRMS (ESI): calculated for $C_{27}H_{34}N_4O_8Na^+$ 565.2257; found 565.2269.

Synthesis of compound A6.

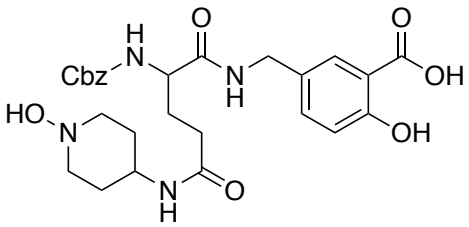

Compound **A5** was stirred in a solution of 20% NaOH at 70°C for 2 hours. The reaction mixture was cooled to room temperature and then acidified using dilute HCl until the pH of the solution was less than 2. The compound was extracted using ethyl acetate and the combined organic phases were dried over sodium sulphate. The solvent was evaporated *in vacuo* to give the compound as a white solid without further purification. ^{1}H NMR (400 MHz, DMSO-D_6): δ 10.37 (s, 1H), 8.39 (t, J = 5.8 Hz, 1H), 7.77 (d, J = 7.1 Hz, 1H), 7.68 (d, J = 2.2 Hz, 1H), 7.41-7.27 (m, 7H), 6.96 (d, J = 8.2 Hz, 1H), 5.09-4.98 (m, 2H), 3.99-3.92 (m, 1H), 3.83=3.76 (m, 2H), 3.72-3.61 (m, 1H), 2.89-2.77 (s, 1H), 2.18-2.06 (m, 2H), 1.96-1.89 (m, 1H), 1.79-1.62 (m 1H). ^{13}C NMR (400 MHz, DMSO-D_6): 169.84, 168.27, 167.31, 162.16, 134.29, 130.58, 128.97, 127.37, 127.48, 126.75, 126.56, 126.26, 125.83, 122.52, 121.89, 121.21, 116.59, 112.39, 110.64, 105.44, 70.39, 69.82, 41.32, 29.43, 25.31.HRMS (ESI): calculated $C_{26}H_{32}N_4O_8Na^+$ 551.2155; found 551.2112.

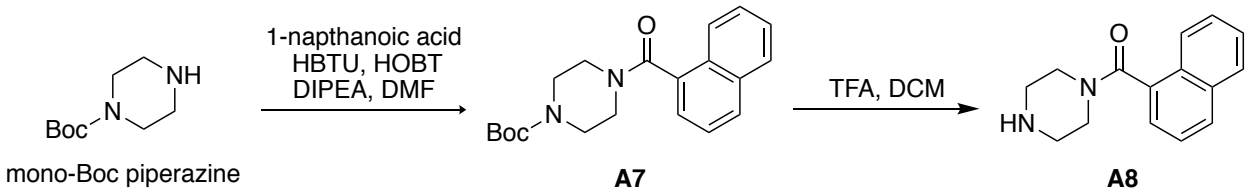

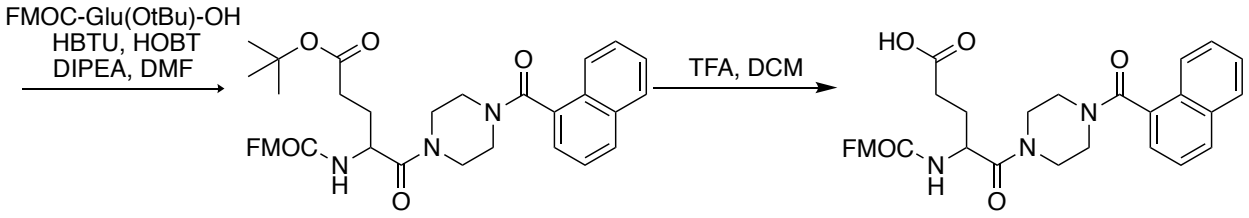

A9 **A10**

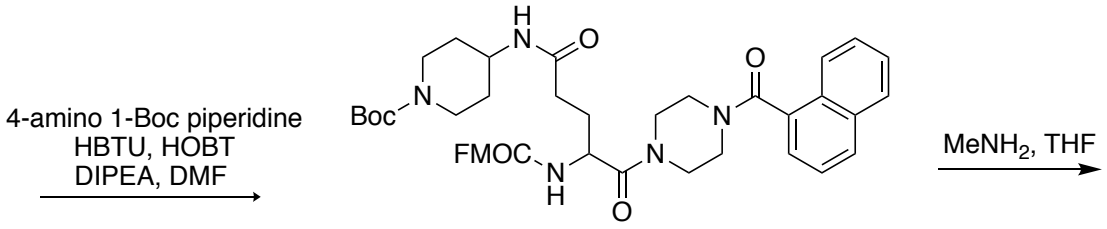

A11

4

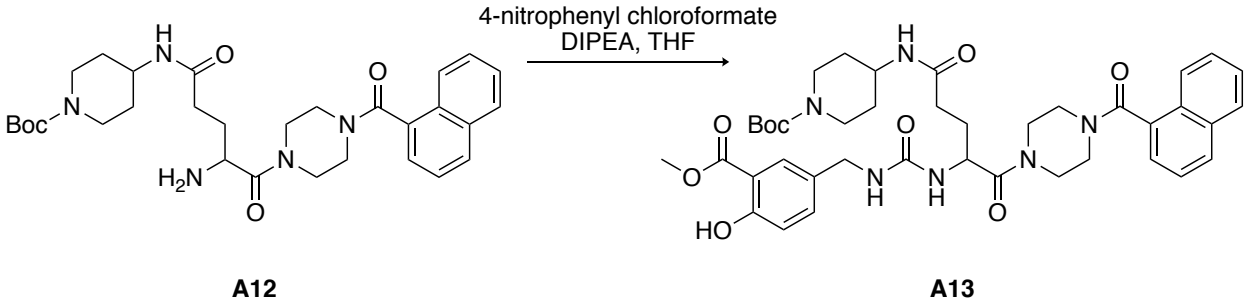

A12 **A13**

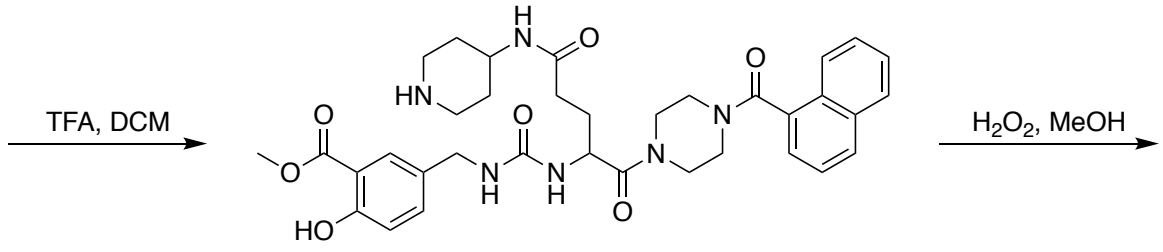

A14

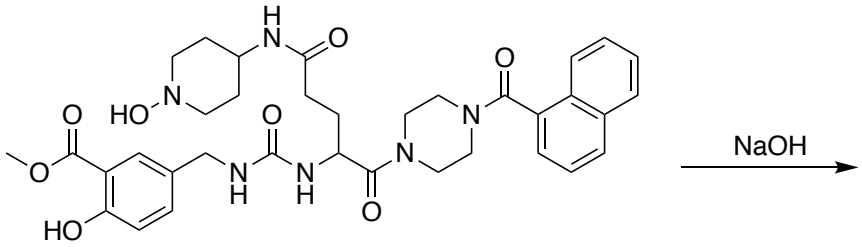

A15

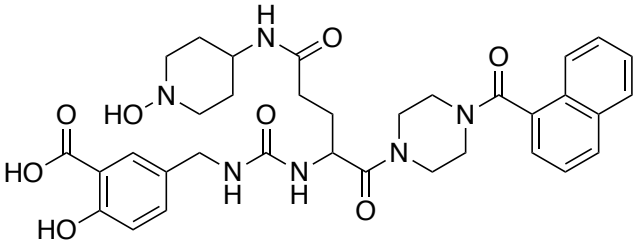

A16

Scheme A2. Synthesis of second generation TG2-activated/FXIII-activated probe.

Synthesis of compound A7.

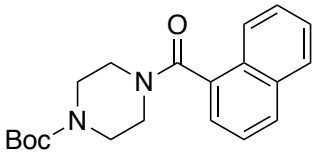

1-napthanoic acid (172 mg, 1 mmol, 1 equi.) was stirred in a solution of 1 mL DMF and 350 µL DIPEA (4 mmol, 4 equi.). HOBT (40.4 mg, 0.3 mmol, 0.3 equi.) and HBTU (379 mg, 1 mmol, 1 equi.) were added and the flask was stirred on ice for 5 minutes. Mono-Boc piperazine (186 mg, 1 mmol, 1 equi.) was added to the flask and the mixture was stirred at room temperature for an additional 18 hours. The compound was isolated using the work-up procedure described for compound **A1**. The crude compound was purified by 3:1 hexanes:acetone and the product was isolated as a yellow residue in 89% yield. ^{1}H NMR (400 MHz, $CDCl_3$): δ 7.91-7.80 (m, 3H), 7.56-7.38 (m, 4H), 4.03-3.82 (m, 2H), 3.66-3.57 (m, 2H), 3.36-3.21 (m, 2H), 3.20-3.14 (m, 2H), 1.46 (s, 9H). ^{13}C NMR (400 MHz, DMSO-D_6): δ 158.12, 143.75, 140.93, 134.05, 133.09, 128.42, 127.77, 127.67, 127.59, 127.16, 127.10, 127.05, 126.55, 125.41, 125.31, 123.87, 120.15,

120.07, 27.78, 27.70, 26.62. HRMS (ESI): calculated for $C_{20}H_{24}N_2O_3Na^+$ 363.1674; found 363.1679.

Synthesis of compound A8.

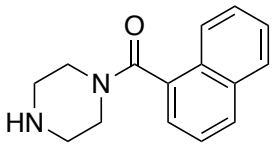

Compound **A8** was synthesized following the Boc deprotection procedure outlined for compound **A2**. The compound was isolated without further purification.

Synthesis of compound A9.

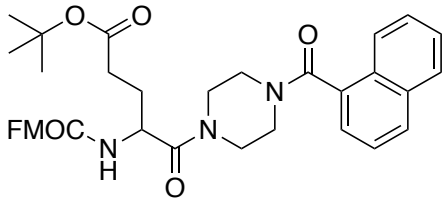

Compound **A9** was synthesized following the coupling procedure outlined for compound **A1** using compound **A8** and FMOC-Glu(OtBu). The product was HPLC purified using a gradient of 1% ACN + 0.1% TFA (in 0.1 TFA in water) to 100% CAN + 0.1% TFA over 25 minutes. The product was isolated as a white fluffy solid. ^{1}H NMR (400 MHz, DMSO-D_6): δ 8.04-7.25 (m, 7H), 4.36-4.21 (m, 2H), 3.77-3.65 (m, 2H), 3.51-3.26 (m, 1H), 3.15-3.10 (m, 1H), 2.34-2.17 (m, 1H), 1.94-1.63 (m, 1H), 1.40 (s, 9H).^{13}C NMR (400 MHz, DMSO-D_6): δ 158.12, 143.75, 140.93, 134.05, 133.09, 128.42, 127.77, 127.67, 127.59, 127.16, 127.10, 127.05, 126.55, 125.41, 125.31, 123.87, 120.15, 120.07, 49.65, 46.73, 46.67, 30.88, 27.78, 27.70, 26.62. HRMS (ESI): calculated for $C_{39}H_{41}N_3O_6Na^+$ 670.2876; found 670.2888.

Synthesis of compound A10.

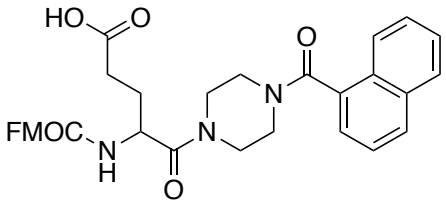

Compound **A10** was synthesized from compound **A9** using the procedure outlined for compound **A2**. The product was isolated as a yellow residue. HRMS (ESI): calculated for $C_{35}H_{33}N_3O_6Na^+$ 614.267; found 614.2241.

Synthesis of compound A11.

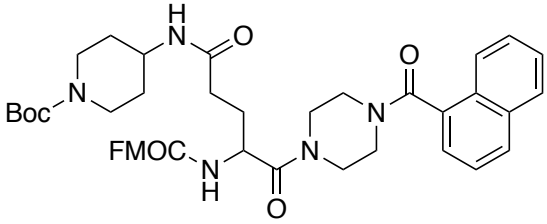

Compound **A11** was synthesized following the amide coupling procedure outlined for compound **A1**. Compound **A10** was coupled to Boc-protected 4-amino piperidine. The crude compound was purified by column chromatography using a elution solvent system of 9:1 DCM:MeOH. The product was isolated as a white solid. ^{1}H NMR (300 MHz, DMSO-D_6): δ 8.03-7.22 (m, 7H), 4.36-4.13 (m, 1H), 3.89-3.67 (m, 2H), 2.89 (s, 1H), 2.69 (s, 2H), 1.37 (d, J = 6.2 Hz, 3H). ^{13}C NMR (400 MHz, DMSO-D_6): δ 158.42, 143.92, 141.21, 134.58, 132.82, 128.45, 127.82, 127.52, 127.29, 127.18, 127.08, 126.92, 126.63, 125.37, 125.24, 123.72, 120.29, 120.03, 49.65, 46.73, 46.67, 30.88, 27.78, 27.70, 26.62.HRMS (ESI): calculated for $C_{35}H_{33}N_3O_6Na^+$ 796.3686; found 796.3674.

Synthesis of compound A12.

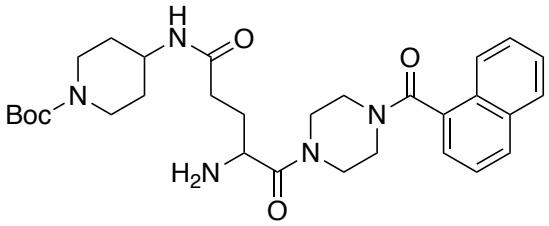

Compound **A11** was stirred in 2 mL of 2.0 M $MeNH_2$ in THF at room temperature for 1 hour. The solvent was evaporated *in vacuo* to give the product without further purification. ^{1}H NMR (400 MHz, DMSO-D_6): δ 8.04-7.98 (m, 2H), 7.84-7.70 (m, 2H), 7.62-7.46 (m, 4H), 3.91-3.55 (m, 7H), 3.19-2.99 (m, 2H), 2.98-2.16 (m, 2H), 2.38-2.03 (m, 2H), 1.90-1.52 (m 4H), 1.38 (s, 9H), 1.28-1.06 (m, 2H).^{13}C NMR (400 MHz, DMSO-D_6): δ 169.30, 165.23, 164.97, 132.74, 127.39, 127.89, 127.43, 126.25, 125.41, 49.52, 46.59, 46.42, 30.25, 27.84, 27.83, 26.25. HRMS (ESI): calculated for $C_{30}H_{41}N_5O_5Na^+$ 574.3005; found 574.2993.

Synthesis of compound A13.

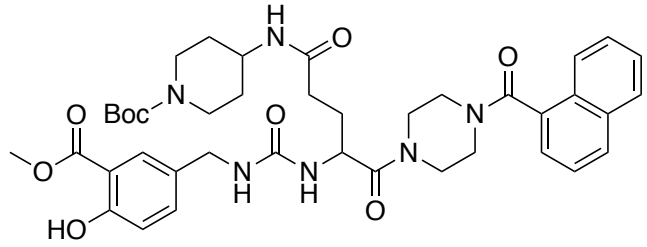

Compound **A12** (40 mg, 0.07 mmol, 1 equi.) was stirred in 2 mL THF and 61 μL DIPEA (0.35 mmol, 5 equi.). The mixture was cooled to 0°C and 4-nitrophenyl chloroformate (17.8 mg, 0.088 mmol, 1.3 equi.) was added. The flask was left on ice for an additional 30 minutes. 4-aminomethyl salicylate methyl ester (**4**) (12.5 mg, 0.07 mmol, 1 equi.) was then added to the reaction mixture and the flask was heated to 50°C. The mixture was stirred at 50°C for 16 hours. After 16 hours, the flask was cooled to room temperature and the reaction was quenched with 1 mL MeOH. The solvents were evaporated *in vacuo* and the residue was purified by column

chromatography using an eluting solvent of 95:5 DCM:MeOH. A light yellow solid was isolated. ^{1}H NMR (400 MHz, $CDCl_3$): δ 10.65 (d, J = 8.8 Hz, 1H), 7.94-7.87 (m, 2H), 7.81-7.69 (m, 2H), 7.57-7.48 (m, 3H), 7.43-7.31 (m 2H), 6.93-6.88 (m, 1H), 5.80-5.65 (broad s, 1H), 5.18-5.02 (broad s, 1H), 4.68-4.58 (m, 1H), 4.33-4.01 (m, 4H), 3.93 (s, 3H), 3.81-3.62 (m, 3H), 3.46-3.11 (m 4H), 2.32-2.17 (m, 2H), 2.09-1.50 (m, 5H), 1.43 (s, 9H), 1.31-1.17 (m, 2H). ^{13}C NMR (400 MHz, DMSO-D_6): δ 169.64, 169.24, 165.23, 164.97, 158.56. 134.29, 132.74, 128.31, 127.39, 127.89, 127.43, 126.25, 125.41, 117.70, 112.34, 52.34, 49.52, 46.59, 46.42, 44.92 30.25, 27.84, 27.83, 26.25. HRMS (ESI): calculated for $C_{40}H_{50}N_6O_9Na^+$ 791.3537; found 781.3535.

Synthesis of compound A14.

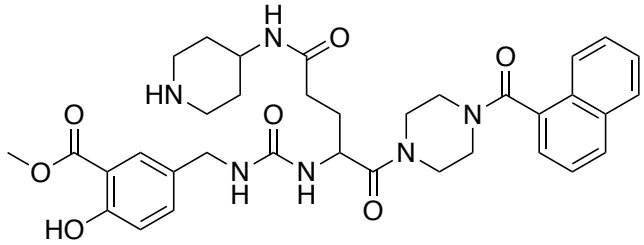

Compound **13** underwent the Boc deprotection procedure, as outlined for compound **A8**. The compound was isolated without further purification. HRMS (ESI): calculated for $C_{35}H_{42}N_6O_7Na^+$ 681.3013; found 681.3041.

Synthesis of compound A15.

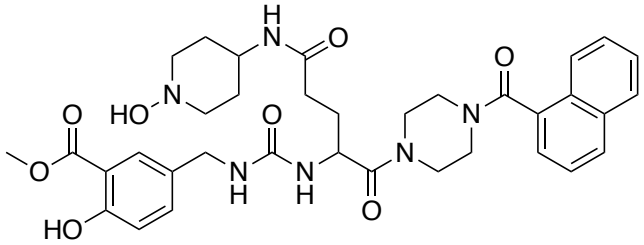

Compound **A15** was oxidized following the procedure outlined for compound **A5**. The product was isolated as a light yellow solid. ^{1}H NMR (400 MHz, $CDCl_3$): δ 10.64 (d, J = 8.7 Hz, 1H), 7.94-7.86 (m, 2H), 7.80-7.69 (m, 2H), 7.56-7.47 (m, 3H), 7.42-7.29 (m 2H), 6.95-6.90 (m, 1H), 5.81-5.70 (broad s, 1H), 5.19-5.04 (broad s, 1H), 4.67-4.59 (m, 1H), 4.30-3.98 (m, 4H), 3.88 (s, 3H), 3.80-3.64 (m, 3H), 3.47-3.14 (m, 4H), 2.32-2.18 (m, 2H), 2.07-1.51 (m, 5H), 1.31-1.17 (m, 2H). ^{13}C NMR (400 MHz, CDCl): δ 169.47, 169.38, 165.52, 164.89, 158.68. 134.22, 132.72, 128.35, 127.32, 127.47, 127.63, 126.15, 125.39, 117.53, 112.15, 52.29, 49.34, 46.26, 46.83, 44.62 30.37. HRMS (ESI): calculated for $C_{35}H_{42}N_6O_8Na^+$ 697.2974; found 697.2956.

Synthesis of compound A16.

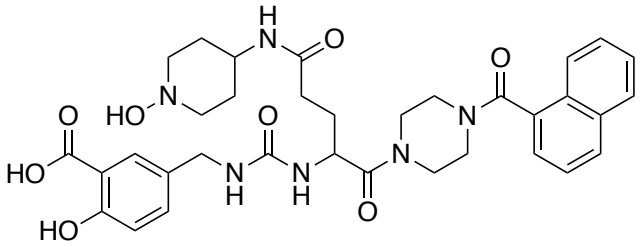

Compound **A15** was hydrolyzed following the procedure outlined for compound **A6**. The product was isolated as a white solid. ^{1}H NMR (400 MHz, $CDCl_3$): δ 10.63 (d, J = 8.8 Hz, 1H), 7.89-7.83 (m, 2H), 7.79-7.62 (m, 2H), 7.53-7.42 (m, 3H), 7.39-7.25 (m, 2H), 6.94-6.89 (m, 1H), 5.81-5.72 (m, 1H), 5.20-5.06 (m, 1H), 4.67-4.58 (m, 1H), 4.29-4.01 (m, 4H), 3.79-3.67 (m, 3H), 3.41-3.15 (m, 4H), 2.32-2.19 (m, 2H), 2.06-1.52 (m, 5), 1.32-1.18 (m, 2H). ^{13}C NMR 170.24, 169.84, 166.24, 165.02, 159.20, 134.25, 128.53, 127.63, 127.42, 126.59, 125.48, 117.39, 111.96, 49.82, 46.79, 44.28, 30.26. HRMS (ESI): calculated for $C_{34}H_{40}N_6O_8Na^+$ 683.2794; found 683.2800.

Appendix B

NMR Spectra

* Some NMR spectra were not remotely accessible and are not included in the appendix, but peak descriptions are provided in the Materials and Methods section.
Compound 1

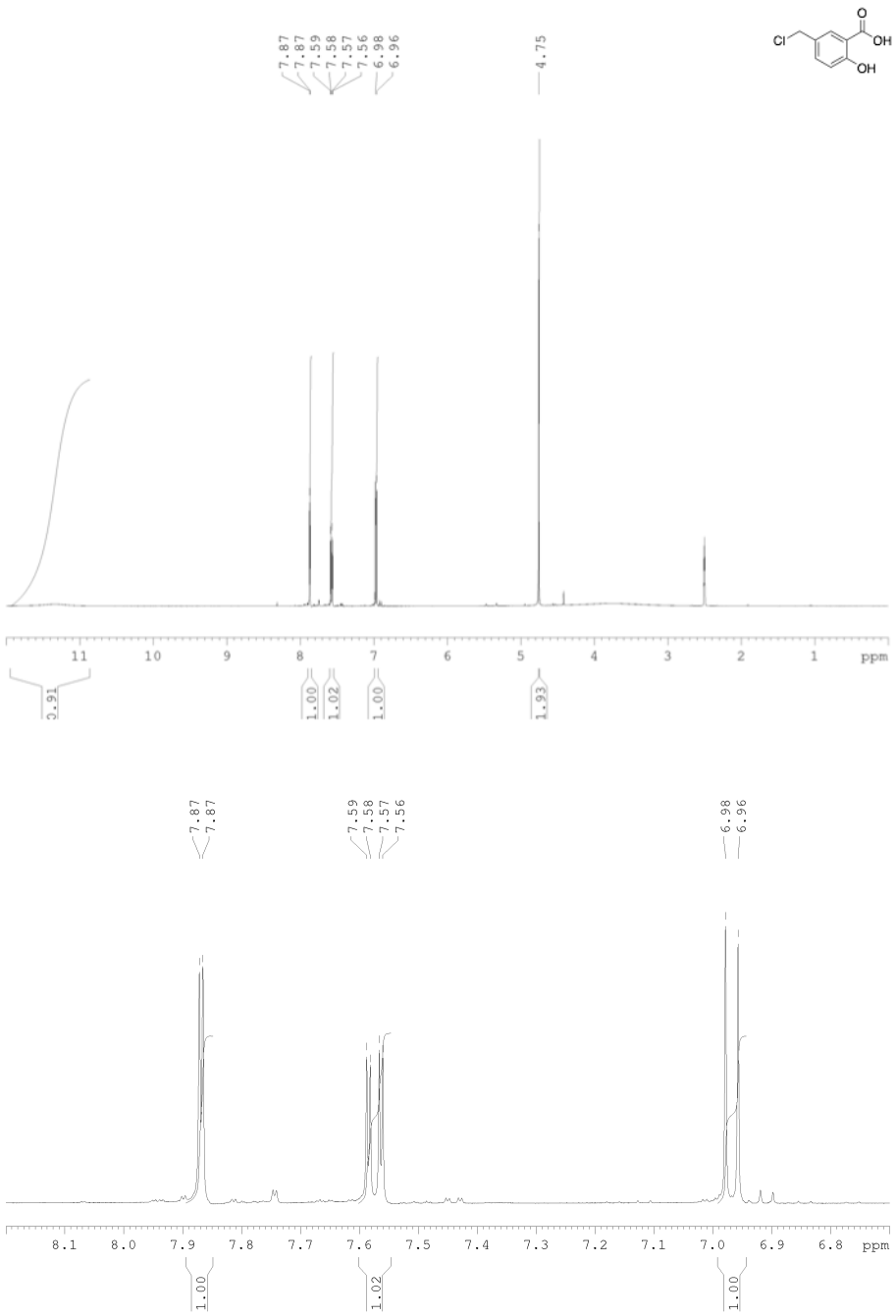

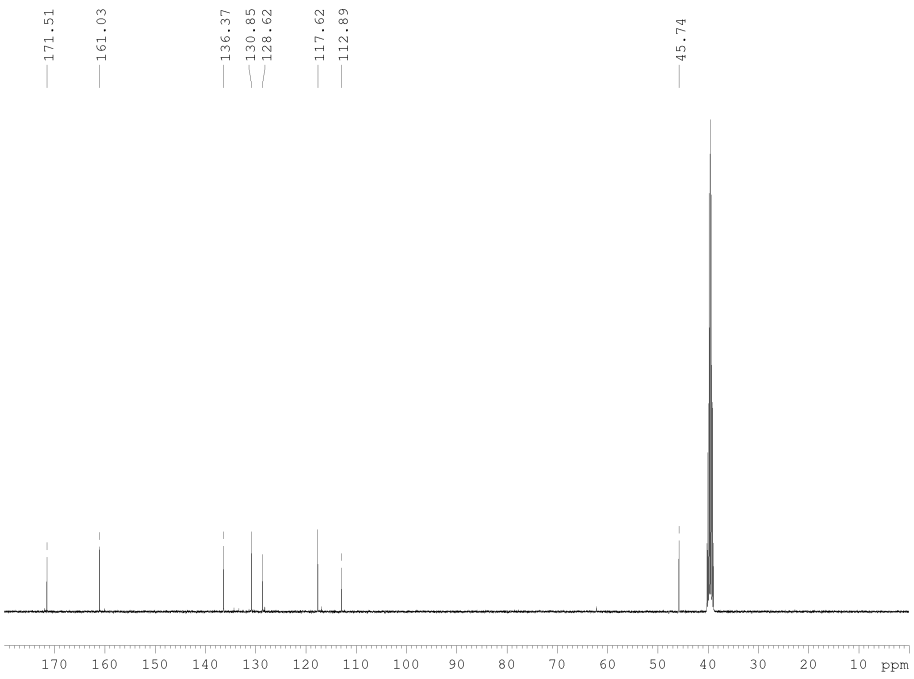
171.51
161.03
136.37
130.85
128.62
117.62
112.89
45.74
170 160 150 140 130 120 110 100 90 80 70 60 50 40 30 20 10 ppm

Compound 2

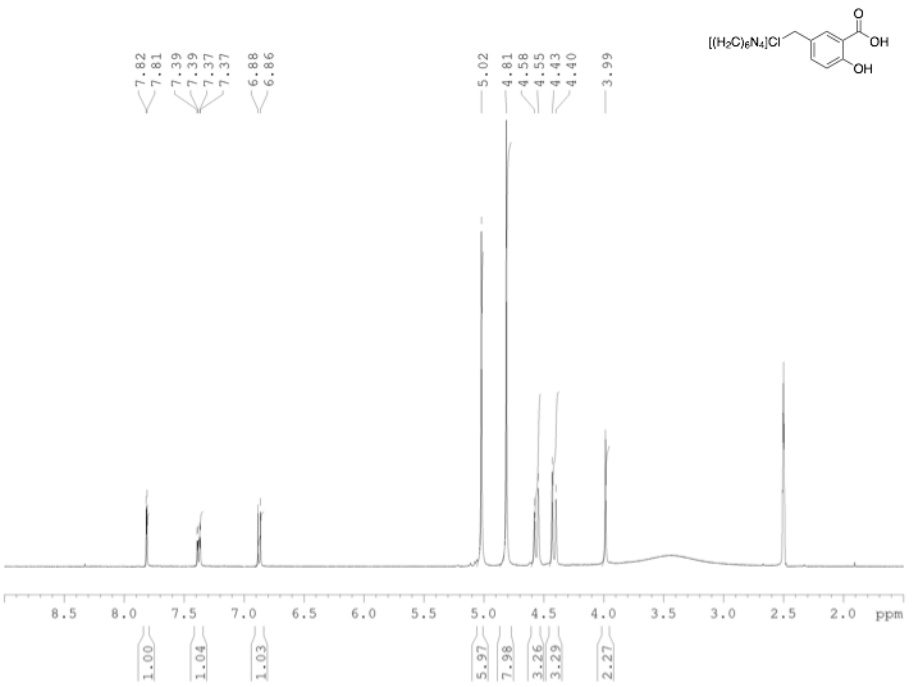
[(H2C)6N4]Cl
OH
OH
7.82
7.81
7.39
7.39
7.37
7.37
6.88
6.86
5.02
4.81
4.58
4.55
4.43
4.40
3.99
8.5 8.0 7.5 7.0 6.5 6.0 5.5 5.0 4.5 4.0 3.5 3.0 2.5 2.0 ppm
1.00
1.04
1.03
5.97
7.98
3.26
3.29
2.27

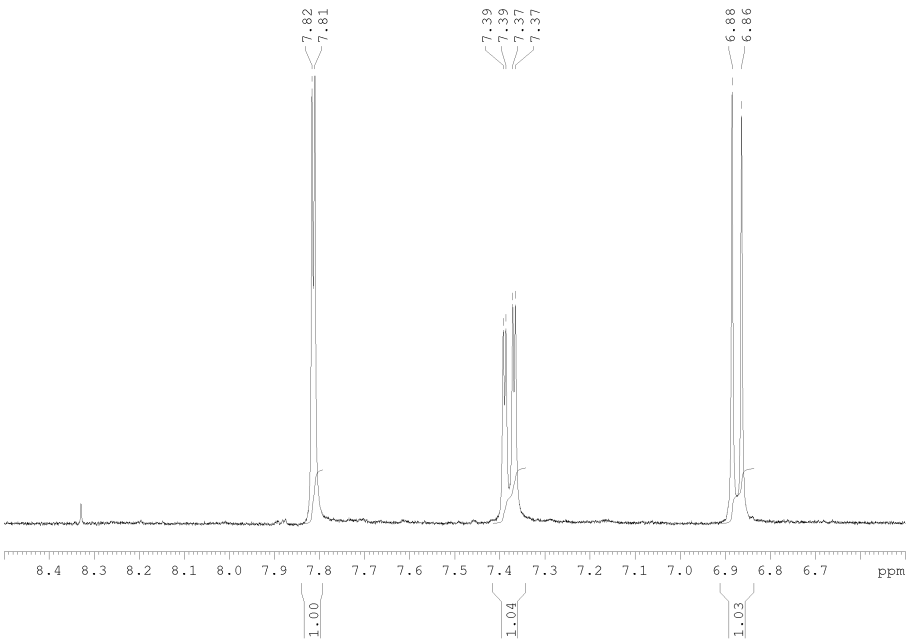
7.82
7.81
7.39
7.39
7.37
7.37
6.88
6.86
8.4 8.3 8.2 8.1 8.0 7.9 7.8 7.7 7.6 7.5 7.4 7.3 7.2 7.1 7.0 6.9 6.8 6.7 ppm
1.00
1.04
1.03

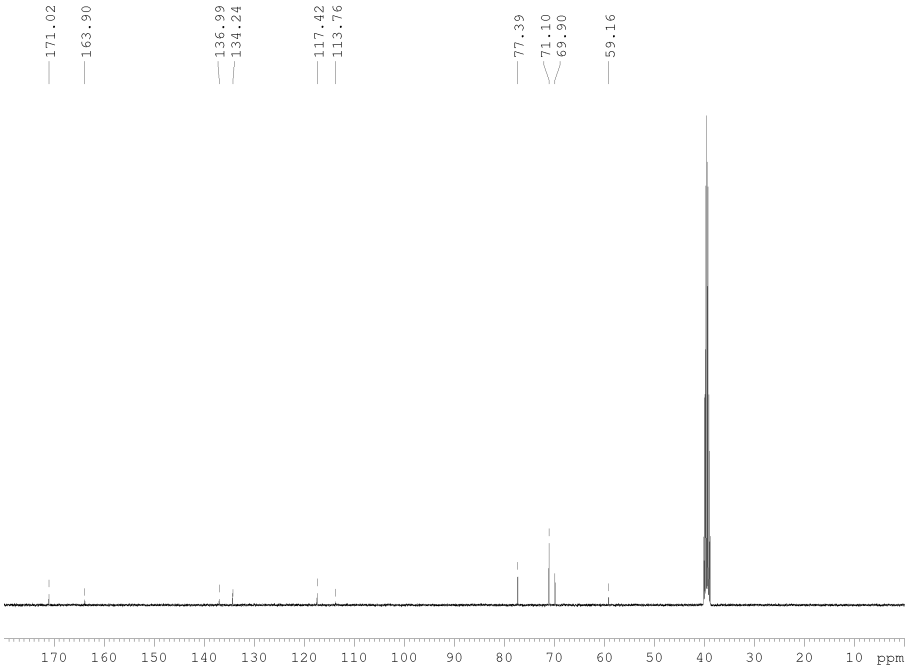
171.02
163.90
136.99
134.24
117.42
113.76
77.39
71.10
69.90
59.16
170 160 150 140 130 120 110 100 90 80 70 60 50 40 30 20 10 ppm

Compound 3

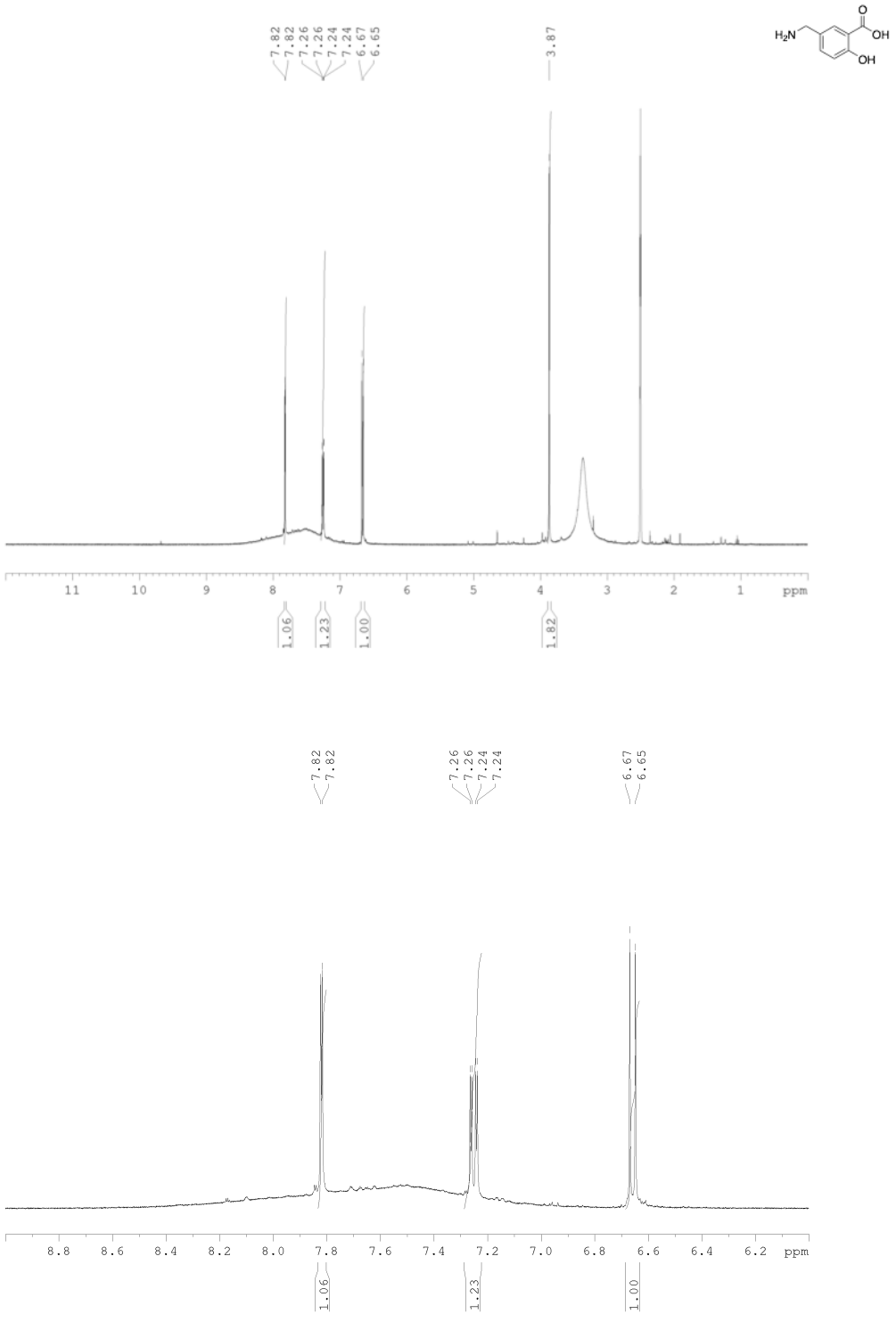
7.82
7.82
7.26
7.26
7.24
7.24
6.67
6.65
3.87
H2N
O
OH
OH
11
10
9
8
7
6
5
4
3
2
1
ppm
1.06
1.23
1.00
1.82
7.82
7.82
7.26
7.26
7.24
7.24
6.67
6.65
8.8
8.6
8.4
8.2
8.0
7.8
7.6
7.4
7.2
7.0
6.8
6.6
6.4
6.2
ppm
1.06
1.23
1.00

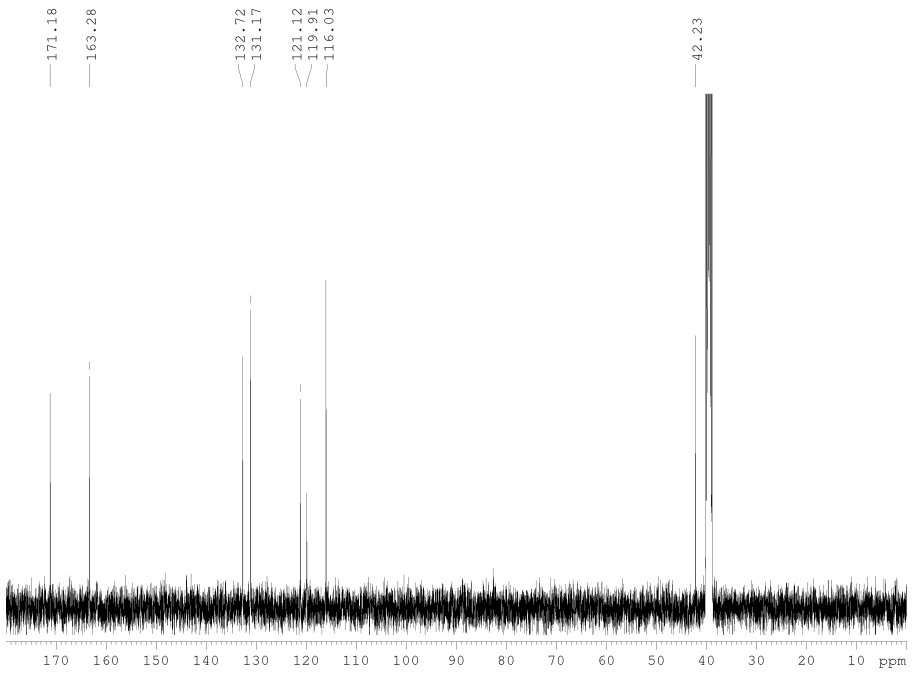
171.18
163.28
132.72
131.17
121.12
119.91
116.03
42.23
170 160 150 140 130 120 110 100 90 80 70 60 50 40 30 20 10 ppm

Compound 4

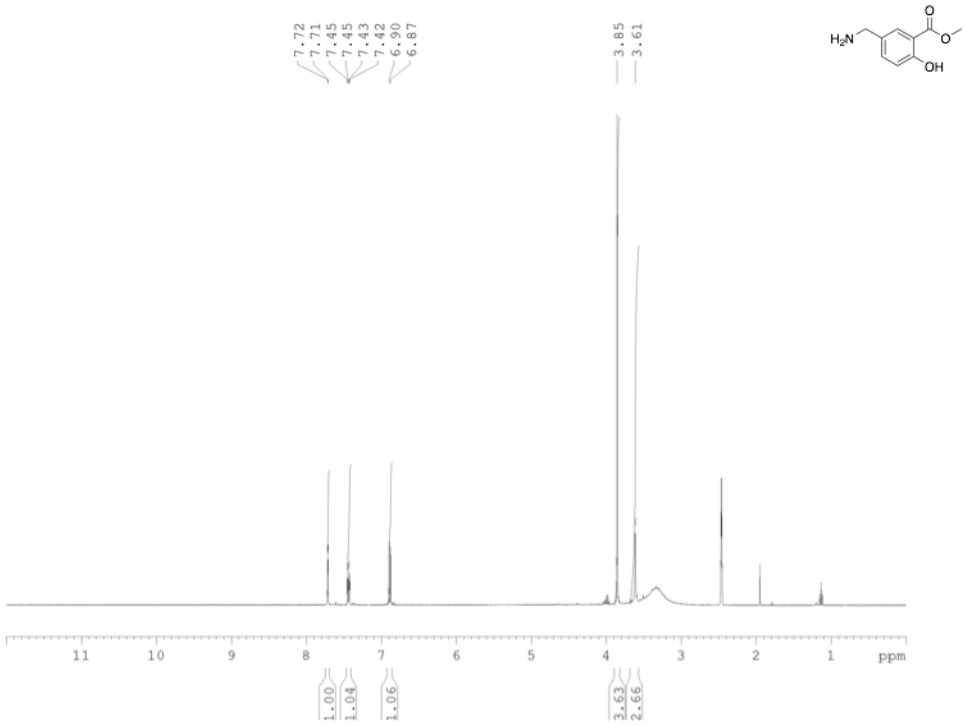
7.72
7.71
7.45
7.45
7.43
7.42
6.90
6.87
3.85
3.61
H2N
O
O
OH
11 10 9 8 7 6 5 4 3 2 1 ppm
1.00
1.04
1.06
3.63
2.66

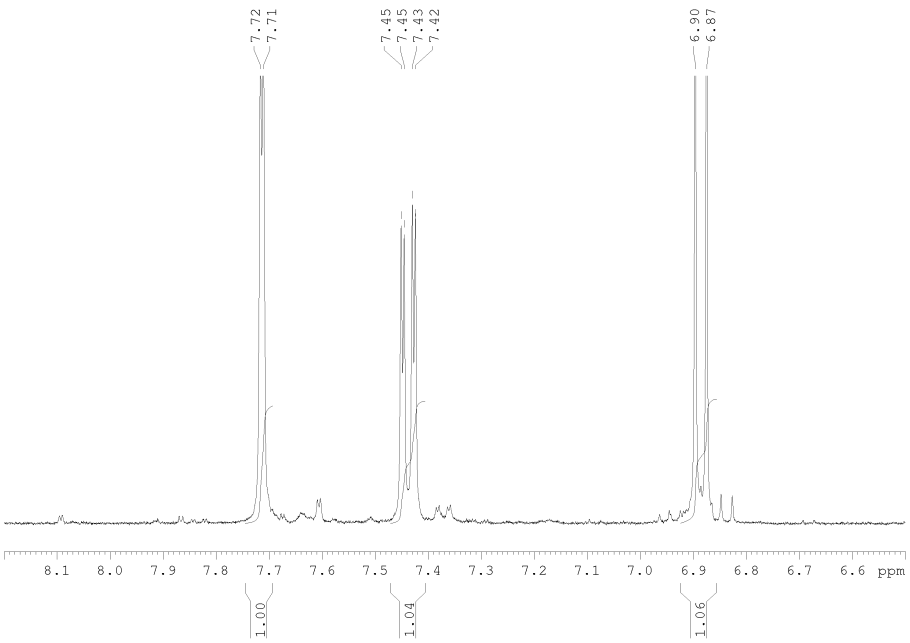
7.72
7.71
7.45
7.45
7.43
7.42
6.90
6.87
8.1 8.0 7.9 7.8 7.7 7.6 7.5 7.4 7.3 7.2 7.1 7.0 6.9 6.8 6.7 6.6 ppm
1.00
1.04
1.06

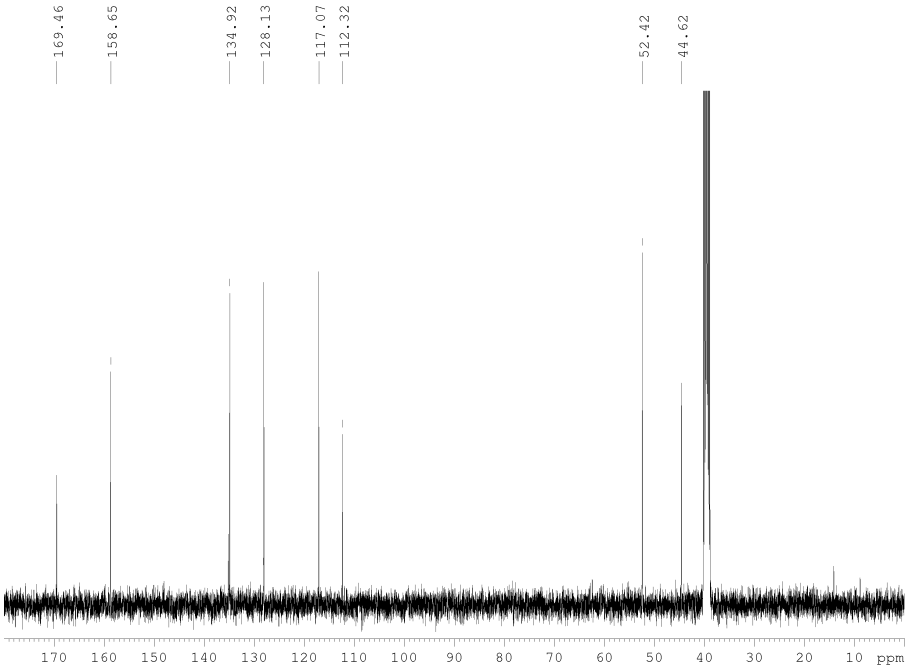
169.46
158.65
134.92
128.13
117.07
112.32
52.42
44.62
170 160 150 140 130 120 110 100 90 80 70 60 50 40 30 20 10 ppm

Compound 5

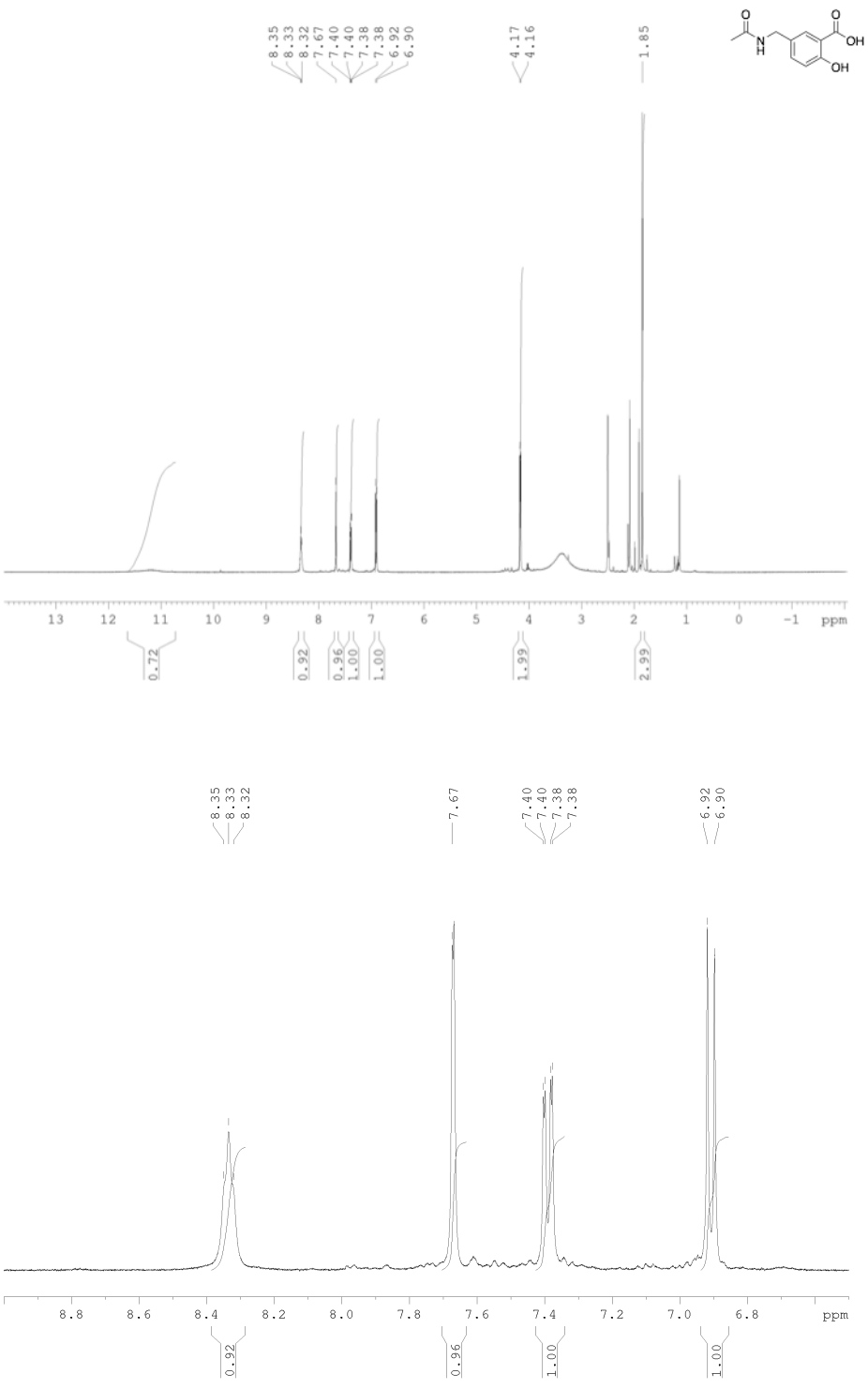
8.35
8.33
8.32
7.67
7.40
7.40
7.38
7.38
6.92
6.90
4.17
4.16
1.85
O
N
H
O
OH
OH
13 12 11 10 9 8 7 6 5 4 3 2 1 0 −1 ppm
0.72
0.92
0.96
1.00
1.00
1.99
2.99
8.35
8.33
8.32
7.67
7.40
7.40
7.38
7.38
6.92
6.90
8.8 8.6 8.4 8.2 8.0 7.8 7.6 7.4 7.2 7.0 6.8 ppm
0.92
0.96
1.00
1.00

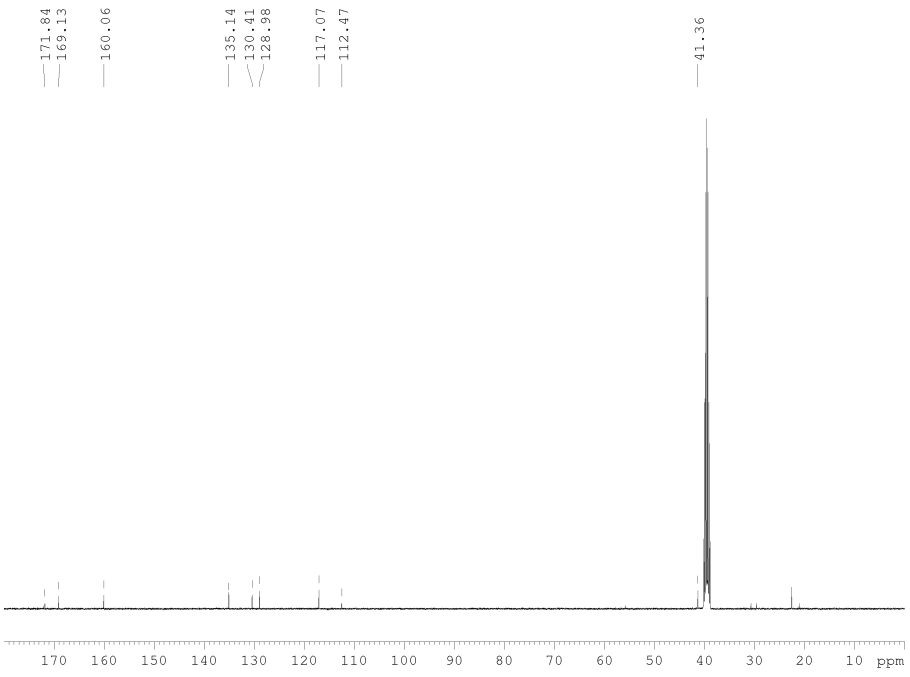
171.84
169.13
160.06
135.14
130.41
128.98
117.07
112.47
41.36
170 160 150 140 130 120 110 100 90 80 70 60 50 40 30 20 10 ppm

Compound 8

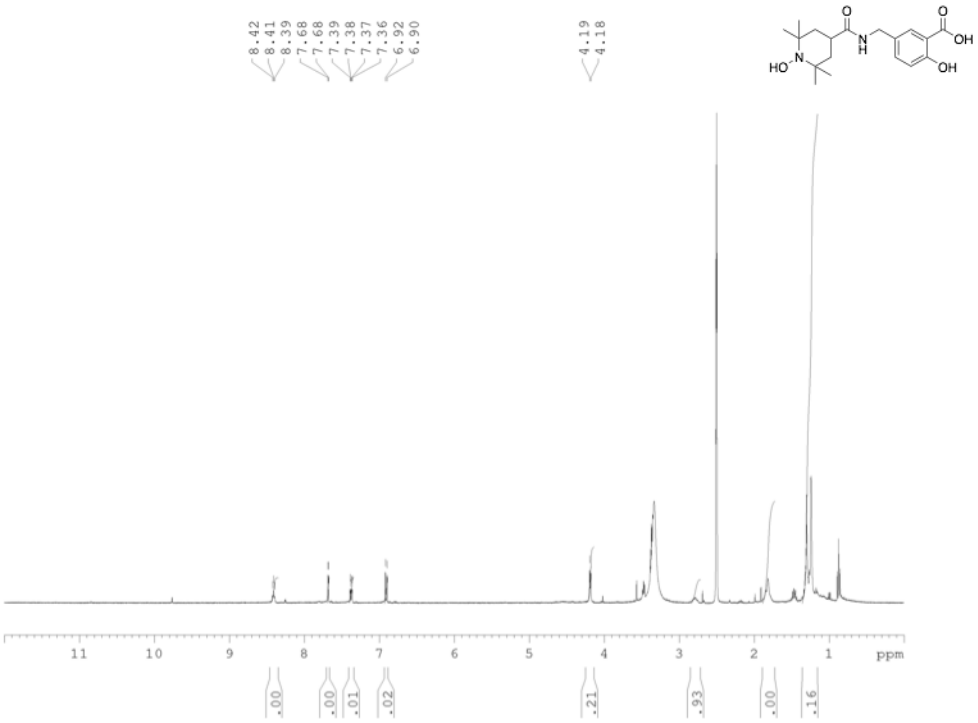
8.42
8.41
8.39
7.68
7.68
7.39
7.38
7.37
7.36
6.92
6.90
4.19
4.18
HO
N
O
N
H
O
OH
OH
11 10 9 8 7 6 5 4 3 2 1 ppm
.00
.00
.01
.02
.21
.93
.00
.16

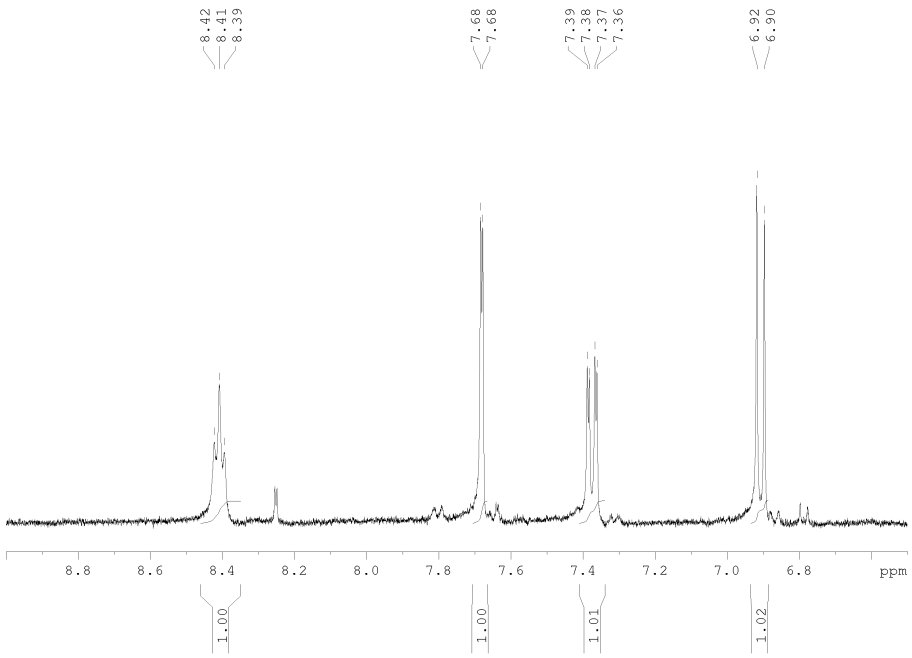
8.42
8.41
8.39
7.68
7.68
7.39
7.38
7.37
7.36
6.92
6.90
8.8
8.6
8.4
8.2
8.0
7.8
7.6
7.4
7.2
7.0
6.8
ppm
1.00
1.00
1.01
1.02

Compound 9

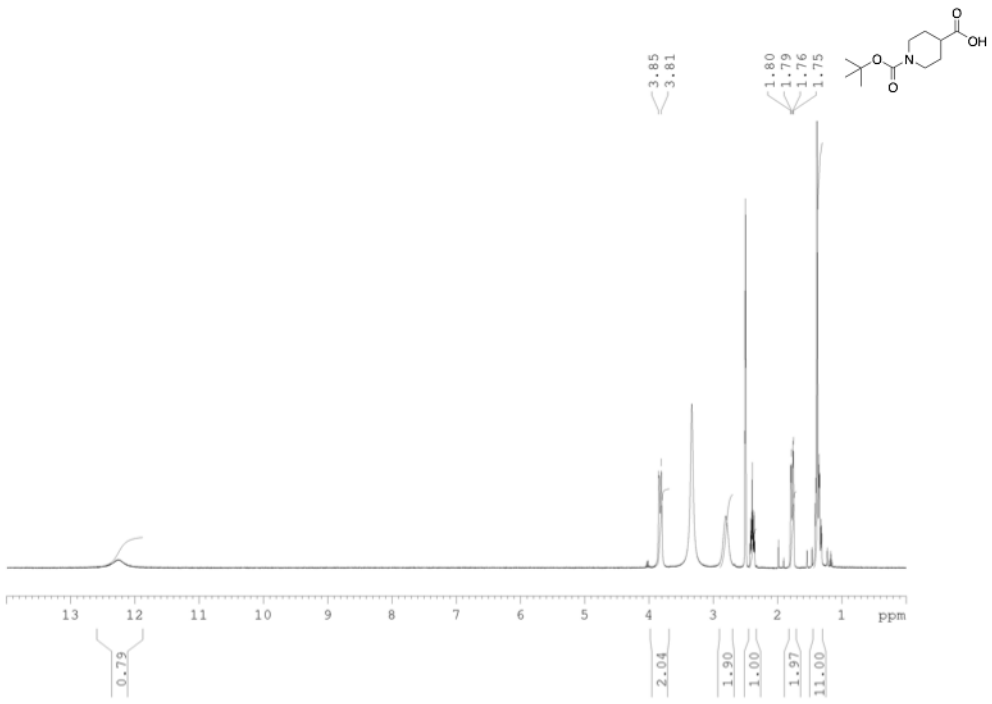
3.85
3.81
1.80
1.79
1.76
1.75
O
OH
O
N
O
13
12
11
10
9
8
7
6
5
4
3
2
1
ppm
0.79
2.04
1.90
1.00
1.97
11.00

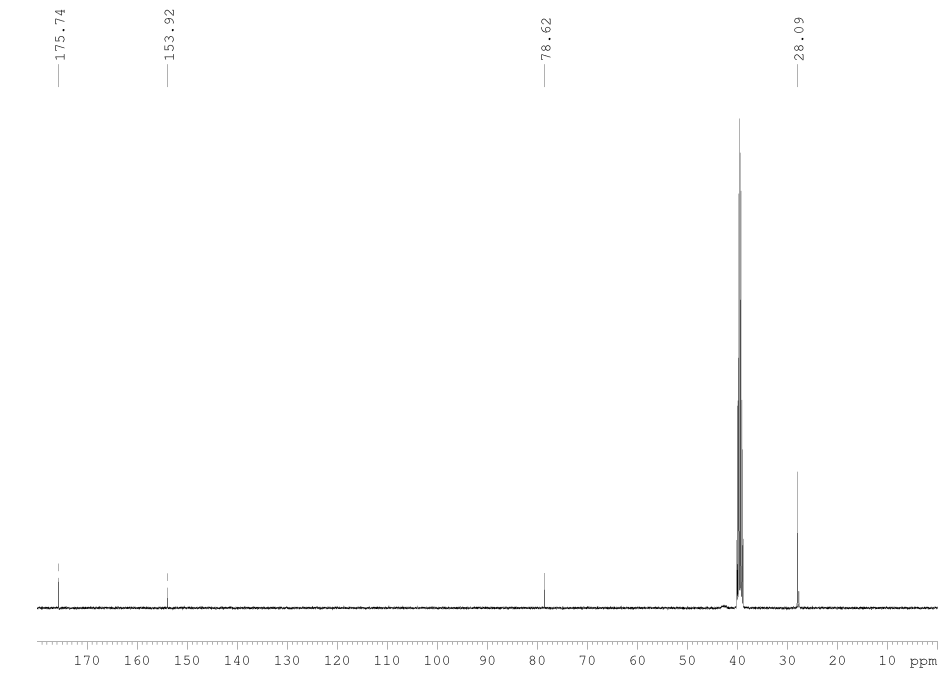
175.74
153.92
78.62
28.09
170 160 150 140 130 120 110 100 90 80 70 60 50 40 30 20 10 ppm

Compound 10

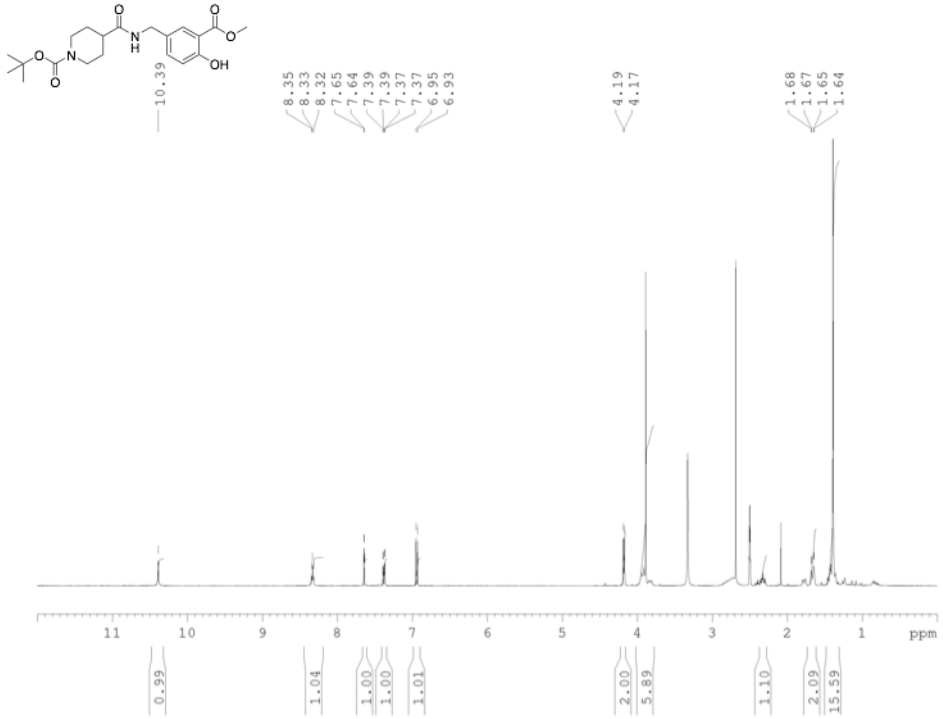
O
O
N
H
O
O
N
O
OH
10.39
8.35
8.33
8.32
7.65
7.64
7.39
7.39
7.37
7.37
6.95
6.93
4.19
4.17
1.68
1.67
1.65
1.64
11 10 9 8 7 6 5 4 3 2 1 ppm
0.99
1.04
1.00
1.00
1.01
2.00
5.89
1.10
2.09
15.59

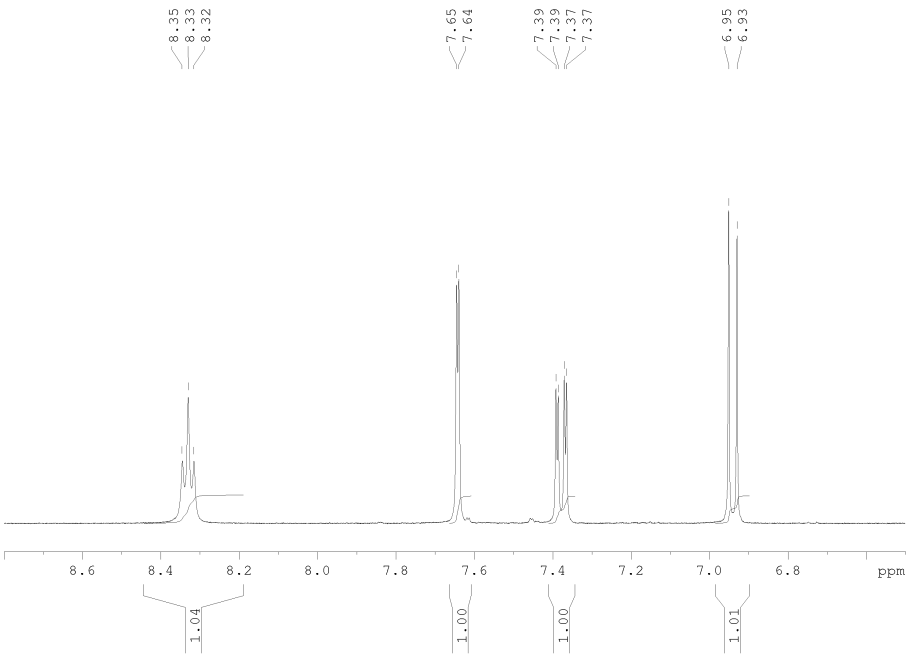
8.35
8.33
8.32
7.65
7.64
7.39
7.39
7.37
7.37
6.95
6.93
8.6
8.4
8.2
8.0
7.8
7.6
7.4
7.2
7.0
6.8
ppm
1.04
1.00
1.00
1.01

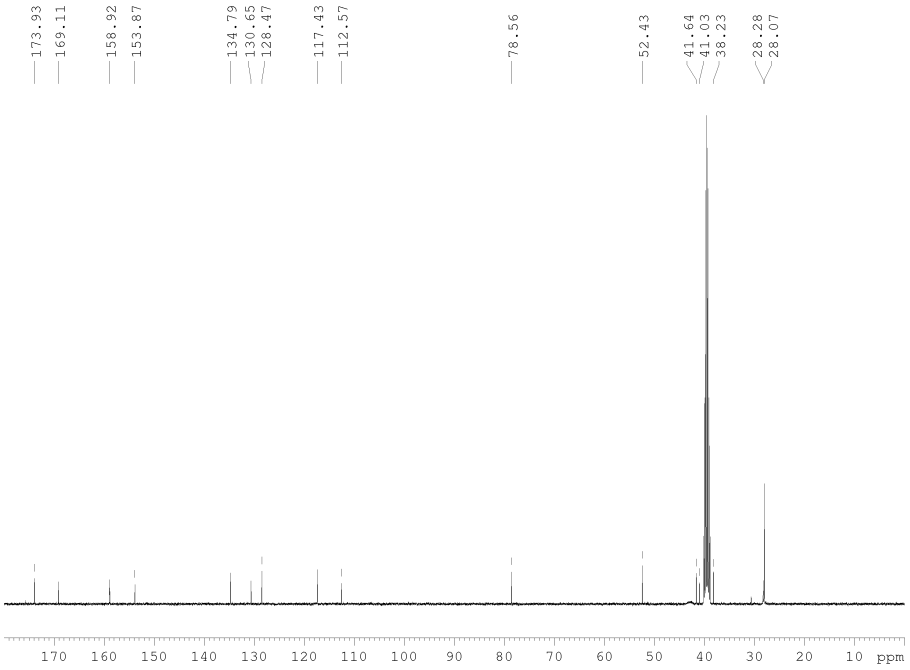
173.93
169.11
158.92
153.87
134.79
130.65
128.47
117.43
112.57
78.56
52.43
41.64
41.03
38.23
28.28
28.07
170
160
150
140
130
120
110
100
90
80
70
60
50
40
30
20
10
ppm

Compound 11

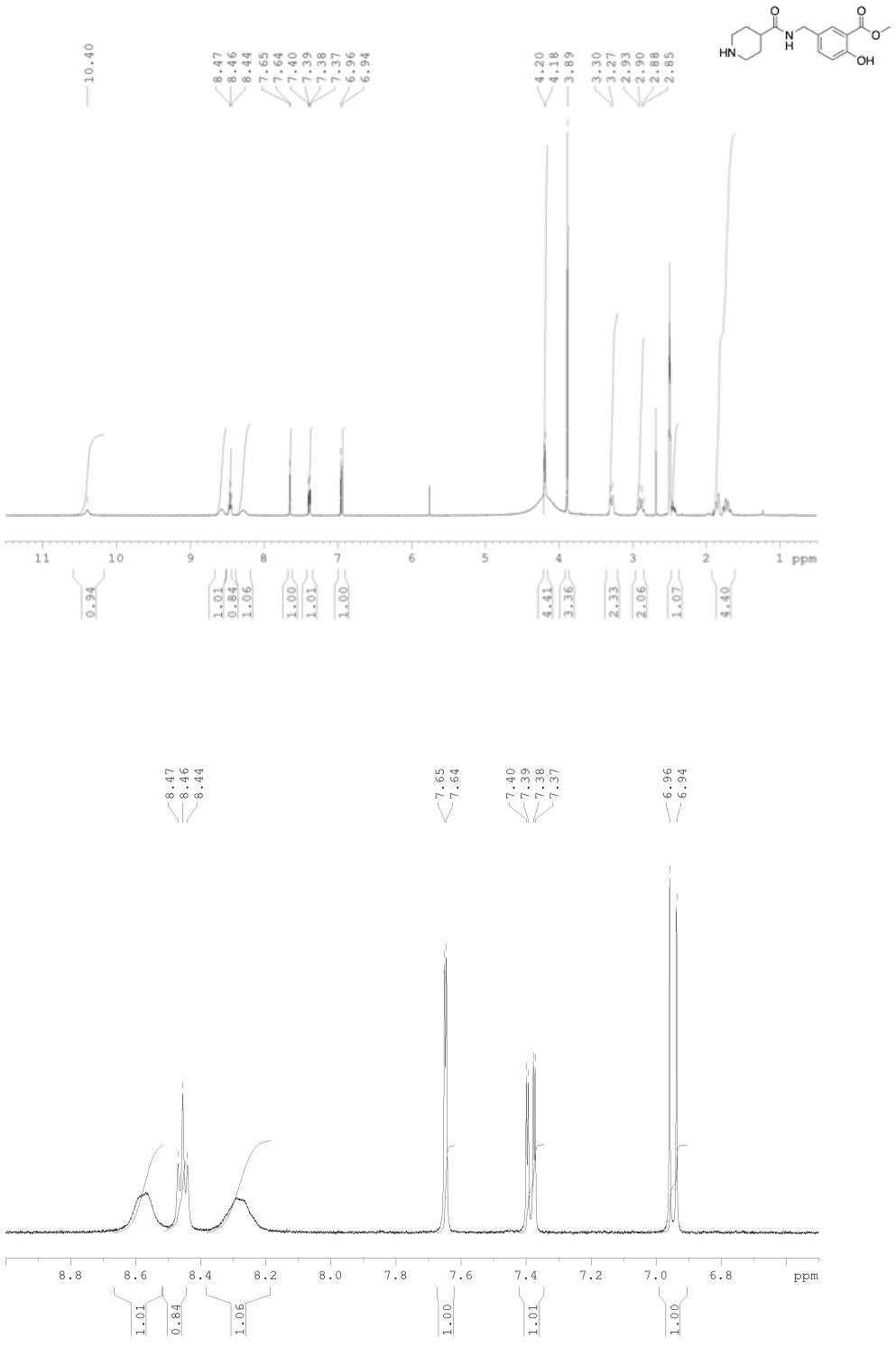
10.40
8.47
8.46
8.44
7.65
7.64
7.40
7.39
7.38
7.37
6.96
6.94
4.20
4.18
3.89
3.30
3.27
2.93
2.90
2.88
2.85
HN
N
H
O
O
O
OH
11
10
9
8
7
6
5
4
3
2
1 ppm
0.94
1.01
0.84
1.06
1.00
1.01
1.00
4.41
3.36
2.33
2.06
1.07
4.40
8.8
8.6
8.4
8.2
8.0
7.8
7.6
7.4
7.2
7.0
6.8
ppm
1.01
0.84
1.06
1.00
1.01
1.00

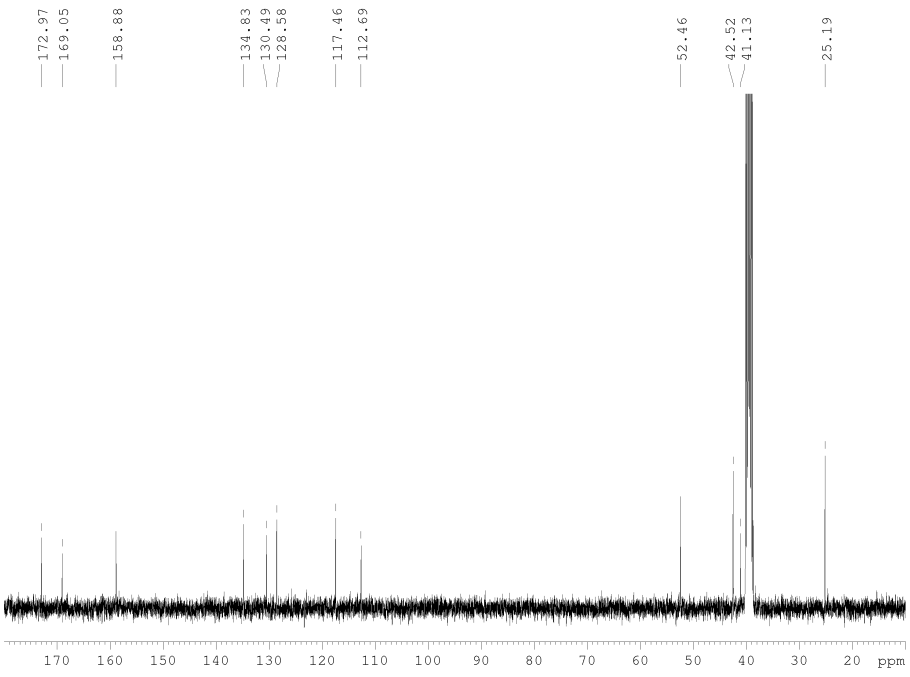
172.97
169.05
158.88
134.83
130.49
128.58
117.46
112.69
52.46
42.52
41.13
25.19
170 160 150 140 130 120 110 100 90 80 70 60 50 40 30 20 ppm

Compound 14

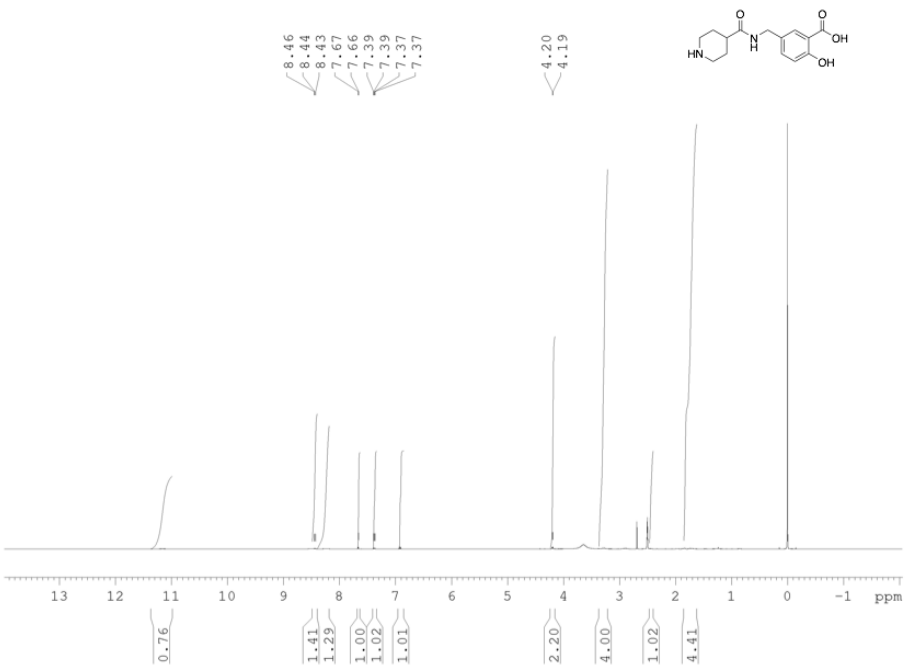
8.46
8.44
8.43
7.67
7.66
7.39
7.39
7.37
7.37
4.20
4.19
HN
O
N
H
O
OH
OH
13 12 11 10 9 8 7 6 5 4 3 2 1 0 -1 ppm
0.76
1.41
1.29
1.00
1.02
1.01
2.20
4.00
1.02
4.41

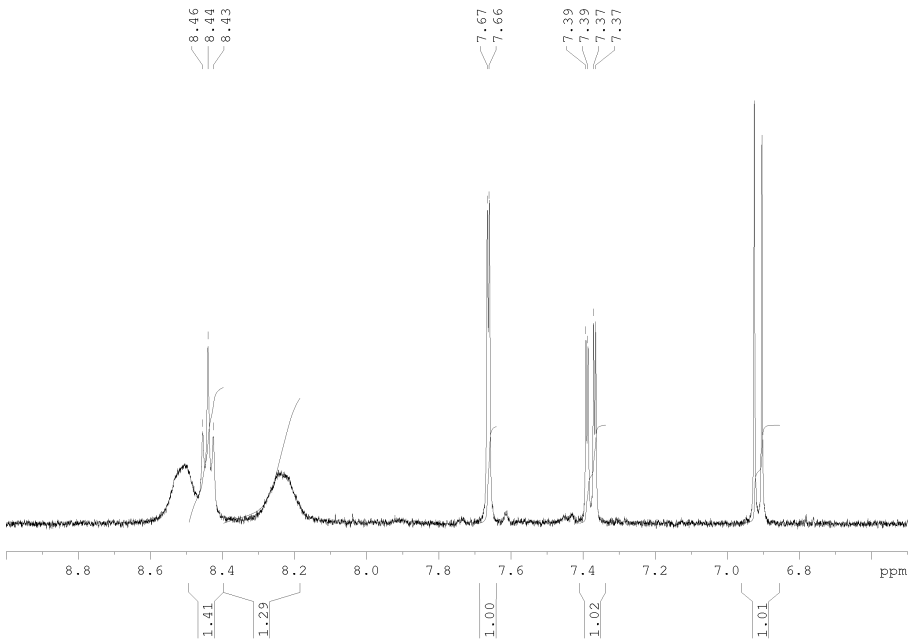
8.46
8.44
8.43
7.67
7.66
7.39
7.39
7.37
7.37
8.8
8.6
8.4
8.2
8.0
7.8
7.6
7.4
7.2
7.0
6.8
ppm
1.41
1.29
1.00
1.02
1.01

Compound 15

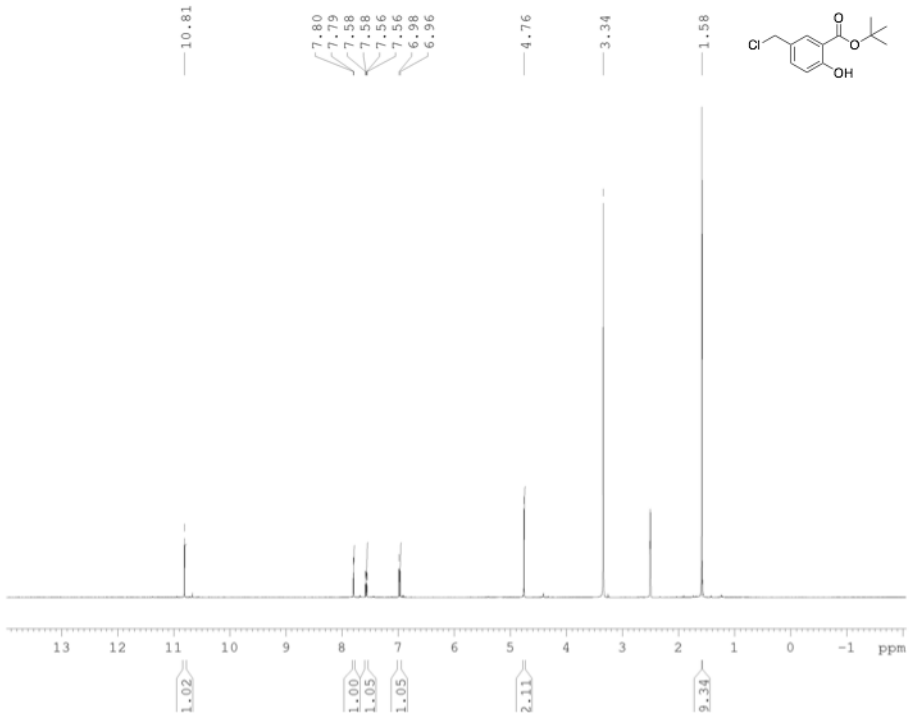
10.81
7.80
7.79
7.58
7.58
7.56
7.56
6.98
6.96
4.76
3.34
1.58
Cl
O
O
OH
13
12
11
10
9
8
7
6
5
4
3
2
1
0
−1
ppm
1.02
1.00
1.05
1.05
2.11
9.34

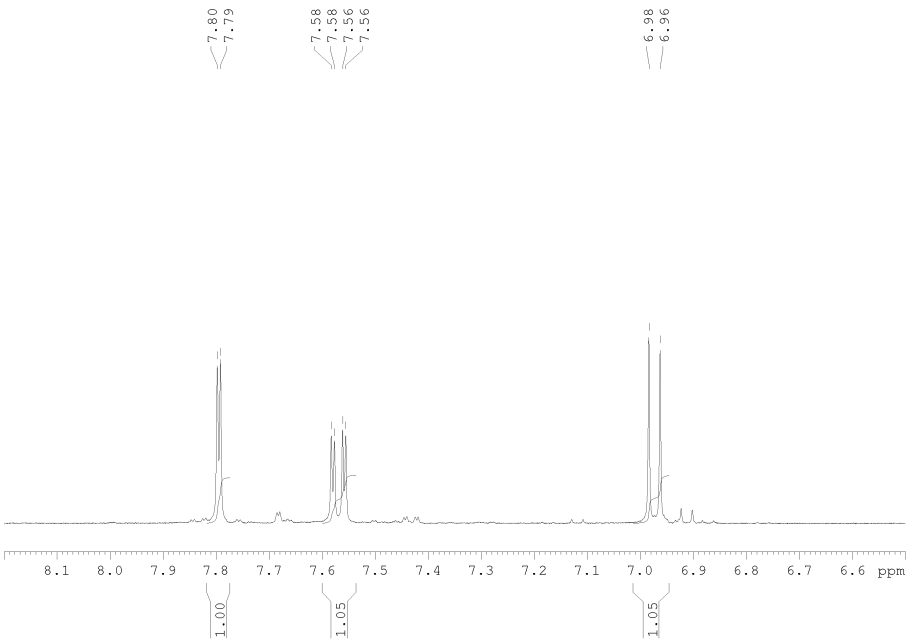
7.80
7.79
7.58
7.58
7.56
7.56
6.98
6.96
8.1 8.0 7.9 7.8 7.7 7.6 7.5 7.4 7.3 7.2 7.1 7.0 6.9 6.8 6.7 6.6 ppm
1.00
1.05
1.05

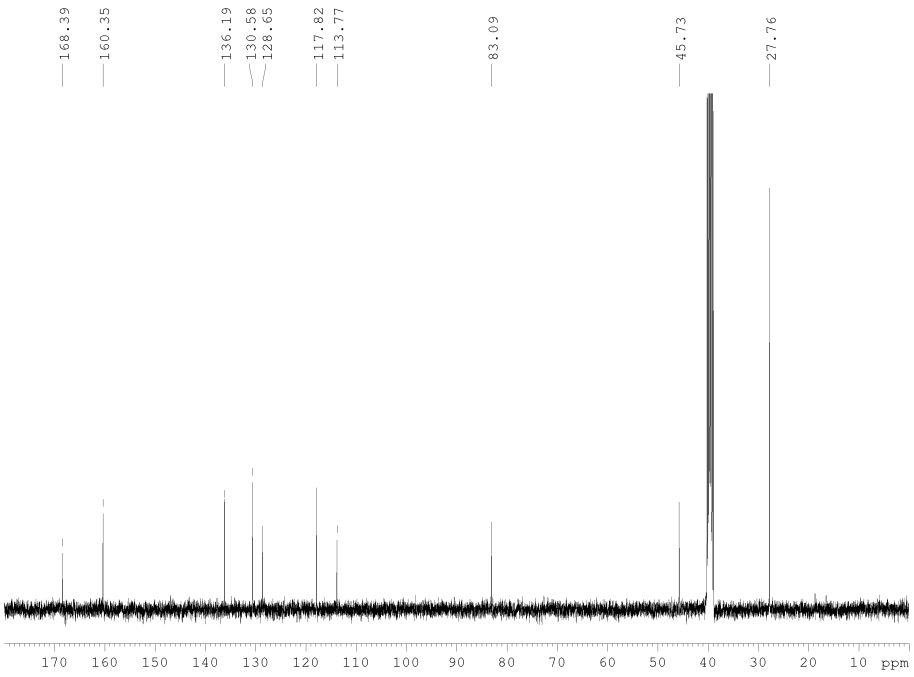
168.39
160.35
136.19
130.58
128.65
117.82
113.77
83.09
45.73
27.76
170 160 150 140 130 120 110 100 90 80 70 60 50 40 30 20 10 ppm

Compound 18

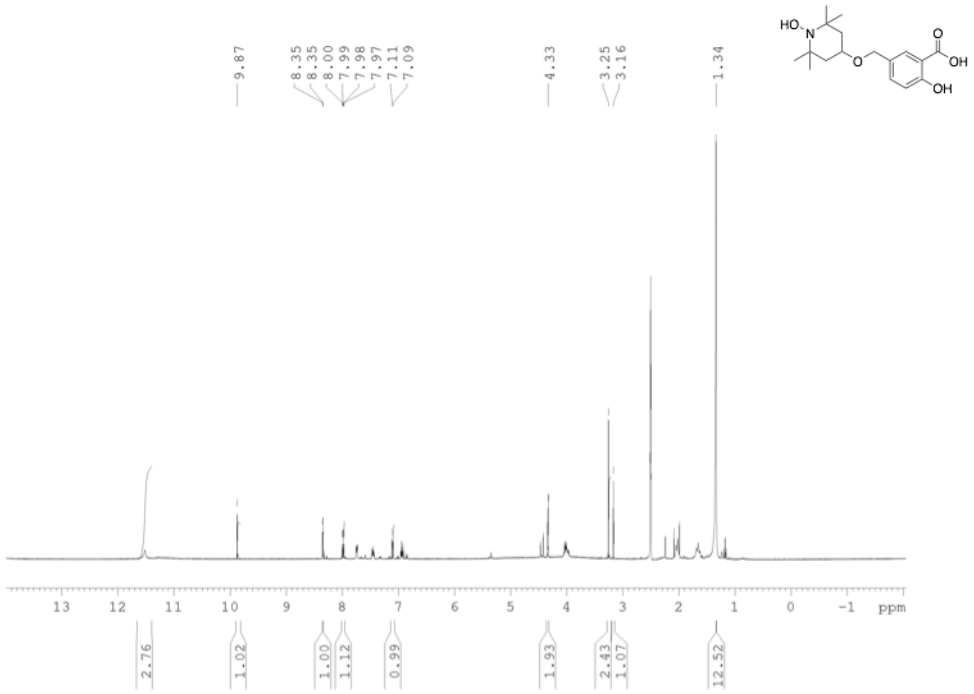

Compound 19

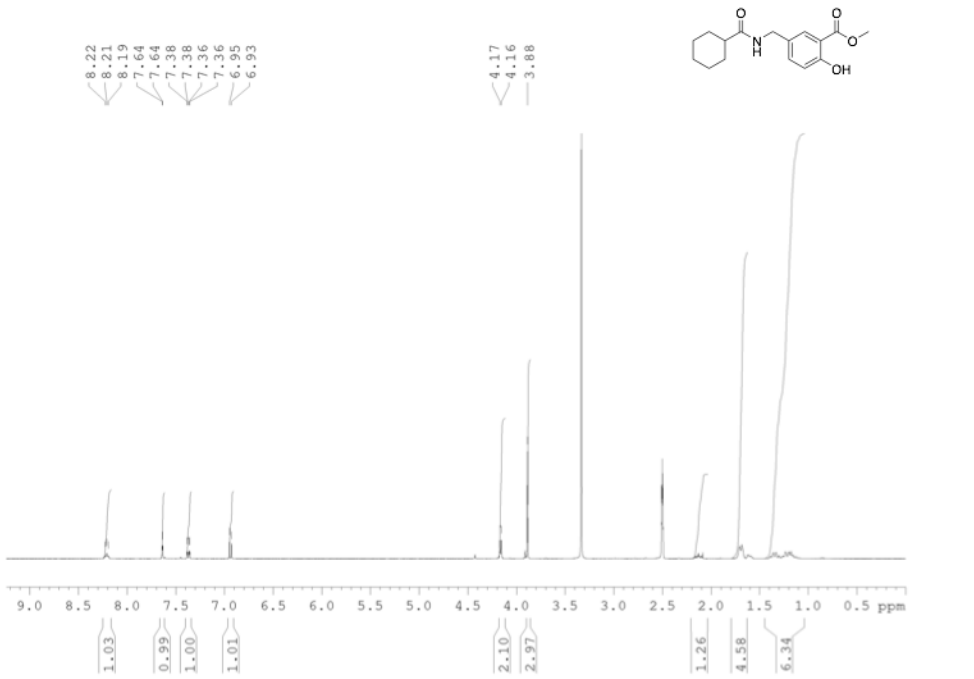

Compound 20

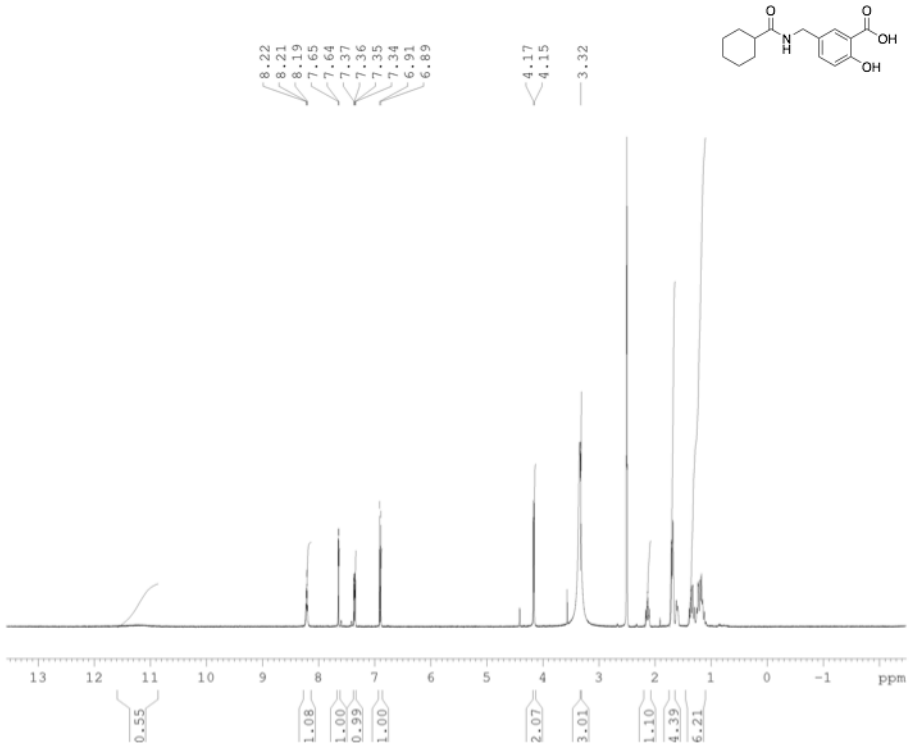
8.22
8.21
8.19
7.65
7.64
7.37
7.36
7.35
7.34
6.91
6.89
4.17
4.15
3.32
OH
OH
13
12
11
10
9
8
7
6
5
4
3
2
1
0
-1
ppm
0.55
1.08
1.00
0.99
1.00
2.07
3.01
1.10
4.39
6.21

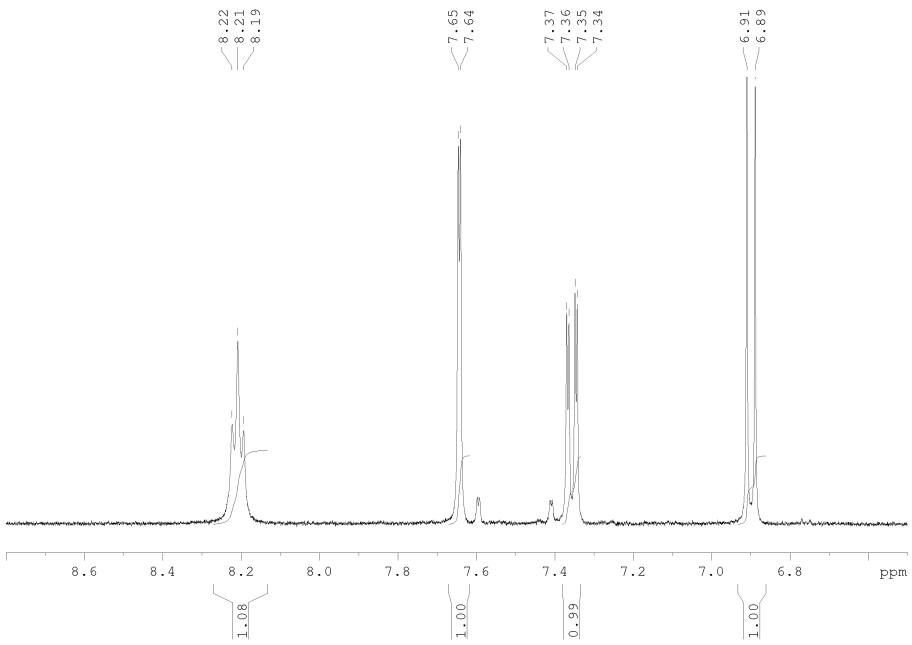
8.22
8.21
8.19
7.65
7.64
7.37
7.36
7.35
7.34
6.91
6.89
8.6
8.4
8.2
8.0
7.8
7.6
7.4
7.2
7.0
6.8
ppm
1.08
1.00
0.99
1.00

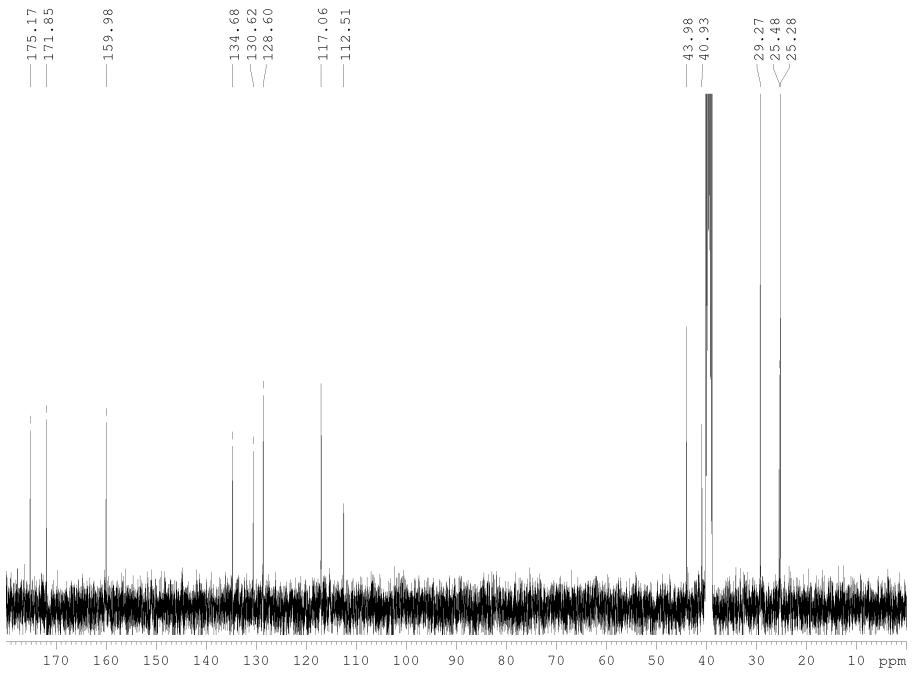
175.17
171.85
159.98
134.68
130.62
128.60
117.06
112.51
43.98
40.93
29.27
25.48
25.28
170 160 150 140 130 120 110 100 90 80 70 60 50 40 30 20 10 ppm

Compound 21

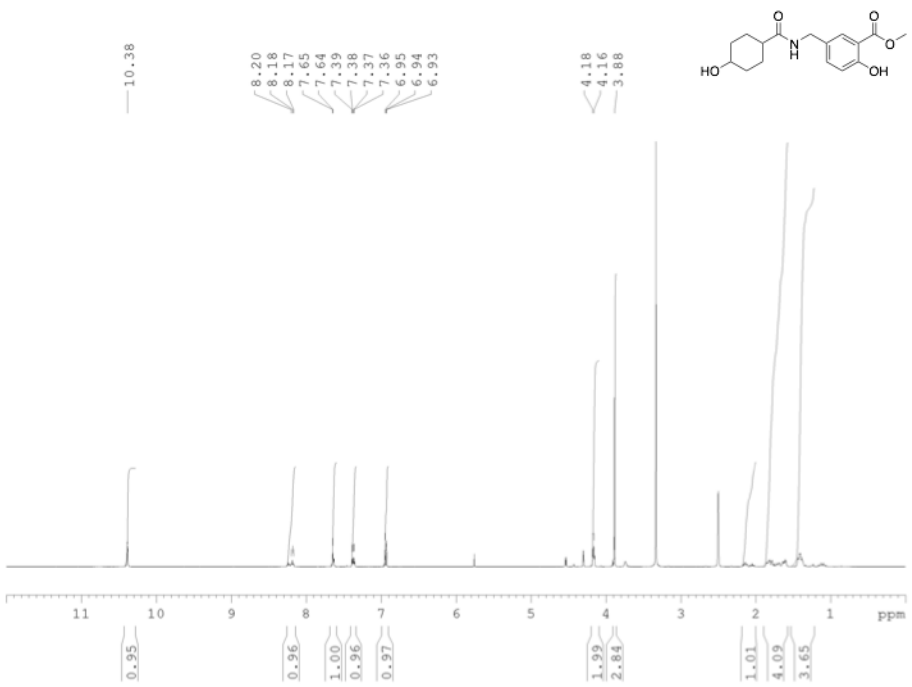
10.38
8.20
8.18
8.17
7.65
7.64
7.39
7.38
7.37
7.36
6.95
6.94
6.93
4.18
4.16
3.88
HO
O
N
H
O
O
OH
11 10 9 8 7 6 5 4 3 2 1 ppm
0.95
0.96
1.00
0.96
0.97
1.99
2.84
1.01
4.09
3.65

Compound 23

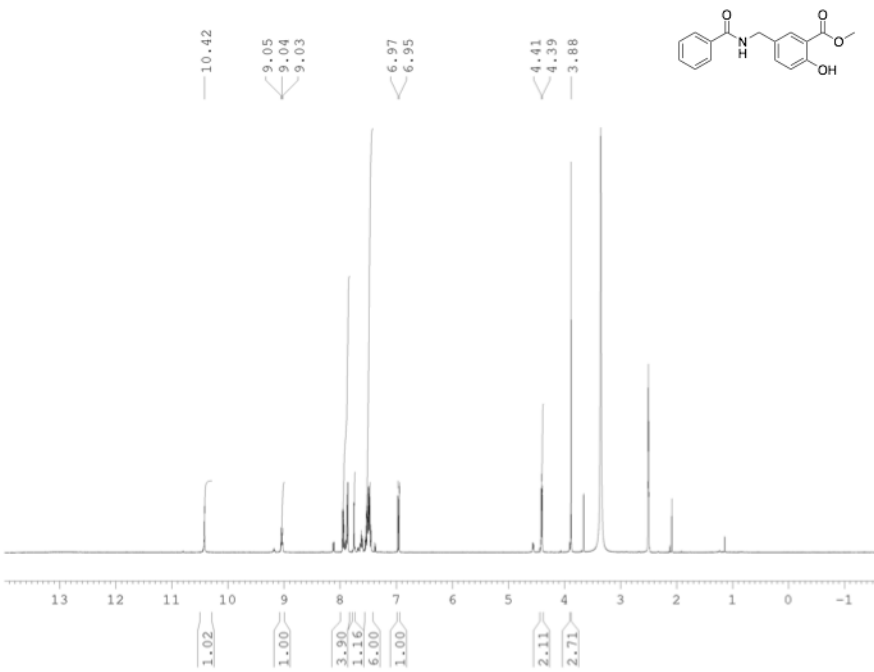

Compound 24

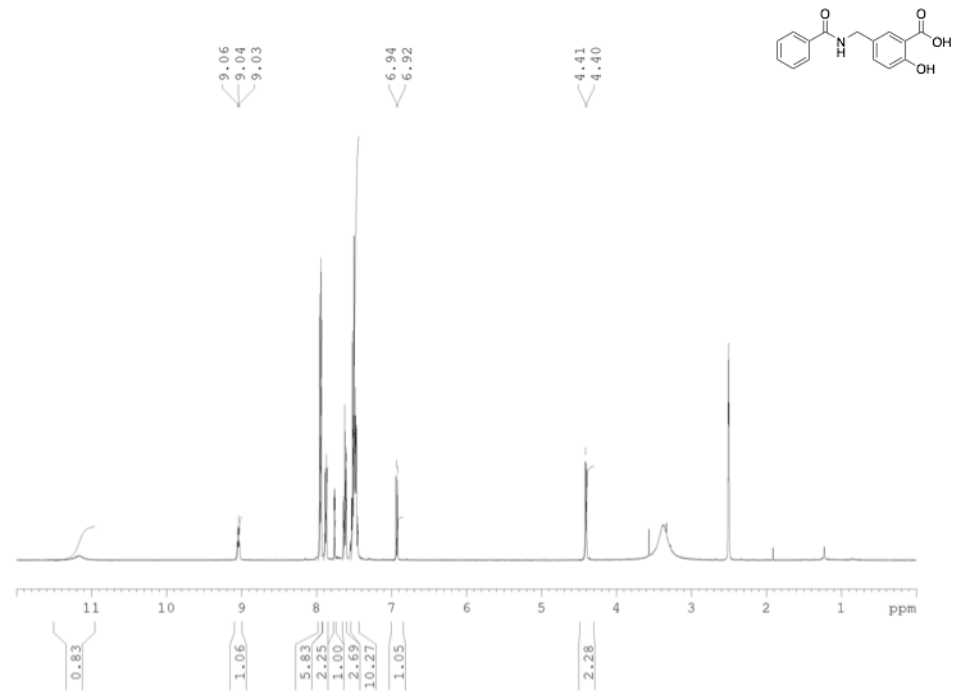

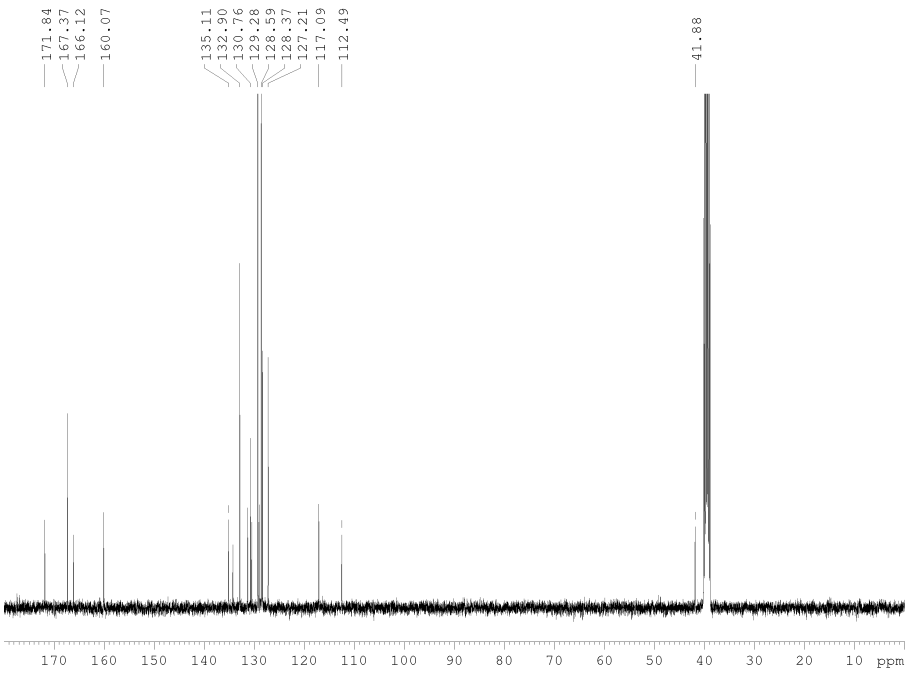
171.84
167.37
166.12
160.07
135.11
132.90
130.76
129.28
128.59
128.37
127.21
117.09
112.49
41.88
170 160 150 140 130 120 110 100 90 80 70 60 50 40 30 20 10 ppm

Compound 25

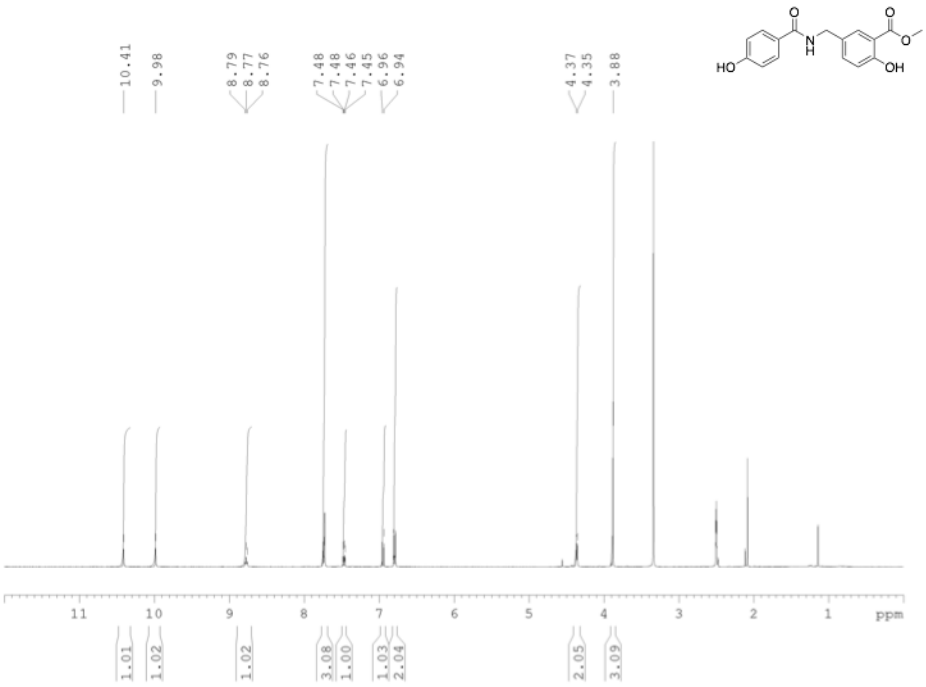
10.41
9.98
8.79
8.77
8.76
7.48
7.48
7.46
7.45
6.96
6.94
4.37
4.35
3.88
HO
O
N
H
O
O
OH
11 10 9 8 7 6 5 4 3 2 1 ppm
1.01
1.02
1.02
3.08
1.00
1.03
2.04
2.05
3.09

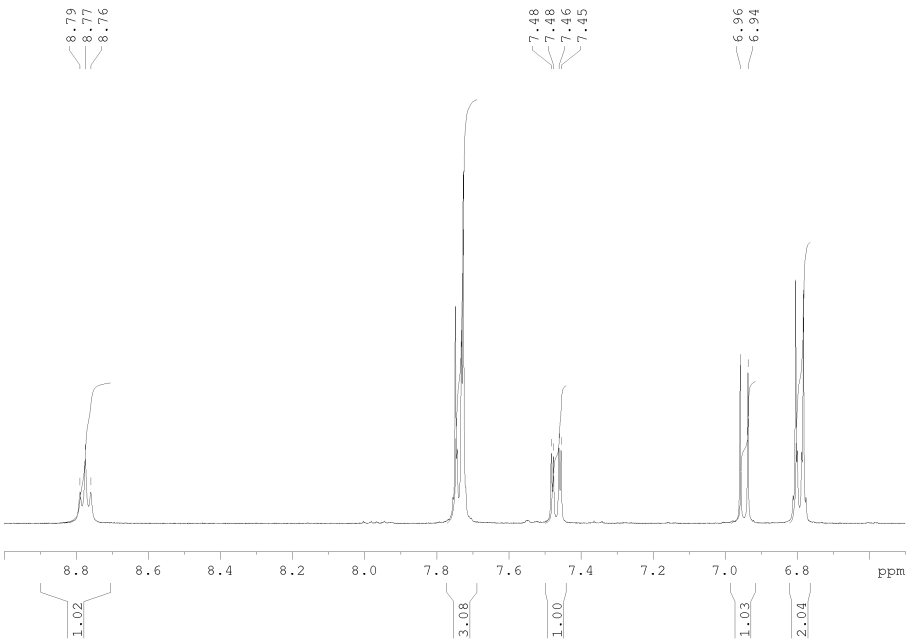
8.79
8.77
8.76
7.48
7.48
7.46
7.45
6.96
6.94
8.8
8.6
8.4
8.2
8.0
7.8
7.6
7.4
7.2
7.0
6.8
ppm
1.02
3.08
1.00
1.03
2.04

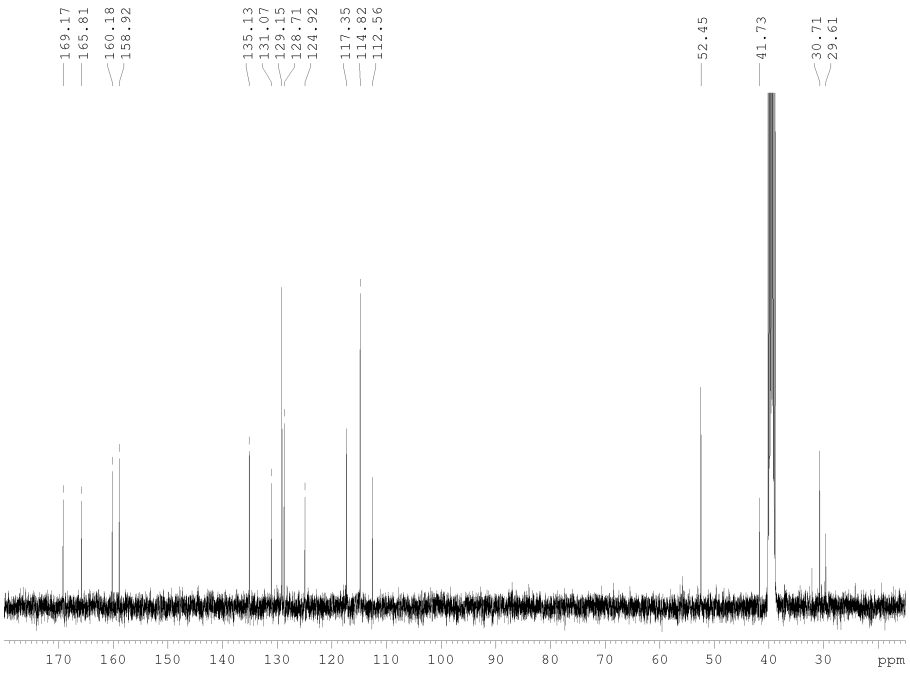
169.17
165.81
160.18
158.92
135.13
131.07
129.15
128.71
124.92
117.35
114.82
112.56
52.45
41.73
30.71
29.61
170
160
150
140
130
120
110
100
90
80
70
60
50
40
30
ppm

Compound 26

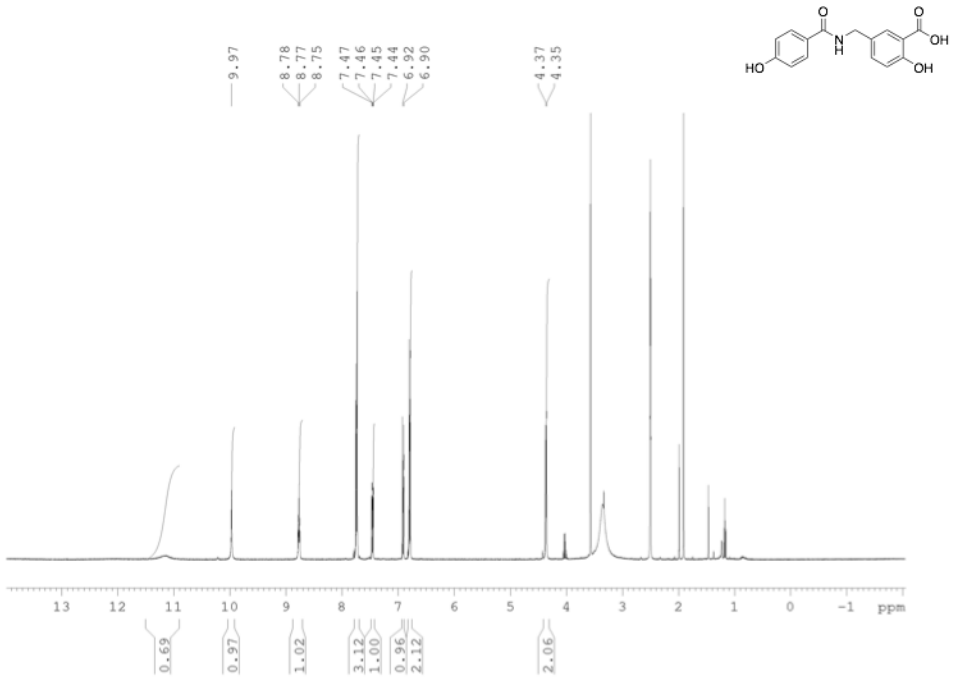
9.97
8.78
8.77
8.75
7.47
7.46
7.45
7.44
6.92
6.90
4.37
4.35
HO
O
N
H
O
OH
OH
13
12
11
10
9
8
7
6
5
4
3
2
1
0
-1
ppm
0.69
0.97
1.02
3.12
1.00
0.96
2.12
2.06

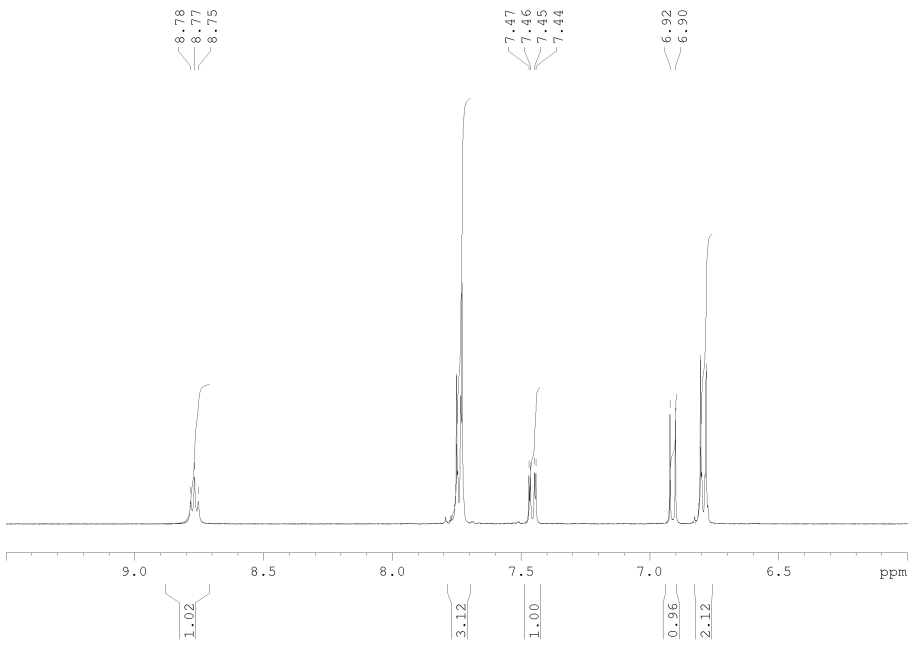
8.78
8.77
8.75
7.47
7.46
7.45
7.44
6.92
6.90
9.0
8.5
8.0
7.5
7.0
6.5
ppm
1.02
3.12
1.00
0.96
2.12

Compound 27

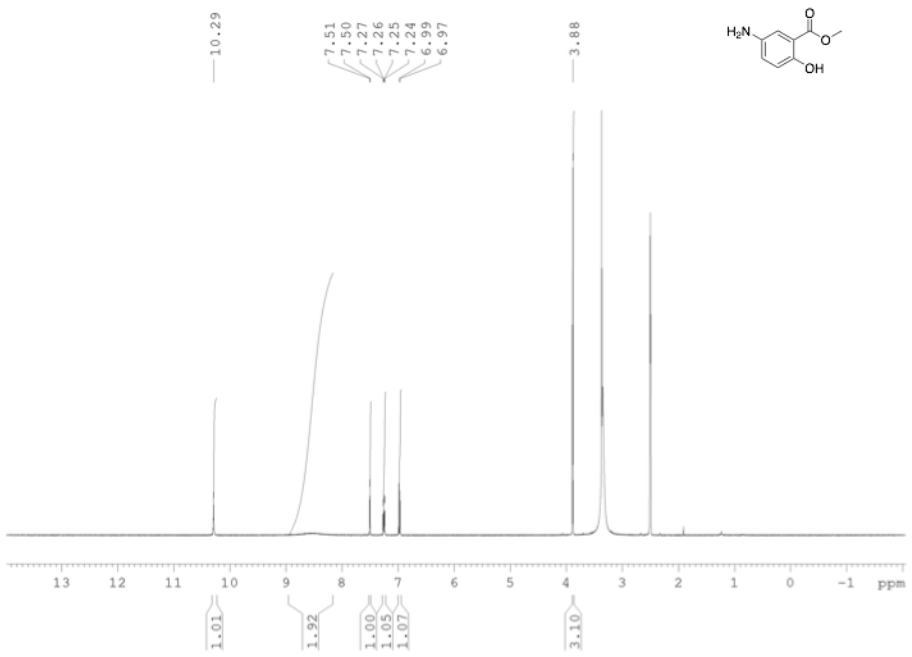
10.29
7.51
7.50
7.27
7.26
7.25
7.24
6.99
6.97
3.88
H2N
O
O
OH
13
12
11
10
9
8
7
6
5
4
3
2
1
0
-1
ppm
1.01
1.92
1.00
1.05
1.07
3.10

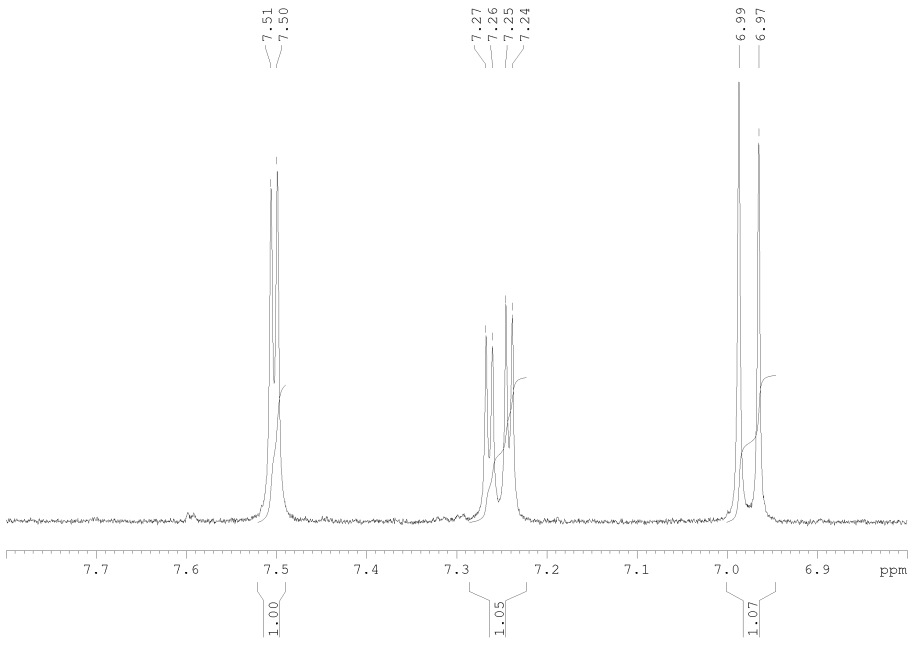
7.51
7.50
7.27
7.26
7.25
7.24
6.99
6.97
7.7
7.6
7.5
7.4
7.3
7.2
7.1
7.0
6.9
ppm
1.00
1.05
1.07

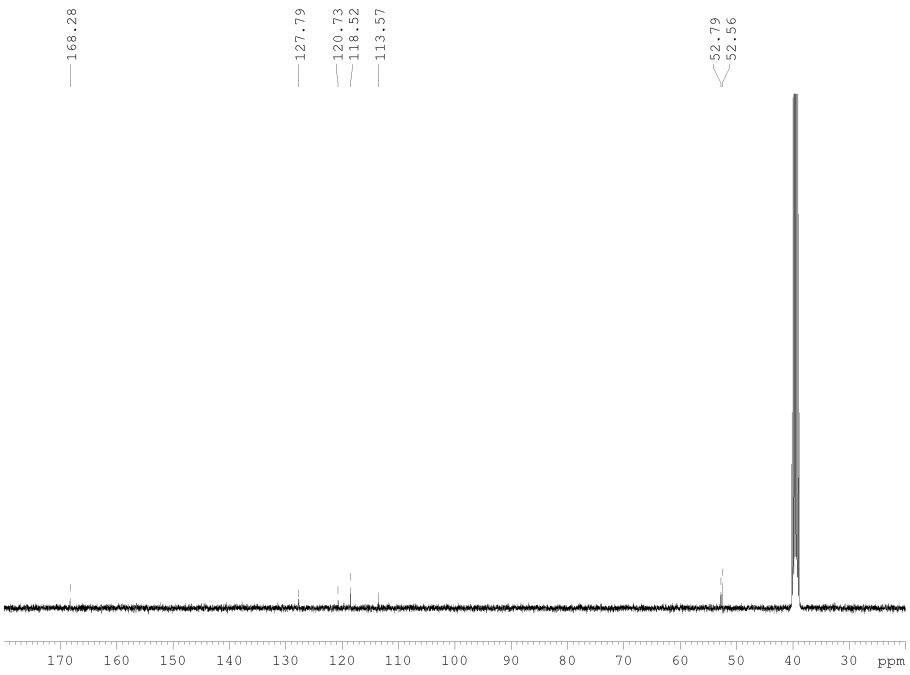
168.28
127.79
120.73
118.52
113.57
52.79
52.56
170 160 150 140 130 120 110 100 90 80 70 60 50 40 30 ppm

Compound 30

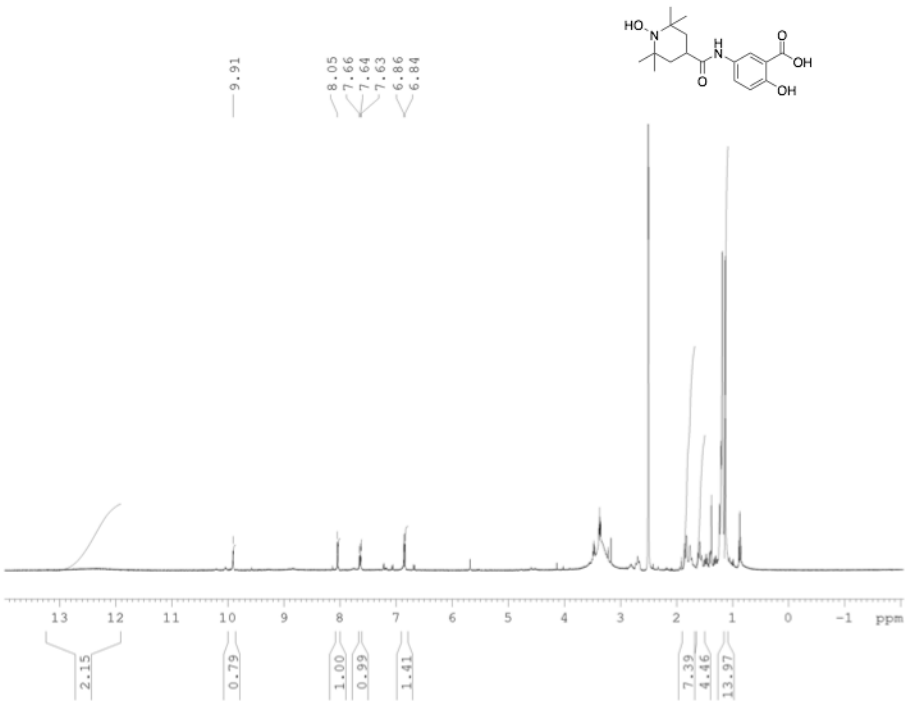
HO
N
H
N
O
O
OH
OH
9.91
8.05
7.66
7.64
7.63
6.86
6.84
13 12 11 10 9 8 7 6 5 4 3 2 1 0 -1 ppm
2.15
0.79
1.00
0.99
1.41
7.39
4.46
13.97

Compound 31

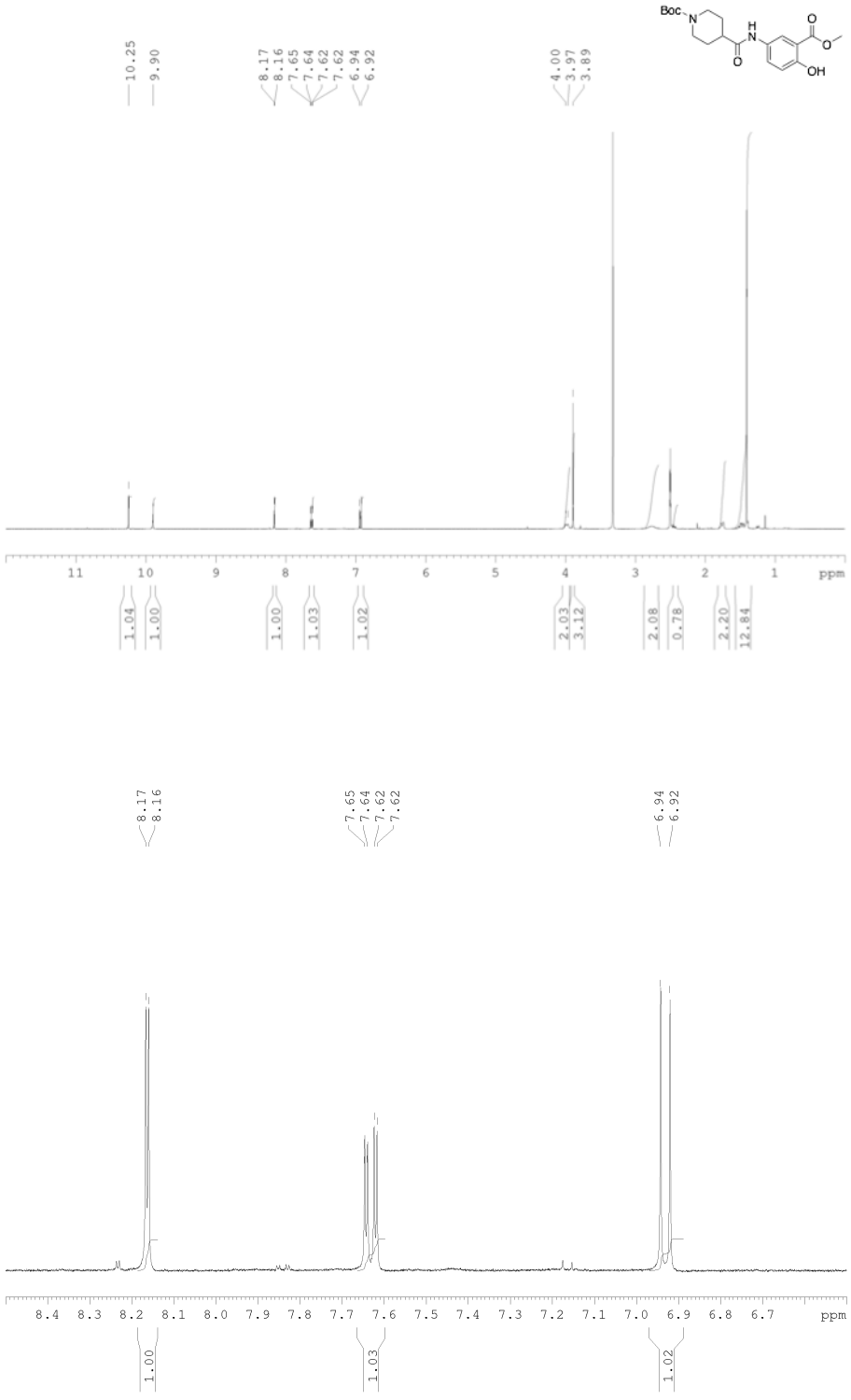
Boc
N
H
N
O
O
O
OH
10.25
9.90
8.17
8.16
7.65
7.64
7.62
7.62
6.94
6.92
4.00
3.97
3.89
11
10
9
8
7
6
5
4
3
2
1
ppm
1.04
1.00
1.00
1.03
1.02
2.03
3.12
2.08
0.78
2.20
12.84
8.17
8.16
7.65
7.64
7.62
7.62
6.94
6.92
8.4
8.3
8.2
8.1
8.0
7.9
7.8
7.7
7.6
7.5
7.4
7.3
7.2
7.1
7.0
6.9
6.8
6.7
ppm
1.00
1.03
1.02

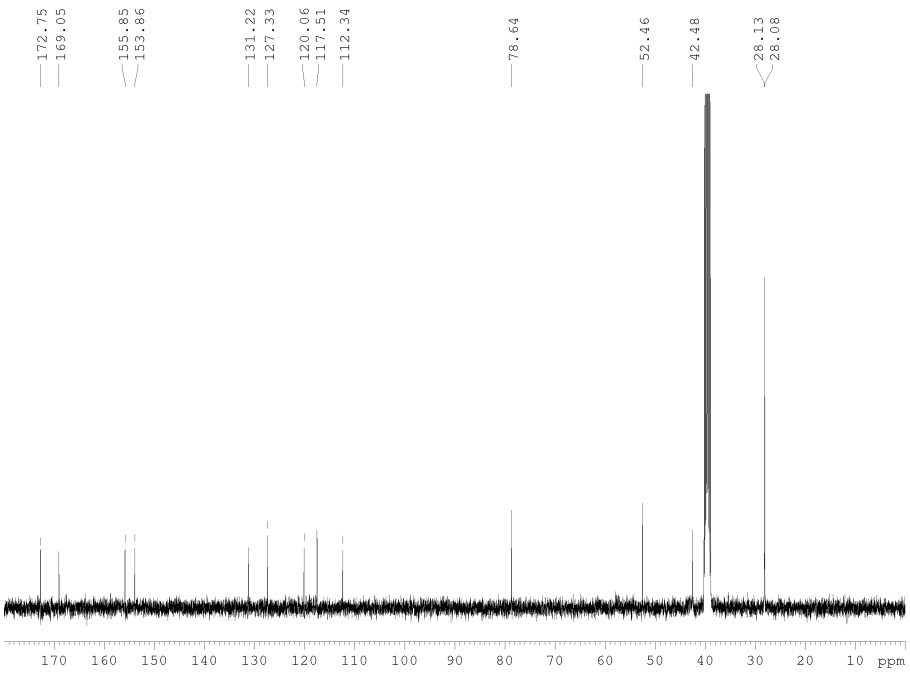
172.75
169.05
155.85
153.86
131.22
127.33
120.06
117.51
112.34
78.64
52.46
42.48
28.13
28.08
170 160 150 140 130 120 110 100 90 80 70 60 50 40 30 20 10 ppm

Compound 32

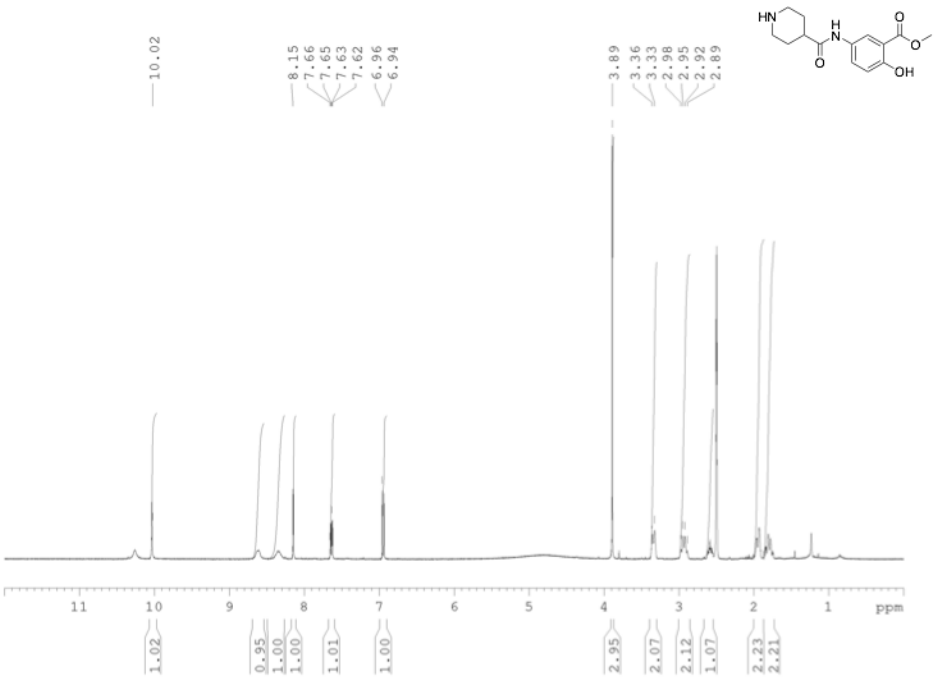
10.02
8.15
7.66
7.65
7.63
7.62
6.96
6.94
3.89
3.36
3.33
2.98
2.95
2.92
2.89
HN
H
N
O
O
O
OH
11 10 9 8 7 6 5 4 3 2 1 ppm
1.02
0.95
1.00
1.00
1.01
1.00
2.95
2.07
2.12
1.07
2.23
2.21

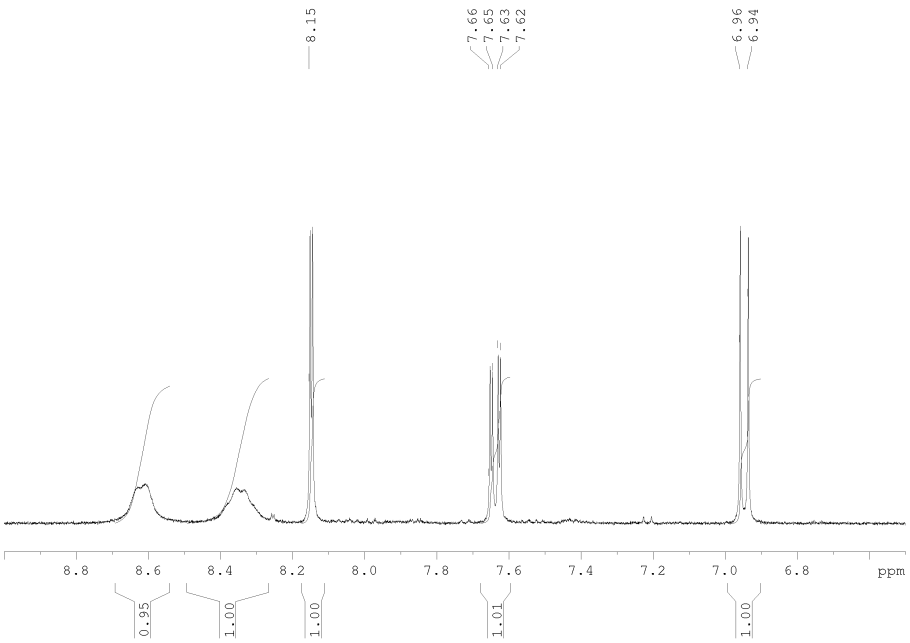
8.15
7.66
7.65
7.63
7.62
6.96
6.94
8.8
8.6
8.4
8.2
8.0
7.8
7.6
7.4
7.2
7.0
6.8
ppm
0.95
1.00
1.00
1.01
1.00

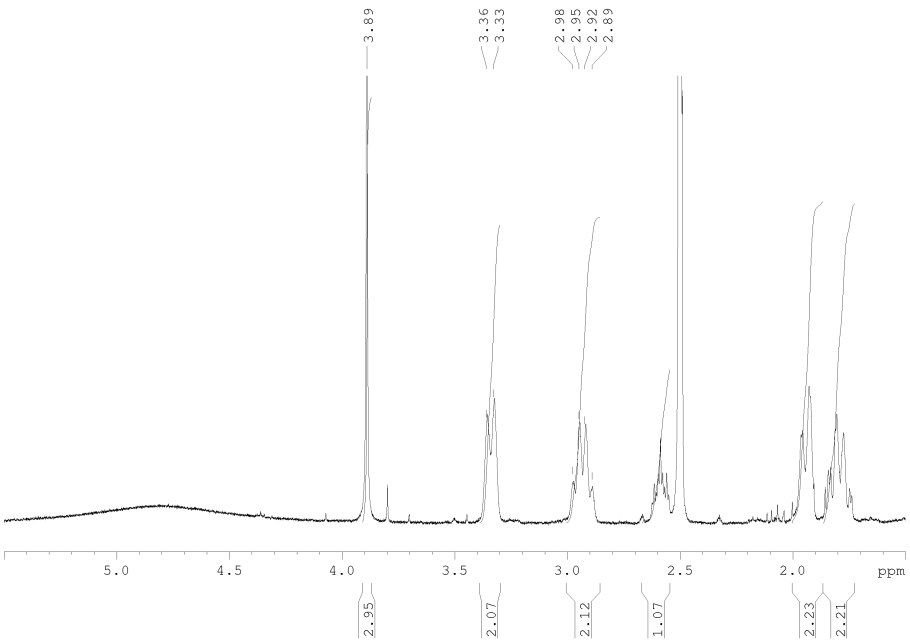
3.89
3.36
3.33
2.98
2.95
2.92
2.89
5.0
4.5
4.0
3.5
3.0
2.5
2.0
ppm
2.95
2.07
2.12
1.07
2.23
2.21

Compound 38

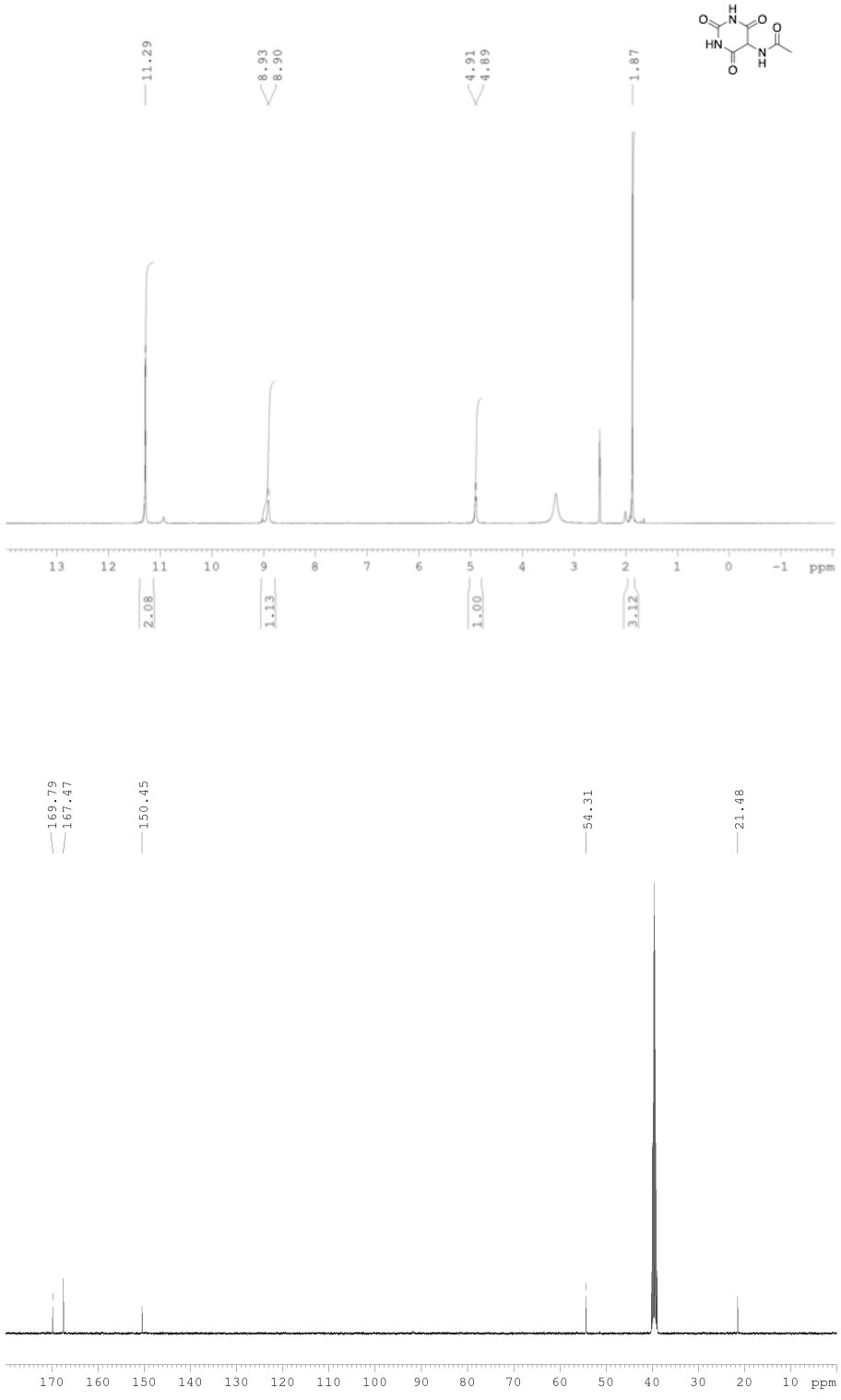
11.29
8.93
8.90
4.91
4.89
1.87
13 12 11 10 9 8 7 6 5 4 3 2 1 0 -1 ppm
2.08
1.13
1.00
3.12
169.79
167.47
150.45
54.31
21.48
170 160 150 140 130 120 110 100 90 80 70 60 50 40 30 20 10 ppm

Compound 39

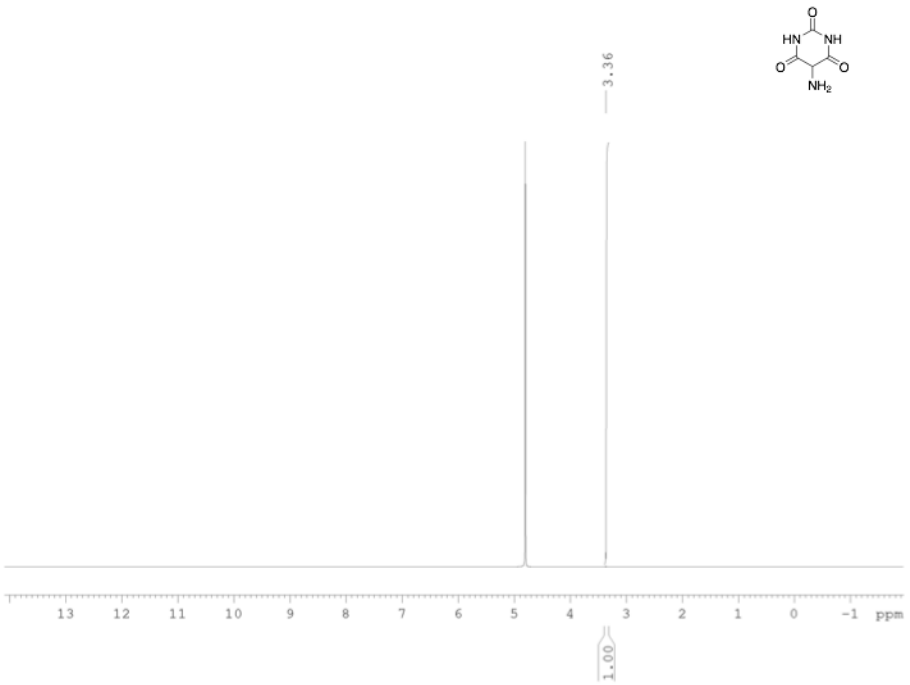
3.36
13 12 11 10 9 8 7 6 5 4 3 2 1 0 -1 ppm
1.00

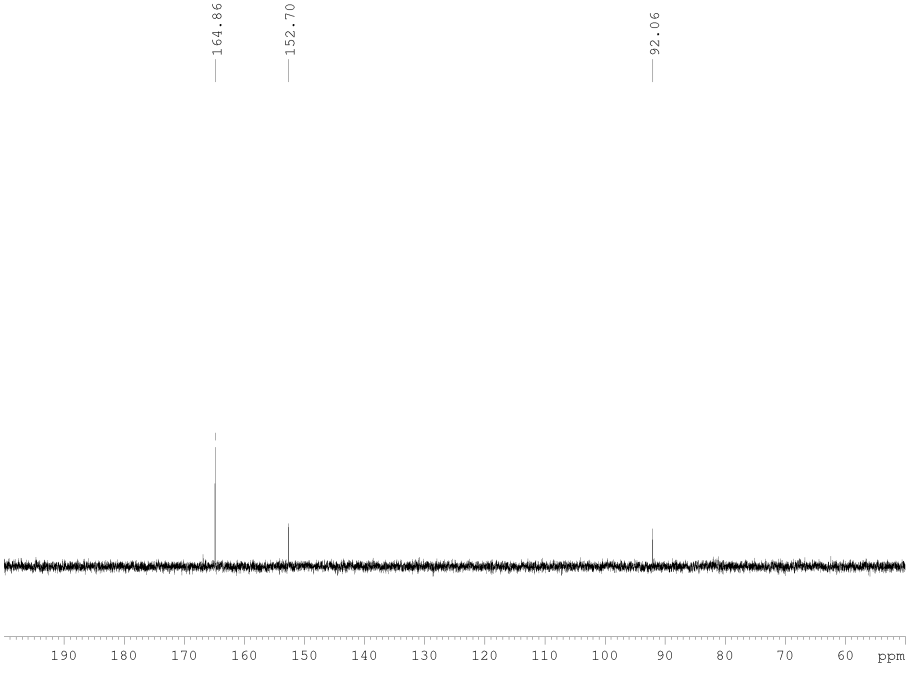
164.86
152.70
92.06
190 180 170 160 150 140 130 120 110 100 90 80 70 60 ppm

Compound 44

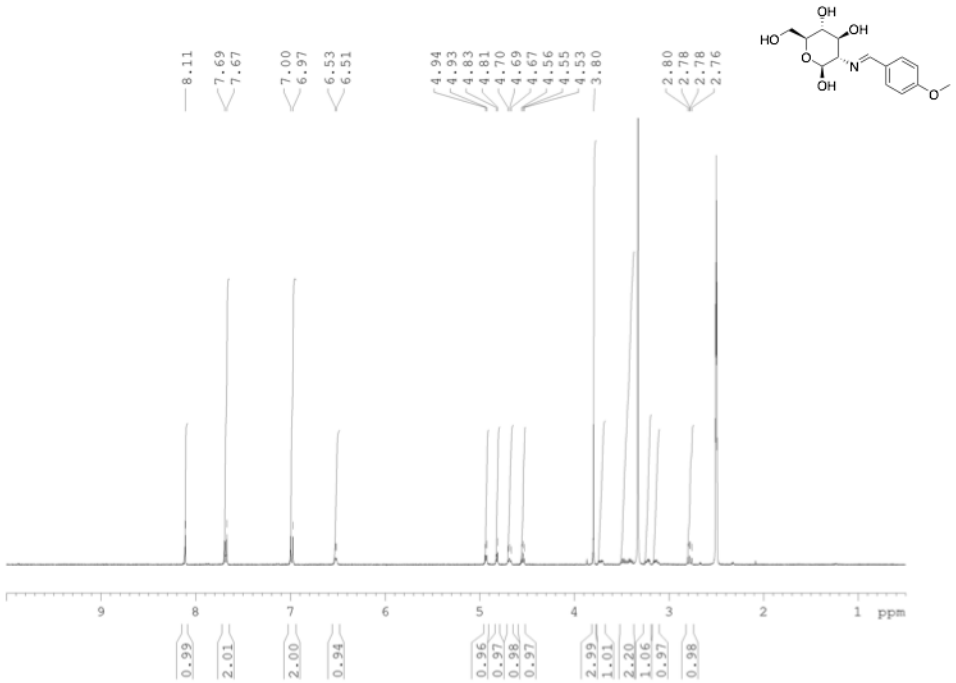
8.11
7.69
7.67
7.00
6.97
6.53
6.51
4.94
4.93
4.83
4.81
4.70
4.69
4.67
4.56
4.55
4.53
3.80
2.80
2.78
2.78
2.76
OH
OH
HO
O
N
OH
O
9
8
7
6
5
4
3
2
1
ppm
0.99
2.01
2.00
0.94
0.96
0.97
0.98
0.97
2.99
1.01
2.20
1.06
0.97
0.98

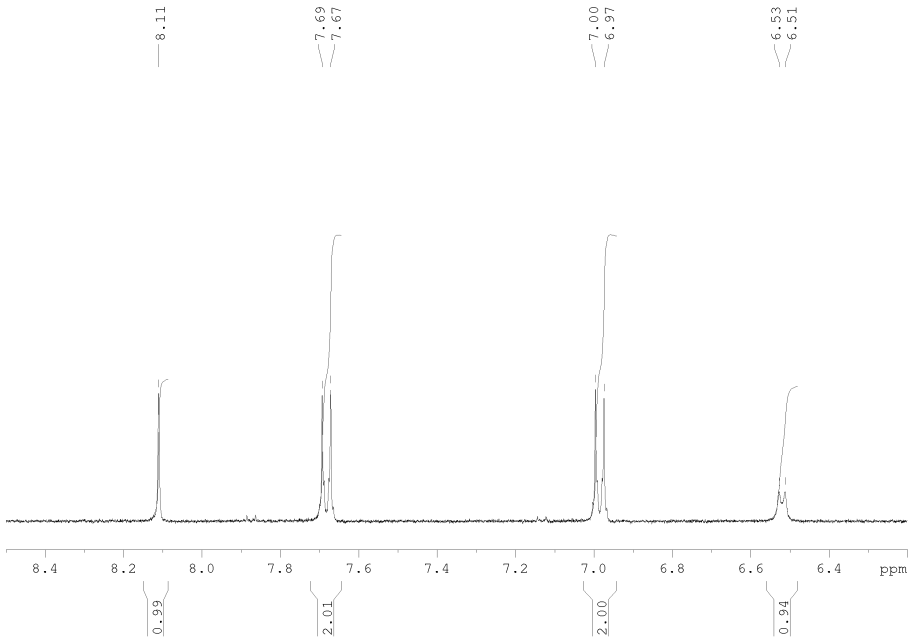
8.11
7.69
7.67
7.00
6.97
6.53
6.51
8.4
8.2
8.0
7.8
7.6
7.4
7.2
7.0
6.8
6.6
6.4
ppm
0.99
2.01
2.00
0.94

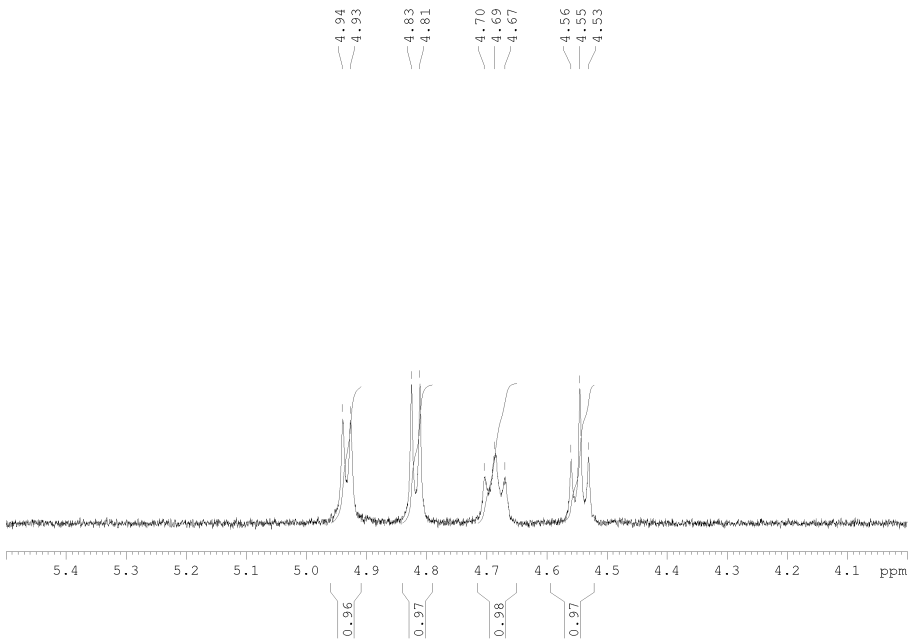
4.94
4.93
4.83
4.81
4.70
4.69
4.67
4.56
4.55
4.53
5.4 5.3 5.2 5.1 5.0 4.9 4.8 4.7 4.6 4.5 4.4 4.3 4.2 4.1 ppm
0.96
0.97
0.98
0.97

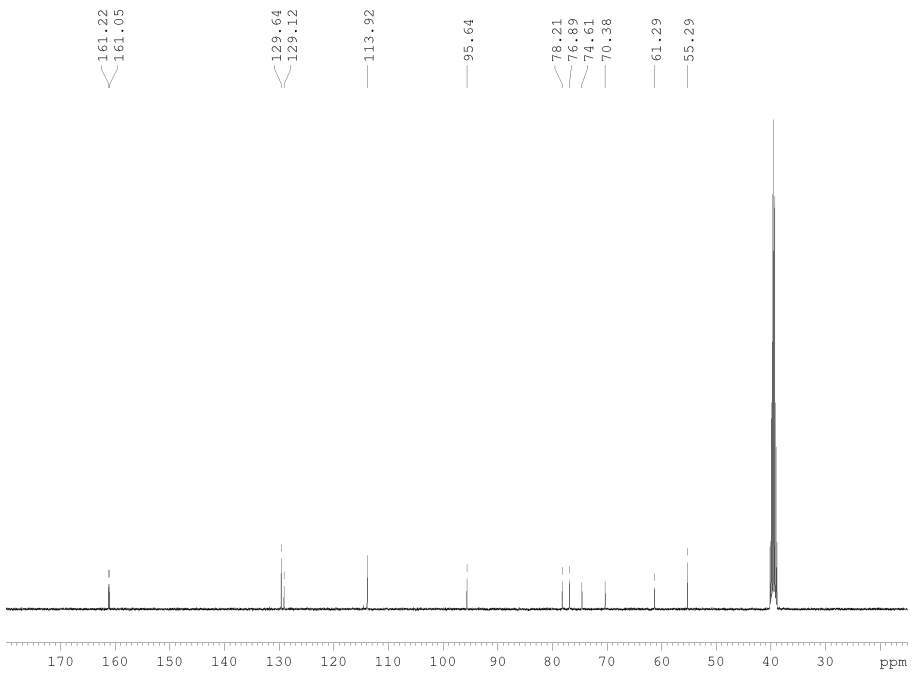
161.22
161.05
129.64
129.12
113.92
95.64
78.21
76.89
74.61
70.38
61.29
55.29
170 160 150 140 130 120 110 100 90 80 70 60 50 40 30 ppm

Compound 45

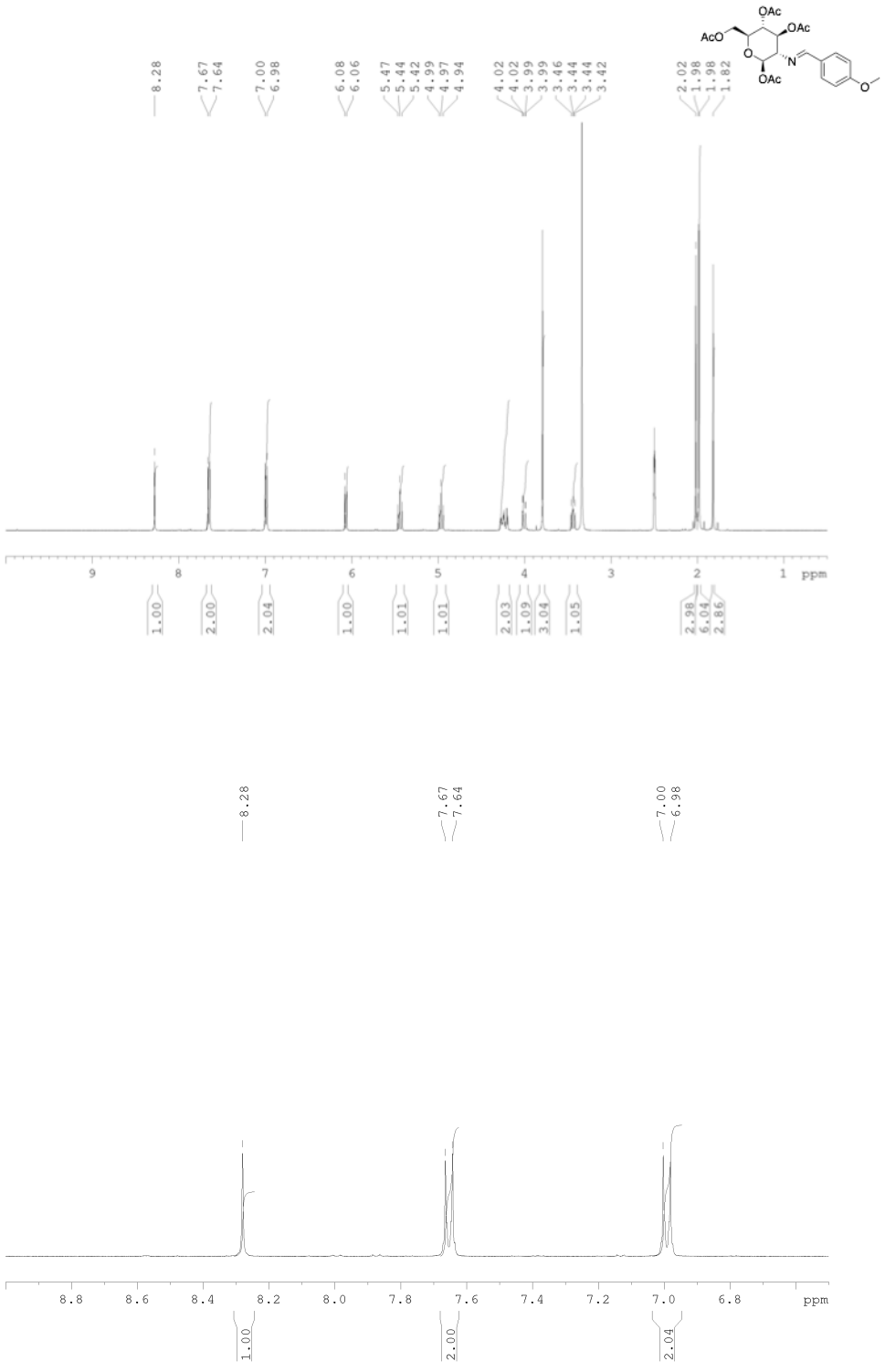
OAc
AcO
OAc
O
N
OAc
O
8.28
7.67
7.64
7.00
6.98
6.08
6.06
5.47
5.44
5.42
4.99
4.97
4.94
4.02
4.02
3.99
3.99
3.46
3.44
3.44
3.42
2.02
1.98
1.98
1.82
9
8
7
6
5
4
3
2
1
ppm
1.00
2.00
2.04
1.00
1.01
1.01
2.03
1.09
3.04
1.05
2.98
6.04
2.86
8.28
7.67
7.64
7.00
6.98
8.8
8.6
8.4
8.2
8.0
7.8
7.6
7.4
7.2
7.0
6.8
ppm
1.00
2.00
2.04

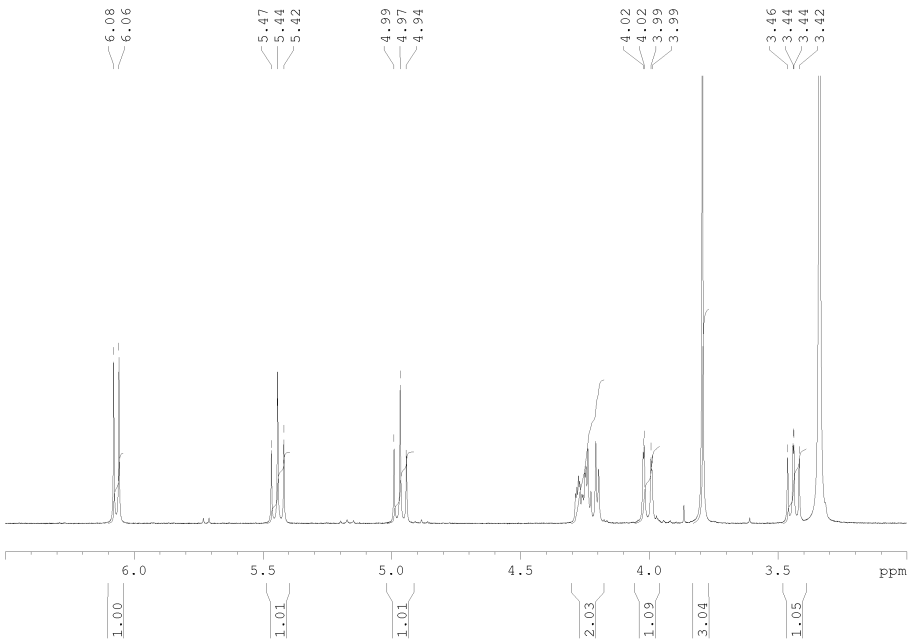
6.08
6.06
5.47
5.44
5.42
4.99
4.97
4.94
4.02
4.02
3.99
3.99
3.46
3.44
3.44
3.42
6.0
5.5
5.0
4.5
4.0
3.5
ppm
1.00
1.01
1.01
2.03
1.09
3.04
1.05

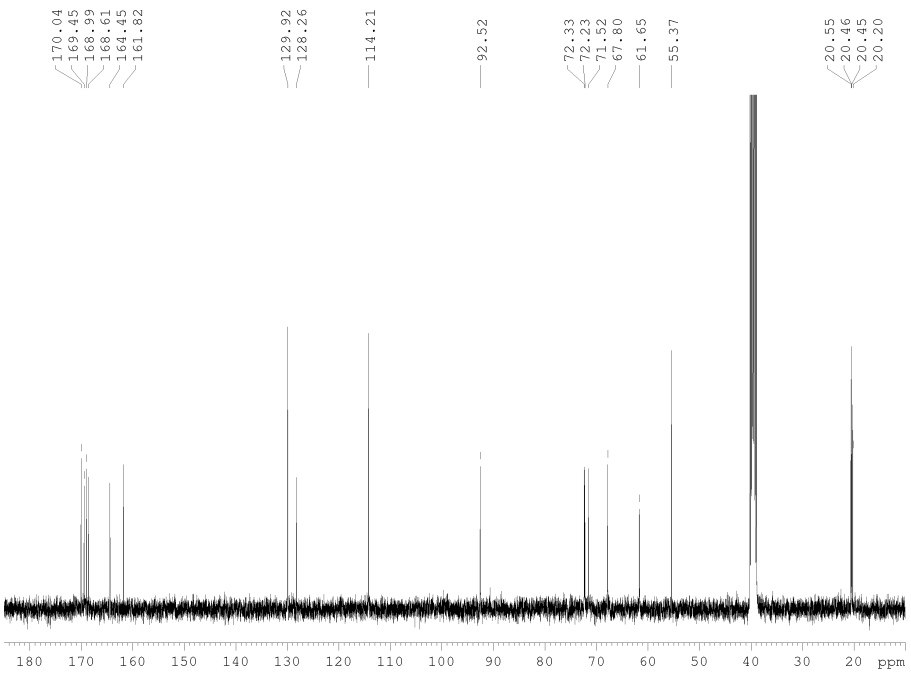
170.04
169.45
168.99
168.61
164.45
161.82
129.92
128.26
114.21
92.52
72.33
72.23
71.52
67.80
61.65
55.37
20.55
20.46
20.45
20.20
180
170
160
150
140
130
120
110
100
90
80
70
60
50
40
30
20
ppm

Compound 46

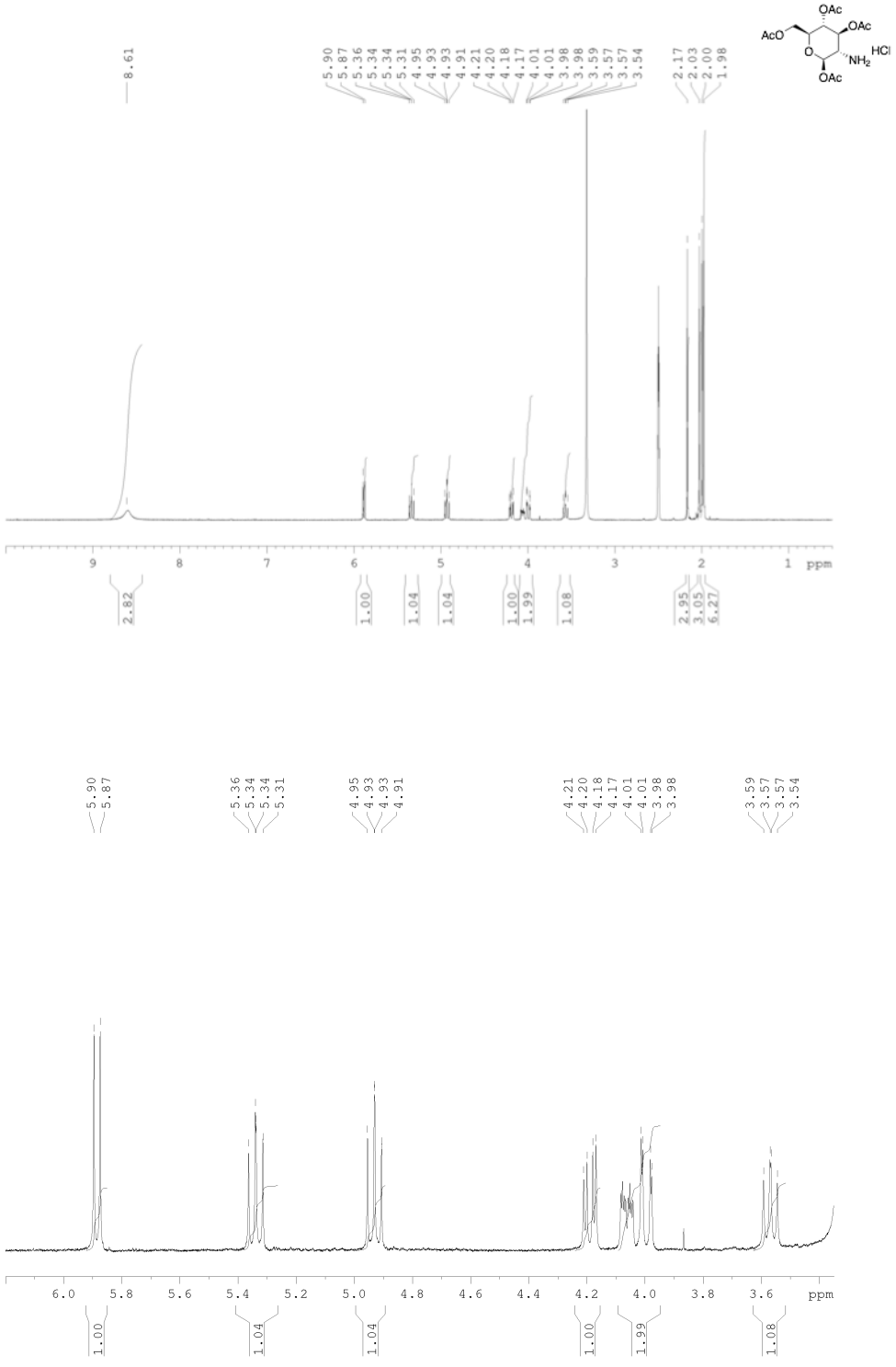
OAc
AcO
OAc
O
NH2
HCl
OAc
8.61
5.90
5.87
5.36
5.34
5.34
5.31
4.95
4.93
4.93
4.91
4.21
4.20
4.18
4.17
4.01
4.01
3.98
3.98
3.59
3.57
3.57
3.54
2.17
2.03
2.00
1.98
ppm
2.82
1.00
1.04
1.04
1.00
1.99
1.08
2.95
3.05
6.27

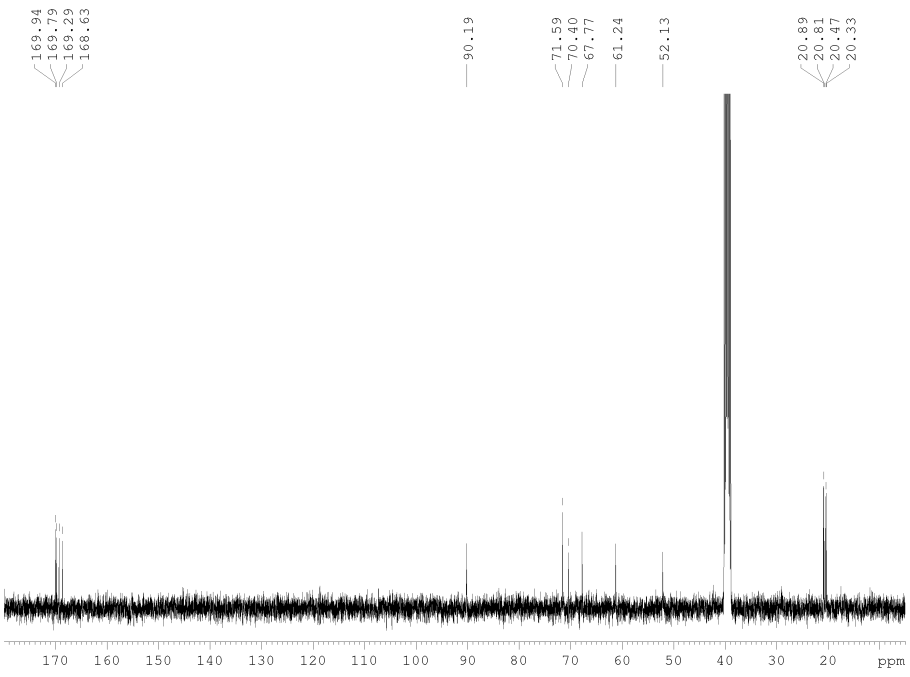
169.94
169.79
169.29
168.63
90.19
71.59
70.40
67.77
61.24
52.13
20.89
20.81
20.47
20.33
170 160 150 140 130 120 110 100 90 80 70 60 50 40 30 20 ppm

Compound 47

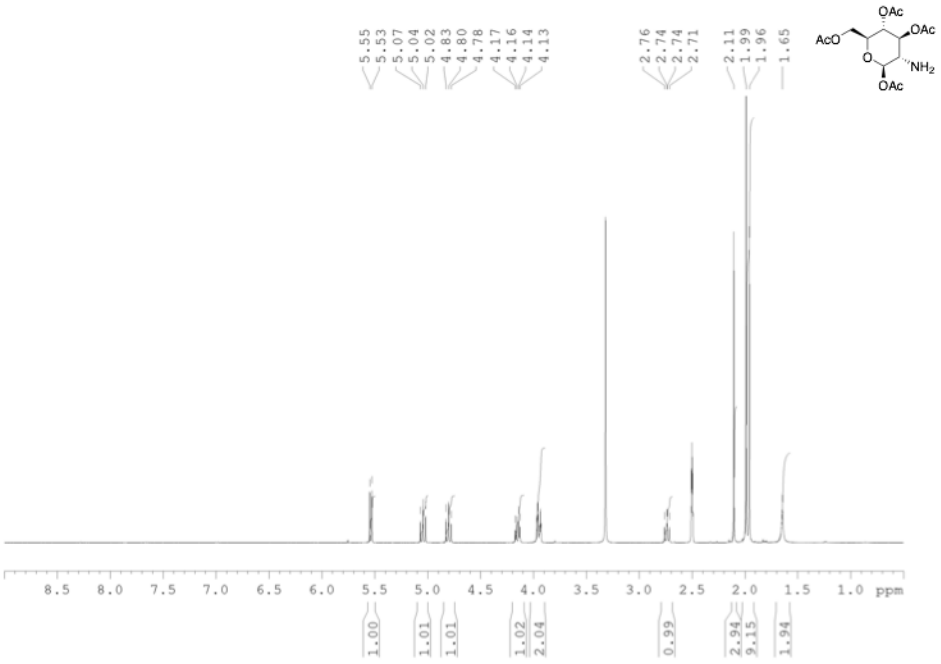
5.55
5.53
5.07
5.04
5.02
4.83
4.80
4.78
4.17
4.16
4.14
4.13
2.76
2.74
2.74
2.71
2.11
1.99
1.96
1.65
OAc
AcO
OAc
NH2
OAc
8.5 8.0 7.5 7.0 6.5 6.0 5.5 5.0 4.5 4.0 3.5 3.0 2.5 2.0 1.5 1.0 ppm
1.00
1.01
1.01
1.02
2.04
0.99
2.94
9.15
1.94

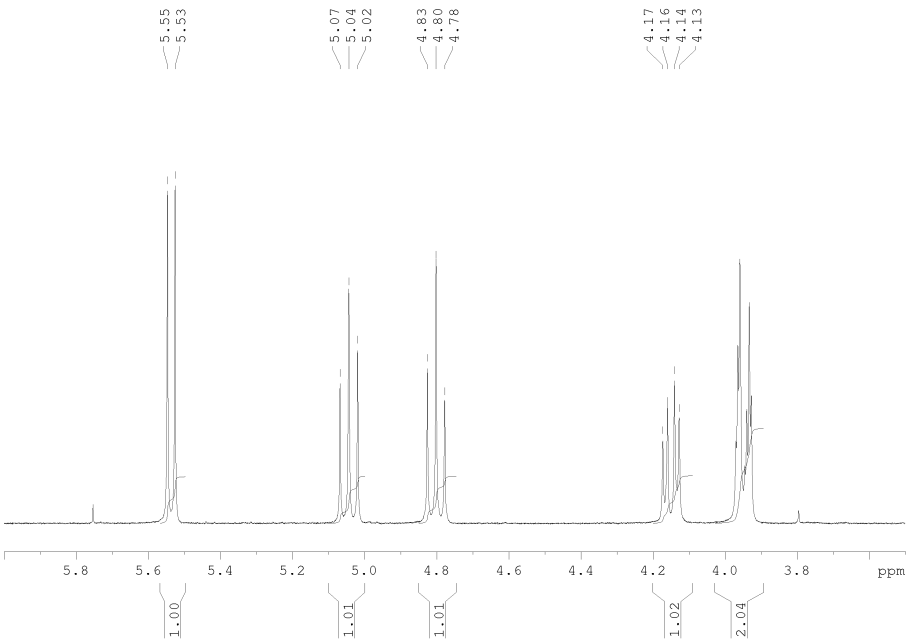
5.55
5.53
5.07
5.04
5.02
4.83
4.80
4.78
4.17
4.16
4.14
4.13
5.8
5.6
5.4
5.2
5.0
4.8
4.6
4.4
4.2
4.0
3.8
ppm
1.00
1.01
1.01
1.02
2.04

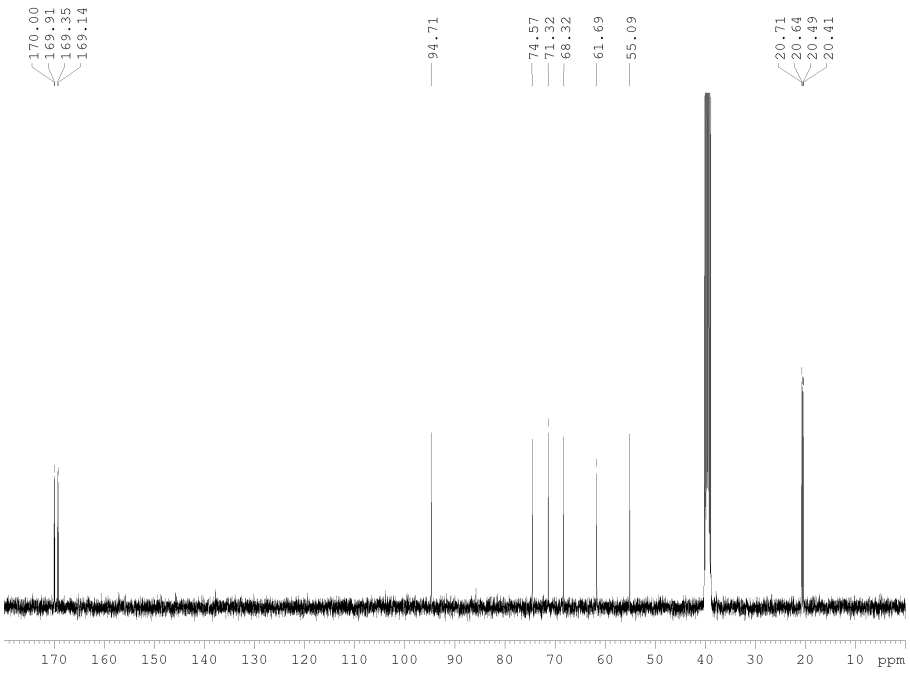
170.00
169.91
169.35
169.14
94.71
74.57
71.32
68.32
61.69
55.09
20.71
20.64
20.49
20.41
170
160
150
140
130
120
110
100
90
80
70
60
50
40
30
20
10
ppm

Compound 50

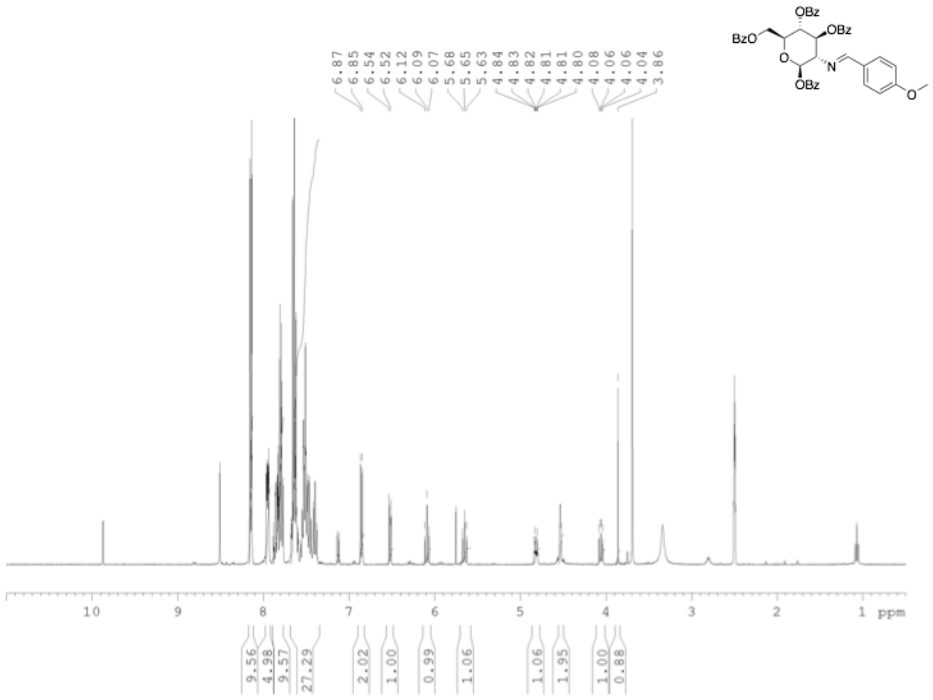
OBz
BzO
OBz
O
N
OBz
O
6.87
6.85
6.54
6.52
6.12
6.09
6.07
5.68
5.65
5.63
4.84
4.83
4.82
4.81
4.80
4.08
4.06
4.06
4.04
3.86
10
9
8
7
6
5
4
3
2
1 ppm
9.56
4.98
9.57
27.29
2.02
1.00
0.99
1.06
1.06
1.95
1.00
0.88

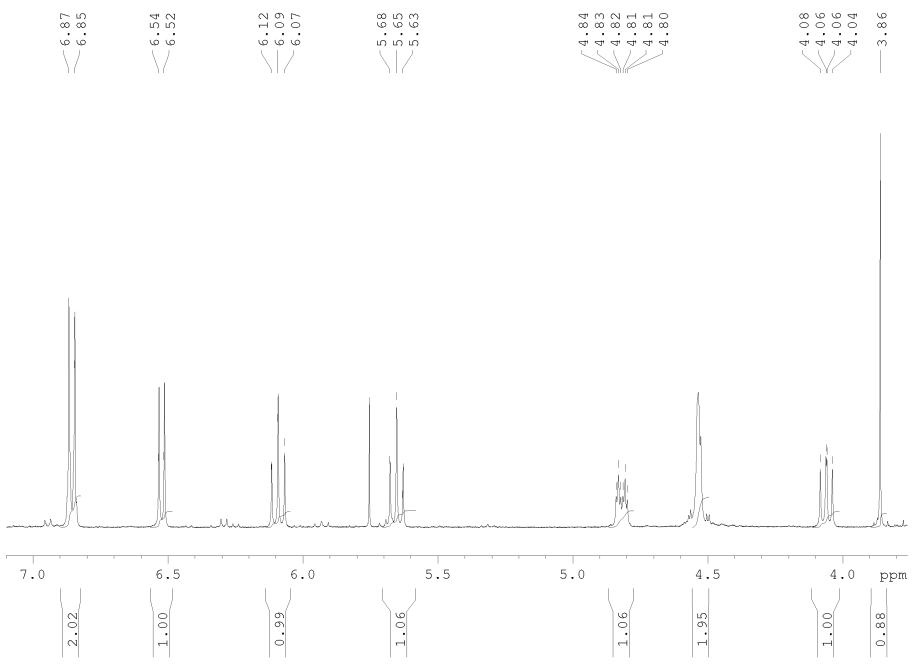
6.87
6.85
6.54
6.52
6.12
6.09
6.07
5.68
5.65
5.63
4.84
4.83
4.82
4.81
4.80
4.08
4.06
4.06
4.04
3.86
7.0
6.5
6.0
5.5
5.0
4.5
4.0
ppm
2.02
1.00
0.99
1.06
1.06
1.95
1.00
0.88

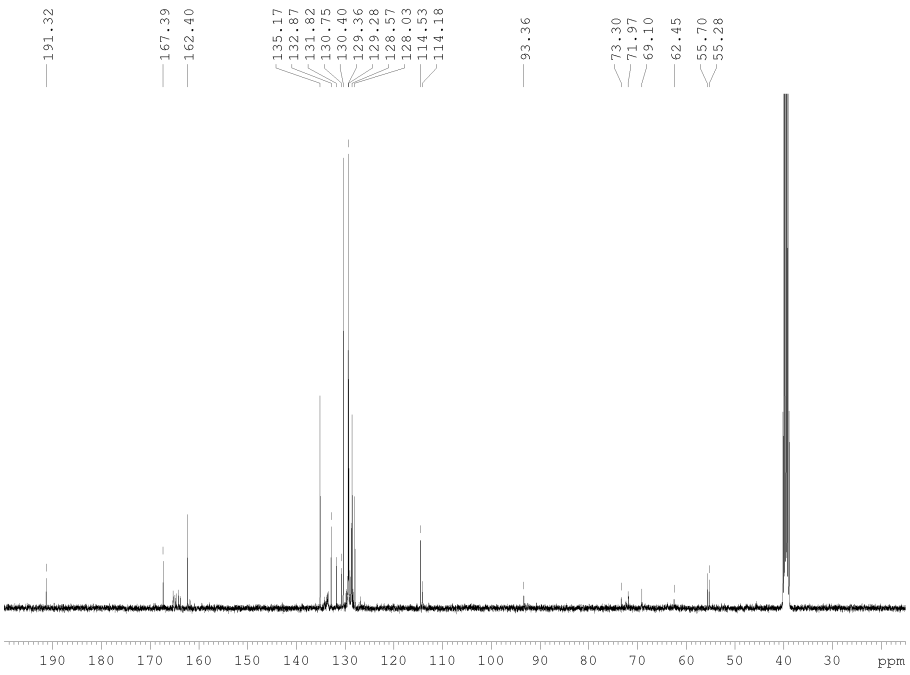
191.32
167.39
162.40
135.17
132.87
131.82
130.75
130.40
129.36
129.28
128.57
128.03
114.53
114.18
93.36
73.30
71.97
69.10
62.45
55.70
55.28
190 180 170 160 150 140 130 120 110 100 90 80 70 60 50 40 30 ppm

Compound 51

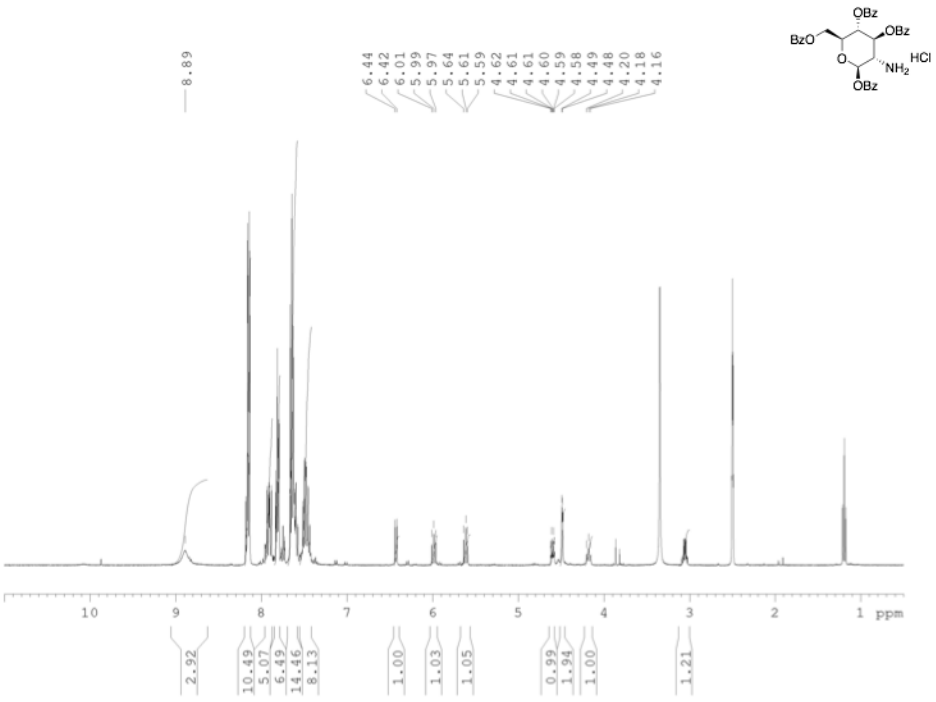
8.89
6.44
6.42
6.01
5.99
5.97
5.64
5.61
5.59
4.62
4.61
4.61
4.60
4.59
4.58
4.49
4.48
4.20
4.18
4.16
OBz
OBz
BzO
O
NH2
HCl
OBz
10 9 8 7 6 5 4 3 2 1 ppm
2.92
10.49
5.07
6.49
14.46
8.13
1.00
1.03
1.05
0.99
1.94
1.00
1.21

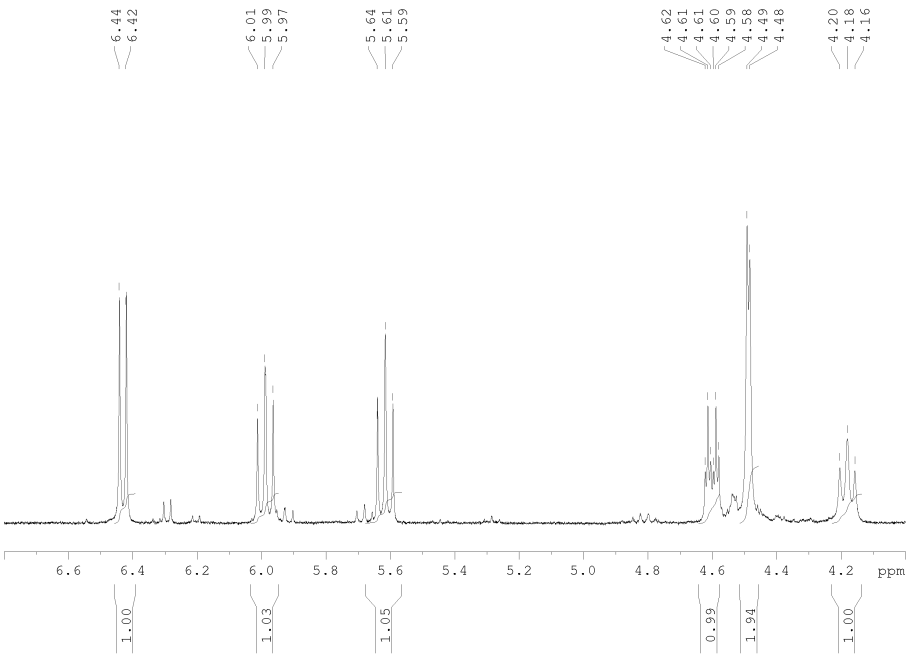
6.44
6.42
6.01
5.99
5.97
5.64
5.61
5.59
4.62
4.61
4.61
4.60
4.59
4.58
4.49
4.48
4.20
4.18
4.16
6.6
6.4
6.2
6.0
5.8
5.6
5.4
5.2
5.0
4.8
4.6
4.4
4.2
ppm
1.00
1.03
1.05
0.99
1.94
1.00

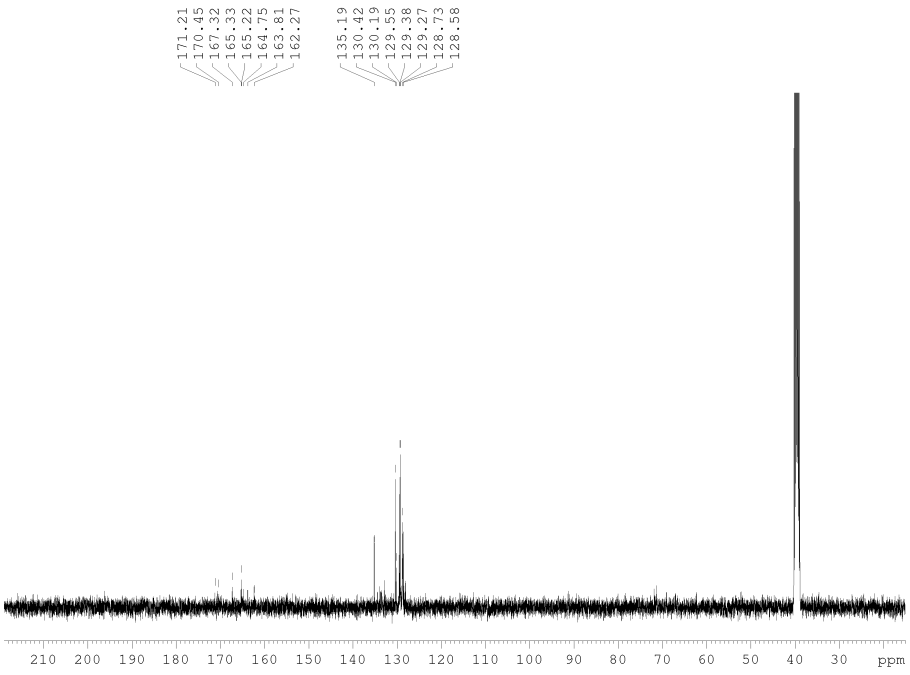
171.21
170.45
167.32
165.33
165.22
164.75
163.81
162.27
135.19
130.42
130.19
129.55
129.38
129.27
128.73
128.58
210
200
190
180
170
160
150
140
130
120
110
100
90
80
70
60
50
40
30
ppm

Compound 52

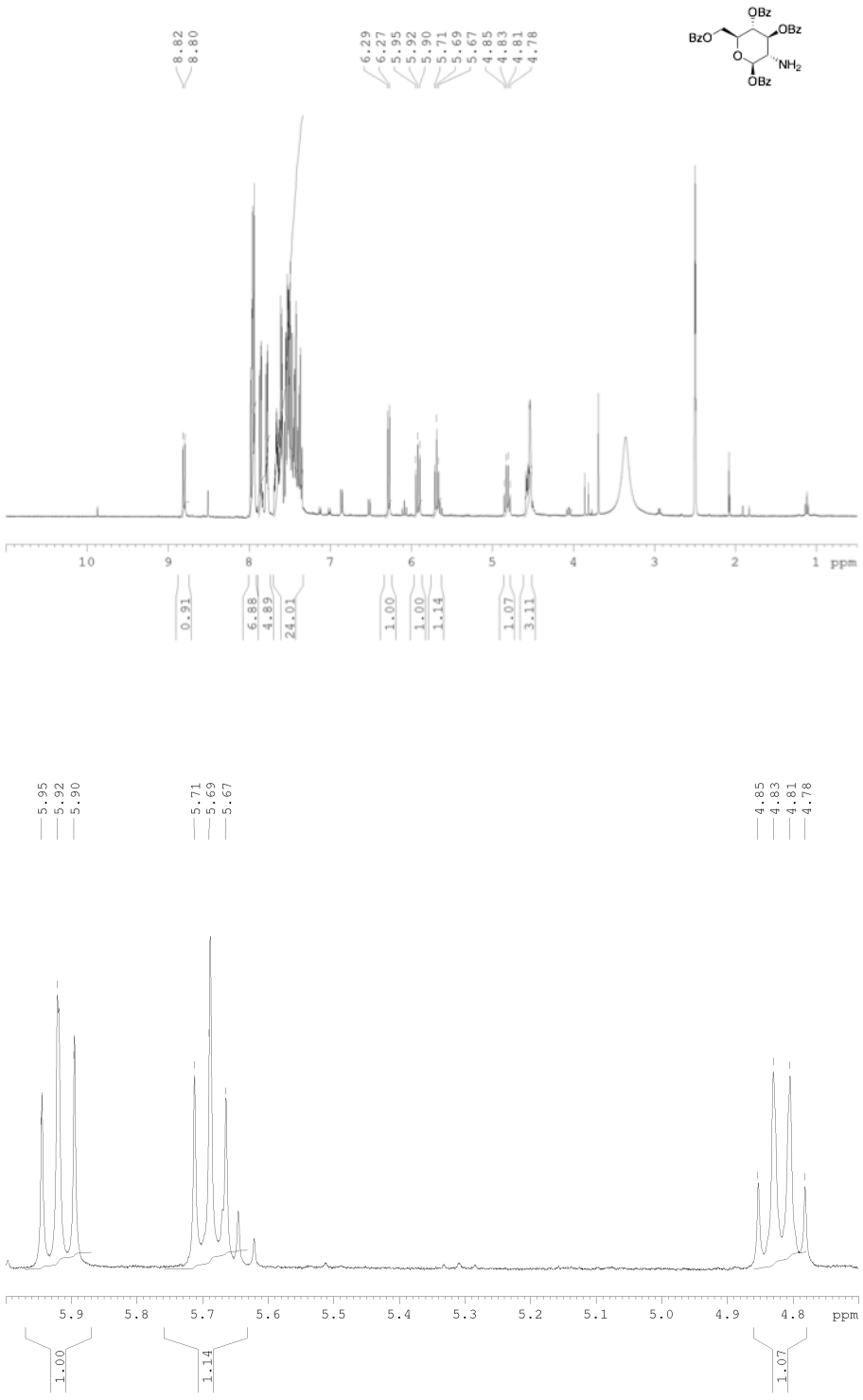
8.82
8.80
6.29
6.27
5.95
5.92
5.90
5.71
5.69
5.67
4.85
4.83
4.81
4.78
OBz
BzO
OBz
NH2
OBz
10
9
8
7
6
5
4
3
2
1 ppm
0.91
6.88
4.89
24.01
1.00
1.00
1.14
1.07
3.11
5.95
5.92
5.90
5.71
5.69
5.67
4.85
4.83
4.81
4.78
5.9
5.8
5.7
5.6
5.5
5.4
5.3
5.2
5.1
5.0
4.9
4.8
ppm
1.00
1.14
1.07

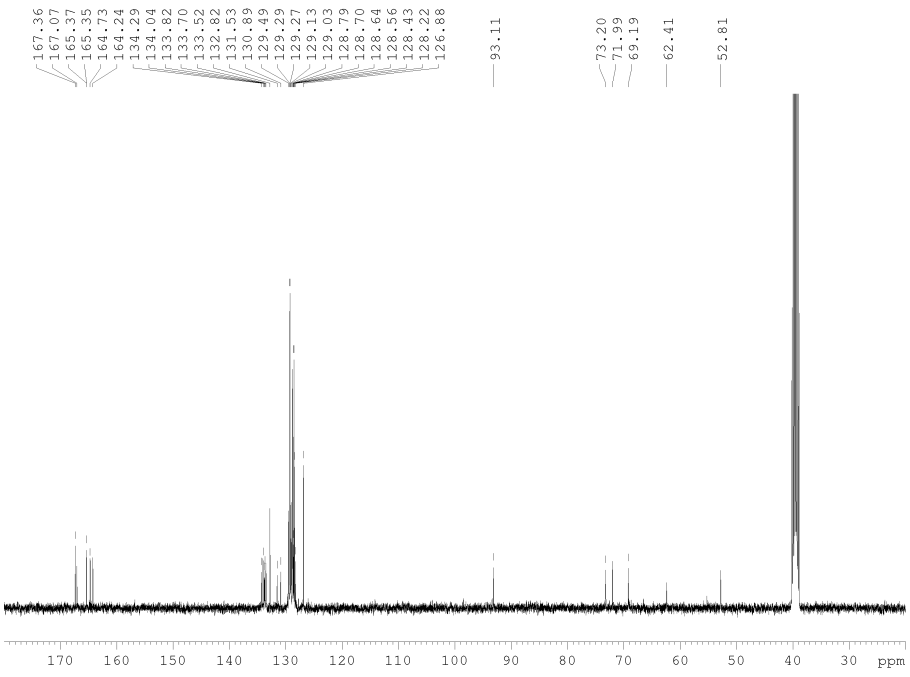
167.36
167.07
165.37
165.35
164.73
164.24
134.29
134.04
133.82
133.70
133.52
132.82
131.53
130.89
129.49
129.29
129.27
129.13
129.03
128.79
128.70
128.64
128.56
128.43
128.22
126.88
93.11
73.20
71.99
69.19
62.41
52.81
170 160 150 140 130 120 110 100 90 80 70 60 50 40 30 ppm

Compound 53

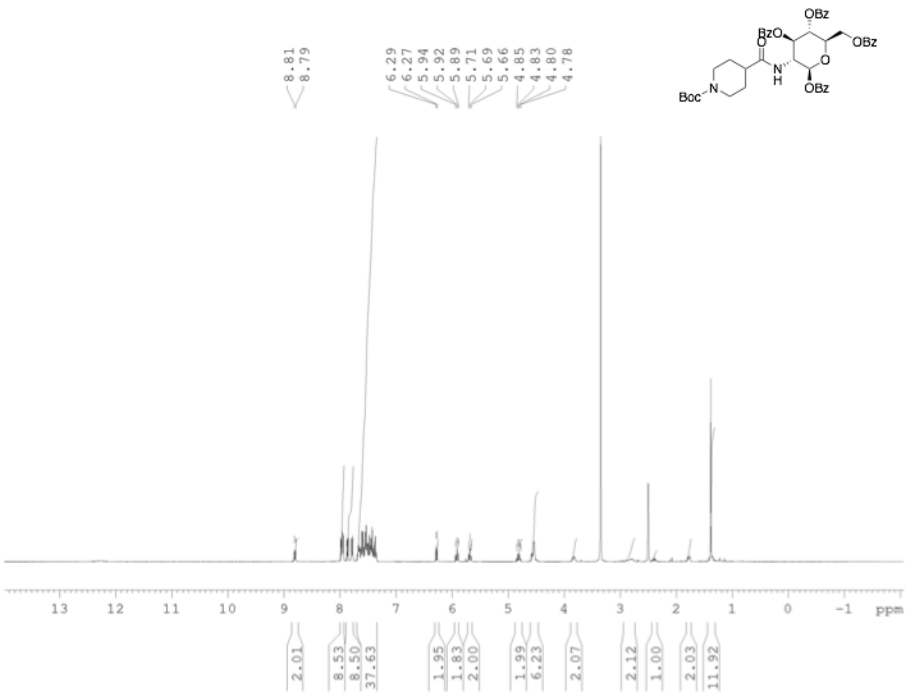
8.81
8.79
6.29
6.27
5.94
5.92
5.89
5.71
5.69
5.66
4.85
4.83
4.80
4.78
OBz
BzO
OBz
O
N
H
OBz
Boc
N
13 12 11 10 9 8 7 6 5 4 3 2 1 0 -1 ppm
2.01
8.53
8.50
37.63
1.95
1.83
2.00
1.99
6.23
2.07
2.12
1.00
2.03
11.92

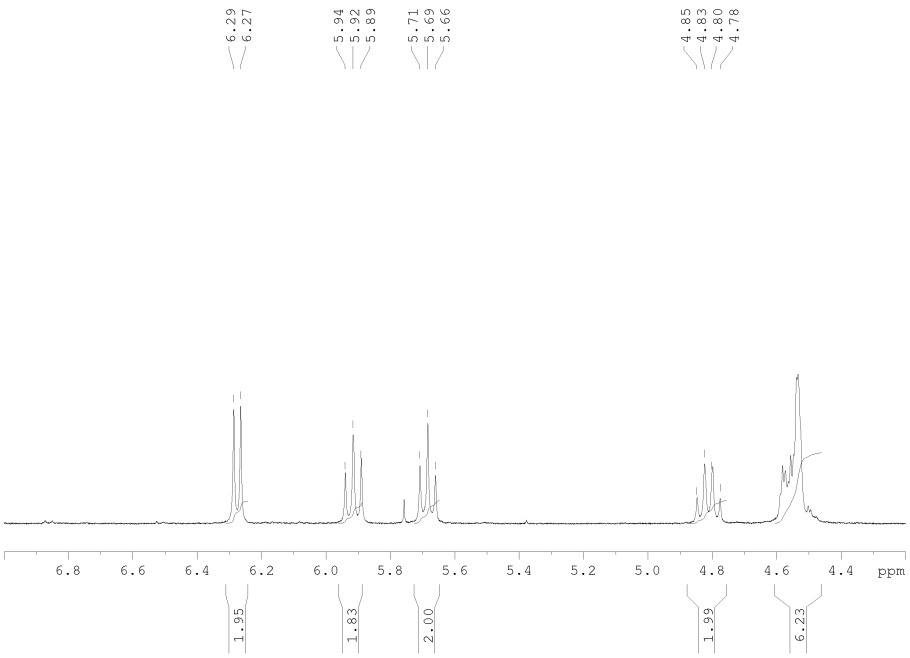
6.29
6.27
5.94
5.92
5.89
5.71
5.69
5.66
4.85
4.83
4.80
4.78
6.8
6.6
6.4
6.2
6.0
5.8
5.6
5.4
5.2
5.0
4.8
4.6
4.4
ppm
1.95
1.83
2.00
1.99
6.23

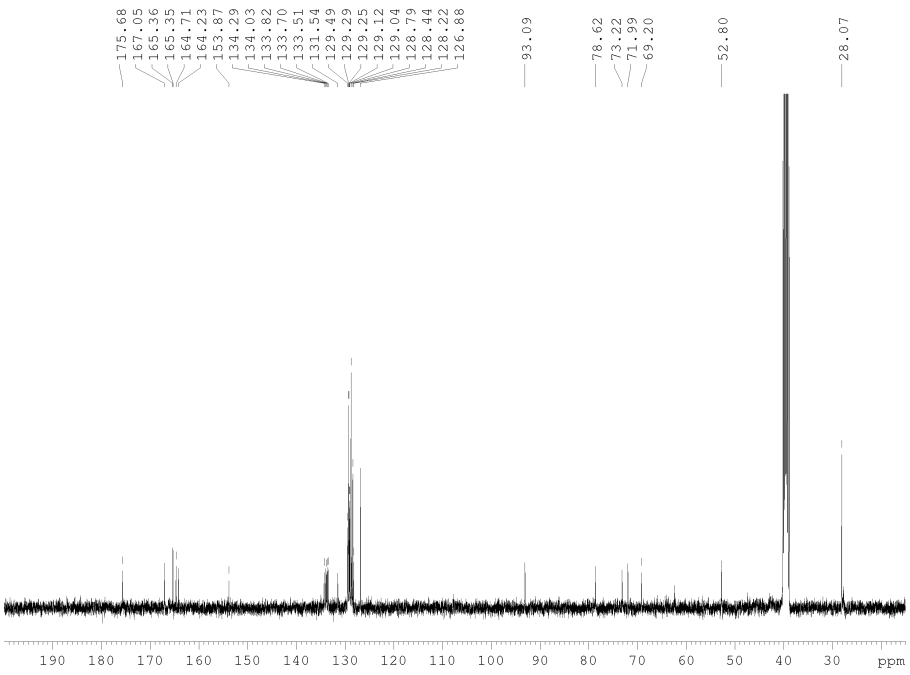
175.68
167.05
165.36
165.35
164.71
164.23
153.87
134.29
134.03
133.82
133.70
133.51
131.54
129.49
129.29
129.25
129.12
129.04
128.79
128.44
128.22
126.88
93.09
78.62
73.22
71.99
69.20
52.80
28.07
190
180
170
160
150
140
130
120
110
100
90
80
70
60
50
40
30
ppm

Compound 54

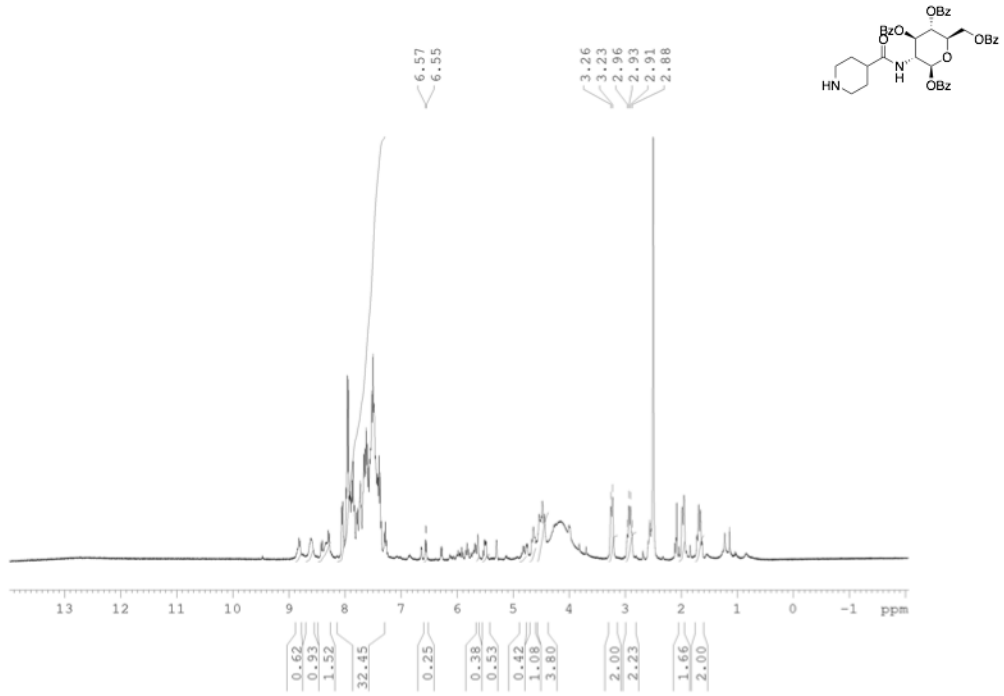
6.57
6.55
3.26
3.23
2.96
2.93
2.91
2.88
OBz
BzO
OBz
HN
N
H
OBz
13 12 11 10 9 8 7 6 5 4 3 2 1 0 -1 ppm
0.62
0.93
1.52
32.45
0.25
0.38
0.53
0.42
1.08
3.80
2.00
2.23
1.66
2.00

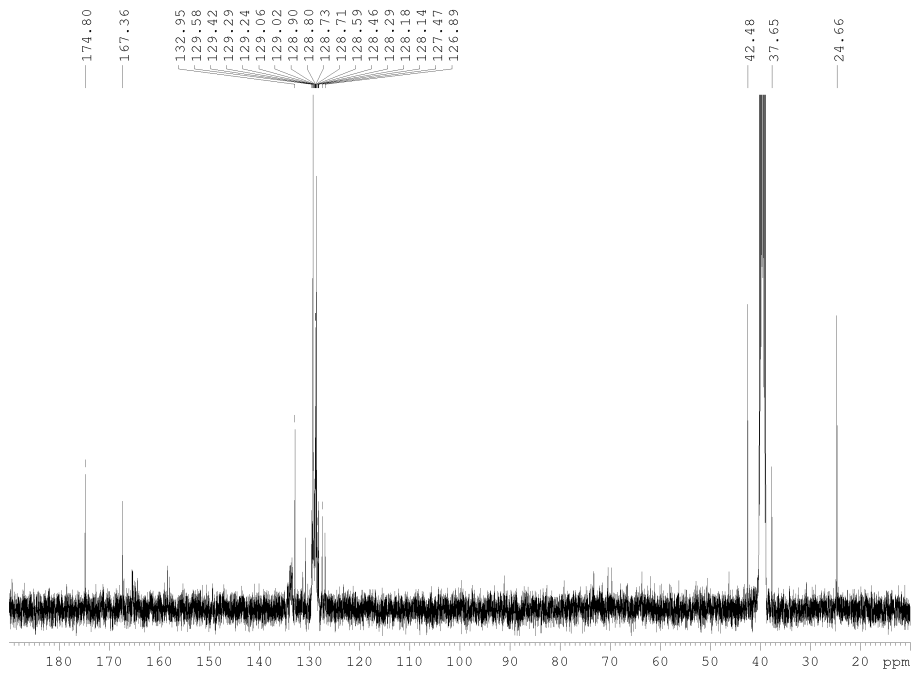
174.80
167.36
132.95
129.58
129.42
129.29
129.24
129.06
129.02
128.90
128.80
128.73
128.71
128.59
128.46
128.29
128.18
128.14
127.47
126.89
42.48
37.65
24.66
180 170 160 150 140 130 120 110 100 90 80 70 60 50 40 30 20 ppm

Compound 57

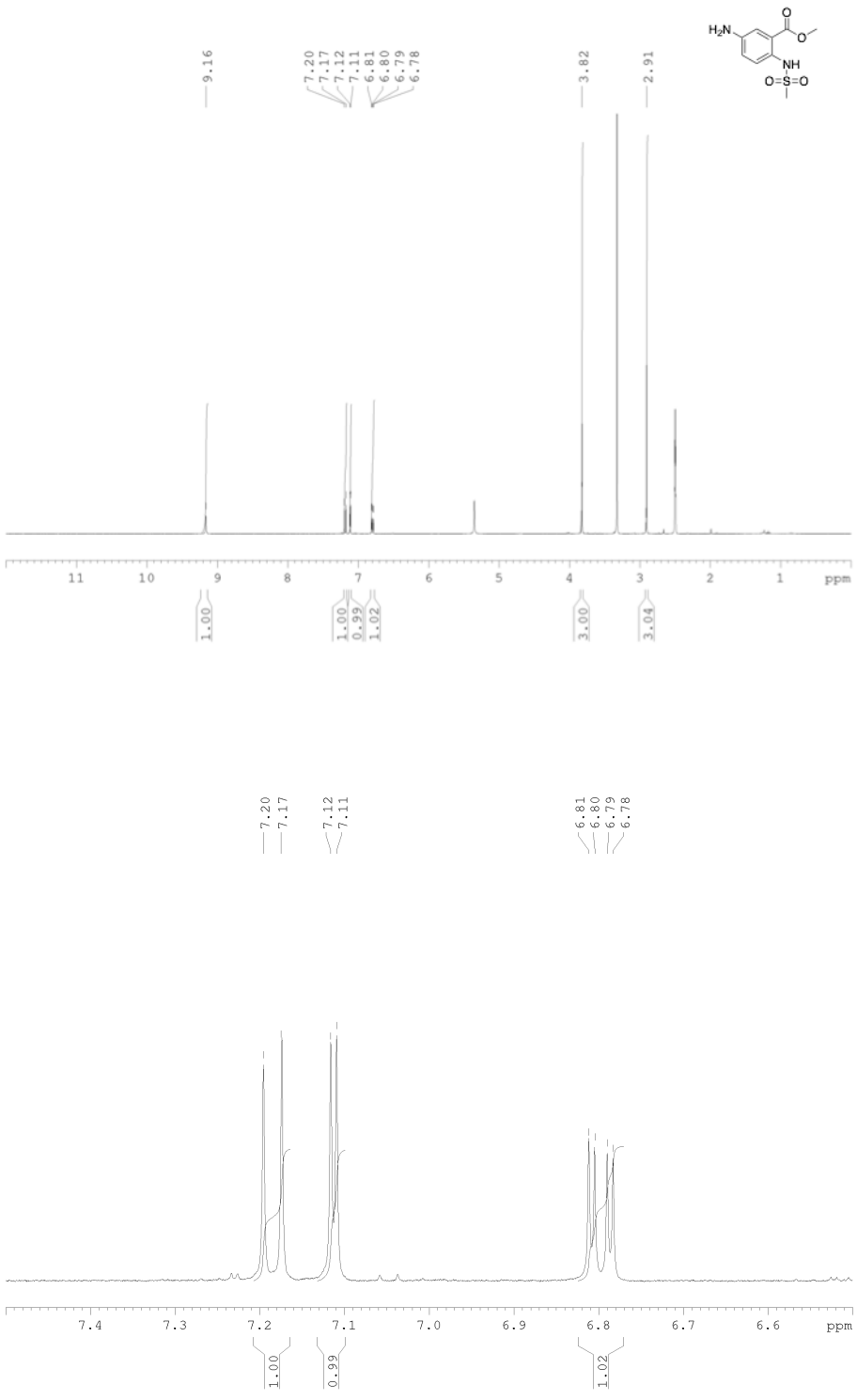
9.16
7.20
7.17
7.12
7.11
6.81
6.80
6.79
6.78
3.82
2.91
ppm
1.00
1.00
0.99
1.02
3.00
3.04

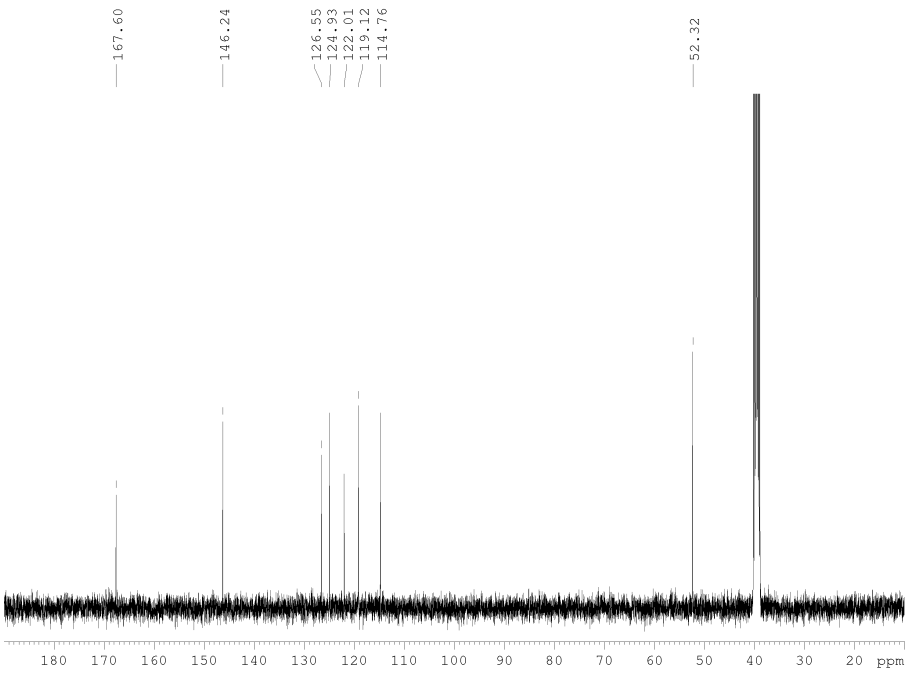
167.60
146.24
126.55
124.93
122.01
119.12
114.76
52.32
180 170 160 150 140 130 120 110 100 90 80 70 60 50 40 30 20 ppm

Compound 60

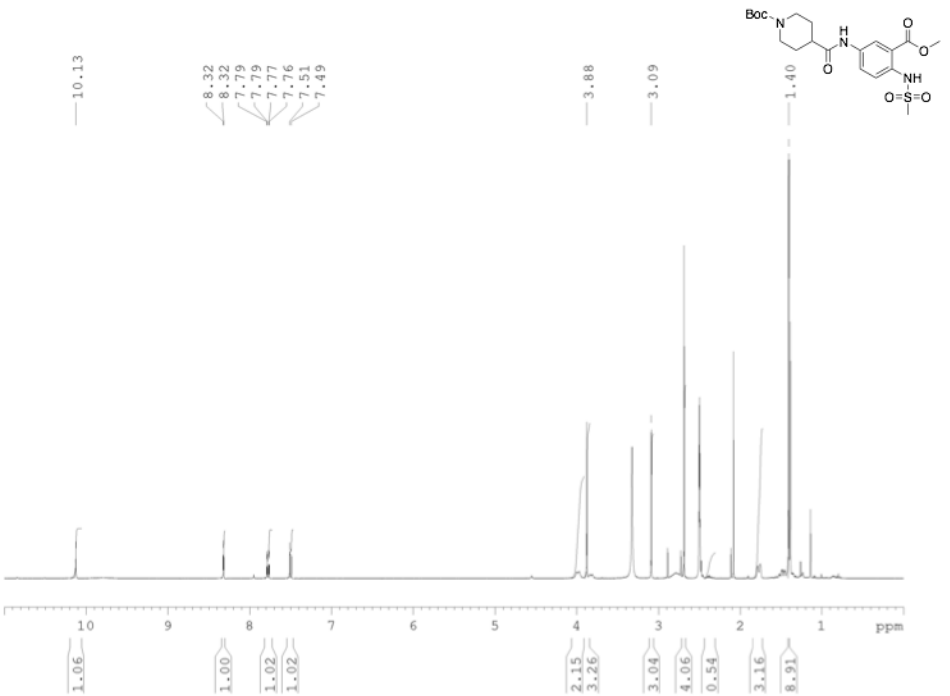
Boc
N
H
N
O
O
O
NH
O=S=O
10.13
8.32
8.32
7.79
7.79
7.77
7.76
7.51
7.49
3.88
3.09
1.40
10 9 8 7 6 5 4 3 2 1 ppm
1.06
1.00
1.02
1.02
2.15
3.26
3.04
4.06
0.54
3.16
8.91

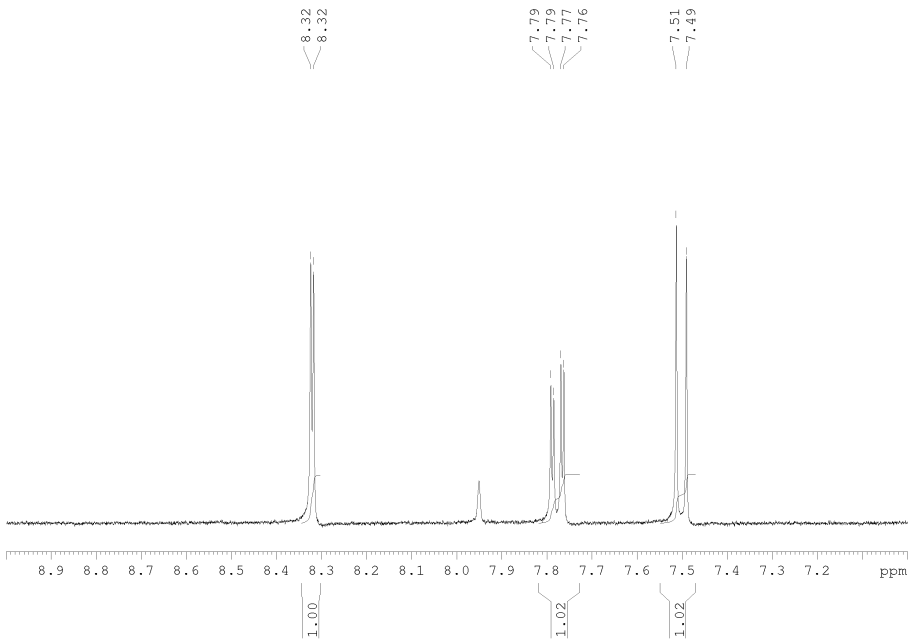
8.32
8.32
7.79
7.79
7.77
7.76
7.51
7.49
8.9 8.8 8.7 8.6 8.5 8.4 8.3 8.2 8.1 8.0 7.9 7.8 7.7 7.6 7.5 7.4 7.3 7.2 ppm
1.00
1.02
1.02

Compound 64

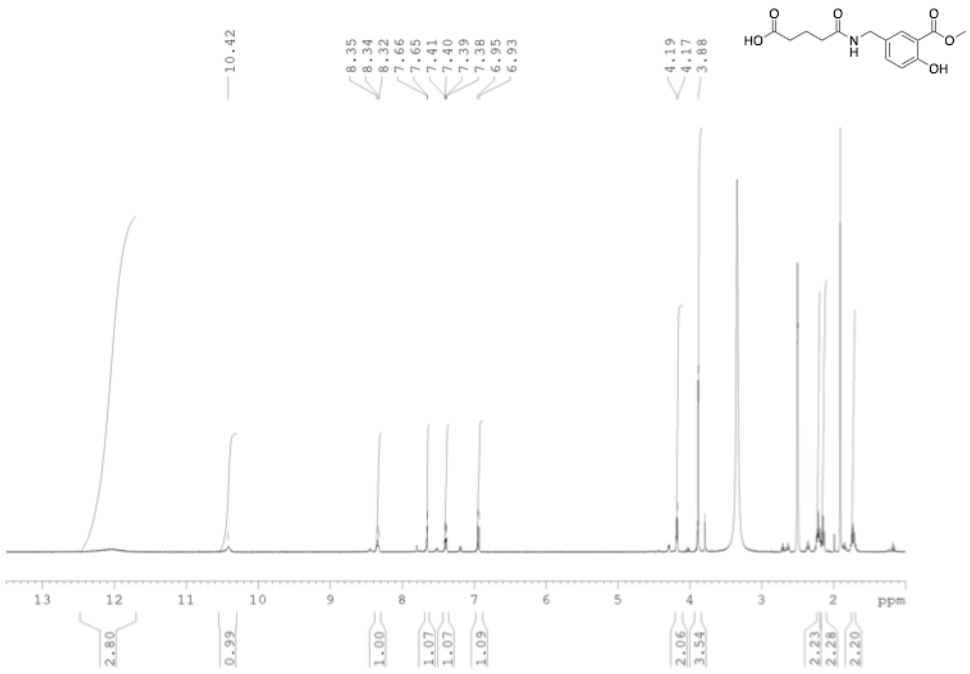
10.42
8.35
8.34
8.32
7.66
7.65
7.41
7.40
7.39
7.38
6.95
6.93
4.19
4.17
3.88
HO
O
O
N
H
O
O
OH
13 12 11 10 9 8 7 6 5 4 3 2 ppm
2.80
0.99
1.00
1.07
1.07
1.09
2.06
3.54
2.23
2.28
2.20

Compound 65

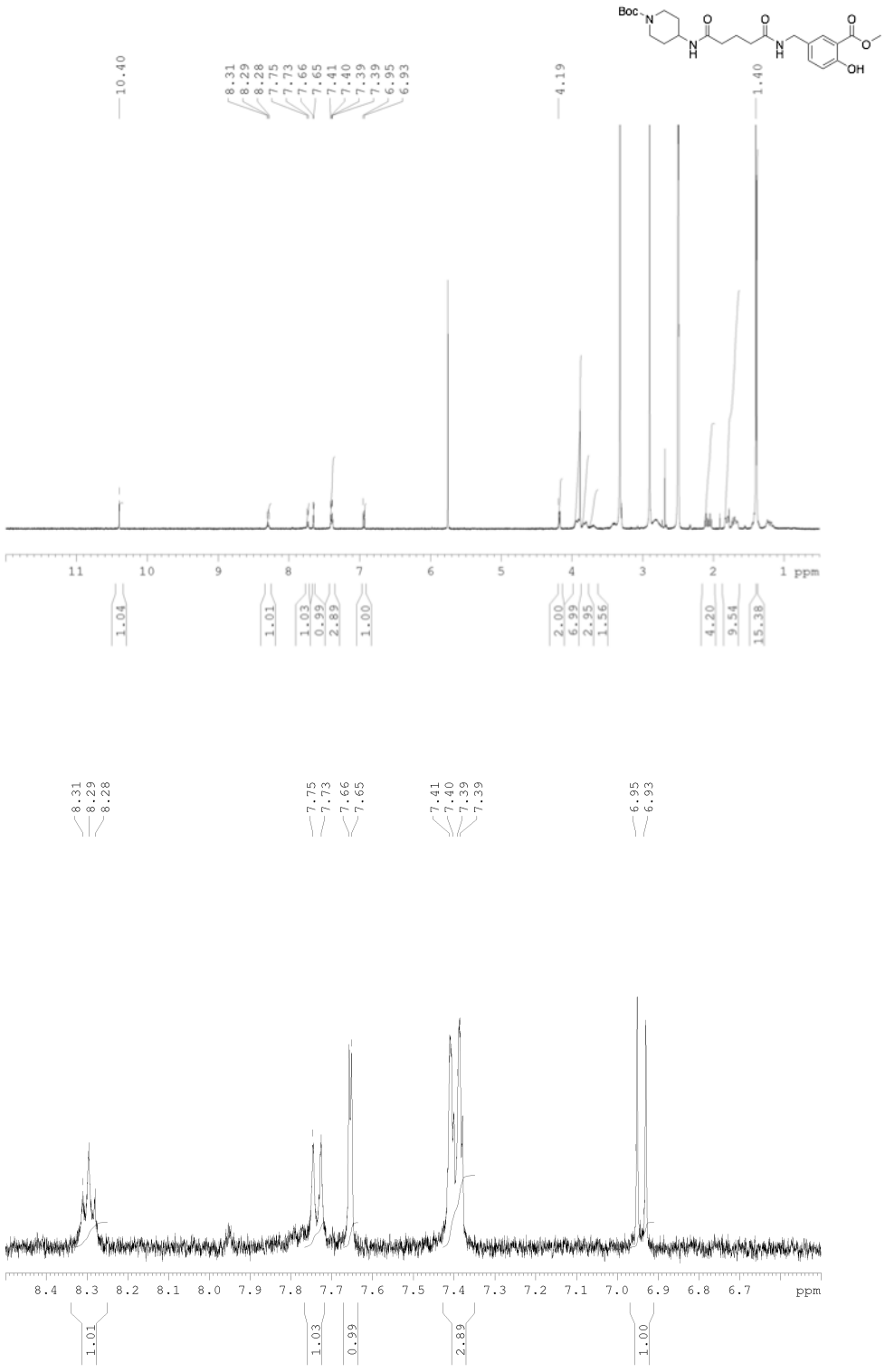
Boc
N
O
O
O
N
H
N
H
O
O
OH
10.40
8.31
8.29
8.28
7.75
7.73
7.66
7.65
7.41
7.40
7.39
7.39
6.95
6.93
4.19
1.40
11
10
9
8
7
6
5
4
3
2
1 ppm
1.04
1.01
1.03
0.99
2.89
1.00
2.00
6.99
2.95
1.56
4.20
9.54
15.38
8.4
8.3
8.2
8.1
8.0
7.9
7.8
7.7
7.6
7.5
7.4
7.3
7.2
7.1
7.0
6.9
6.8
6.7
ppm
1.01
1.03
0.99
2.89
1.00

Compound 69

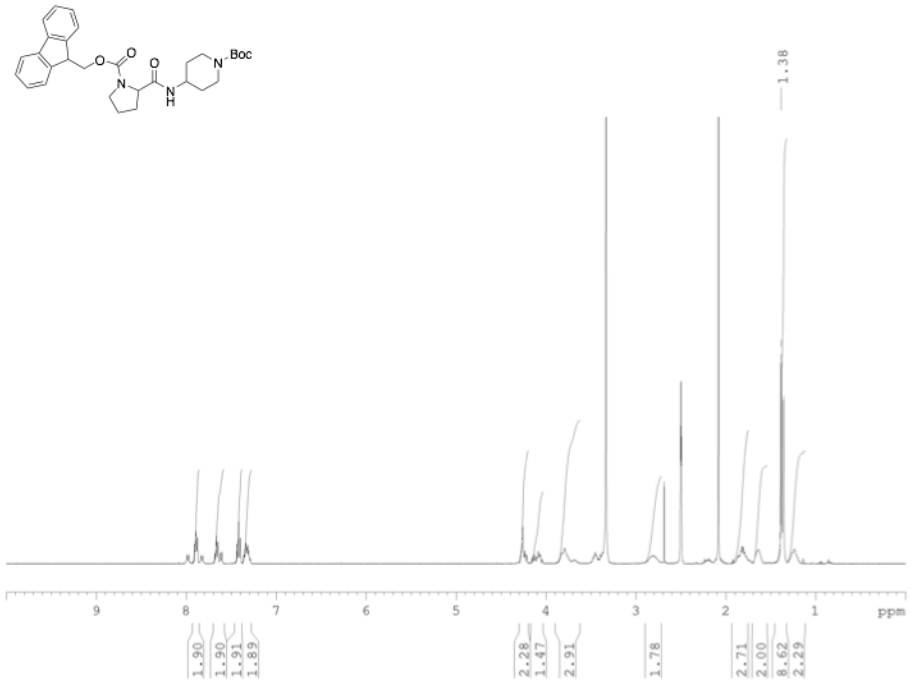
Boc
1.38
9
8
7
6
5
4
3
2
1
ppm
1.90
1.90
1.91
1.89
2.28
1.47
2.91
1.78
2.71
2.00
8.62
2.29

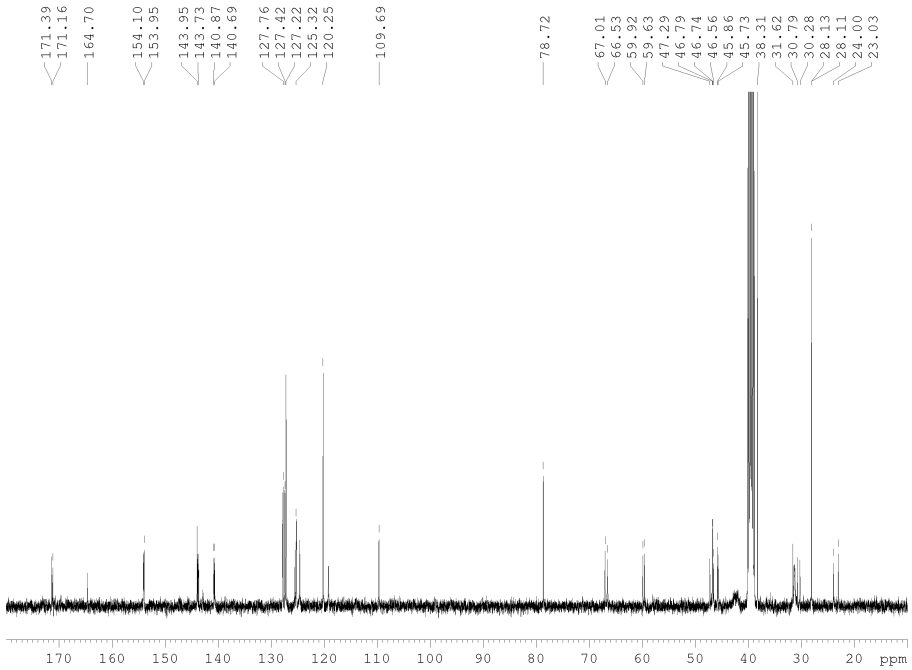
171.39
171.16
164.70
154.10
153.95
143.95
143.73
140.87
140.69
127.76
127.42
127.22
125.32
120.25
109.69
78.72
67.01
66.53
59.92
59.63
47.29
46.79
46.74
46.56
45.86
45.73
38.31
31.62
30.79
30.28
28.13
28.11
24.00
23.03
170
160
150
140
130
120
110
100
90
80
70
60
50
40
30
20
ppm

Compound 70

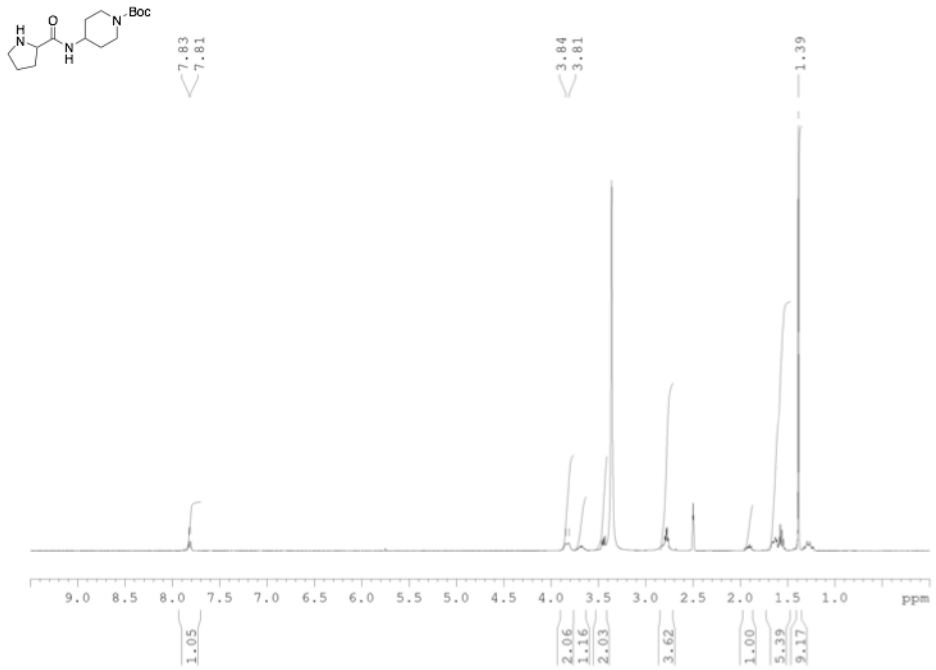
Boc
7.83
7.81
3.84
3.81
1.39
9.0 8.5 8.0 7.5 7.0 6.5 6.0 5.5 5.0 4.5 4.0 3.5 3.0 2.5 2.0 1.5 1.0 ppm
1.05
2.06
1.16
2.03
3.62
1.00
5.39
9.17

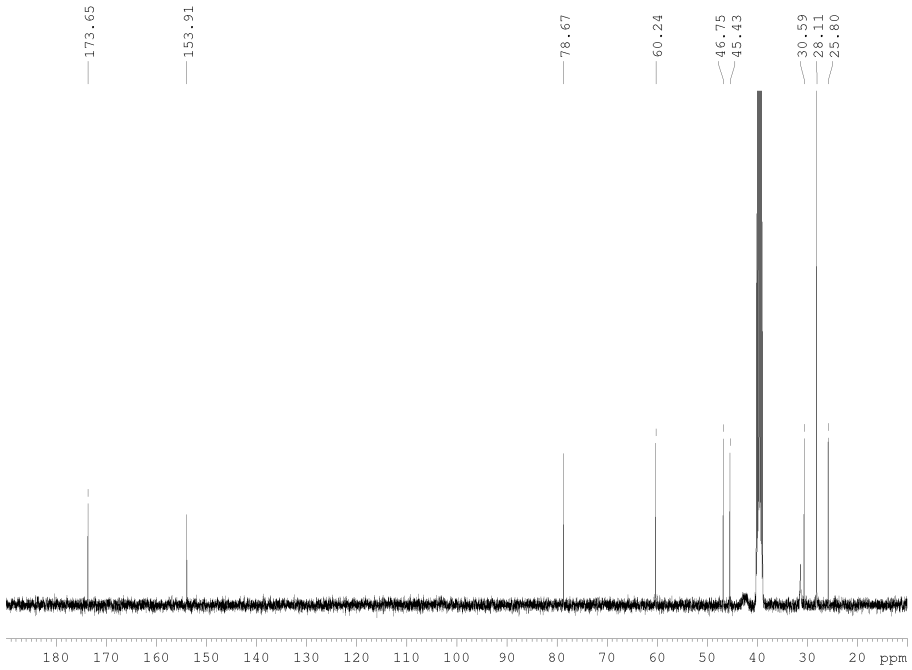
173.65
153.91
78.67
60.24
46.75
45.43
30.59
28.11
25.80
180 170 160 150 140 130 120 110 100 90 80 70 60 50 40 30 20 ppm

Compound 71

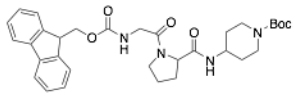
O
O
N
H
O
N
O
N
H
N
Boc

2.88
2.73
1.38
9.0 8.5 8.0 7.5 7.0 6.5 6.0 5.5 5.0 4.5 4.0 3.5 3.0 2.5 2.0 1.5 1.0 ppm
2.50
2.25
4.43
3.45
3.44
2.84
2.36
5.05
7.84
2.00

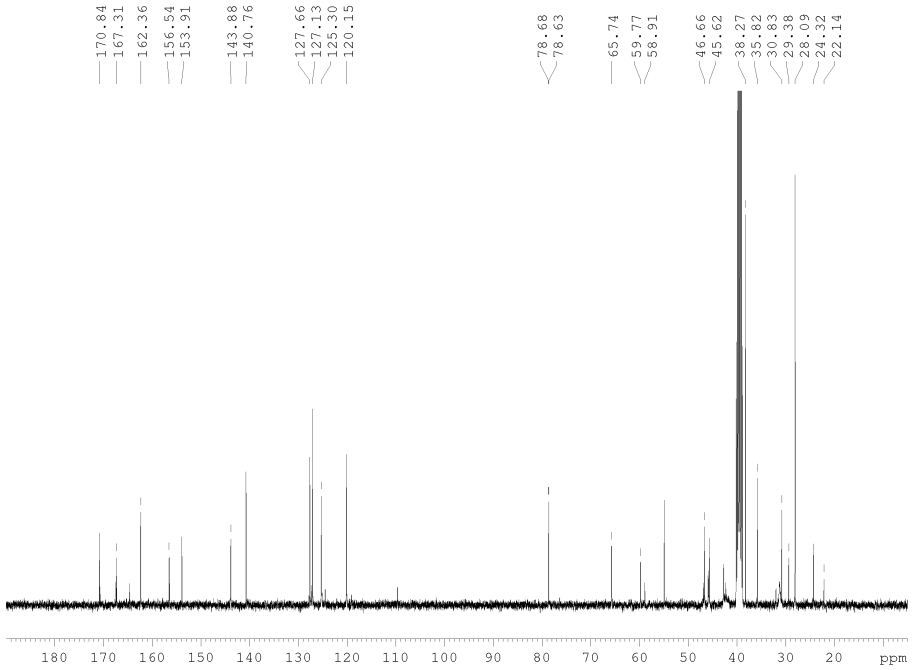
170.84
167.31
162.36
156.54
153.91
143.88
140.76
127.66
127.13
125.30
120.15
78.68
78.63
65.74
59.77
58.91
46.66
45.62
38.27
35.82
30.83
29.38
28.09
24.32
22.14
180 170 160 150 140 130 120 110 100 90 80 70 60 50 40 30 20 ppm

Compound 72

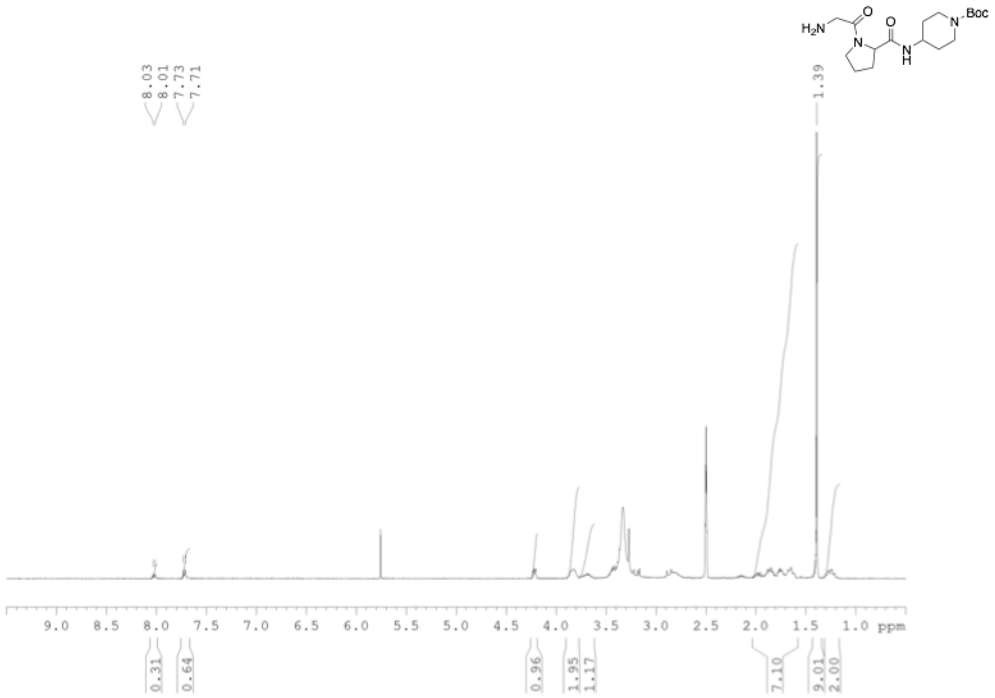
8.03
8.01
7.73
7.71
1.39
9.0 8.5 8.0 7.5 7.0 6.5 6.0 5.5 5.0 4.5 4.0 3.5 3.0 2.5 2.0 1.5 1.0 ppm
0.31
0.64
0.96
1.95
1.17
7.10
9.01
2.00

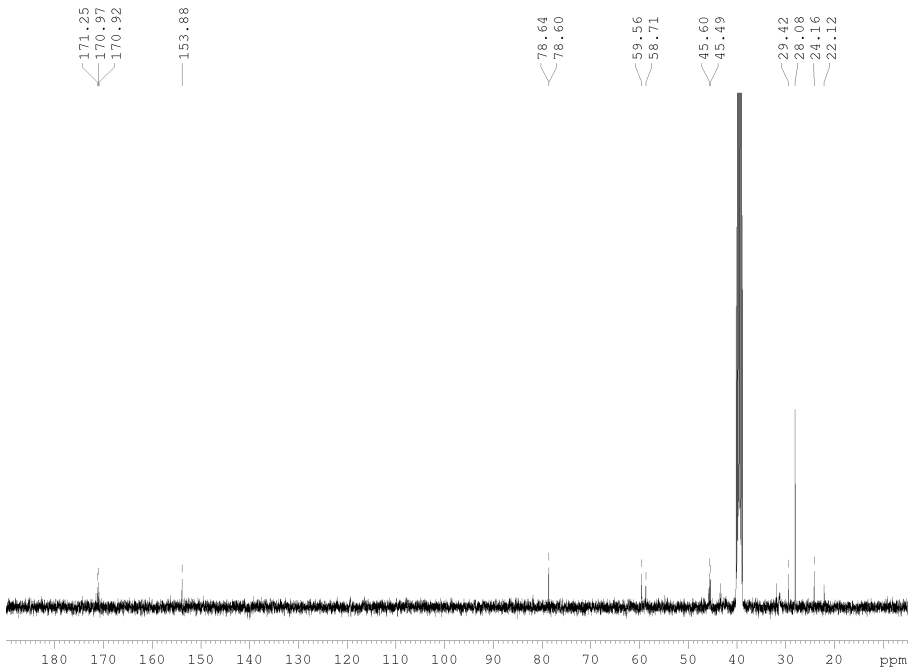
171.25
170.97
170.92
153.88
78.64
78.60
59.56
58.71
45.60
45.49
29.42
28.08
24.16
22.12
180 170 160 150 140 130 120 110 100 90 80 70 60 50 40 30 20 ppm

Compound 73

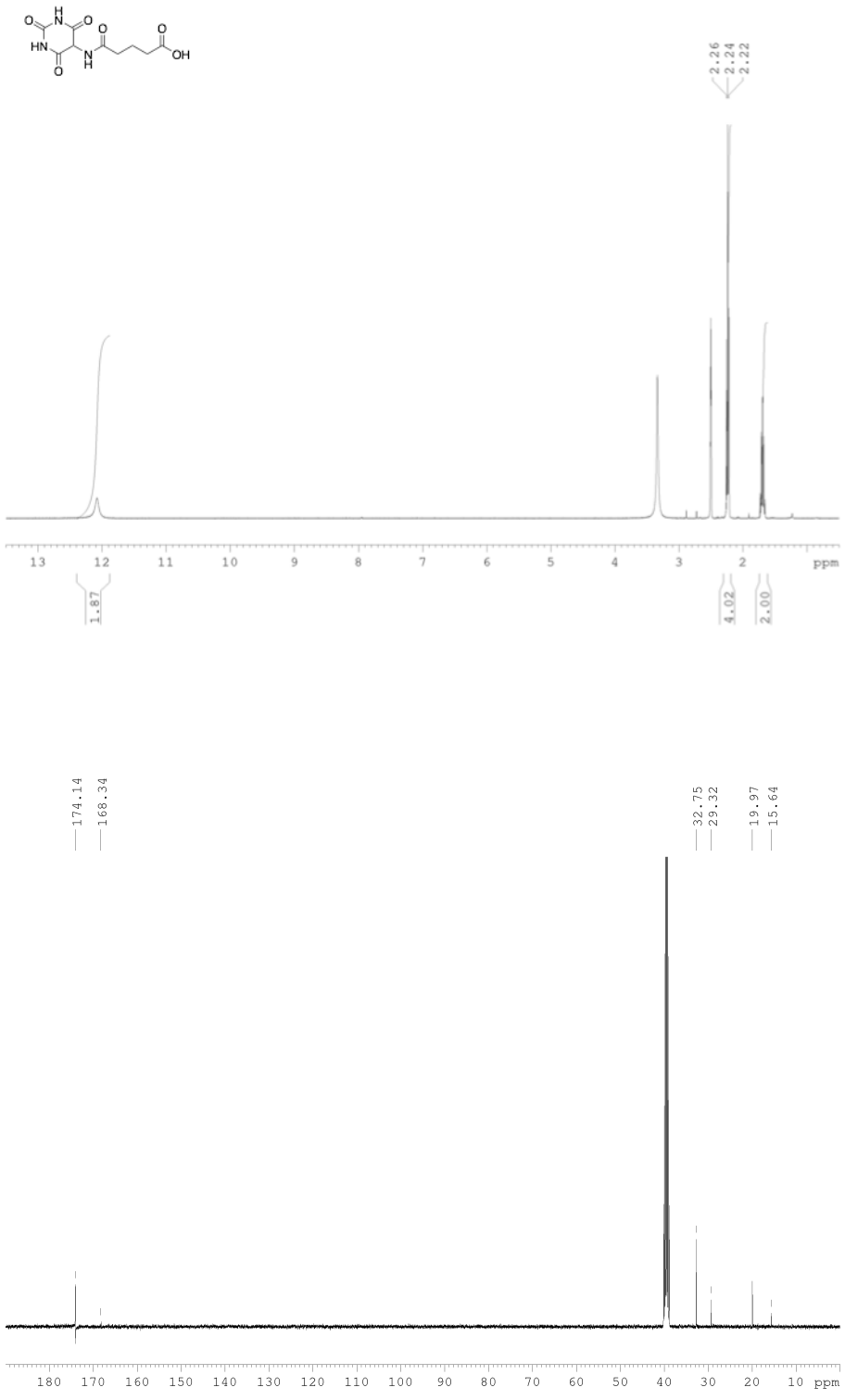
2.26
2.24
2.22
13
12
11
10
9
8
7
6
5
4
3
2
ppm
1.87
4.02
2.00
174.14
168.34
32.75
29.32
19.97
15.64
180
170
160
150
140
130
120
110
100
90
80
70
60
50
40
30
20
10 ppm

Compound 78

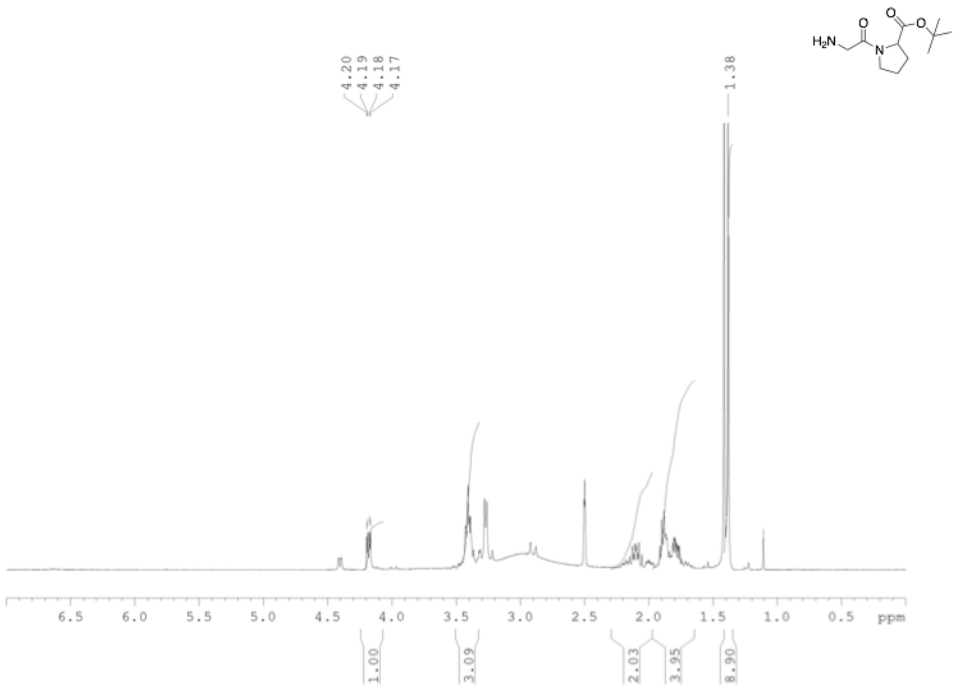
4.20
4.19
4.18
4.17
1.38
6.5 6.0 5.5 5.0 4.5 4.0 3.5 3.0 2.5 2.0 1.5 1.0 0.5 ppm
1.00
3.09
2.03
3.95
8.90

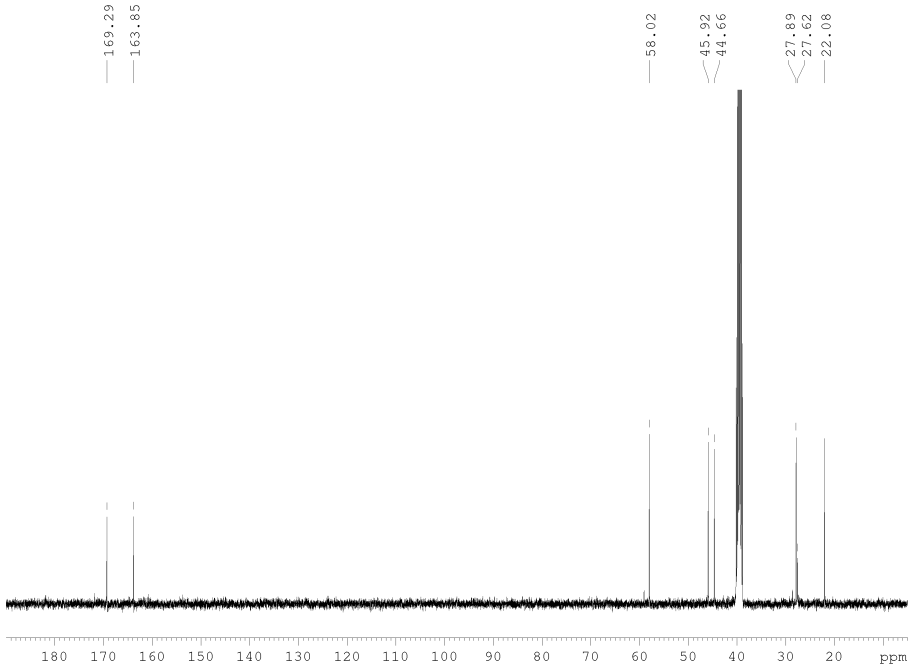
169.29
163.85
58.02
45.92
44.66
27.89
27.62
22.08
180 170 160 150 140 130 120 110 100 90 80 70 60 50 40 30 20 ppm

Compound 83

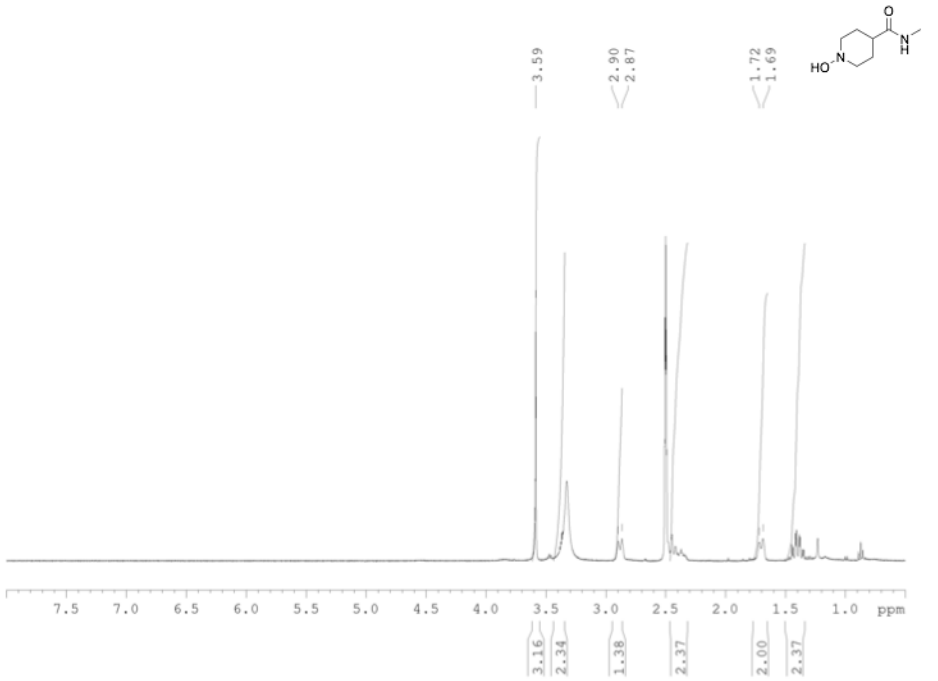
3.59
2.90
2.87
1.72
1.69
HO
N
O
N
H
7.5 7.0 6.5 6.0 5.5 5.0 4.5 4.0 3.5 3.0 2.5 2.0 1.5 1.0 ppm
3.16
2.34
1.38
2.37
2.00
2.37

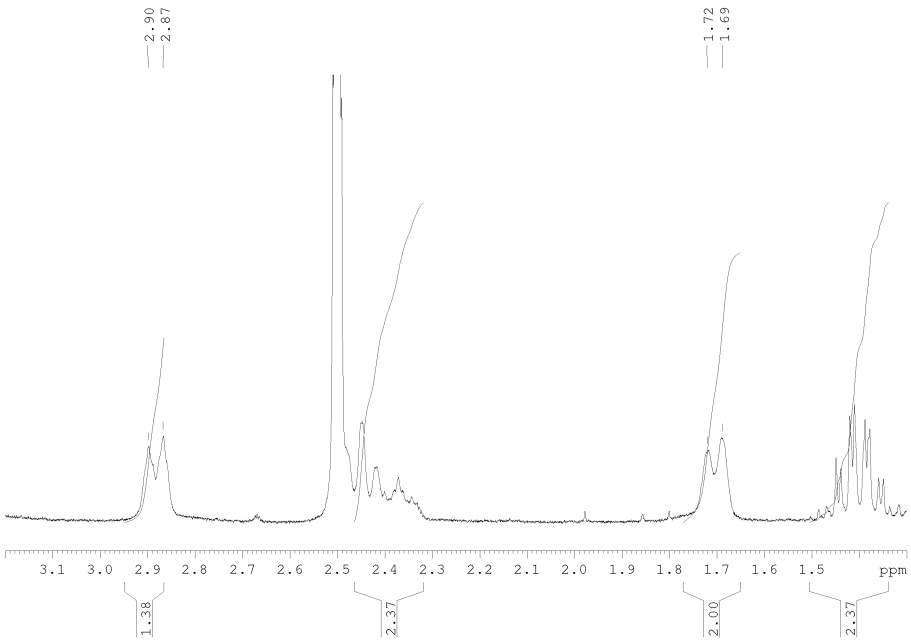
2.90
2.87
1.72
1.69
3.1 3.0 2.9 2.8 2.7 2.6 2.5 2.4 2.3 2.2 2.1 2.0 1.9 1.8 1.7 1.6 1.5 ppm
1.38
2.37
2.00
2.37

Compound A1

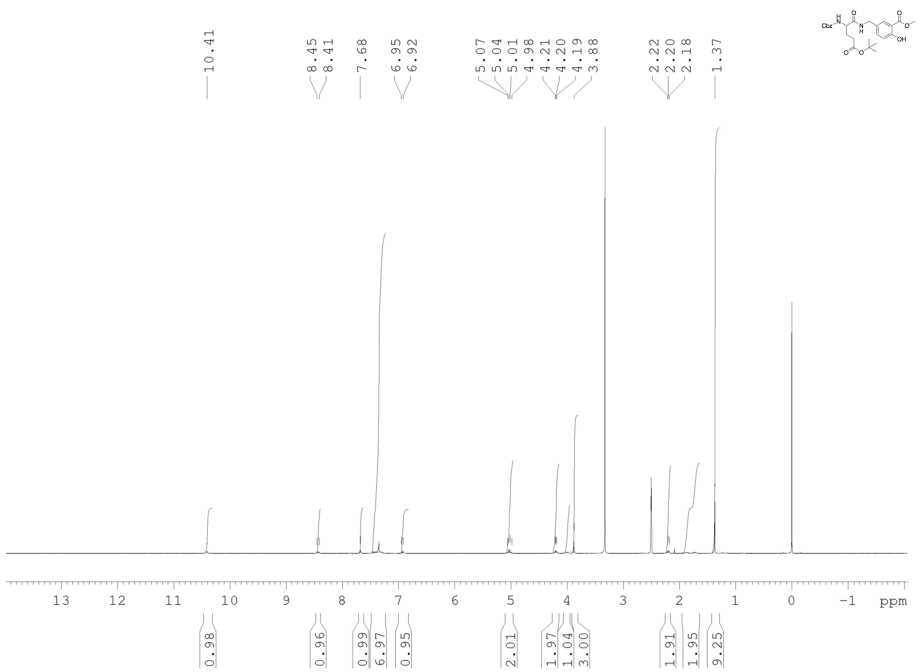

Compound A2

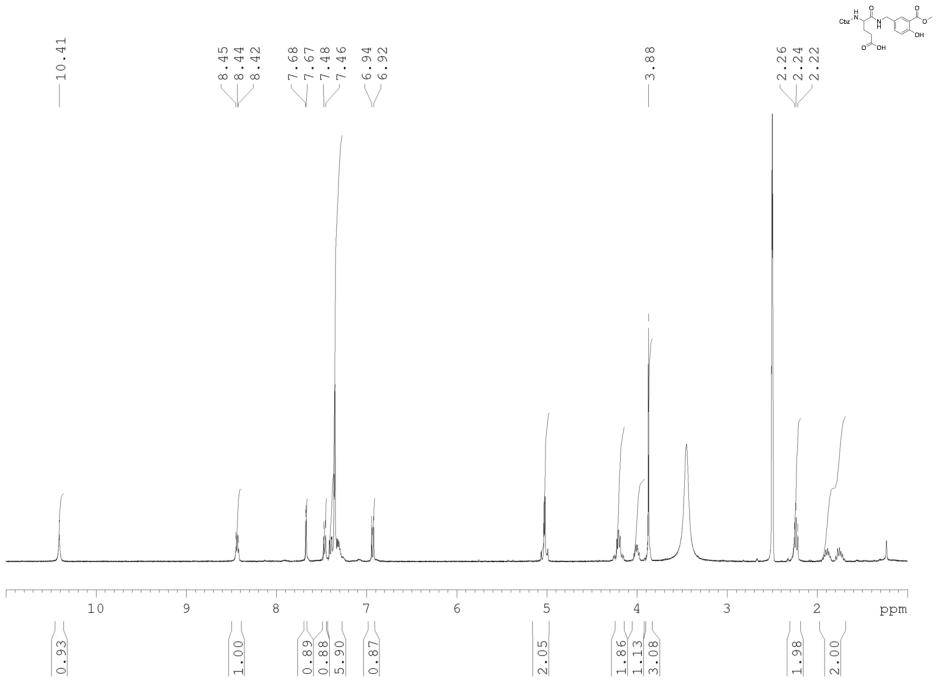

Compound A3

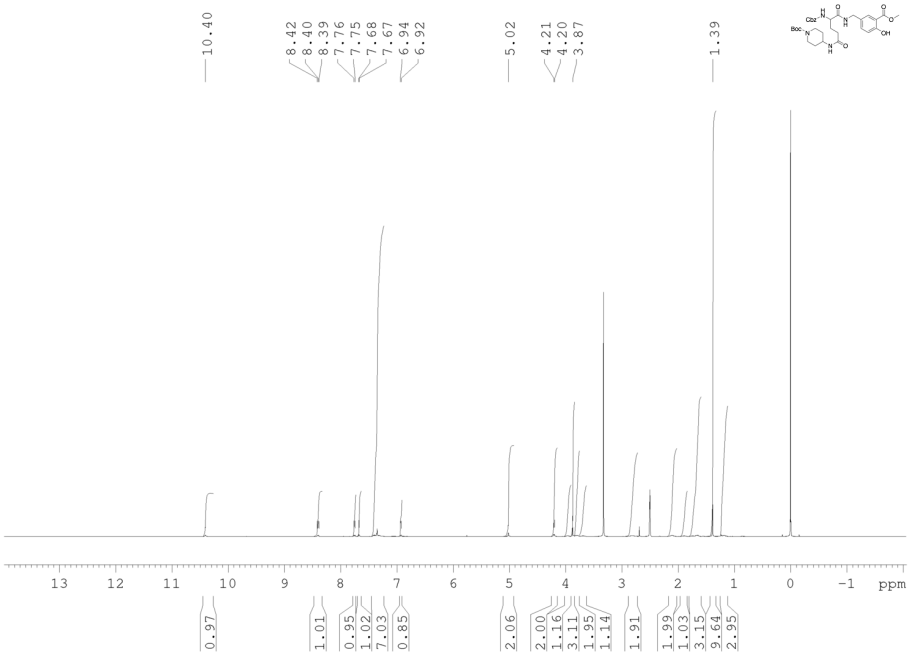

Compound A7

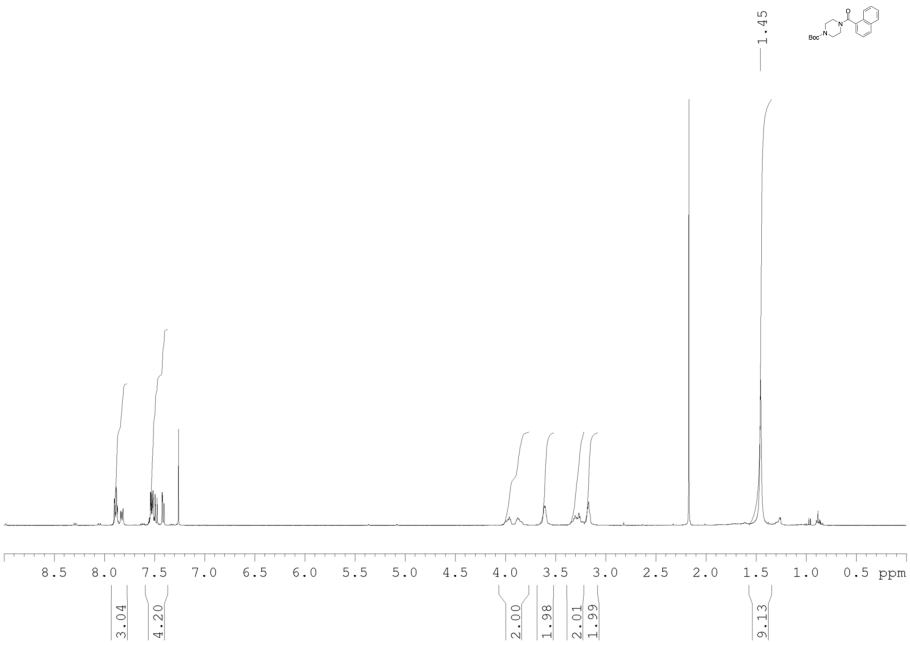

Compound A9

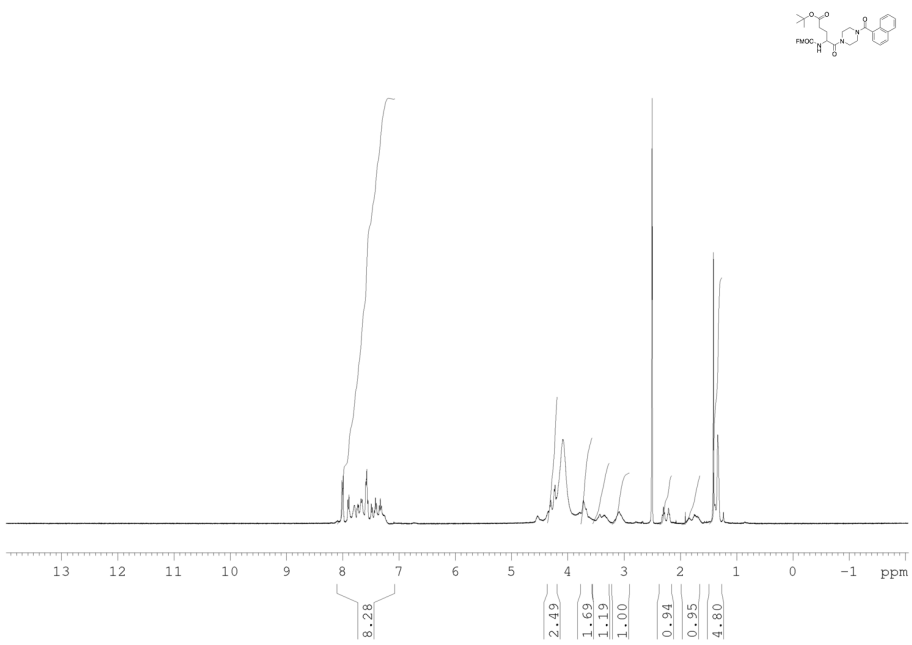
13 12 11 10 9 8 7 6 5 4 3 2 1 0 −1 ppm
8.28
2.49
1.69
1.19
1.00
0.94
0.95
4.80

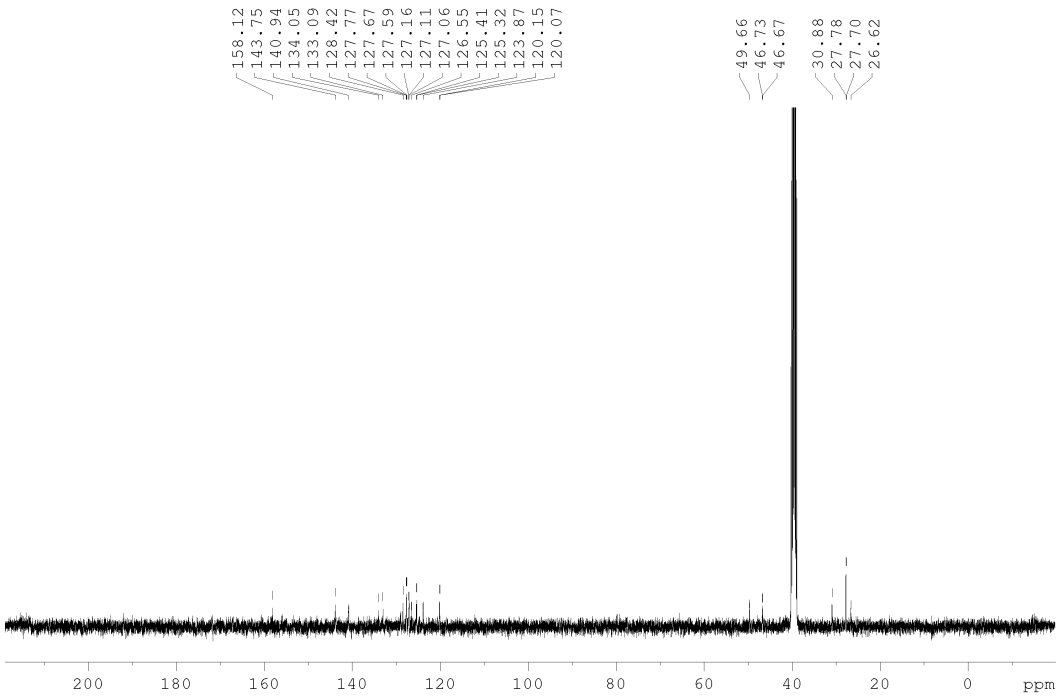
158.12
143.75
140.94
134.05
133.09
128.42
127.77
127.67
127.59
127.16
127.11
127.06
126.55
125.41
125.32
123.87
120.15
120.07
49.66
46.73
46.67
30.88
27.78
27.70
26.62
200 180 160 140 120 100 80 60 40 20 0 ppm

Compound A11

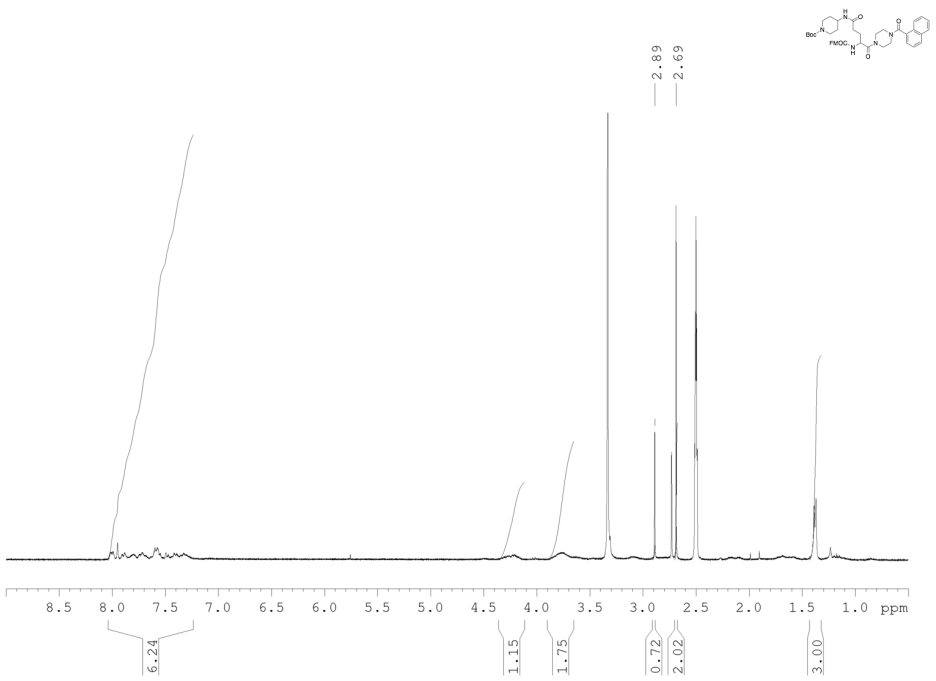

Compound A12

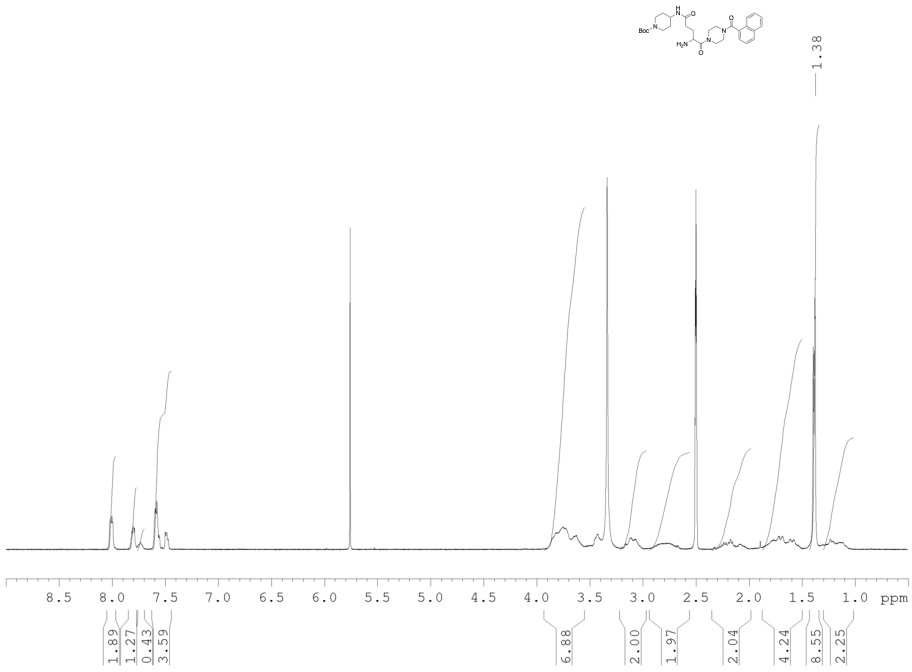

EPR Spectra of Final Compounds

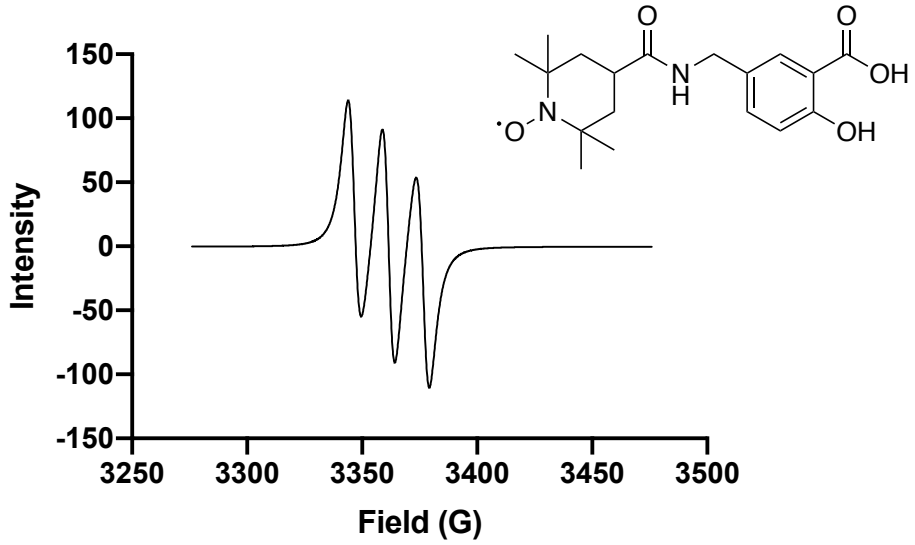

Compound 7

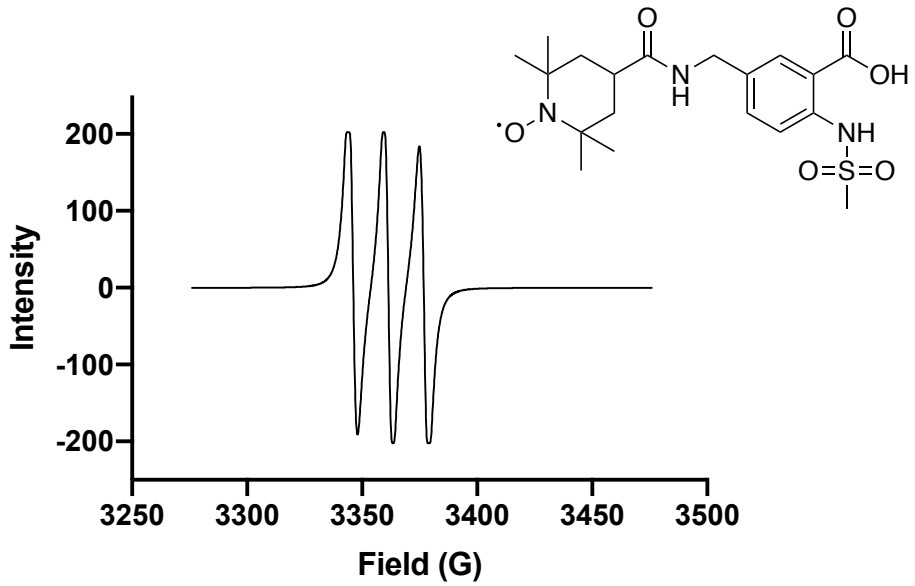

Compound 59

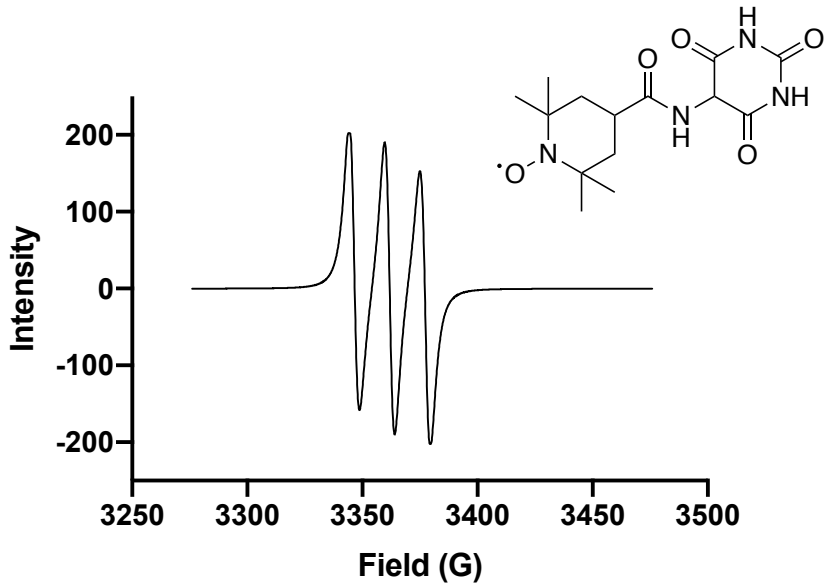

Compound 40

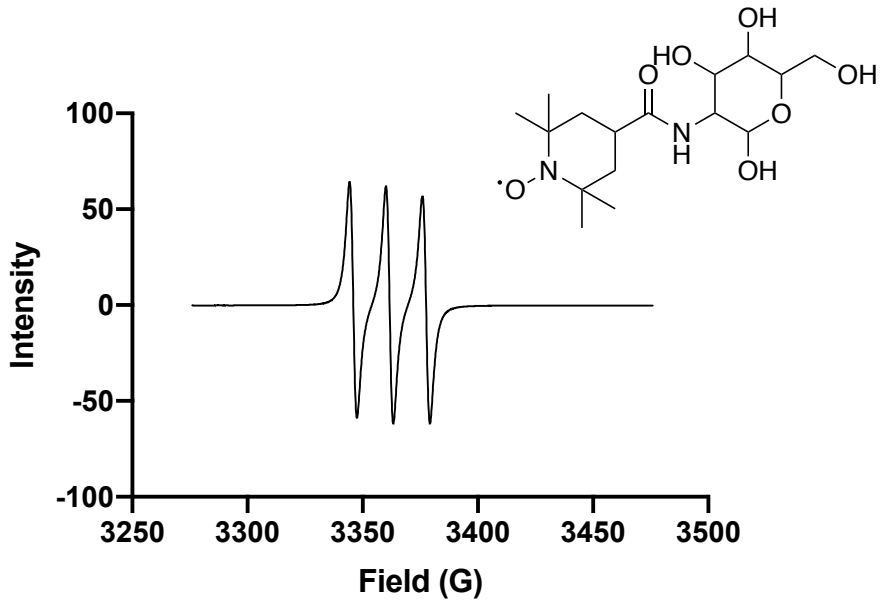

Compound 49